

**PHOTOINDUCED ELECTRON TRANSFER IN  
CYCLODEXTRIN BASED DONOR-ACCEPTOR SYSTEMS**

LIBRARY & INFORMATICS  
NIST(CSIR) TRIVANDRUM



G2931

THESIS SUBMITTED TO  
**THE UNIVERSITY OF KERALA**  
FOR THE DEGREE OF  
**DOCTOR OF PHILOSOPHY**  
IN CHEMISTRY  
UNDER THE FACULTY OF SCIENCE

*By*

**BIJITHA BALAN**



**PHOTOSCIENCES AND PHOTONICS  
CHEMICAL SCIENCES AND TECHNOLOGY DIVISION  
NATIONAL INSTITUTE FOR INTERDISCIPLINARY SCIENCE  
AND TECHNOLOGY (CSIR)  
TRIVANDRUM 695 019, KERALA, INDIA**

**AUGUST 2007**

**PHOTOINDUCED ELECTRON TRANSFER IN  
CYCLODEXTRIN BASED DONOR-ACCEPTOR SYSTEMS**

THESIS SUBMITTED TO  
**THE UNIVERSITY OF KERALA**  
FOR THE DEGREE OF  
**DOCTOR OF PHILOSOPHY**  
IN CHEMISTRY  
UNDER THE FACULTY OF SCIENCE

*By*

**BIJITHA BALAN**



LIBRARY & INFORMATICS  
NIST(CSIR) TRIVANDRUM



G2931

**PHOTOSCIENCES AND PHOTONICS  
CHEMICAL SCIENCES AND TECHNOLOGY DIVISION  
NATIONAL INSTITUTE FOR INTERDISCIPLINARY SCIENCE  
AND TECHNOLOGY (CSIR)  
TRIVANDRUM 695 019, KERALA, INDIA**

**AUGUST 2007**

## STATEMENT

I hereby declare that the matter embodied in the thesis entitled: **“Photoinduced Electron Transfer in Cyclodextrin based Donor-Acceptor Systems”** is the result of investigations carried out by me at the Photosciences and Photonics, Chemical Sciences and Technology Division of the National Institute for Interdisciplinary Science and Technology (CSIR), Thiruvananthapuram, under the supervision of Dr. K. R. Gopidas and the same has not been submitted elsewhere for a degree.

In keeping with the general practice of reporting scientific observations, due acknowledgement has been made wherever the work described is based on the findings of other investigators.



**Bijitha Balan**

---

**Chemical Sciences and Technology Division**  
**National Institute for Interdisciplinary Science and Technology**  
(formerly Regional Research Laboratory, Trivandrum)



**K. R. Gopidas**  
Scientist EII

**Council of Scientific and Industrial Research (CSIR)**  
Industrial Estate P.O., Trivandrum 695 019  
Kerala, INDIA  
<http://www.niist.res.in>

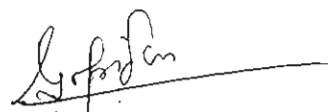
ISO 9001 REGISTERED  
  
DNV  
MGMT. SYS.  
RVA C 024  
gopidaskr@rediffmail.com  
Tel.: +91-471-2515364  
Fax: +91-471-2490186

---

August 3, 2007

**CERTIFICATE**

This is to certify that the work embodied in the thesis entitled:  
**“Photoinduced Electron Transfer in Cyclodextrin based Donor-Acceptor Systems”** has been carried out by Ms. Bijitha Balan under my supervision and the same has not been submitted elsewhere for a degree.



**K. R. Gopidas**  
Thesis Supervisor

## ACKNOWLEDGEMENTS

*I have great pleasure in placing on record my deep sense of gratitude to Dr. K. R. Gopidas, my thesis supervisor for suggesting the research problem and for his guidance, support, encouragement and help, leading to the successful completion of this work.*

*I would like to express my sincere thanks to Professor M. V. George for being an inspiration.*

*I wish to thank Professor. T. K. Chandrashekar, Director, NIIST, Trivandrum for providing necessary facilities for carrying out the work. I also thank Dr. G. Vijay Nair, Dr. B. C. Pai and Professor Javed Iqbal, former Directors of this institute.*

*I sincerely thank Dr. Suresh Das, Dr. A. Ajayaghosh, Dr. K. George Thomas and Dr. D. Ramaiah, Scientists of the Photosciences and Photonics section, Chemical Sciences and Technology Division, for all the help and support extended to me.*

*I thank all the members of the Photosciences and Photonics and in particular Dr. Sumalekshmy, Dr. M. A. Smitha, Dr. S. Dileesh, Dr. E. Prasad, Ms. Deepthi L. Sivadas, Mr. K. Sreenath, Mr. C. V. Suneesh, Mr. G. Ajayakumar and Mr. V. K. Ratheesh Kumar. I also thank Mr. V. K. Praveen, Mr. C. Vijayakumar, Dr. T. D. Suja and Ms. Elizabeth Kuruvilla for their constant help and motivation. I also extend my thanks to Mr. Robert Philip, Ms. Priya A. Nair and Mrs. Sarada Nair for their help and cooperation. I thank Mrs. S. Viji and Mrs. Soumini Shoji for NMR and elemental analyses. I also thank my friends in other Divisions of the NIIST, Trivandrum for their cooperation.*

*I am deeply indebted to my parents and sisters for their love and affection which has always been a great source of inspiration and in particular Baby aunty for her invaluable support and constant encouragement. I would also like to thank all my teachers for their help and blessings.*

*Financial assistance from the Council of Scientific and Industrial Research (CSIR) and the Department of Science and Technology (DST) is gratefully acknowledged.*

*Bijitha Balan*

## CONTENTS

	<b>Page</b>
Statement	i
Certificate	ii
Acknowledgements	iii
Preface	viii
<b>Chapter 1:      <i>Photoinduced Electron Transfer in Cyclodextrin-Appended Donor-Acceptor Systems – An Overview</i></b>	<b>01-34</b>
1.1.      Introduction	1
1.2.      Photoinduced Electron and Energy Transfer in CD-based Donor-Acceptor systems	12
1.3.      Origin of the Present Work	27
1.4.      References	29
<b>Chapter 2:      <i>Free Energy Dependence of Photoinduced Electron Transfer Rates in <math>\alpha</math>-CD appended Donor-Acceptor Systems</i></b>	<b>35-86</b>
2.1.      Abstract	35
2.2.      Introduction	36
2.3.      Results and Discussion	39
2.3.1.      Synthesis and Characterization of <b>PYCD</b>	39
2.3.2.      Photophysical Properties of <b>PYCD</b>	44
2.3.3.      Interaction of Acceptors with <b>PYCD</b>	45
2.3.4.      Fluorescence Quenching	49
2.3.5.      Calculation of $\Delta G^0$ Values	61
2.3.6.      Free Energy Dependence of $k_{et}$ and $k_q$	64

2.3.7.	Electronic Coupling and Reorganization Energy	67
2.3.8.	The Inverted Region	69
2.3.9.	Visual Demonstration of the Inverted Region	74
2.4.	Conclusions	78
2.5.	Experimental Section	79
2.6.	References	81
<b>Chapter 3: Self-Assembly and Photoinduced Electron Transfer Processes in a <math>\beta</math>-Cyclodextrin-Appended Anthracene - Pyromellitic Diimide Dyad System</b>		<b>87-146</b>
3.1.	Abstract	87
3.2.	Introduction	88
3.3.	Results and Discussion	92
3.3.1.	Synthesis and Characterization of <b>ANCD</b> and <b>PMDI</b>	92
3.3.2.	Photophysical Properties and Conformation of <b>ANCD</b>	97
3.3.3.	Properties of Electron Acceptor	106
3.3.4.	Interaction of <b>ANCD</b> with <b>PMDI</b>	107
3.3.5.	Photoinduced Electron Transfer between <b>ANCD</b> and <b>PMDI</b>	116
3.3.6.	Laser Flash Photolysis Studies	123
3.4.	Conclusions	134
3.5.	Experimental Section	135
3.6.	References	140
<b>Chapter 4: Self-Assembly and Photoinduced Electron Transfer Processes in a Donor-Cyclodextrin-Acceptor Type Ternary System</b>		<b>147-195</b>
4.1.	Abstract	147



4.2.	Introduction	148
4.3.	Results and Discussion	151
4.3.1.	Interactions of <b>PMDI</b> Derivatives with $\beta$ -CD and <b>ANCD</b>	151
4.3.2.	Design and Study of Donor- $\beta$ -CD-Acceptor Ternary System	165
4.4.	Conclusions	188
4.5.	Experimental Section	189
4.6.	References	193

<b>List of Publications</b>	<b>196</b>
-----------------------------	------------

## PREFACE

Photoinduced Electron Transfer (PET) plays a central role in photobiological processes such as photosynthesis and has drawn much interest in view of designing photochemical molecular devices and light energy conversion systems. The most important requirement in the design of such systems is the assembly of a donor and an acceptor at fixed distances and proper orientations. The supramolecular approach wherein the donor and acceptor are assembled by non-covalent interactions has attracted considerable interest in the study of PET reactions. Cyclodextrins (CDs) are ideal molecular receptors for building supramolecular functional systems in aqueous solution. CDs are cyclic oligosaccharides with hydrophobic cavities capable of encapsulating suitably sized organic molecules from aqueous solutions. Because of their water solubility, guest-encapsulation properties and ability to mimic natural enzymatic systems, CDs are now increasingly used in the design of supramolecular photoinduced electron transfer (PET) systems. First chapter of this thesis is a review of the literature dealing with the use of CD as an assembler of donor-acceptor systems for PET reactions.

Previous studies have already established that PET from a CD-appended chromophore to encapsulated guest is feasible. However, several important aspects of PET in CD-appended systems remain unaddressed. For example, the magnitude of the electronic coupling between the CD-appended chromophore and the

encapsulated guest, dependence of the electron transfer rate on free energy change and influence of the CD cavity on the reorganization energy of the encapsulated guest, etc are some of the important aspects that need to be addressed. In the second chapter of the thesis an attempt is made in this direction. In this chapter we have studied the PET between  $\alpha$ -cyclodextrin-appended pyrene (**PYCD**) and a few acceptor molecules in aqueous solutions. The pyrene moiety in **PYCD** is placed above the small rim of the CD and is fully exposed to water. The acceptors selected were monocyclic organic molecules and upon dissolution in water in the presence of **PYCD**, a fraction of the donor-acceptor systems are present as supramolecular dyads and the remaining fraction as free molecules. Free energy dependence studies showed that electron transfer in the supramolecular dyads follow the Marcus equation. The donor-acceptor coupling and reorganization energy were determined from fits of the data to the Marcus equation. The electronic coupling was found to be similar to those reported for hydrogen bonded systems. It appears that actual  $\lambda_{\text{out}}$  values in these systems are somewhat lower than values calculated using the continuum model. Our experimental design also has allowed, for the first time, a visual demonstration of the inverted region using the raw fluorescence lifetime data.

Acceptors employed in Chapter 2 have low association constants and hence a significant fraction of PET took place through the diffusion-mediated route. In biological ET systems the diffusion component is absent and an important aim of

our research in this area is to reduce the diffusion-mediated component of ET. To achieve this we require acceptor molecules, which fit the CD cavity rather tightly with high association constants. We observed that pyromellitic diimide (**PMDI**) derivatives associate better with  $\beta$ -CD. Chapter 3 of the thesis deals with the study of self-assembly and PET processes of an anthracene donor appended  $\beta$ -CD and **PMDI** acceptor. Anthracene appended  $\beta$ -CD (termed **ANCD**) was synthesized and characterized by usual spectroscopic techniques. Self-assembly of **ANCD** and **PMDI** was studied by absorption, fluorescence, induced circular dichroism, NMR and cyclic voltammetry. PET processes in the self-assembled **ANCD:PMDI** dyad were studied by fluorescence quenching and laser flash photolysis. At  $[\text{PMDI}] < 10^{-4}$  M, the equilibrium is in favour of the free molecules and under these conditions fluorescence quenching is negligible and diffusion mediated electron transfer involving the triplet-excited state of anthracene predominates. At higher concentrations of **PMDI**, the equilibrium is largely in favour of the supramolecular dyad and intra-ensemble PET processes predominate. The experimentally determined electron transfer rate constants agreed very well with those calculated using the Marcus equation. It was observed that a fraction of the ion pairs survived the fast back electron transfer and persisted for more than 200  $\mu$ s.

During the course of our study we observed that the synthesis and purification protocols of CD-appended systems are very tedious. Hence

developing a methodology to co-encapsulate the donor and acceptor into a CD cavity appeared very attractive. A useful strategy in this context was to search for donor (or acceptor) molecules that can selectively bind to the rim or to the outside of CD cavity. The acceptor (or donor) molecule can then be encapsulated into the CD cavity, leading to the formation of CD-based, non-covalent ternary systems capable of undergoing photoinduced electron or energy transfer reactions. Chapter 4 of the thesis is an attempt in this direction. Our studies with **PMDI** derivatives showed that these molecules complexed with native  $\beta$ -CD in a non-inclusion manner wherein the **PMDI**s lie just outside of the narrow rim of  $\beta$ -CD. In this conformation the  $\beta$ -CD cavity is mostly empty opening up the possibility of co-inclusion of a donor molecule in the cavity. The very high affinity of adamantane moiety for  $\beta$ -CD cavity and the propensity of **PMDI** for rim binding with the primary rim of  $\beta$ -CD cavity were utilized in the design of CD based non-covalent ternary system. Formation of the ternary ensemble was studied using NMR, ICD and MALDI-TOF experiments. In the ternary system described here CD act as a scaffold to keep the donor and acceptor moieties at a fixed distance. Steady state and time resolved fluorescence experiments confirm photoinduced electron transfer in the ternary system. Self-assembly of donor and acceptor components in

aqueous solution and study of PET processes in such systems is an extremely important task in the context of understanding and mimicking natural photosynthetic process.

---

*Note: The numbers of the various compounds given in each chapter correspond to those given under the respective chapters.*

# Chapter 1

---

## Photoinduced Electron Transfer in Cyclodextrin-Appended Donor-Acceptor Systems – An Overview

---

### 1.1. Introduction

Photoinduced Electron Transfer (PET) involves the transfer of an electron from a donor (D) to an acceptor (A), with either D or A placed in one of its excited states, ultimately leading to the formation of a charge-separated (CS) state. PET plays a central role in photo biological processes such as photosynthesis and in various light driven physical and chemical processes. Photosynthesis in green plants involves absorption of light by the antenna molecules, followed by a series of electron transfer reactions between donors and acceptors that are placed at specific distances and orientations relative to one another by the surrounding protein matrix, ultimately leading to storage of the absorbed photon energy in the form of charge separation. The energy stored in the charge-separated state is utilized for the reduction of  $\text{CO}_2$  to glucose and in this process water is oxidized to molecular oxygen. A fundamental understanding of the processes taking place in natural photosynthesis is required for the development of efficient systems for the conversion and storage of solar energy.

---

The photosynthetic apparatus in both bacteria and plants consists of two distinct units called antennae and the reaction centre. Antennae are the light gathering complexes consisting of chlorophyllous pigments as well as carotenoids arranged in the protein matrix. These pigment-protein complexes absorb light and efficiently transfer the excitation to the reaction centre. The reaction centre consists mainly of organic donor and acceptor molecules embedded within a protein matrix. The photosynthetic reaction centre of purple bacteria *Rhodospseudomonas viridis* comprises of four bacteriochlorophylls (**BCl**), two bacteriopheophytins (**BPh**), two quinones, namely ubiquinone and menaquinone, and a non-heme iron atom.<sup>1</sup> The spatial arrangement of these components within the reaction centre is shown in Figure 1.1. It may be noted that with the exception of the iron atom, the constituents occur in pairs and the reaction centre has approximate  $C_2$  symmetry. Of the four **BCl** molecules, two are positioned very close. Hence they are strongly coupled electronically and are termed “special pair” of **BCls**.

The photosynthetic process within the reaction centre begins with the excitation of special pair **BCls** by excitation transfer from the antennae units. The singlet excited state of the special pair transfers an electron to the bacteriopheophytin (**BPh L**) on the L side of the branch within 3 ps leading to the formation of special pair radical cation and **BPh** radical anion.<sup>2</sup> It is believed that **BCl L** plays a role in this electron transfer reaction. The M branch of the reaction



centre is almost inactive in the electron-transfer process. The **BPh** radical anion decays in 200 ps moving the electron to the menaquinone from where it is further transported to the ubiquinone in about 100  $\mu$ s. The positive charge remaining on the special pair is quenched by electron transfer from an iron porphyrin on the outer side of the membrane. The net result of this multistep electron transfer is the generation of a trans-membrane CS state with a quantum yield of near unity. Since the positive and negative charges are separated by the thickness of the lipid bilayer, back electron transfer, which leads to the wastage of stored energy, is precluded.

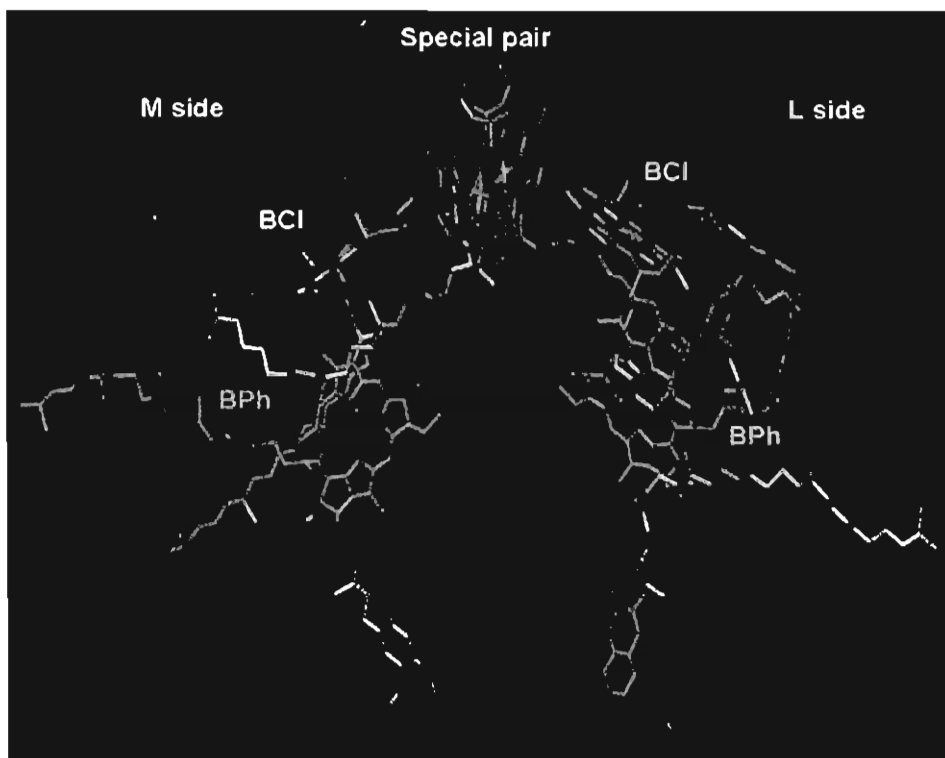


Figure 1.1. Arrangement of the chromophores, electron donors and electron acceptors in the bacterial reaction centre of *Rhodospseudomonas viridis*.

Considerable effort has been devoted to mimicking the natural photosynthetic process in the laboratory and this area of electron transfer chemistry is known as artificial photosynthesis. Extremely high quantum yield of the PET processes in the natural systems is attributed to the high degree of organization of the donors and acceptors in the reaction centre. It was believed that some degree of organization could be achieved by covalently linking the donor and acceptor. Following this approach a large number of covalently linked dyads, triads, tetrads etc. were synthesized and studied as model systems for artificial photosynthesis and these studies have contributed a great deal to our understanding of the fundamental processes taking place in photosynthesis.<sup>3</sup> Few examples of covalently linked D-A systems are given in Figure 1.2 A-B.

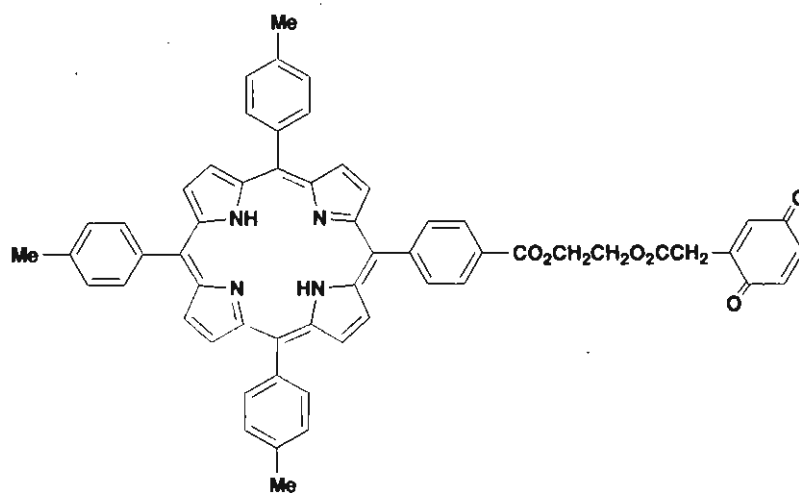


Figure 1.2 A. Structure of a Donor-Acceptor Dyad.

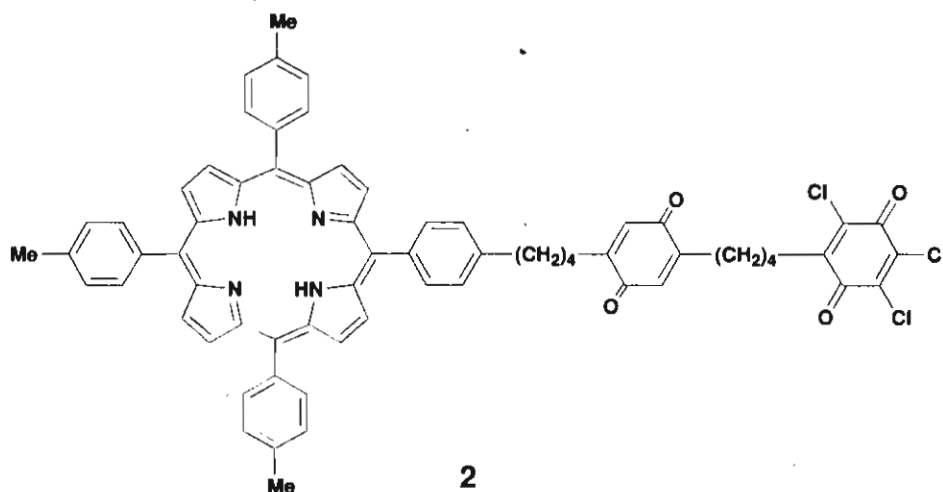


Figure 1.2 B. Structure of a Donor-Acceptor-Acceptor Triad.

In these systems donors and acceptors are covalently assembled to build linear arrays of the type **D-A**, **D<sub>2</sub>-D<sub>1</sub>-A**, **D-A<sub>1</sub>-A<sub>2</sub>**, **D<sub>2</sub>-D<sub>1</sub>-A<sub>1</sub>-A<sub>2</sub>**, **D-A<sub>1</sub>-A<sub>2</sub>-A<sub>3</sub>** etc. Following light absorption, sequential electron transfer occurs whereby the electron moves in one direction and the holes move in the opposite direction. This leads to increased quantum yield and lifetime for the CS state. Triads and tetrads with microsecond lifetimes for the CS state have been designed in this way.

In the covalent approach, the donor and acceptor moieties are linked by chemical bonds. In the natural photosynthetic reaction centre, the constituents are held together by non-covalent interactions, which also help in the mediation of electron and energy transfer processes. Awareness of these interactions has led to a surge of interest in the use of non-covalent binding interactions termed - *supramolecular interactions* - to assemble chromophore-quencher systems.<sup>4</sup> The

complexity involved in covalent synthesis also encouraged the non-covalent approach.

Non-covalent or supramolecular assembling of components relies on the principles of molecular recognition. Non-covalent interactions of interest in this context are coordinate bonds, hydrogen bonds, van der Waals interactions, aromatic  $\pi$ -stacking, ionic interactions etc. A large number of donors and acceptors were assembled using these interactions and PET processes taking place in them were studied in the past decade. Selected examples are given in Figure 1.3 A-B. Dependence of PET rates on factors such as free energy, distance and temperature in hydrogen-bonded D-A systems were studied in detail in our own laboratory.<sup>5</sup>

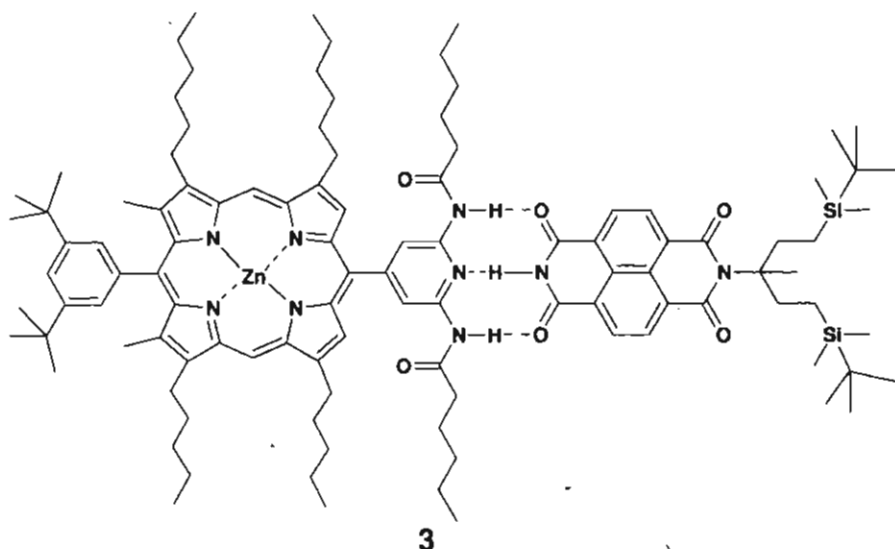


**Figure 1.3 A.** Example of a Hydrogen-bonded D-A system.

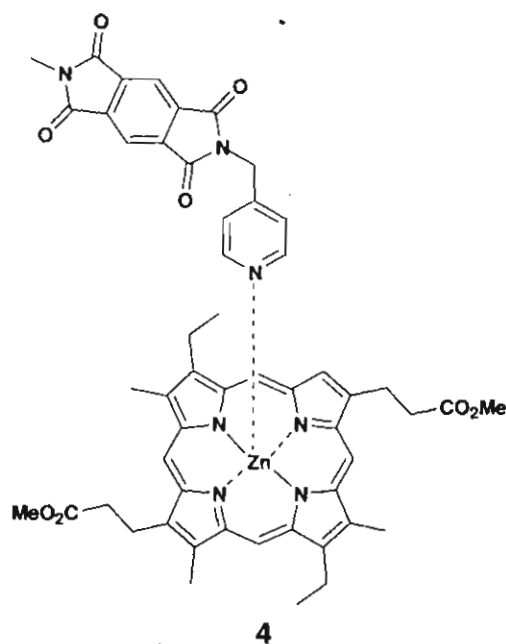


**Figure 1.3 B.** Example of a D-A system assembled through coordinate bond.

A major drawback of this approach is that non-covalent interactions mentioned above fail to perform in aqueous environments. Biological electron transfer processes occur in aqueous environments and mimicry of natural systems requires self-assembly in water. Encapsulation in cyclodextrin cavity is one of the most important methods available for self-assembly in water. In the present thesis, several important aspects of photoinduced electron transfer reactions in cyclodextrin based D-A systems are reported. In order to put our work in proper perspective, a review of the literature that makes use of CD as an assembler of D-A systems is attempted here. Origin of the present work and outline of the thesis is then briefly discussed.

Cyclodextrins (CDs) are a family of cyclic, water-soluble oligosaccharides made up of  $\alpha$ -(+)-glucopyranose units, which adopt a  ${}^4C_1$  chair conformation.<sup>6</sup> They are shaped like truncated cones. The most common CDs consist of 6, 7 or 8 glucose units and these are named  $\alpha$ -,  $\beta$ - and  $\gamma$ -CD, respectively. A schematic representation of the CDs, along with approximate sizes of the inner and outer cavities, are shown in Figure 1.4. Because of their bucket like shape, they exhibit a narrower and larger cavity entrance or rims. The former bearing the primary hydroxyl groups is referred to as the primary rim and the latter bearing the secondary hydroxyl groups is referred to as the secondary rim. The cavity interior is lined with the H-3 and H-5 hydrogens and the O-4 oxygen atoms, thus conferring a hydrophobic character to the cavity.

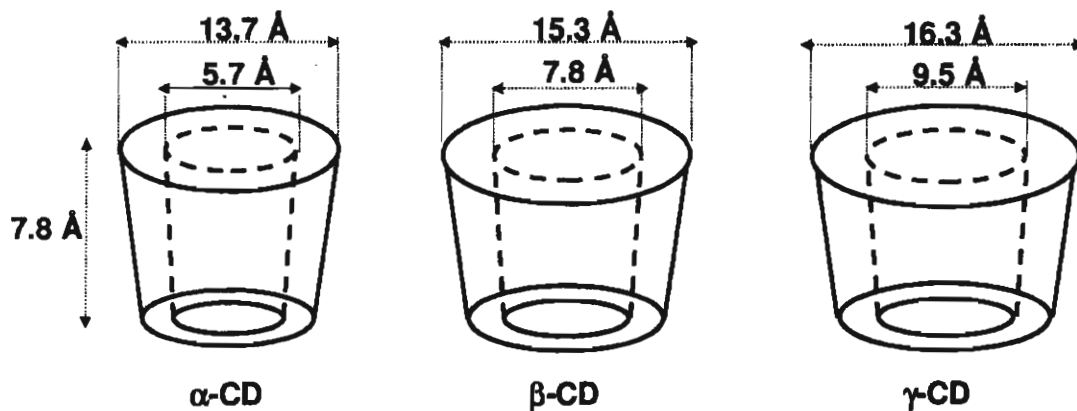


Figure 1.4

The hydrophobic cavity enables CDs to form inclusion complexes with suitably sized organic molecules. Several factors contribute towards the driving

---

force for encapsulation. In an aqueous solution, the slightly apolar cyclodextrin cavity is occupied by water molecules which are energetically unfavored (polar-apolar interaction), and therefore can be readily replaced by appropriate “guest molecules” which are less polar than water. Substitution of high enthalpy water molecules by an appropriate guest contributes significantly towards the driving force for encapsulation. Other contributing factors are the van der Waals interactions and possible hydrogen bonding interactions between the CD and the guest. Geometrical factors also play an important role. The  $\alpha$ -,  $\beta$ - and  $\gamma$ -CDs with different internal diameters are able to accommodate molecules of different sizes. Larger molecules also complex with CDs, but in these cases only small segments of the molecules are encapsulated into the cavity.

CDs are optically transparent in the UV and visible region of the spectrum where organic and inorganic molecules absorb. They are water-soluble, non-toxic and environmentally friendly. Some of the CDs, particularly  $\beta$ -CD are manufactured in large amounts because they find applications in a variety of areas such as cosmetics, drug formulation, food technology, toiletry, pesticides, phase transfer catalysts etc. CDs can be modified by introduction of suitable groups on to the rims through reaction at the hydroxyl groups. Substitution reactions can occur at the primary or secondary rims. On a given rim, substitution can occur at one or more hydroxyl groups, or a given organic fragment can link two hydroxyl groups

like a bridge. The hydrophobic area available in modified CDs is different from native CDs and these derivatives also find several applications.<sup>7</sup>

The most important attribute of CDs is their ability to form complexes with other molecules and almost all applications of CDs, either in research or in industry, are related to complex formation. In the CD complexes, the guest molecules are either completely or partially encapsulated in to the CD cavity and hence CD complexes are known as inclusion complexes. Most commonly CDs form 1:1 complexes with guests, but 1:2, 2:1 etc. type complexes are also known. Consider the formation of a complex between a guest (G) and CD.



where,  $G \supset CD$  represents the inclusion complex and  $K_a$  is the equilibrium association constant for complex formation. Several experimental techniques are available for the study of CD complexation and determination of  $K_a$  values. For example, the  $^1\text{H}$  NMR chemical shifts ( $\delta$ ) of the guest molecule quite often exhibit changes upon complexation with CD. A quantitative study of the dependence of  $\Delta\delta$  on CD concentration can yield  $K_a$  values. Likewise, changes in the absorption spectra, fluorescence spectra or fluorescence lifetimes could be used to study the complexation process. In this context, circular dichroism spectra proved to be a valuable tool. Achiral molecules do not exhibit circular dichroism spectra, but upon complexation with CD they exhibit induced circular dichroism



---

(ICD). The sign and intensity of ICD bands can give valuable information regarding the complexation. In this thesis all the above methods are used to study complexation of guests with CDs.

The advantages of easy availability, potential utilizations and good economic reasons play a very important role in the growing interest in CDs for industrial applications. CDs can be used in drug formulations either as complexing agents or as auxiliary additives (such as carriers, diluents, solubilizers etc). The main use of CDs in both food technology and cosmetics is for the molecular encapsulation of flavours and fragrances. Pesticides can be complexed with CDs and this encapsulation may result in interesting effects, which lead to the formulation of poorly soluble or volatile and unstable pesticides. CDs find various applications in research also. Several chemical reactions, both in solution and solid state, are accelerated or inhibited by CDs. CDs are used as chiral NMR shift reagents. CDs and their soluble or insoluble polymers are used as mobile phases in chromatographic applications. CD-based systems find applications as catalysts, sensors, molecular machines, enzyme-mimics, and molecular wires.<sup>8</sup> Of particular interest is the role of CDs as an assembler of D-A systems for energy and electron transfer reactions. A detailed account of this aspect is presented below.

## 1.2. Photoinduced Electron and Energy Transfer in CD-based Donor-Acceptor systems

CDs have been used in the past as constrained media to carry out photochemical reactions both in solution and in the solid state.<sup>9</sup> In this thesis CD is used as an assembler of donor and acceptor systems for PET reactions. A large body of experimental data is available in this area and the remaining part of this chapter is a survey of the literature in this area. A general strategy employed in all these studies is to link one of the components to the primary or secondary rim of the CD and then assemble the second component through encapsulation in the cavity. Several variations of this theme are available and in the following section a few of them are presented.

Kuroda and co-workers were among the first to design donor-acceptor systems based on CDs. The system they designed consisted of a porphyrin (**P**) sandwiched between the primary rims of two  $\beta$ -CD units through covalent bonds as shown in Figure 1.5. The porphyrin performed the roles of sensitizer and donor and quinones (**Q**) encapsulated into the open cavity of CD acted as acceptor in this study. The authors employed benzoquinone (**BQ**), naphthoquinone (**NQ**) and anthraquinone-2-sulfonate (**AQ**) as acceptors.<sup>10</sup> Fluorescence from the porphyrin unit in **5** was quenched upon the addition of **NQ** and **AQ** and this is attributed to electron transfer from  $^1\text{P}^*$  to **Q**. The authors observed that quenching by **BQ** was very inefficient and this was attributed to weak binding of **BQ** to the cavity.

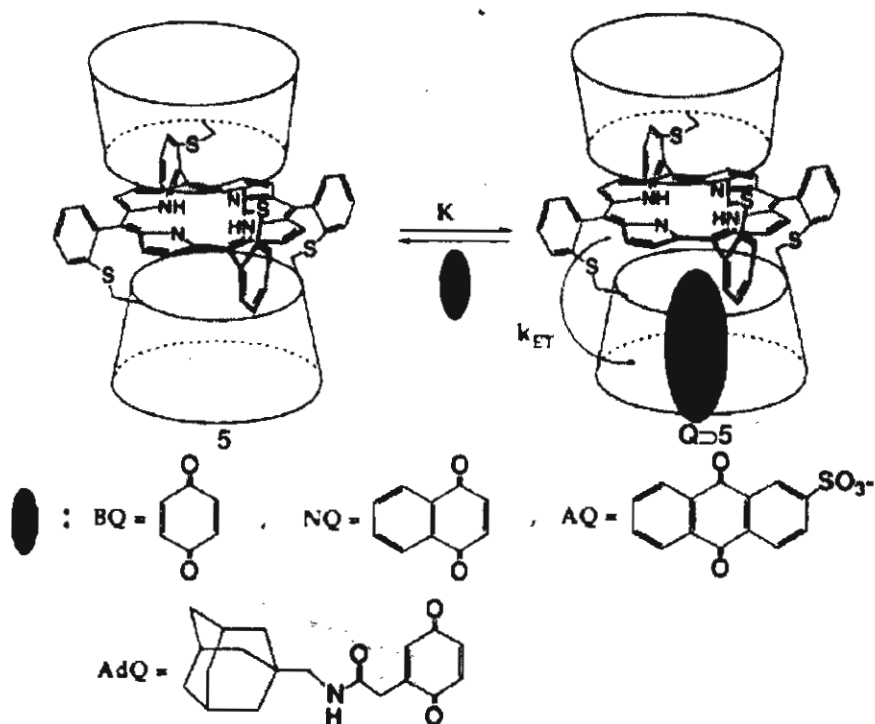


Figure 1.5

Hamachi and coworkers have studied photoinduced electron transfer in the protein-based and non-covalently linked donor-sensitizer-acceptor triad.<sup>11</sup> Incorporation of synthetic dyad or triad systems consisting of cyclodextrins into a protein matrix could be an alternative approach for construction of an excellent photochemical system. This semisynthetic approach was used in the reconstitution of apo-hemoproteins like apomyoglobin with chemically modified protoporphyrin derivatives. Protoporphyrins was attached to CDs and reconstitution of these with Myoglobin yielded **6** as shown in Figure 1.6.

The triad consisted of  $\beta$ -CD-appended Zn-myoglobin **6** (**Zn-Mb-CD**), an adamantane-modified  $\text{Ru}(\text{bpy})_3$  (**Ad-Rubp**), and a bis(viologen)cyclophane (**BXV<sup>4+</sup>**) **7** as shown in Figure 1.6. Photoexcitation of the  $\text{Ru}(\text{bpy})_3$  at 460 nm leads to initial electron transfer from  $\text{Ru}(\text{bpy})_3$  to the cyclic viologen, followed by a second electron transfer from Zn porphyrin to  $\text{Ru}(\text{bpy})_3$  to yield the final charge separated state. Estimated quantum yield of CS state was 0.03 and its lifetime was 640 ns.

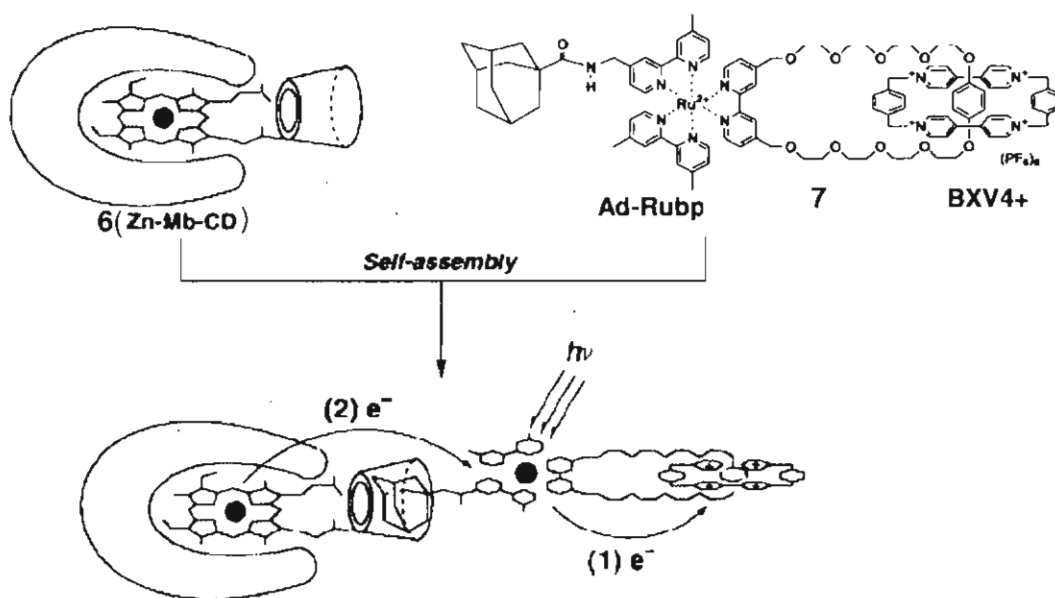


Figure1.6

Tung and coworkers have studied photoinduced electron transfer between *p*-nitrobenzoyl- $\beta$ -cyclodextrin **8** (**NBCD**), which acts as the acceptor, and various naphthalene derivatives (**NP**) as donors (Figure 1.7).<sup>12</sup> Significant fluorescence quenching was observed for the naphthalene derivatives when **NBCD** was added

to it and this was attributed to the occurrence of electron transfer. Decay of  $^1\text{NP}^*$  in water was monoexponential in the absence of **NBCD**. The decay became biexponential when **NBCD** was added. Biexponential decays arise due to the two types of electron transfers shown by arrows in Figure 1.7.

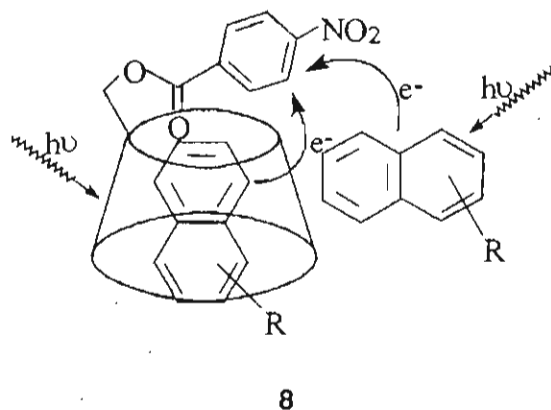


Figure 1.7

In another example, Liu, Guo and coworkers studied the PET reaction between **NBCD** and porphyrin-linked adamantane **9** (**ZnPC<sub>n</sub>A**).<sup>13</sup> Since the adamantane unit has high affinity for  $\beta$ -CD, simple mixing of the two moieties lead to self-assembly of the D-A system as shown in Figure 1.8. By the use of redox potentials and excitation energy,  $\Delta G_{\text{ET}}$  values for all the porphyrin compounds were calculated.  $\Delta G_{\text{ET}}$  values were found to be negative indicating that electron transfer may take place between **ZnPC<sub>n</sub>A** and **NBCD**. Detailed steady state and time resolved fluorescence studies revealed two pathways for electron transfer, static and dynamic. The static component arises due to electron transfer in

the self-assembled system. The rate of PET determined for the complex was  $1 \times 10^9 \text{ s}^{-1}$  and this value was found to be very close to that of a covalently linked porphyrin-nitrobenzene dyad.

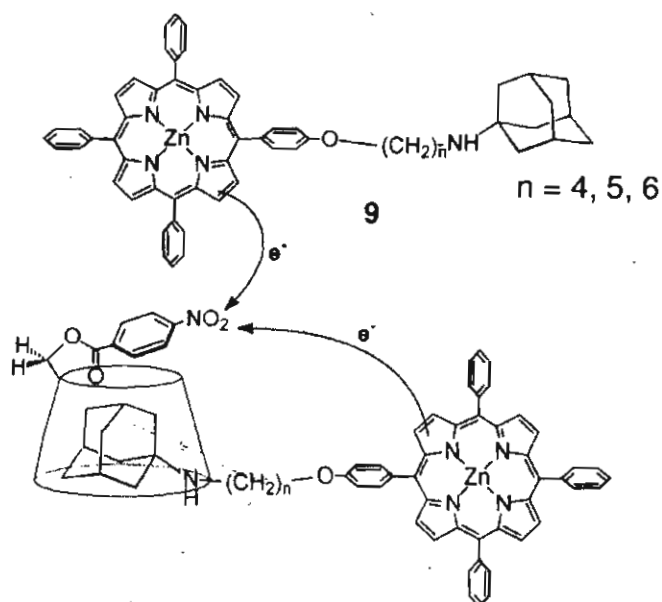
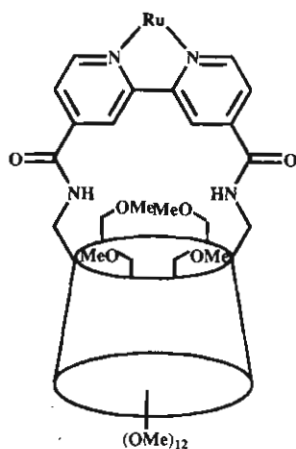


Figure 1.8

The introduction of photoactive metal centres on to cyclodextrin receptors opens up new possibilities for the design of various energy and electron transfer systems. These are known as metallocyclodextrins. Capping of  $\alpha$ -CD with photoactive Ruthenium(II) centre was carried out for the first time by the use of difunctionalized 2,2'-bipyridyl ligand (Figure 1.9).<sup>14</sup> Luminescence from the metal complex **10** was quenched upon addition of 1,4-benzoquinone (**BQ**). Stern-Völmer plot showed positive deviation from linearity, which indicated that both static and dynamic quenchings are taking place in the system. Quenching was

attributed to electron transfer from the triplet excited metal complex to **BQ**, although the radical ion products could not be detected by transient absorption spectroscopy.



10

Figure 1.9

Pikramenou and coworkers synthesized terpyridine functionalized cyclodextrins and their ruthenium complexes (**11**) and investigated the electron transfer quenching of these systems with several quinones (Figure 1.10).<sup>15</sup> The ruthenium emission intensity at 640 nm was quenched upon addition of quinone. The luminescence quenching was attributed to an intercomponent electron transfer from the appended ruthenium centre to the quinone guest. Control experiments using  $[\text{Ru}(\text{tp})_2][\text{PF}_6]$  and quinones under the same conditions showed no effect on the ruthenium luminescence. The same authors have successfully demonstrated

PET from the Ru terpyridyl to self-assembled Os terpyridyl as shown in Figure 1.10.

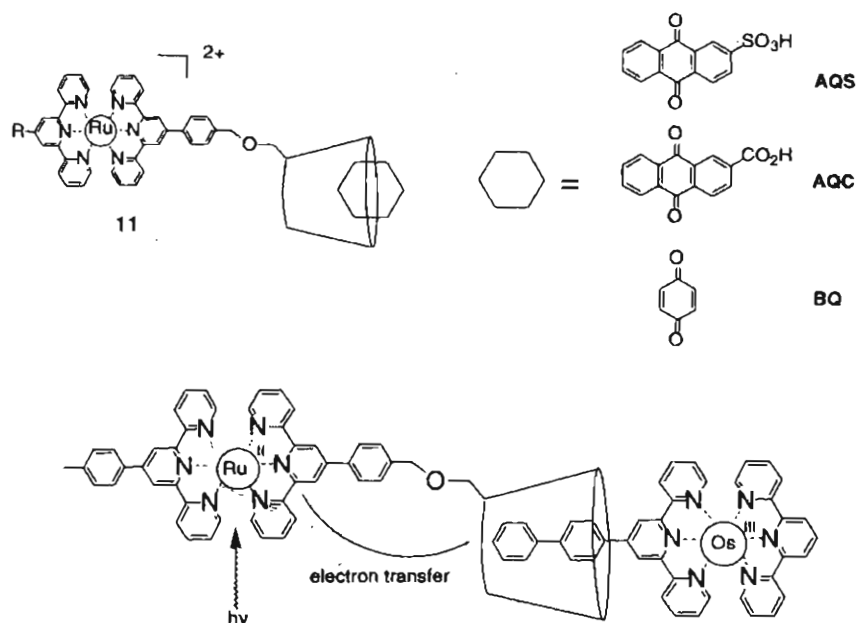


Figure 1.10

Keyes and coworkers have synthesized Ruthenium and Rhenium substituted  $\beta$ -Cyclodextrin systems where a fullerene moiety is noncovalently included between two metallocyclodextrins as shown in Figure 1.11.<sup>16</sup> Fullerene is not fully included in to the cavity and the system is stabilized by intermolecular H-bonding between adjacent  $\beta$ -Cyclodextrins and water. Photophysical and electrochemical properties of model complexes in the absence of  $C_{60}$  were examined and compared with the  $C_{60}$  bridged dimer centres. Inclusion of fullerene centres induced significant changes in the photophysical properties of the CD



appended chromophores. The lifetime and quantum yield of the emission of the complexes were significantly reduced upon the inclusion of  $C_{60}$  to these complexes. On the basis of thermodynamic considerations, this reduction in lifetime was attributed to either energy or electron transfer as shown in Figure 1.11.

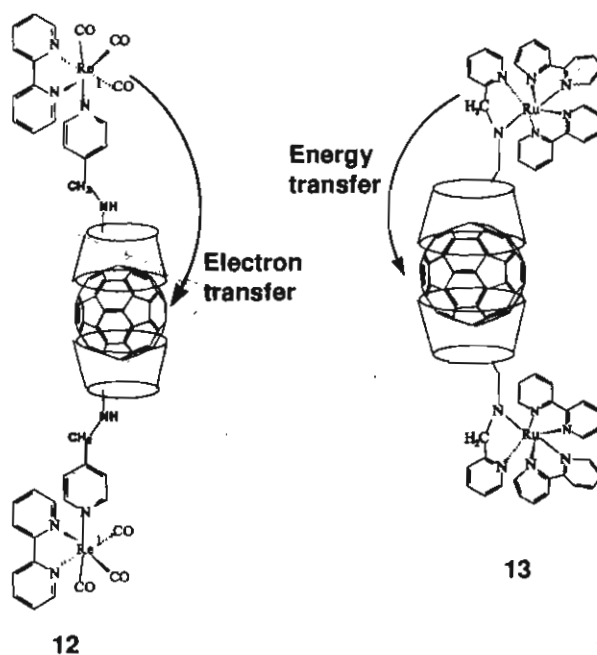


Figure 1.11

In the case of Ru- $C_{60}$  complex, the quantum yield was reduced by nearly an order of magnitude upon fullerene inclusion, with a concomitant decrease in lifetime of approximately 80%. In addition, a weak shoulder on the emission centered around 710 nm appears. This emission was assigned to  $C_{60}$  fluorescence arising as a result of energy transfer from Ru complex. The Re analogue also

exhibits comparable reduction in quantum yield and lifetime, but no new emission were observed at longer wavelengths indicating that no energy transfer was involved in this system. The quenching in this case was attributed to electron transfer. The rate constants were determined from the luminescence lifetimes and the values obtained were  $1.3 \times 10^8 \text{ s}^{-1}$  and  $7 \times 10^7 \text{ s}^{-1}$  for the Ru and Re complexes, respectively. These large rate constants indicated efficient communication between excited metal centres and encapsulated fullerene across the cyclodextrin bridge.

Increasing the number of guest interaction sites in cyclodextrin recognition systems was another interesting area of study. Pikramenou and coworkers described an assembly of CDs using coordination principles to yield complexes with multiple cyclodextrin recognition sites around a central metal core. Octahedral metal centres and nine-coordinate lanthanide ions were used to spatially organize CDs functionalized with bidentate bipyridine units **14** ( $\beta$ -CD-mbpy) and tridentate tolyl terpyridine units **16** ( $\beta$ -CD-ttp). Addition of Fe(II) to a methanolic solution of **14** results in a deep red color due to the formation of the  $[\text{Fe}(\beta\text{-CD-mbpy})_3]^{2+}$  complex **15** (Figure 1.12).<sup>17</sup> Likewise the Fe(II) complex **17** and Eu(III) complex **18** were prepared as shown in Figure 1.13. **18** exhibited strong red luminescence due to Eu ion upon excitation at the ligand band. The ttp units acted as light harvesting centres for collecting energy and transferring it to the lanthanide centre. The metalloreceptors described here can take part in

photoactive processes occurring in more than one direction in space through the metal core and the guests.

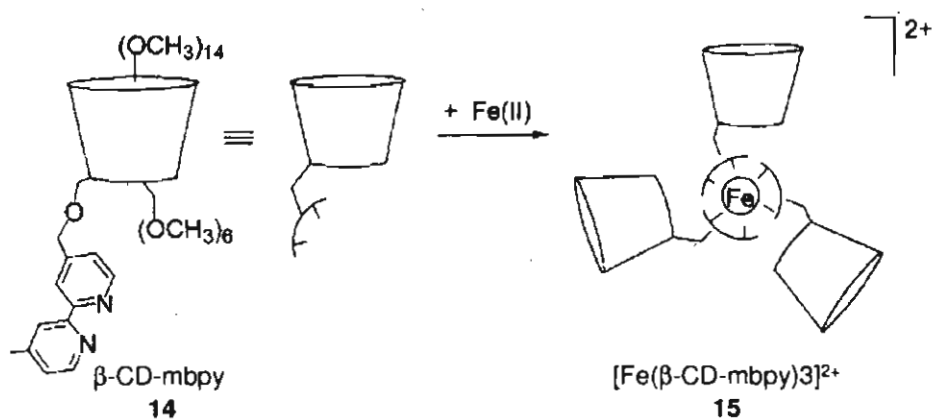


Figure 1.12

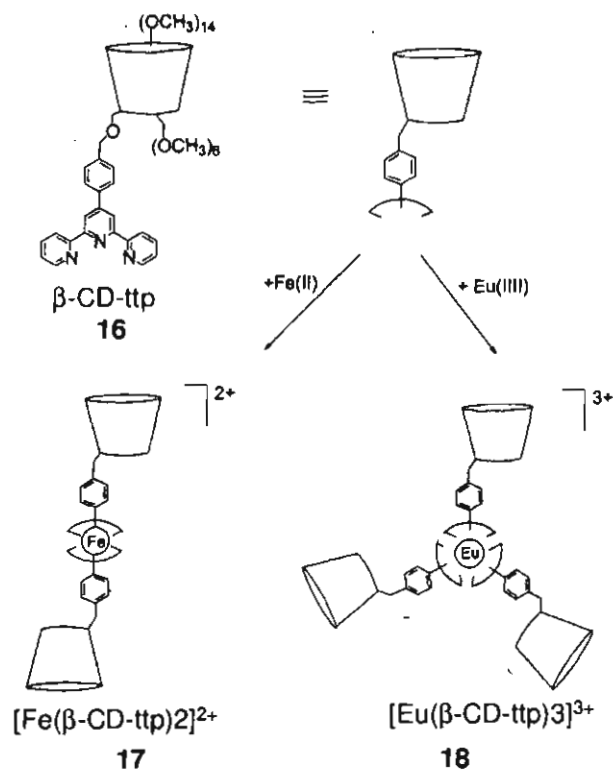
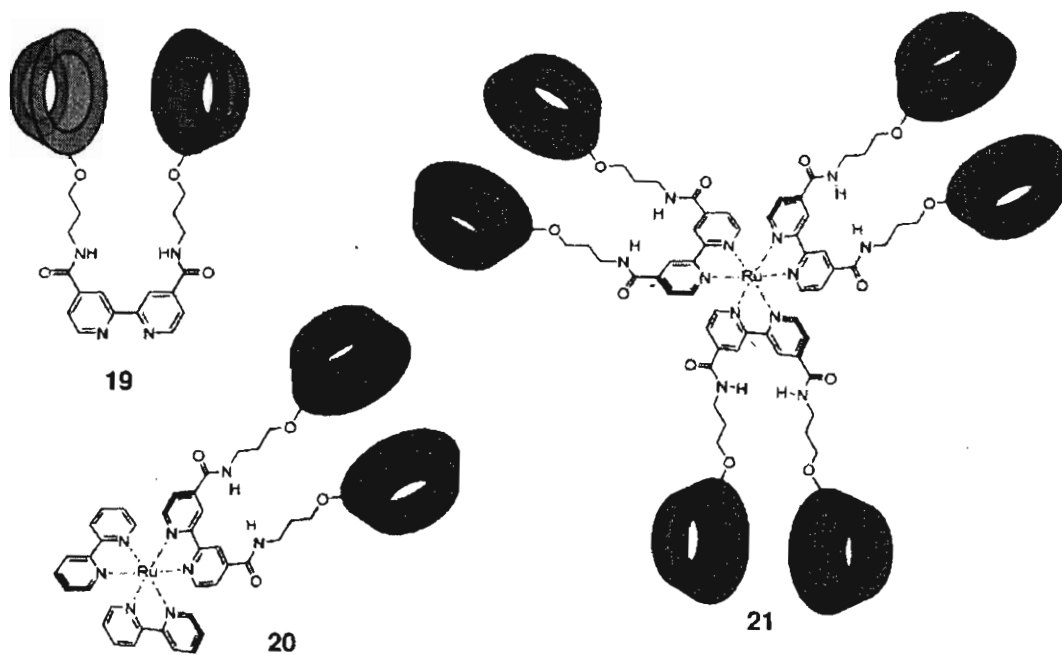


Figure 1.13

Another example which demonstrated the importance of multiple recognition sites was furnished by De Cola and coworkers. They synthesized ligand **19** and using this prepared  $\text{Ru}(\text{bpy})_3^{2+}$  complexes **20** and **21**, bearing two and six  $\beta$ -CD units, respectively on their ligands as shown in Figure 1.14.<sup>18</sup> In these systems the ruthenium complexes acted as electron donors while the cyclodextrins functioned as binding sites for viologen acceptors as shown in Figure 1.14. Every viologen is bound by two CDs in a cooperative mode leading to higher binding constants. Hence PET could be observed even at very low concentrations of viologen guests. Long alkyl chains were needed for efficient binding between the two cyclodextrins. For viologens with only one alkyl tail the quenching was inefficient.



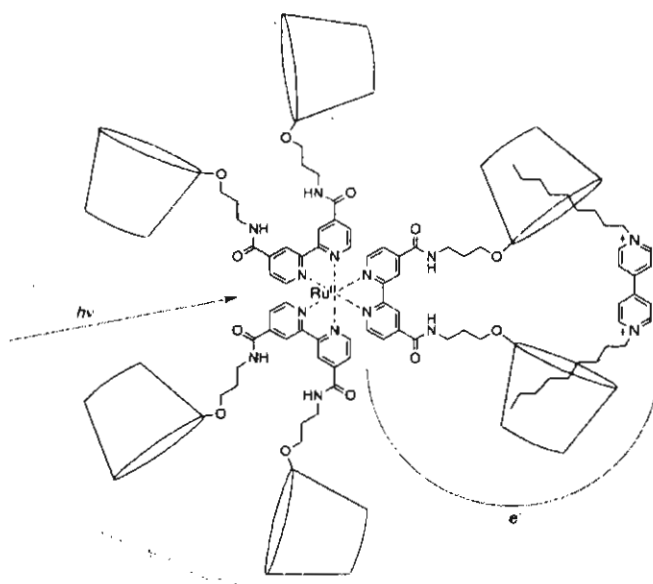


Figure 1.14

Harada and coworkers constructed a supramolecular system with the components shown in Figure 1.15.<sup>19</sup> Electron acceptors **22** and **23**, having viologen moieties attached to a  $\beta$ -CD through cinnamic and hydrocinnamic groups, respectively, were synthesized. Earlier studies indicated that CDs with flexible hydrocinnamic groups could form intra- and intermolecular inclusion complexes while rigid cinnamic group inhibits formation of intramolecular complexes. Both **22** and **23** form stable 1:1 complexes with 5,10,15,20-tetrakis(4-carboxyphenyl)-21*H*,23*H*-porphyrin **24** (TCPP) although binding constant for **22** ( $8.7 \times 10^5 \text{ M}^{-1}$ ) with TCPP is greater than that for **23** ( $2.5 \times 10^4 \text{ M}^{-1}$ ). Enhancement of binding constant of **22** is due to the rigid double bond, which prevents self-inclusion. The extraordinary stability of the 1:1 complexes of **22** and

**23** with  $\beta$ -CD is attributed to the cooperative effect of electrostatic attraction and charge transfer interactions. The binding constant of **TCPP** with  $\beta$ -CD alone was only  $7.4 \times 10^3 \text{ M}^{-1}$ . Steady state and time resolved studies indicated that efficient PET occurs from the **TCPP** to the acceptors **22** and **23**.

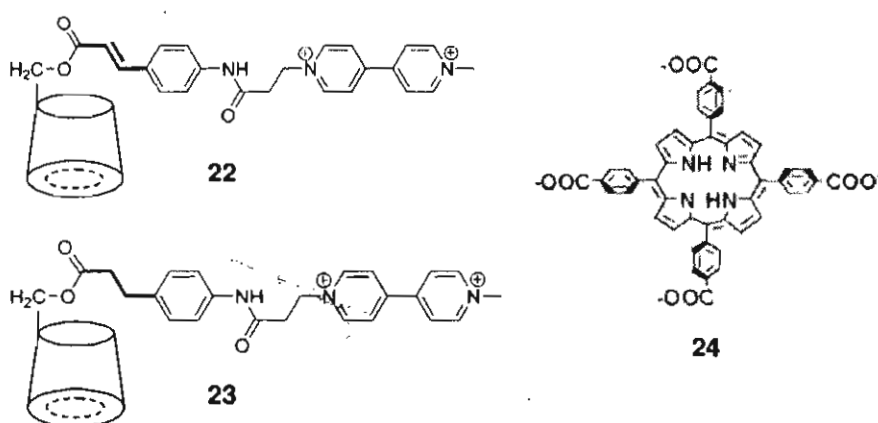


Figure 1.15

Pikramenou and coworkers have developed a light harvesting system using the encapsulation technique.<sup>20</sup> The  $\text{Ru}(\text{bpy})_3^{2+}$  system **25** shown in Figure 1.16 has two bpy groups with  $\alpha$ -CD attached to them and one bpy group with a  $\beta$ -CD. Since adamantane exhibits high selectivity for  $\beta$ -CD and alkyl chains prefer  $\alpha$ -CD, mixing **25** with the adamantane substituted Os complex **26** and alkyl chain attached anthracene **27** in 1:1:2 ratio led to the self-assembled system **28** shown in Figure 1.16. There are two anthracene chromophores in **28**, which when excited funnels their excitation out to the Ru centre, which in turn transfers it to the Os centre. The authors have used ultrafast techniques to probe the energy transfer

process. Each of the excited states were monitored and the energy hopping mechanisms in the assembly were studied carefully. The rate of energy transfer process was  $1.8 \times 10^{10} \text{ s}^{-1}$  in step *a* and  $9 \times 10^8 \text{ s}^{-1}$  in step *b*. This type of strategy allows the construction of unidirectional wires of nanoscale dimensions.

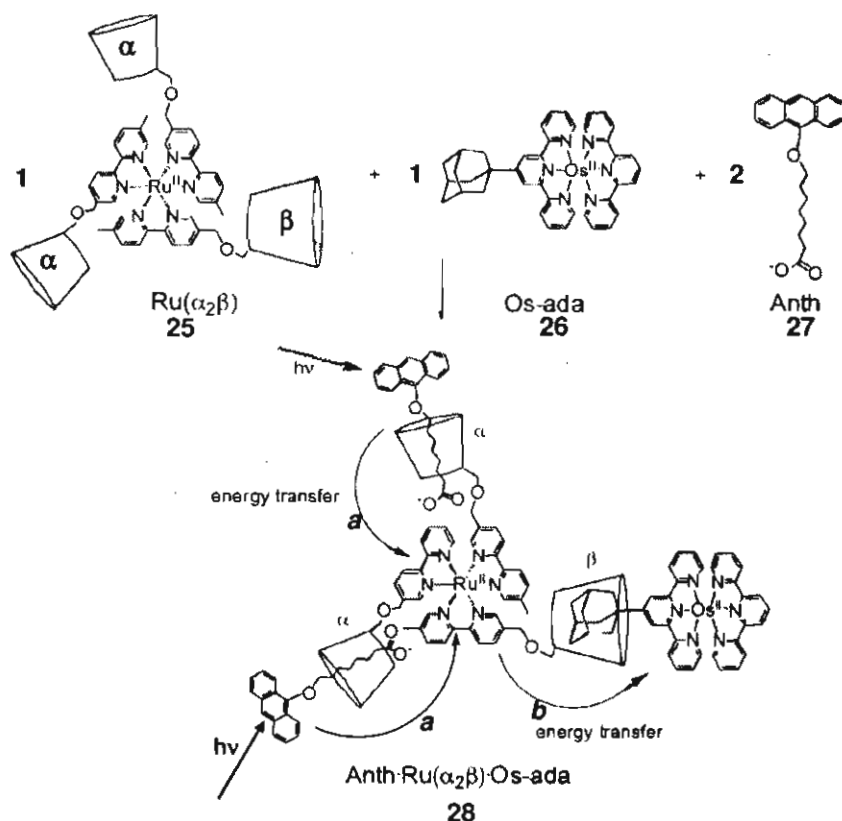


Figure 1.16

De Cola, Pikramenou and coworkers have presented a Ruthenium tris(bipyridyl) cyclodextrin “wheel”  $[\text{Ru}(\beta\text{-CD-mbpy})_3]^{2+}$  (29) that could act as energy donor or acceptor.<sup>21</sup> Metal-complexes based on Osmium(II) and Iridium(III) terpyridine species with biphenyl or adamantyl tails were employed as

guest molecules (30-31) (Figure 1.17). When Os(II) based guests with biphenyl linkers were employed, excitation of ruthenium moiety leads to energy transfer from Ru to the Os(II) unit at a rate of  $8.3 \times 10^{10} \text{ s}^{-1}$ .

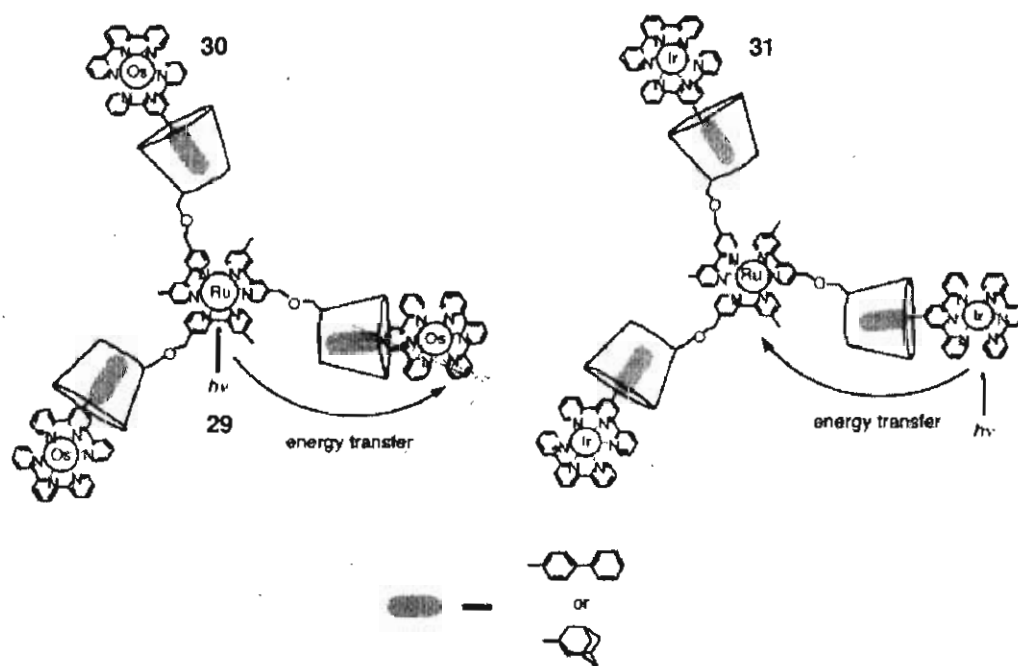


Figure 1.17

In the case of Iridium complex, with biphenyl linker, excitation of Ru centre did not lead to energy or electron transfer. Excitation of the Ir complex, however, led to energy transfer from Ir to Ru centre at a rate of  $3.3 \times 10^8 \text{ s}^{-1}$ . In both cases, changing the tail from biphenyl to adamantane lead to a decrease in the rates. This is attributed to the electronic interaction between CD and biphenyl or CD and



---

adamantyl groups. Aliphatic spacers are known to reduce the energy transfer rates much more than conjugated spacers in covalently linked systems.

### 1.3. Origin of the Present Work

In the preceding section we have presented a survey of the experiments, which utilized the principle of encapsulation to assemble D-A systems capable of undergoing photoinduced energy or electron transfer. Extension of the principle to more and more complex situations resulted in the development of complex systems such as shown in Figure 1.16. Strictly speaking, all these systems have focused more on the self-assembly than on the energy or electron transfer process. Our primary interest is in the PET process and an examination of the literature in this perspective brings forth the following deficiencies.

Although the previous studies have established that electron transfer from a CD-appended chromophore to an encapsulated guest is feasible, several important aspects of electron transfer in these systems remain unaddressed. For example, one can ask the following questions: (1) Does the electron transfer process in these systems conform to any established electron transfer theory? What happens after PET? Does it result in long-lived charge separation? Most importantly, one can ask if we can use CDs to enhance the yield and lifetime of charge separated states. To answer these and similar other questions, systematic studies of the encapsulation processes and also of the rates of the PET reactions in these systems are required. The present thesis is an attempt in this direction.

---

PET in weakly interacting D-A systems is most generally explained using the Marcus theory. The second chapter of the thesis is an attempt to see if the PET process in CD-based systems conforms to the Marcus theory. According to Marcus theory the plot of reaction rate ( $k_{et}$ ) vs free energy change ( $\Delta G^0$ ) is bell-shaped with a normal and inverted region. Thus, a straightforward procedure to establish the conformity to Marcus theory is to study the  $\Delta G^0$  dependence of  $k_{et}$  in these systems. For this purpose we have prepared a pyrene attached  $\alpha$ -CD and employed it as sensitizer and donor. A series of benzene derivatives capable of encapsulation in the  $\alpha$ -CD cavity are used as acceptors. Using these systems, a  $\Delta G^0$  range of 0 to -1.5 eV could be achieved. Results of the  $k_{et}$  vs  $\Delta G^0$  study are presented in Chapter 2 of the thesis.

A very important objective of PET studies is to achieve high yield and long lifetime for the CS state. In order to study the charge separation process we have selected an anthracene appended  $\beta$ -CD as donor. The selection was made because anthracene can be easily excited using 355 nm laser light and the anthracene radical cation generated is easily observable. Our investigations showed that pyromellitic diimide has very high affinity for  $\beta$ -CD and is a suitable acceptor in PET reactions. The third chapter of the thesis is an in-depth study of self-assembly and PET processes in the anthracene-appended  $\beta$ -CD-pyromellitic diimide system.

In almost all the PET systems based on CD, one component is attached to CD by a covalent bond and the other component is assembled through the encapsulation ability of the CD. The synthesis and purification of chromophore appended CD is a challenge in itself. In this context development of alternate strategies for assembling supramolecular D-A systems that does not involve synthesis and purification of CD-appended systems gain considerable importance. The fourth chapter of the thesis is an attempt in that direction. We have observed that an adamantane attached pyrene donor and a pyromellitic diimide with a pyridinium ion end group could be self assembled into a native  $\beta$ -CD to give a ternary system which is capable of undergoing PET reaction. Details of this study are presented in Chapter 4 of the thesis.

#### 1.4. References

1. (a) Reimers, J. R.; Hutter, M. C.; Hughes, J. M.; Hush, N. S. *Int. J. Quant. Chem.* **2000**, *80*, 1224-1243. (b) Hutter, M. C.; Hughes, J. M.; Reimers, J. R.; Hush, N. S. *J. Phys. Chem. B* **1999**, *103*, 4906-4915.
2. (a) Breton, J.; Martin, J.-L.; Migus, A.; Antonetti, A.; Orszag, A. *Proc. Natl. Acad. Sci. USA* **1986**, *83*, 5121-5125. (b) Wasielewski, M. R.; Tiede, D. M. *FEBS Lett.* **1986**, *204*, 368-372. (c) Woodbury, N. W.; Becker, M.; Middendorf, D.; Parson, W. W. *Biochemistry* **1985**, *24*, 7516-7521. (d) Martin, J.-L.; Breton, J.; Hoff, A. J.; Migus, A.; Antonetti, A. *Proc. Natl. Acad. Sci. USA* **1986**, *83*, 957-961.

- 
3. (a) Gust, D.; Moore, T. A.; Moore, A. L. *Acc. Chem. Res.* **2001**, *34*, 40-48. (b) Guldi, D. M.; Prato, M. *Acc. Chem. Res.* **2000**, *33*, 695-703. (c) Blanco, M.-J.; Jimenez, M. C.; Chambron, J.-C.; Heitz, V.; Linke, M.; Sauvage, J.-P. *Chem. Soc. Rev.* **1999**, *28*, 293-305. (d) Harriman, A.; Sauvage, J.-P. *Chem. Soc. Rev.* **1996**, *26*, 41-48. (e) Paddon-Row, M. N. *Acc. Chem. Res.* **1994**, *27*, 18-25. (f) Wasielewski, M. R. *Chem. Rev.* **1992**, *92*, 435-461. (g) Jordan, K. D.; Paddon-Row, M. N. *Chem. Rev.* **1992**, *92*, 395-410. (h) Wasielewski, M. R. in *Photoinduced Electron Transfer, Part D*; Fox, M. A., Channon, M., Eds.; Elsevier: Amsterdam, 1988; pp 303-393.
4. (a) Nijhuis, C. A.; Ravoo, B. J.; Huskens, J.; Reinhoudt, D. N. *Coord. Chem. Rev.* **2007**, *251*, 1761-1780. (b) Lomozik, L.; Gasowska, A.; Bregier-jarzebowska, R.; Jastrzab, R. *Coord. Chem. Rev.* **2005**, *249*, 2335-2350. (c) Keizer, H. M.; Sijbesma, R. P. *Chem. Soc. Rev.* **2005**, *34*, 226-234. (d) *Electron Transfer in Chemistry, Vol. 3*; Balzani, V., Ed.; Wiley-VCH: Weinheim, 2001. (e) Piotrowiak, P. *Chem. Soc. Rev.* **1999**, *28*, 143-150. (f) Hayashi, T.; Ogoshi, H. *Chem. Soc. Rev.* **1997**, *26*, 355-364. (g) Ward, M. D. *Chem. Soc. Rev.* **1997**, *26*, 365-375. (h) Sessler, J. L.; Wang, B.; Springs, S. L.; Brown, C. T. in *Comprehensive Supramolecular Chemistry, Vol. 4*; Atwood, J. L., Davies, J. E. D., Macnicol, D. D., Vögtle, F., Murakami, Y., Eds.; Pergamon: UK, 1996; pp 311-336. (i) Balzani, V.; Scandola, F. in *Comprehensive Supramolecular Chemistry, Vol. 10*;

- Atwood, J. L., Davies, J. E. D., Macnicol, D. D., Vögtle, F., Reinhoudt, D. N., Eds.; Pergamon: UK, 1996; pp 687-746. (j) Lehn, J.-M. *Supramolecular chemistry: Concepts and Perspectives*; VCH: New York, 1995. (k) Schneider, H.-J.; Dürr, H. *Frontiers in Supramolecular Organic Chemistry and Photochemistry*; VCH: New York, 1991.
5. (a) Smitha, M. A.; Prasad, E.; Gopidas, K. R. *J. Am. Chem. Soc.* **2001**, *123*, 1159-1165. (b) Prasad, E.; Gopidas, K. R. *J. Am. Chem. Soc.* **2000**, *122*, 3191-3196.
6. (a) Szejtli, J. *Chem. Rev.* **1998**, *98*, 1743-1754. (b) *Comprehensive Supramolecular Chemistry, Vol. 3*; Atwood, J. L., Davies, J. E. D., Macnicol, D. D., Vögtle, F., Szejtli, J., Osa, T., Eds.; Pergamon: Oxford, 1996.
7. (a) Kano, K.; Kitagishi, H.; Dagallier, C.; Kodera, M.; Matsuo, T.; Hayashi, T.; Hisaeda, Y.; Hirota, S. *Inorg. Chem.* **2006**, *45*, 4448-4460. (b) Liu, Y.; Song, Y.; Chen, Y.; Yang, Z.-X.; Ding, F. *J. Phys. Chem. B* **2005**, *109*, 10717-10726. (c) Park, J. W.; Lee, S. Y.; Song, H. J.; Park, K. K. *J. Org. Chem.* **2005**, *70*, 9505-9513. (d) Pagliari, S.; Corradini, R.; Galaverna, G.; Sforza, S.; Dossena, A.; Montalti, M.; Prodi, L.; Zaccheroni, N.; Marchelli, R. *Chem. Eur. J.* **2004**, *10*, 2749-2758. (e) Engeldinger, E.; Armspach, D.; Matt, D. *Chem. Rev.* **2003**, *103*, 4147-4173. (f) Engeldinger, E.; Armspach, D.; Matt, D.; Jones, P. G. *Chem. Eur. J.* **2003**, *9*, 3091-3105. (g) Yuan, D.-

- Q.; Yamada, T.; Fujita, K. *Chem. Commun.* **2001**, 2706-2707 (h) Rekharsky, M. V.; Inoue, Y. *Chem. Rev.* **1998**, *98*, 1875-1917. (i) Jullien, L.; Canceill, J.; Valeur, B.; Bardez, E.; Lefèvre, J.-P.; Lehn, J.-M.; Marchi- Artzner, V.; Pansu, R. *J. Am. Chem. Soc.* **1996**, *118*, 5432-5442.
8. (a) Haider, J. M.; Pikramenou, Z. *Chem. Soc. Rev.* **2005**, *34*, 120-132. (b) Monti, S.; Sortino, S. *Chem. Soc. Rev.* **2002**, *31*, 287-300. (c) Cacialli, F.; Wilson, J. S.; Michels, J. J.; Daniel, C.; Silva, C.; Friend, R. H.; Severin, N.; Anderson, H. L. *Nat. Mater.* **2002**, *1*, 160-164. (d) Hossain, M. A.; Hamasaki, K.; Takahashi, K.; Mihara, H.; Ueno, A. *J. Am. Chem. Soc.* **2001**, *123*, 7435-7436. (e) Harada, A. *Acc. Chem. Res.* **2001**, *34*, 456-464. (f) Narita, M.; Mima, S.; Ogawa, N.; Hamada, F. *Anal. Sci.* **2000**, *16*, 865-869. (g) Rizzarelli, E.; Vecchio, G. *Coord. Chem. Rev.* **1999**, *188*, 343-364. (h) Nepogodiev, S. A.; Stoddart, J. F. *Chem. Rev.* **1998**, *98*, 1959-1976. (i) Bonomo, R. P.; Pedotti, S.; Vecchio, G.; Rizzarelli, E. *Inorg. Chem.* **1996**, *35*, 6873-6877. (j) Ueno, A. *Supramol. Sci.* **1996**, *3*, 31-36. (k) Eastburn, S. D.; Tao, B. Y. *Biotechnol. Adv.* **1994**, *12*, 325-339.
9. (a) Ito, T.; Ujiie, T.; Naka, M.; Nakamura, H. *Chem. Phys. Lett.* **2001**, *340*, 308-316. (b) Masuhara, A.; Fujitsuka, M.; Ito, O. *Bull. Chem. Soc. Jpn.* **2000**, *73*, 2199-2206. (c) Park, J. W.; Lee, B. A.; Lee, S. Y. *J. Phys. Chem. B* **1998**, *102*, 8209-8215. (d) Yonemura, H.; Kusano, S.; Matsuo, T.; Yamada, S. *Tetrahedron Lett.* **1998**, *39*, 6915-6918. (e) Yonemoto, E. H.;

- Saupe, G. B.; Schmehl, R. H.; Hubig, S. M.; Riley, R. L.; Iverson, B. L.; Mallouk, T. E. *J. Am. Chem. Soc.* **1994**, *116*, 4786-4795. (f) Seiler, M.; Duerr, H.; Willner, I.; Joselevich, E.; Doron, A.; Stoddart, J. F. *J. Am. Chem. Soc.* **1994**, *116*, 3399-3404. (g) Chesta, C. A.; Whitten, D. G. *J. Am. Chem. Soc.* **1992**, *114*, 2188-2197. (h) Ueno, A.; Osa, T. in *Photochemistry in Organized and Constrained Media*; Ramamurthy, V., Ed.; VCH: New York, 1991; pp 739-782. (i) Yonemura, H.; Saito, H.; Matsushima, S.; Nakamura, H.; Matsuo, T. *Tetrahedron Lett.* **1989**, *30*, 3143-3146. (j) Yonemura, H.; Nakamura, H.; Matsuo, T. *Chem. Phys. Lett.* **1989**, *155*, 157-161.
10. Kuroda, Y.; Ito, M.; Sera, T.; Ogoshi, H. *J. Am. Chem. Soc.* **1993**, *115*, 7003-7004.
11. Hamachi, I.; Takashima, H.; Hu, Y.-Z.; Shinkai, S.; Oishi, S. *Chem. Commun.* **2000**, 1127-1128.
12. Wang, Y.-H.; Zhang, H.-M.; Liang, Z.-X.; Liu, L.; Guo, Q.-X.; Tung, C.-H.; Inoue, Y.; Liu, Y.-C. *J. Org. Chem.* **2002**, *67*, 2429-2434.
13. Wang, Y.-H.; Zhu, M.-Z.; Ding, X.-Y.; Ye, J.-P.; Liu, L.; Guo, Q.-X. *J. Phys. Chem. B* **2003**, *107*, 14087-14093.
14. Armspach, D.; Matt, D.; Harriman, A. *Eur. J. Inorg. Chem.* **2000**, 1147-1150.

- 
15. Haider, J. M.; Chavarot, M.; Weidner, S.; Sadler, I.; Williams, R. M.; De Cola, L.; Pikramenou, Z. *Inorg. Chem.* **2001**, *40*, 3912-3921.
  16. McNally, A.; Forster, R. J.; Russell, N. R.; Keyes, T. E. *Dalton. Trans.* **2006**, 1729-1737.
  17. Haider, J. M.; Pikramenou, Z. *Eur. J. Inorg. Chem.* **2001**, 189-194.
  18. Nelissen, H. F. M.; Kercher, M.; De Cola, L.; Feiters, M. C.; Nolte, R. J. M. *Chem. Eur. J.* **2002**, *8*, 5407-5414.
  19. Deng, W.; Onji, T.; Yamaguchi, H.; Ikeda, N.; Harada, A. *Chem. Commun.* **2006**, 4212-4214.
  20. Faiz, J. A.; Williams, R. M.; Silva, M. J. J. P.; De Cola, L.; Pikramenou, Z. *J. Am. Chem. Soc.* **2006**, *128*, 4520-4521.
  21. Haider, J. M.; Williams, R. M.; De Cola, L.; Pikramenou, Z. *Angew. Chem.* **2003**, *115*, 1874-1877.



### Free Energy Dependence of Photoinduced Electron Transfer Rates in $\alpha$ -CD appended Donor- Acceptor Systems

---

#### 2.1. Abstract

*$\alpha$ -Cyclodextrin-appended pyrene (PYCD) was synthesized and fully characterized. Photoinduced electron transfer (PET) between PYCD and a few acceptor molecules were investigated in aqueous solution. The pyrene moiety in PYCD is located above the narrower rim of the  $\alpha$ -CD and is fully exposed to water. The acceptors were monocyclic aromatic molecules and, upon dissolution in water in the presence of PYCD, a fraction of the donor-acceptor systems existed as supramolecular dyads and the remaining fraction as free molecules. Free-energy-dependence studies showed that electron transfer in the supramolecular dyads followed the Marcus equation. The donor-acceptor coupling and the reorganization energy were determined from fits of the data to the Marcus equation. The electronic coupling was found to be similar to those reported for hydrogen-bonded systems. It appears that the actual  $\lambda_{out}$  values are somewhat lower than values calculated with the continuum model. The*

*experimental design has also allowed, for the first time, a visual demonstration of the inverted region on the basis of the raw fluorescence lifetime data.*

## 2.2. Introduction

During the last decade, a large number of donor–acceptor (D-A) systems were assembled using the encapsulation ability of CDs. Some of the systems are capable of undergoing PET reactions and a brief survey of these systems are presented in Chapter 1 of this thesis. Although these studies have established that electron transfer between CD-appended chromophore and an encapsulated guest is feasible, several important aspects of electron transfer in these systems remain unaddressed. The obvious question is whether the electron transfer in CD based systems conform to any established electron transfer theory? Cyclodextrin based systems belong to the group of weakly interacting donors and acceptors and electron transfer in such systems are best explained by the Marcus equation which relates the rate of electron transfer ( $k_{et}$ ) to the free energy change as given in equation (1),<sup>1</sup>

$$k_{et} = (2\pi/\hbar) H_{el}^2 (4\pi\lambda k_B T)^{-1/2} \exp[-(\Delta G^0 + \lambda)^2/4\lambda k_B T] \quad (1)$$

where,  $\hbar$  is Planck's constant divided by  $2\pi$ ,  $H_{el}$  is the coupling matrix element,  $\lambda$  is the reorganization energy,  $k_B$  is the Boltzmann constant,  $T$  is the absolute temperature and  $\Delta G^0$  is the free energy change. The reorganization energy  $\lambda$  is the energy required to structurally reorganize the donor, acceptor and their solvation spheres upon electron transfer. Depending on the relative values of  $\Delta G^0$  and  $\lambda$ ,

equation (1) envisages three typical kinetic regimes for electron-transfer reactions: i) a normal region ( $\Delta G^0 > -\lambda$ ) where electron transfer is thermally activated and is favoured by an increase in the driving force, ii) an “activation-less” regime ( $\Delta G^0 = -\lambda$ ) where the rate is maximum, and iii) an “inverted region” for strongly exergonic reactions ( $\Delta G^0 < -\lambda$ ), where the rate actually decreases with increase in driving force. The existence of an inverted region was the most important prediction of Marcus theory. Although definitive evidence for its existence was lacking for a long time, the inverted region is now well established in fixed-distance electron-transfer reactions.<sup>2</sup>

A major objective of this chapter is to investigate whether PET processes in CD based systems could be described by Marcus theory. We were also interested in determining the magnitude of electronic coupling between the CD-appended chromophore and encapsulated guest as well as the reorganization energy for the PET reaction. Study of the dependence of  $k_{et}$  on  $\Delta G^0$  is the most straightforward strategy to achieve this aim. Herein we describe a study of the free-energy dependence of the PET reaction between  $\alpha$ -CD-appended pyrene (**PYCD**) and encapsulated acceptors. The reaction involves the excitation of the pyrene moiety to the singlet state, which then transfers an electron to the acceptor encapsulated in the  $\alpha$ -CD cavity. Pyrene was selected for this study because of its long lifetime. The acceptors employed are mono- or 1,4-disubstituted benzene derivatives and

these molecules could provide a  $\Delta G^0$  range of  $\approx 0$  to  $-1.5$  eV. Since all the quenchers are monocyclic benzene derivatives, the reorganization energy associated with their one-electron reduction are expected to be similar. Thus the systems selected form a truly homogeneous series for a free energy-dependence study. The study was performed in water so as to resemble the biological electron-transfer conditions more closely. The molecules employed for the study are shown in Chart 2.1.

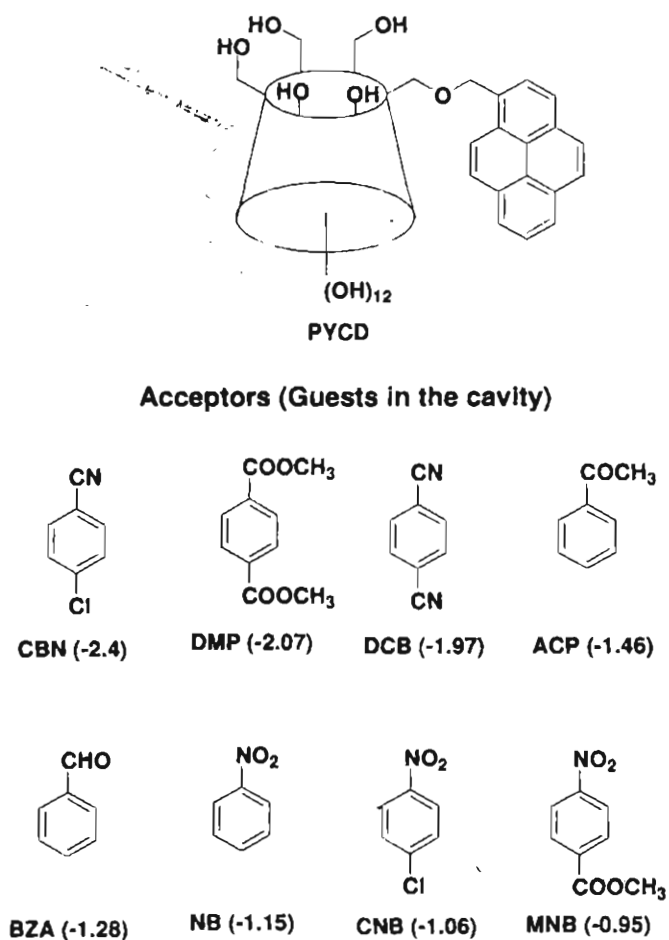
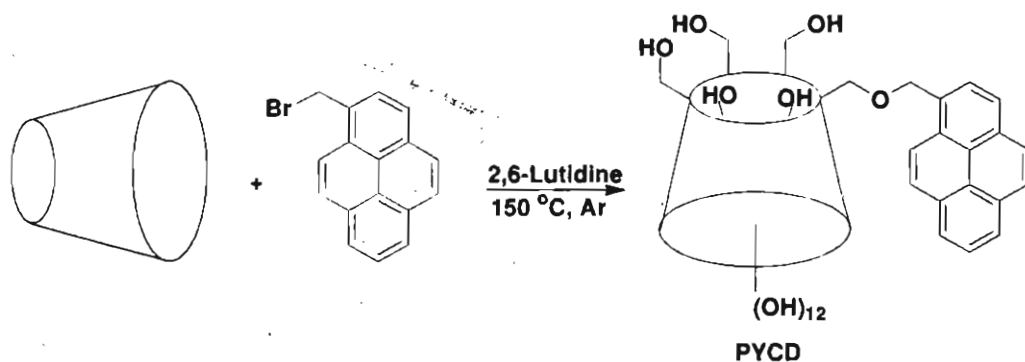


Chart 2.1

## 2.3. Results and Discussion

### 2.3.1. Synthesis and Characterization of PYCD

The strategy for the selective functionalization of the narrower rim of  $\alpha$ -CD is well established in the literature<sup>3</sup>, and we adapted this procedure for the synthesis of **PYCD**. The reaction involved heating of 1-bromomethylpyrene with  $\alpha$ -CD in lutidine as shown in Scheme 2.1. The crude product was obtained in 30% yield and this was purified by repeated column chromatography over silica gel.



Scheme 2.1

The structure of **PYCD** was assigned based on spectral evidence. For example, the MALDI-TOF showed a peak at  $m/z$  1209.2, which corresponds to  $[\text{PYCD}+\text{Na}]^+$  (Figure 2.1). The peak corresponding to native CD is not observed. The extinction coefficient (calculated assuming a molecular weight of 1186) of the **PYCD** absorption maximum is very close to that of the unsubstituted pyrene, and this confirms that only one pyrene unit is attached to the CD ring.

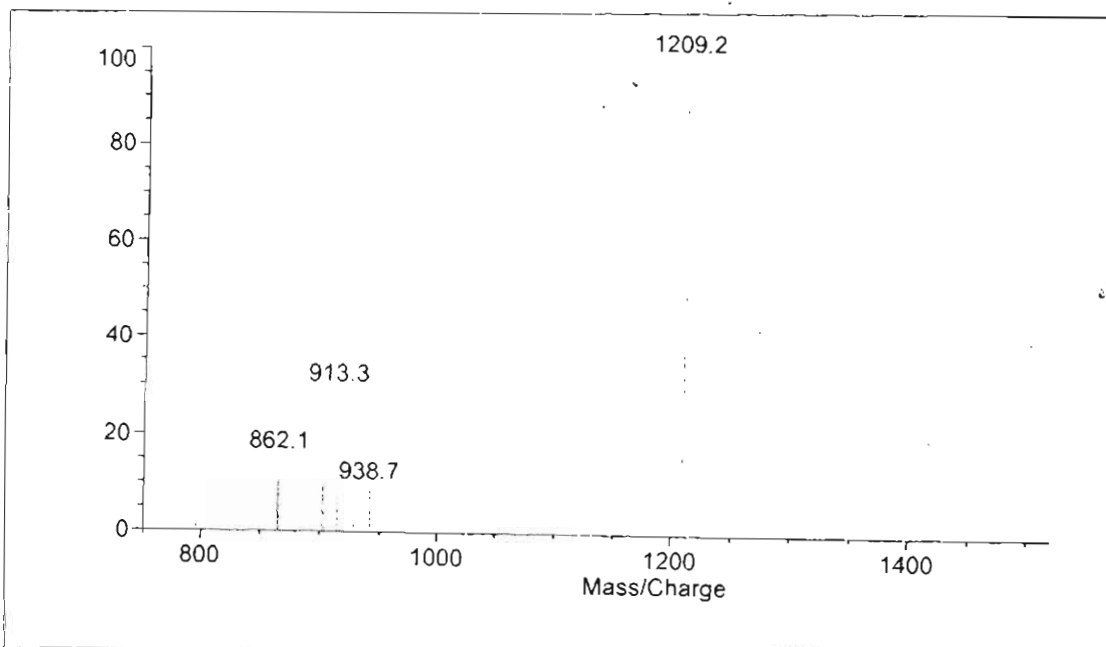


Figure 2.1. MALDI-TOF Spectrum of RYCD.

The  $^1\text{H}$  NMR spectrum of **PYCD** exhibited peaks due to the  $\alpha$ -CD part at  $\delta = 3.3$ – $5.7$  ppm and the aromatic residue at  $\delta = 7.8$ – $8.4$  ppm as shown in Figure 2.2. Integration for proton signals showed 1:1 stoichiometry for  $\alpha$ -CD and pyrene.

The regiochemistry (i.e., position of attachment of pyrene on the CD) was assigned based on a comparison of  $^{13}\text{C}$  NMR chemical shifts of **PYCD** with those in earlier reports (*vide infra*).  $\alpha$ -CD is built up of six glucose units, and **PYCD** has a pyrene attached to one of these glucose units.  $^{13}\text{C}$  chemical shifts of the pyrene-attached glucose unit are expected to differ somewhat relative to those for unsubstituted glucose units. Within the pyrene-attached glucose unit,  $^{13}\text{C}$  chemical shifts are expected to vary depending on the position of attachment.

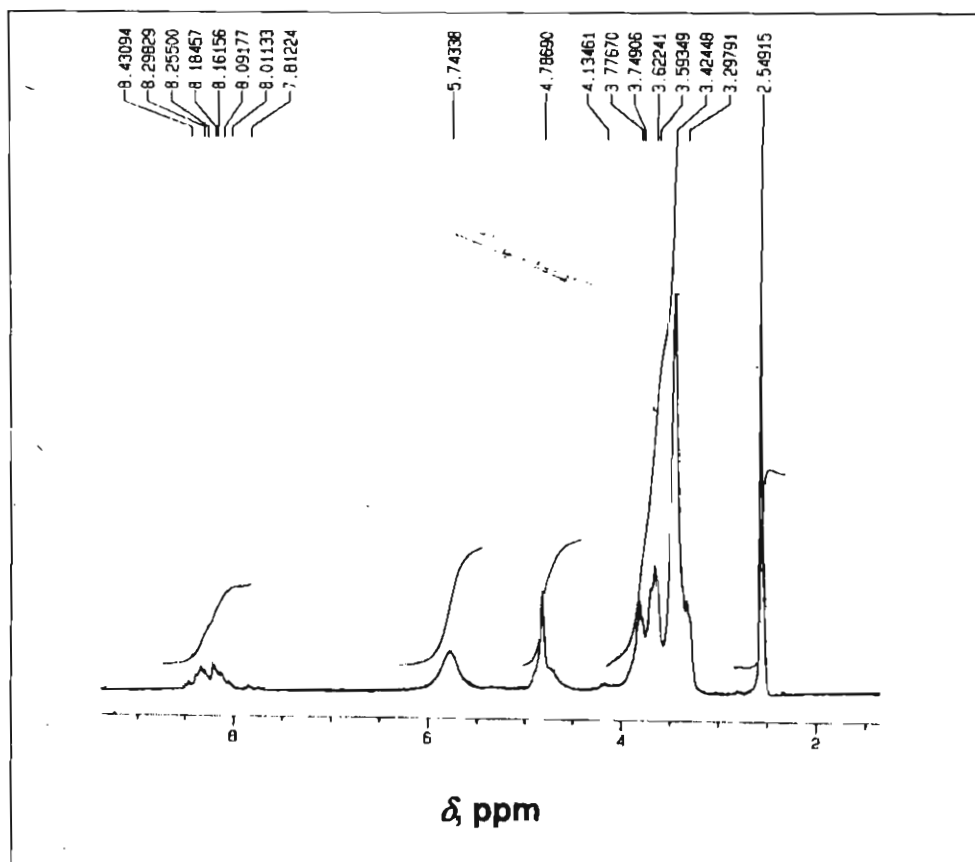


Figure 2.2.  $^1\text{H}$  NMR spectrum of PYCD in DMSO.

When an alcohol is alkylated, the  $^{13}\text{C}$  NMR chemical shifts of the  $\alpha$ - and  $\gamma$ -carbon atoms are known to move downfield by approximately 10 and 1 ppm, respectively, and that of the  $\beta$ -carbon atom is known to move upfield by  $\approx 2$  ppm. D'Souza and co-workers<sup>3</sup> used this argument to assign the regiochemistry of monosubstituted cyclodextrins. They assumed that, if C6-OH is substituted, the C6 carbon is expected to shift downfield by  $\approx 10$  ppm, C5 is expected to shift upfield  $\approx 1$  ppm, and C4 is expected to shift downfield by  $\approx 0.3$  ppm.  $^{13}\text{C}$  NMR

spectrum of **PYCD** is shown in Figure 2.3. There are five intense peaks in the carbohydrate region. Based on a comparison with the spectrum of  $\alpha$ -CD and literature precedence, these intense peaks are assigned to the carbon atoms in the five unsubstituted glucose units at  $\delta = 102.09$  (C1), 82.23 (C4), 73.45 (C3), 72.23 (C2 and C5), and 60.19 ppm (C6). In addition to this, there are eight smaller peaks. The small peak at  $\delta = 71.02$  ppm is assigned to the CH<sub>2</sub> group attached to pyrene. Six of the remaining seven peaks can then be assigned to the six carbons in the pyrene-attached glucose ring. Of these, the peak at  $\delta = 69.34$  is assigned to the C6 carbon and this signal is 9.15 ppm downfield from the normal value because of attachment to the pyrene unit. The other signals were: C5 at  $\delta = 71.29$  (0.94 ppm upfield), C4 at 82.61 (0.4 ppm downfield), C3 at 73.05 (0.4 ppm upfield), C2 at 72.59 (0.36 ppm downfield) and C1 at 102.52 ppm (0.43 ppm downfield). Because the C6 signal is shifted by more than 9 ppm and C5 is shifted by nearly 1 ppm, this confirms that the pyrene is attached to the C6 carbon, which is on the narrower rim of  $\alpha$ -CD. The above assignments are consistent with those given by D'Souza and co-workers.<sup>3</sup> A small signal at  $\delta = 60.68$  ppm (0.49 ppm downfield from unmodified C6 signal) remains unaccounted. D'Souza and co-workers<sup>3</sup> also observed such a peak, but they have not assigned it.



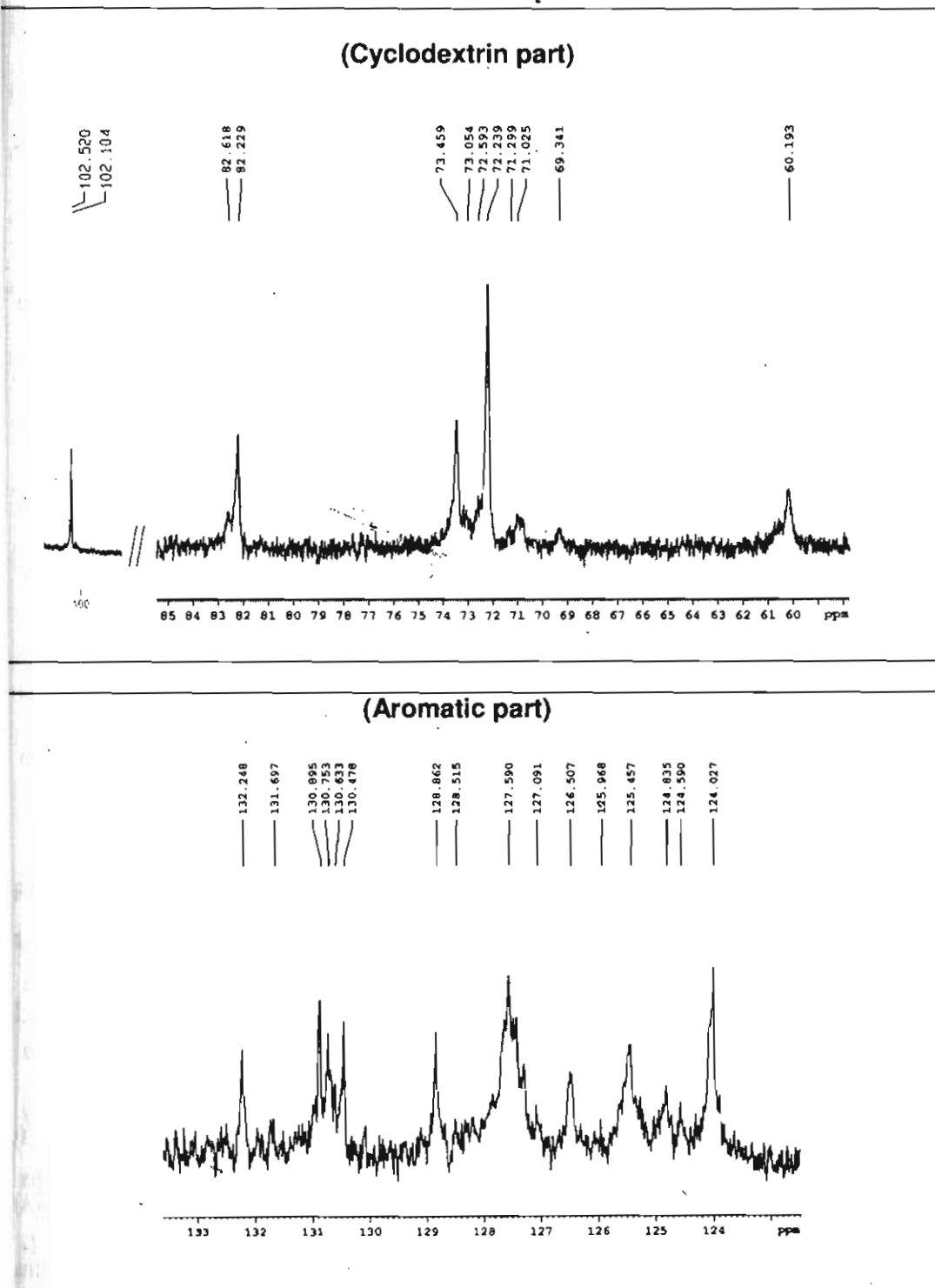


Figure 2.3.  $^{13}\text{C}$  NMR spectrum of PYCD. (spectrum is presented as two parts for clarity)

When a relatively large molecule, such as pyrene, is attached to the narrower rim of  $\alpha$ -CD, the  $\text{CH}_2\text{OH}$  groups projecting out of the narrower rim may experience steric crowding. This effect may be greater on adjacent glucose rings. In consideration of this, we tentatively assign this signal to the C6 carbon atoms of the glucose unit(s) adjacent to the one to which pyrene is attached.

Several examples of pyrene attached to  $\gamma$ -CD are reported in the literature and some of these are useful as sensors of organic molecules in aqueous solutions.<sup>4</sup> In these systems, pyrene is hosted by the  $\gamma$ -CD cavity. Because of its relatively large size, pyrene cannot be hosted in the cavities of  $\alpha$ - and  $\beta$ -CDs.<sup>5</sup> Nevertheless, size considerations cannot rule out partial inclusion of pyrene within the  $\alpha$ -CD cavity in **PYCD**. Absorption and emission spectral studies described below, however, suggested that the pyrene moiety in **PYCD** is fully exposed to water.

### 2.3.2. Photophysical Properties of **PYCD**

The absorption and emission spectra of **PYCD** in water are shown in Figure 2.4. The absorption spectral profile and extinction coefficient of **PYCD** closely resemble those of pyrene in common solvents. This indicates that there is only negligible interaction between pyrene and  $\alpha$ -CD moieties in **PYCD**. The emission spectrum of **PYCD** was superimposable on the emission spectrum of 1-pyrenemethanol in water (as shown by the dotted line in Figure 2.4), which again

indicated that the pyrene moiety is fully exposed to water in the most stable conformation of **PYCD**. On the basis of the absorption and emission maxima, the excitation energy ( $E_{0,0}$ ) of **PYCD** was calculated and the value obtained was 3.5 eV. The fluorescence decay of **PYCD** was monoexponential with a lifetime of 204 ns.

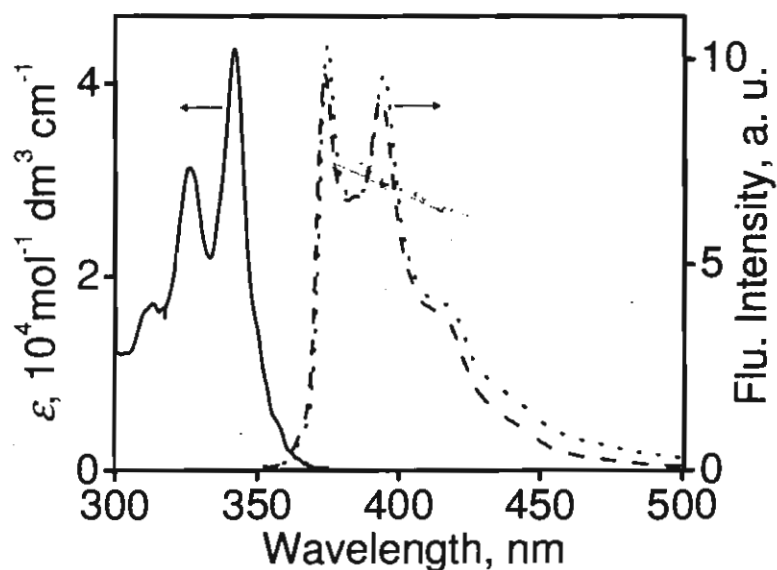
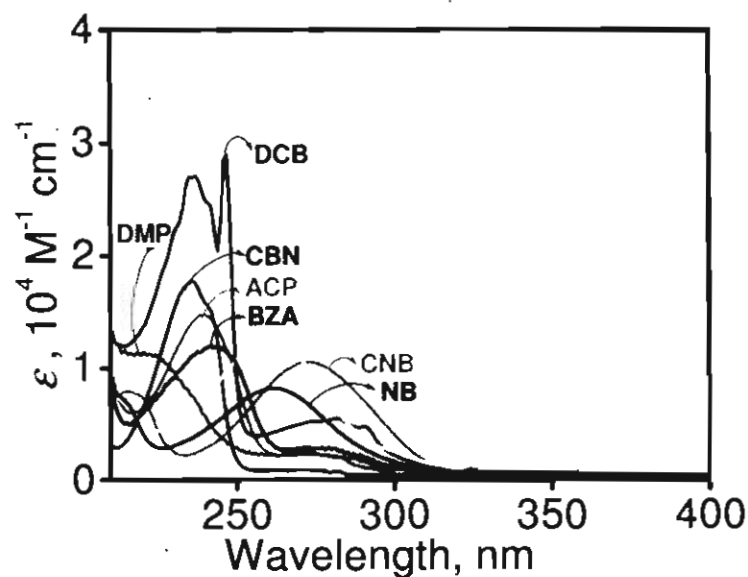


Figure 2.4. Absorption (—) and emission (- -) spectra of **PYCD** in water, and the emission spectrum (.....) of 1-pyrenemethanol in water.

### 2.3.3. Interaction of Acceptors with **PYCD**

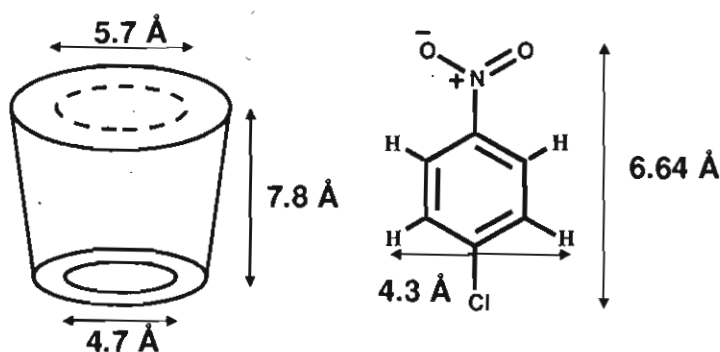
The acceptor molecules employed in the study are 4-chlorobenzonitrile (**CBN**), dimethylterephthalate (**DMP**), 1,4-dicyanobenzene (**DCB**), acetophenone (**ACP**), benzaldehyde (**BZA**), nitrobenzene (**NB**), 4-chloronitrobenzene (**CNB**), and methyl-4-nitrobenzoate (**MNB**). Structures of the acceptor molecules are shown in Chart 2.1. The reduction potentials of all these molecules are known in

the literature<sup>6</sup> and the values are also given in Chart 2.1. These molecules have been employed as acceptors in several photoinduced electron-transfer reactions. Earlier workers have documented photoinduced electron-transfer reactions between pyrene and most of the quenchers listed in Chart 2.1 by means of fluorescence quenching and/or laser flash-photolysis techniques.<sup>7</sup> The onset of absorption for all these acceptors is below  $\lambda = 320$  nm as shown in Figure 2.5. This indicates that singlet energies of these molecules are higher than that of pyrene. Hence singlet-singlet energy transfer from pyrene to the acceptors would be endothermic and this eliminates the possibility of pyrene fluorescence being quenched by these acceptors by the energy-transfer mechanism.



**Figure 2.5.** Absorption spectra of acceptors employed in the study.

The known dimensions of  $\alpha$ -CD and calculated dimensions of one of the acceptors is shown in Scheme 2.2. It is clear from Scheme 2.2 the all the quencher molecules in Chart 2.1 could be included into the  $\alpha$ -CD cavity with their long molecular axis parallel to the  $C_6$ -axis of  $\alpha$ -CD. In fact, inclusion behaviours of several mono- and 1,4-disubstituted benzene derivatives in  $\alpha$ -CD (including some molecules shown in Chart 2.1) were studied, both theoretically and experimentally.<sup>8</sup> These compounds were found to associate with  $\alpha$ -CD in water with association constants ( $K_a$ ) in the range 50–400  $M^{-1}$ .



**Scheme 2.2.** Molecular dimensions of  $\alpha$ -CD and CNB.

All the acceptor molecules were soluble in water in the  $10^{-4}$ – $10^{-3}$  M concentration range. Upon addition of the quenchers to aqueous **PYCD** solutions, the long wavelength absorption of **PYCD** remained unaffected as shown in Figure 2.6 A. This indicates that the pyrene moiety in **PYCD** has no ground state interactions with the acceptors.

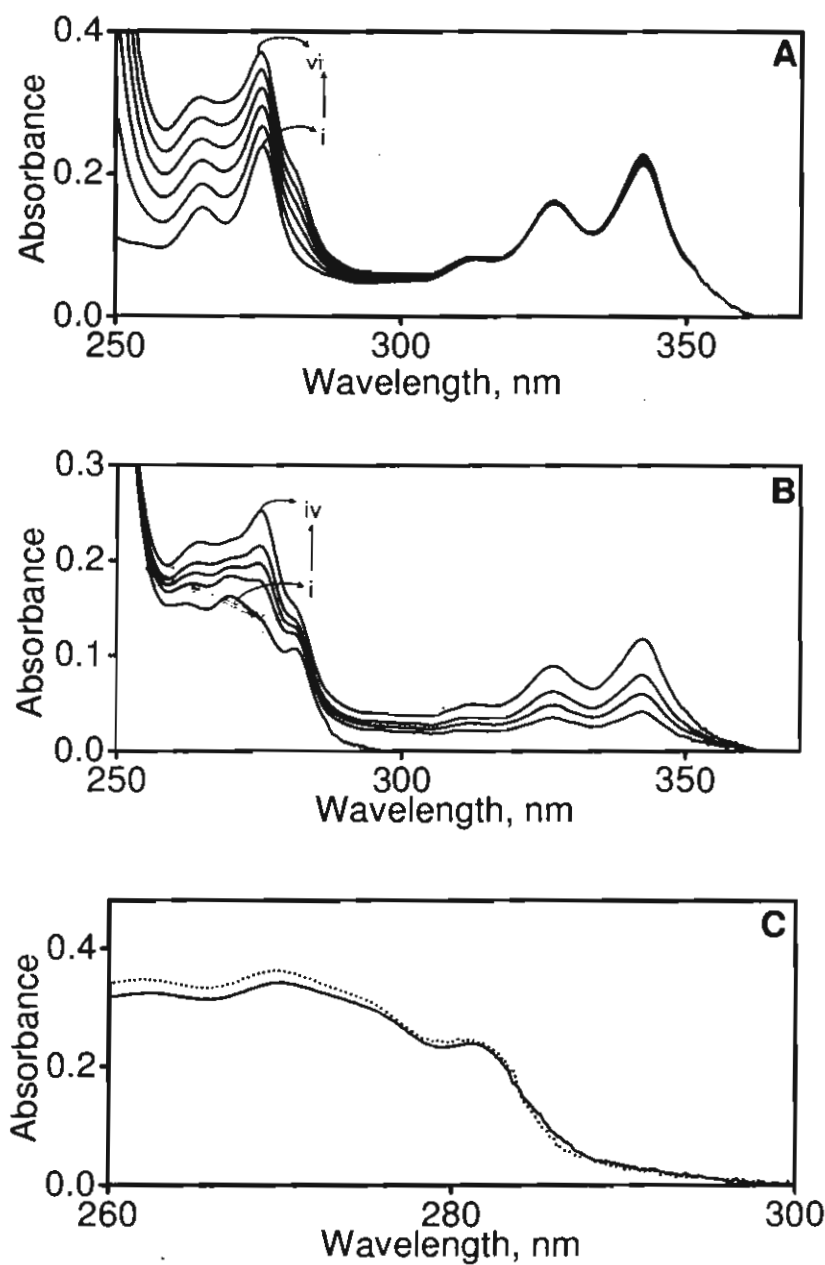


**Figure 2.6.** (A) Changes in the absorption spectrum of PYCD (i) ( $5 \times 10^{-6}$  M) with varying concentrations ( $8\text{--}40 \times 10^{-4}$  M) of CBN (ii–vi); (B) Changes in absorption spectrum of CBN (i) ( $4 \times 10^{-4}$  M) with varying concentrations ( $1.0\text{--}2.5 \times 10^{-6}$  M) of PYCD (ii–iv); (C) Change in absorption spectrum of CBN ( $8 \times 10^{-4}$  M) in the absence (—) and presence (.....) of native  $\alpha$ -CD ( $1 \times 10^{-5}$  M).

On the other hand, the absorption spectra of the quenchers undergo slight changes upon addition of small amounts of **PYCD** as shown in Figure 2.6 B for **CBN/PYCD** system. Because the pyrene moiety of **PYCD** also absorbs in the same region, the spectral shifts of the **CBN** moiety could not be analyzed to obtain  $K_a$  values. In Figure 2.6 C, absorption spectra of **CBN**, in the absence and presence of native  $\alpha$ -CD are presented, which clearly shows the association of **CBN** with  $\alpha$ -CD. Other quencher molecules also exhibited similar behaviours. Figure 2.6 seems to suggest that **PYCD** interacts with the quenchers, but the interactions are with the  $\alpha$ -CD part of **PYCD** and the pyrene moiety remains unaffected by this interaction. Inclusion of the acceptors probably occurs through the wider rim of  $\alpha$ -CD, which is away from the pyrene moiety. Park et al. have recently shown that encapsulation of guest molecules in CDs preferably takes place through the secondary face.<sup>9</sup>

## 2.3.4. Fluorescence Quenching

### 2.3.4.1. Steady State Experiments

All the acceptors shown in Chart 2.1 quench the fluorescence of **PYCD** in aqueous solutions. Figure 2.7 shows an example where the fluorescence of **PYCD** is progressively quenched with addition of increasing amounts of **DCB**.

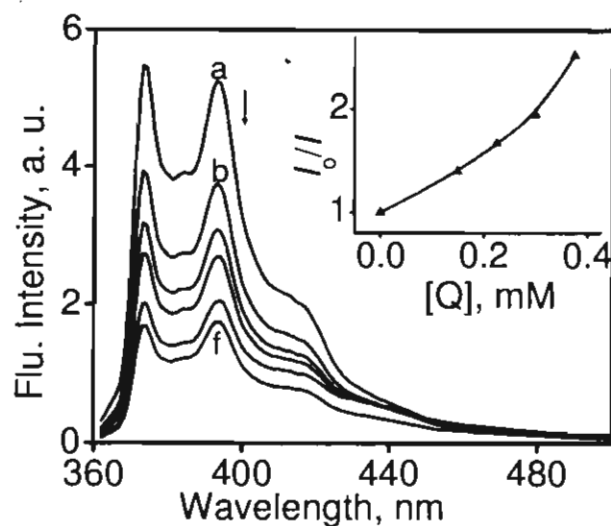


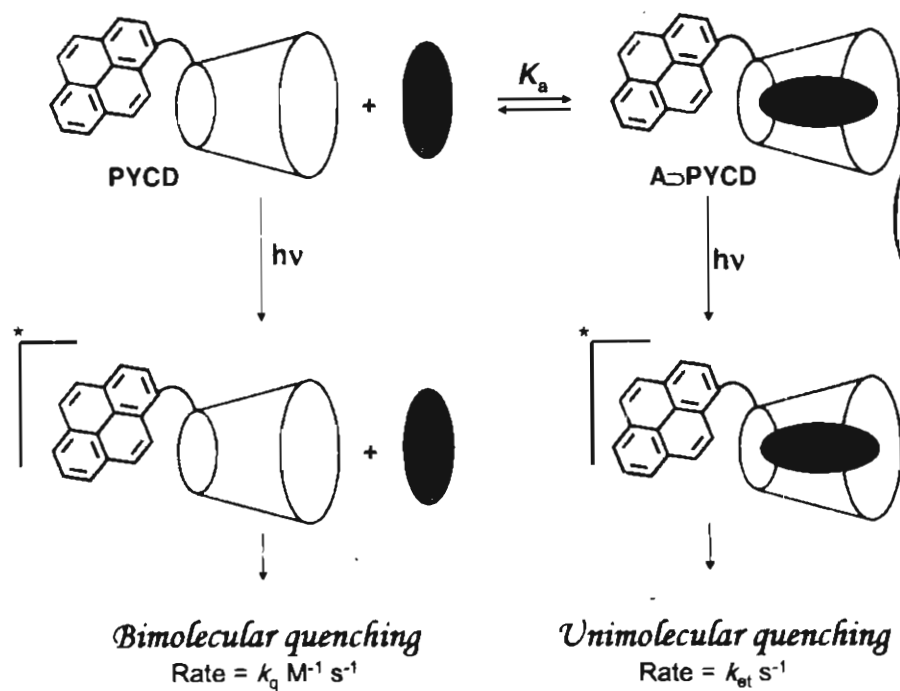
**Figure 2.7.** Fluorescence spectra of **PYCD** in the absence (a) and in the presence (b–f) of **DCB**. Concentration of **DCB** varied from  $1-4 \times 10^{-4}$  M. Inset is a plot of  $I_0/I$  for this quenching.

The  $I_0/I$  plot for the fluorescence quenching shown in the insert in Figure 2.7 exhibits an upward curvature at higher concentrations of the quencher. Upward curvature in the Stern-Völmer plot indicates the presence of more than one quenching pathway.<sup>10</sup> Similar behaviours were observed with other quenchers also. We have already ruled out the possibility of quenching by energy transfer. Hence, quenching reactions in all the systems were attributed to electron transfer from pyrene moiety to the acceptors. The upward curvature in the Stern-Völmer plot prompted us to suggest that 2 types of electron transfer quenchings are taking place in these systems.

The model shown in Scheme 2.3 can explain the different types of electron transfer quenching mechanism operating in the **PYCD**/acceptor systems. Up on mixing the acceptor **A** with **PYCD** in aqueous solution, a fraction of **A** undergoes



encapsulation in the cavity of **PYCD** to give **A $\supset$ PYCD** and an equilibrium as shown in Scheme 2.3 is established. When irradiated, the pyrene moieties in free **PYCD** and **A $\supset$ PYCD** are excited. As shown in Scheme 2.3, free **\*PYCD** is quenched by free moving **A** molecules in a bimolecular, diffusion-mediated electron-transfer reaction. The excitation in **A $\supset$ \*PYCD**, on the other hand, is quenched by the encapsulated **A**, in a fixed-distance, unimolecular electron-transfer reaction. The unimolecular and bimolecular components of the electron-transfer reactions can be evaluated separately by fluorescence lifetime quenching experiments.



**Scheme 2.3.** Scheme showing unimolecular and bimolecular quenching pathways for  $\alpha$ -CD-appended pyrene.

### 2.3.4.2. Time Resolved Fluorescence Experiments

Fluorescence decay of **PYCD** was monoexponential in the absence of acceptors and lifetime ( $\tau_0$ ) obtained from single photon counting experiment was 204 ns. Addition of an acceptor resulted in unimolecular and bimolecular quenching pathways. As a result the fluorescence decays became biexponential. Fluorescence decay profiles of **PYCD** were collected in the presence of different concentrations of all the acceptors. Decay profiles are presented in Figure 2.8 A-H. The biexponential nature of the decay is very evident from these figures.

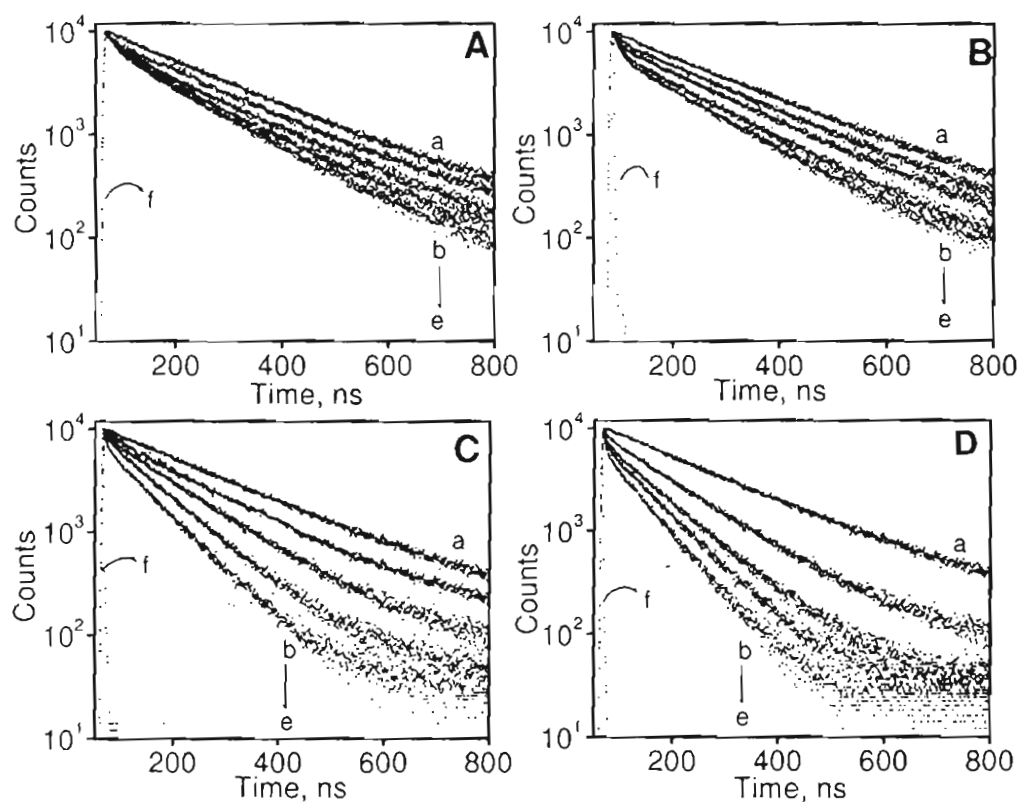
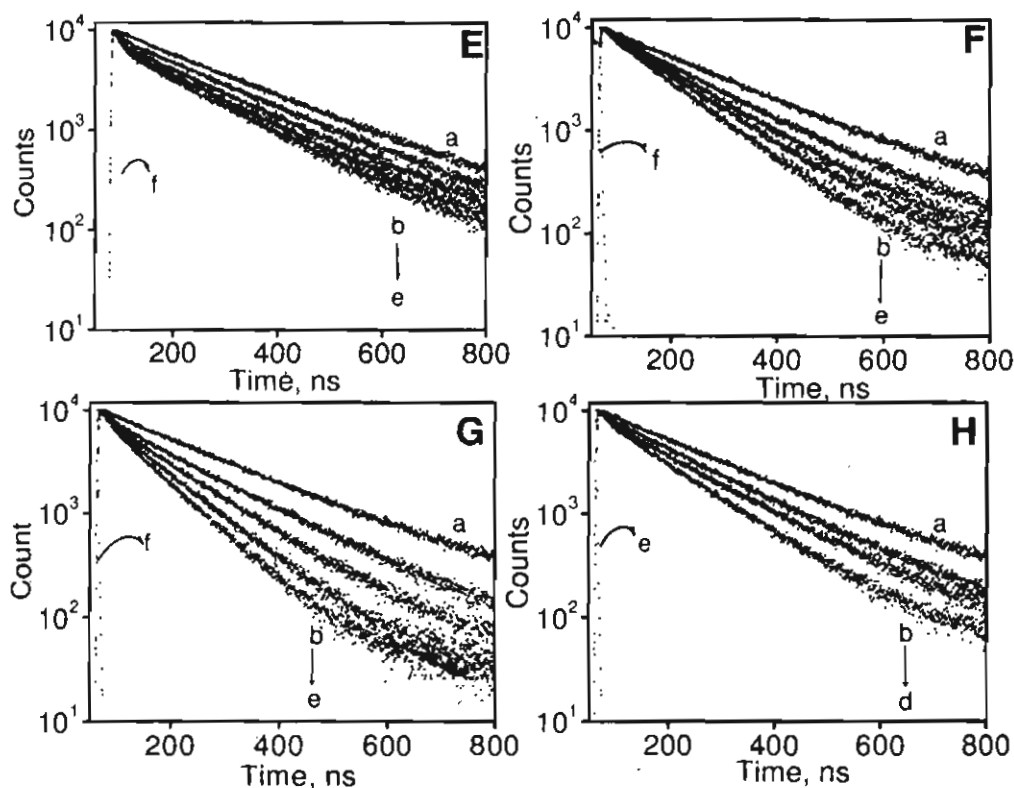


Figure 2.8 A-D: Fluorescence decay profiles of PYCD with various Acceptors (A) CBN (B) DMP (C) DCB (D) ACP



**Figure 2.8 E-H:** Fluorescence decay profiles of PYCD with various Acceptors (E) BZA (F) NB (G) CNB (H) MNB.

The short lifetime component ( $\tau_1$ ) of the decay arises due to intra-ensemble electron transfer and the long component ( $\tau_2$ ) is due to diffusion mediated electron transfer. Hence the biexponential fluorescence decays can be expressed by equation (2),<sup>11</sup>

$$I_t = \chi_{(A \supset PYCD)} \exp(-t/\tau_1) + \chi_{(PYCD)} \exp(-t/\tau_2) \quad (2)$$

where  $\chi_{(A \supset PYCD)}$  is the mole fraction of the encapsulated species and  $\chi_{(PYCD)}$  is the mole fraction of free PYCD. The above assumptions lead to equations (3) and (4).

$$\tau_1 = (k_0 + k_{et})^{-1} \quad (3)$$

$$\tau_2 = (k_0 + k_q \tau_0 [A])^{-1} \quad (4)$$

where,  $k_0$  ( $= 1/\tau_0$ ) is the intrinsic decay rate of the probe,  $k_{et}$  is the unimolecular rate constant of electron transfer within the encapsulated segment,  $k_q$  is the bimolecular quenching rate constant for the unassociated **PYCD** molecules and  $[A]$  is the concentration of the acceptor. According to equations (2)–(4), the short lifetime component ( $\tau_1$ ) is independent of the acceptor concentration and the long lifetime component ( $\tau_2$ ) is dependent on the acceptor concentration. From the short lifetime component, the rate constant for electron transfer within the encapsulated complex **A**⊃**PYCD** can be calculated with equation (5).

$$k_{et} = 1/\tau_1 - 1/\tau_0 \quad (5)$$

$k_q$  for the bimolecular process can be obtained by the usual Stern-Völmer method.

$$\tau_0/\tau_2 = 1 + k_q \tau_0 [A] \quad (6)$$

According to equation (6), a plot of  $\tau_0/\tau_2$  versus acceptor concentration will give a straight line, the slope of which when divided by  $\tau_0$  gives  $k_q$ . Thus, the rate constants  $k_{et}$  and  $k_q$  can be obtained from the same set of experiments. The equilibrium association constant,  $K_a$  for the encapsulation process shown in Scheme 2.3 can also be determined from these experiments.  $\chi_{(A \supset PYCD)}$  and  $\chi_{(PYCD)}$  values, obtained from fitting the lifetime data, are proportional to the concentrations of the associated and unassociated fractions, respectively. Since the

concentration of the acceptor is large compared to that of the associated complex, we can write equation (7),

$$K_a = \frac{\chi_{(A \rightarrow PYCD)}}{\chi_{(PYCD)}[A]} \quad (7)$$

A plot of  $\chi_{(A \rightarrow PYCD)}/\chi_{(PYCD)}$  versus  $[A]$  will be linear and gives  $K_a$  as the slope.

The bimolecular decays obtained for all systems were analyzed to obtain  $\tau_1$ ,  $\tau_2$ ,  $\chi_{(A \rightarrow PYCD)}$ , and  $\chi_{(PYCD)}$ . These, along with the  $\chi^2$  values obtained for the fits are presented in Table 2.1 A-H. Notice that  $\chi^2$  values were  $< 1.2$  for all the fits.

**Table 2.1.** Fluorescence lifetimes ( $\tau_1$  and  $\tau_2$ ), fractional contributions ( $\chi_{(A \rightarrow PYCD)}$  and  $\chi_{(PYCD)}$ ) and  $\chi^2$  values obtained in the fluorescence quenching of PYCD by various quenchers.

Table 2.1 A: Fit parameters for PYCD/CBN system

[CBN], $10^{-3}$ M	$\tau_1$ , ns	$\chi_{(A \rightarrow PYCD)}$	$\tau_2$ , ns	$\chi_{(PYCD)}$	$\chi^2$
0	--	--	204	100	1.1
0.15	11.7	4.1	200	95.9	1.1
0.25	11.5	5.8	198	94.2	1.0
0.35	11.5	7.4	196	92.6	1.1
0.45	11	8.5	193	91.5	1.2

Table 2.1 B: Fit parameters for PYCD/DMP system

[DMP], $10^{-3}$ M	$\tau_1$ , ns	$\chi_{(A \rightarrow PYCD)}$	$\tau_2$ , ns	$\chi_{(PYCD)}$	$\chi^2$
0			204	100	1.1
0.05	2.4	7.7	198	92.3	1.0
0.15	2.4	9.5	190	90.5	1.2
0.35	2.2	12.4	182	87.6	1.1
0.55	2.2	15.5	172	84.5	1.1

Table 2.1 C: Fit parameters for PYCD/DCB system

[DCB], $10^{-3}$ M	$\tau_1$ , ns	$\chi_{(A \rightarrow PYCD)}$	$\tau_2$ , ns	$\chi_{(PYCD)}$	$\chi^2$
0			204	100	1.1
0.15	1.4	4.1	196	95.9	1.1
0.55	1.3	9.5	183	90.5	1.1
0.95	1.4	14	170	86	1.1
1.05	1.3	15	167	85	1.1

Table 2.1 D: Fit parameters for PYCD/ACP system

[ACP], $10^{-3}$ M	$\tau_1$ , ns	$\chi_{(A \rightarrow \text{PYCD})}$	$\tau_2$ , ns	$\chi_{(\text{PYCD})}$	$\chi^2$
0			204	100	1.1
0.12	1.2	9.3	175	90.7	1.2
0.4	1.2	11.1	154	89.9	1.1
0.5	1.1	12.6	144	87.4	1.1
0.6	1.2	14	136	86	1.1

Table 2.1 E: Fit parameters for PYCD/BZA system

[BZA], $10^{-3}$ M	$\tau_1$ , ns	$\chi_{(A \rightarrow \text{PYCD})}$	$\tau_2$ , ns	$\chi_{(\text{PYCD})}$	$\chi^2$
0			204	100	1.1
0.04	2.4	4.7	196	95.3	1.2
0.05	2.4	5.4	194	94.6	1.1
0.07	2.4	6.2	191	93.8	1.1
0.09	2.3	7.0	189	93	1.2

Table 2.1 F: Fit parameters for PYCD/NB system

[NB], $10^{-3}$ M	$\tau_1$ , ns	$\chi_{(A \rightarrow PYCD)}$	$\tau_2$ , ns	$\chi_{(PYCD)}$	$\chi^2$
0			204	100	1.1
0.03	13.3	4.0	195	96	1.1
0.07	13.0	4.4	190	95.6	1.0
0.10	13.2	5.0	187	95	1.0
0.13	12.9	5.5	182	94.5	1.0

Table 2.1 G: Fit parameters for PYCD/CNB system

[CNB], $10^{-3}$ M	$\tau_1$ , ns	$\chi_{(A \rightarrow PYCD)}$	$\tau_2$ , ns	$\chi_{(PYCD)}$	$\chi^2$
0			204	100	1.1
0.1	28.6	2.8	188	97.2	1.1
0.2	28	6.0	172	94	1.0
0.3	28	8.8	161	91.2	1.1
0.4	28.5	12.5	151	87.5	1.1



2.1 H: Fit parameters for **PYCD/MNB** system

[MNB], 10 <sup>-3</sup> M	$\tau_1$ , ns	$\chi_{(A \rightarrow PYCD)}$	$\tau_2$ , ns	$\chi_{(PYCD)}$	$\chi^2$
0			204	100	1.1
0.05	40	3.0	194	97	1.0
0.1	39	4.2	187	95.8	1.1
0.15	40	5.3	178	94.7	1.1
0.2	40	6.2	172	93.8	1.1

An examination of the fit parameters given in the Tables 2.1 A-H confirms the following. (1) For all **PYCD**/acceptor systems,  $\tau_1$  values were independent of acceptor concentration (within the limits of experimental error) and  $\chi_{(A \rightarrow PYCD)}$  increased with acceptor concentration; (2)  $\tau_2$  and  $\chi_{PYCD}$  values decreased with increase in acceptor concentration. We also noted that the short lifetime component disappears upon addition of methanol (15% by volume) to the above solutions. The role of methanol is to prevent the hydrophobic interaction between **PYCD** and acceptors, thereby preventing the encapsulation process. The bimolecular fluorescence quenching component will be absent in this case. These findings further confirmed that the excited state processes taking place in **PYCD**/acceptor systems are adequately explained by Scheme 2.3.

Scheme 2.3 lists three important rate constants namely  $k_{et}$ ,  $k_q$  and  $K_a$ .  $k_{et}$  values were calculated using equation (5) by employing  $\tau_1$  and  $\tau_0$  values shown in Table 2.1.  $k_q$  values were obtained from plots of  $\tau_0/\tau_2$  vs acceptor concentration. As per equation (6) straight lines are expected. Representative examples of these are given in Figure 2.9.  $k_q$  values are obtained from the slopes of these plots.

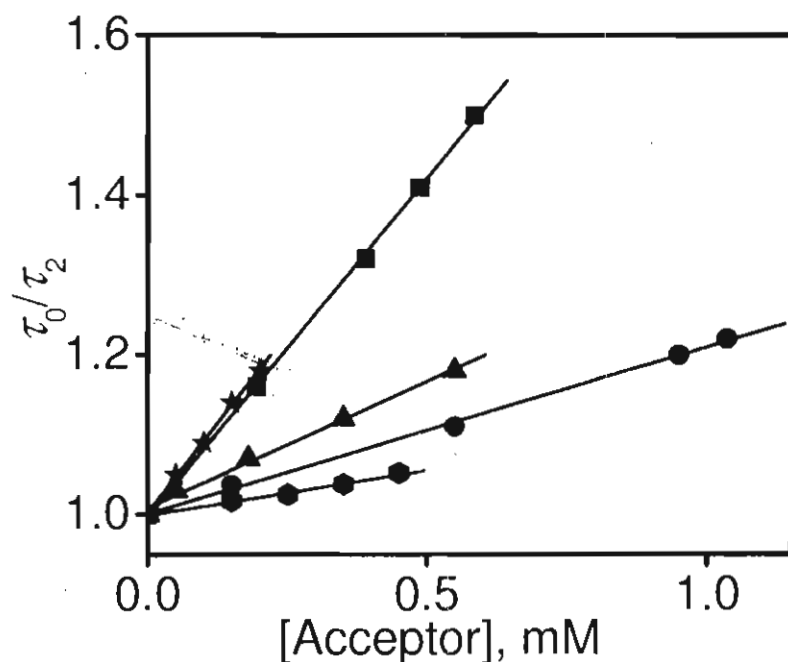


Figure 2.9.  $\tau_0/\tau_2$  plot for the lifetime quenching of PYCD by CBN (●), DCB (○), DMP (▲), ACP (■) and MNB (★).

Plots of  $\chi_{(A \rightarrow PYCD)}/\chi_{(PYCD)}$  against acceptor concentrations gave straight lines some examples of which are given in Figure 2.10.  $K_a$  values are obtained from the slopes of these plots. Values of  $k_{et}$ ,  $k_q$ , and  $K_a$  obtained by the analysis mentioned above are given in Table 2.2 for all systems.

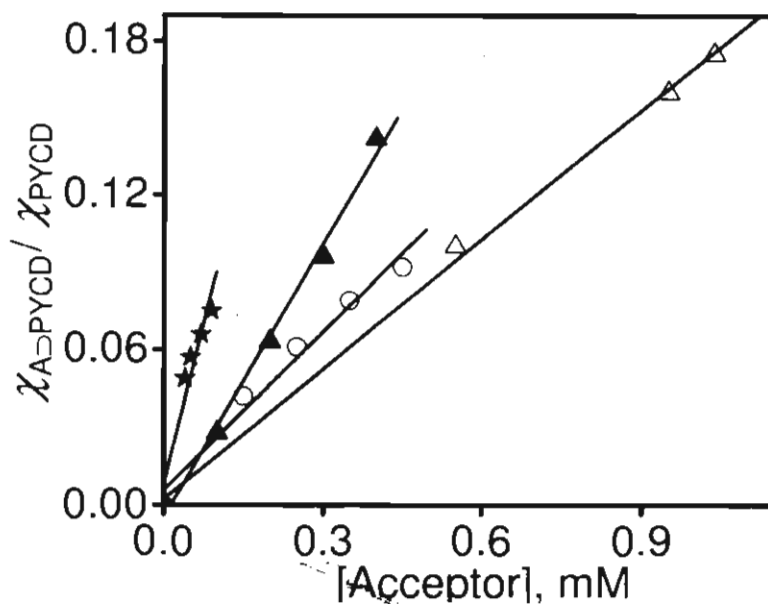


Figure 2.10. Plots of  $\chi_{A \rightarrow PYCD} / \chi_{PYCD}$  vs [Acceptor] for CNB ( $\blacktriangle$ ), DCB ( $\triangle$ ), CBN ( $\circ$ ) and BZA ( $\star$ ).

### 2.3.5. Calculation of $\Delta G^0$ values.

With redox potentials of pyrene and acceptors measured in acetonitrile, the free-energy change for electron-transfer  $\Delta G^0$  can be calculated using equation (8).<sup>12</sup>

$$\Delta G^0 = E_{ox} - E_{red} - E_{0,0} - \frac{e^2}{2} \left( \frac{1}{r_P} + \frac{1}{r_A} \right) \left( \frac{1}{37} - \frac{1}{\epsilon_s} \right) - \frac{e^2}{\epsilon_s d} \quad (8)$$

where  $E_{ox}$  is the oxidation potential of the pyrene moiety in **PYCD** and  $E_{red}$  are the reduction potentials of the acceptors,  $r_P$  and  $r_A$  are the radii of the pyrene and

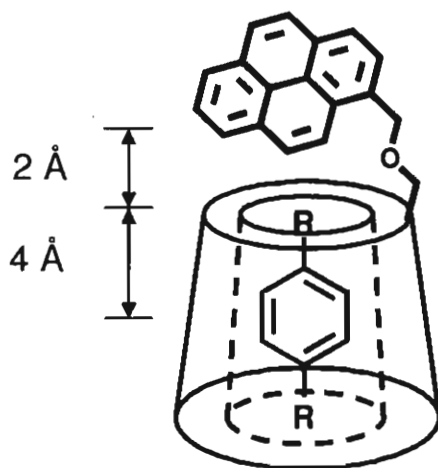
acceptor moieties, respectively,  $\epsilon_s$  is the dielectric constant of water, and  $d$  is the distance separating the pyrene and acceptor units.

**Table 2.2.** Free energies ( $\Delta G^0$ ), Association constants ( $K_a$ ) and Rate constants ( $k_{et}$  and  $k_q$ ) for the PYCD/Acceptor systems

D-A system	$K_a, M^{-1}$	$\Delta G^0, (eV)$	$k_q, 10^8 M^{-1} s^{-1}$	$k_{et}, 10^7 s^{-1}$
<b>PYCD/CBN</b>	145	-0.11	5.3	$8.3 \pm 0.3$
<b>PYCD/DMP</b>	193	-0.44	15.7	$43.1 \pm 2.0$
<b>PYCD/DCB</b>	140	-0.53	10.4	$73.5 \pm 2.5$
<b>PYCD/ACP</b>	179	-1.07	38.0	$86.6 \pm 3.8$
<b>PYCD/BZA</b>	461	-1.22	42.5	$42.0 \pm 0.9$
<b>PYCD/NB</b>	172	-1.35	42.9	$7.1 \pm 0.10$
<b>PYCD/CNB</b>	375	-1.44	42.8	$3.0 \pm 0.04$
<b>PYCD/MNB</b>	236	-1.55	44.0	$2.0 \pm 0.03$

The oxidation potential of **PYCD** in water was measured and we obtained the value as 0.9 V versus SCE. The reduction potentials of the acceptors, however, could not be measured in water because the reduction potentials of most of them lay outside the range possible in water. Hence we were forced to use the redox potentials of pyrene and the acceptors measured in acetonitrile or DMF and make the necessary corrections for the difference in solvation by means of the fourth

term in equation (8). We used  $r_P = 3.6 \text{ \AA}$ ,  $r_A = 3.5 \text{ \AA}$  for monosubstituted benzenes, and  $r_A = 4.0\text{-}4.5 \text{ \AA}$  for disubstituted benzenes. These values were obtained with AM1 methods.<sup>13</sup> In order to calculate  $d$ , we assumed that the acceptors are centrally positioned in the  $\alpha$ -CD cavity and that the midpoint of the pyrene moiety in **PYCD** is positioned  $\approx 2 \text{ \AA}$  above the narrower rim of  $\alpha$ -CD as shown in Scheme 2.4. This gives a  $d$  value of  $6 \text{ \AA}$  for the intra-ensemble electron transfer. For diffusion-mediated electron transfer,  $d$  may be slightly different; however, the same values were assumed for the sake of simplicity.  $\Delta G^0$  values thus calculated are presented in Table 2.2. It can be seen that  $\Delta G^0$  values for the selected systems spanned a range of  $\approx 0$  to  $-1.5 \text{ eV}$ .



Scheme 2.4

### 2.3.6. Free Energy Dependence of $k_{et}$ and $k_q$ .

Figure 2.11 is a plot of the bimolecular quenching rate constant,  $k_q$  versus  $\Delta G^0$  (see Table 2.2 for actual values). It can be seen that, as the driving force for the reaction ( $-\Delta G^0$ ) increases,  $k_q$  first increases, reaches a maximum, and then stays nearly invariant with further increase in the driving force. This type of behaviour is known as Rehm–Weller behaviour.

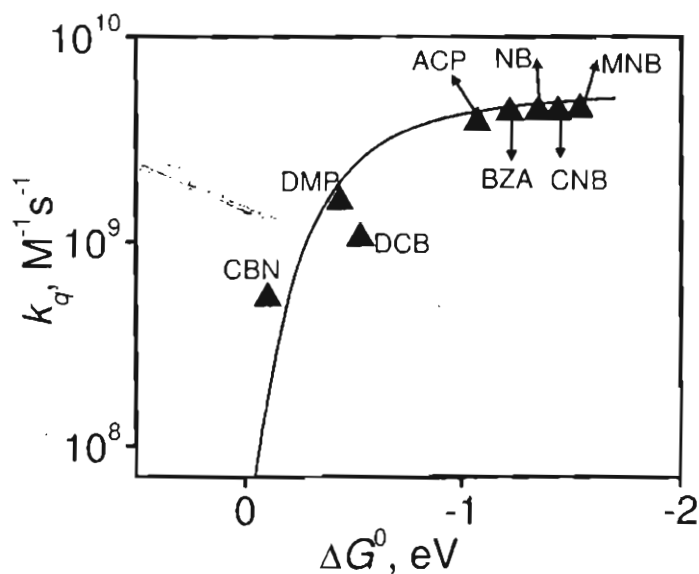


**Figure 2.11.** Plot of bimolecular quenching rate constants ( $k_q$ ) vs  $\Delta G^0$ . The solid line is a fit using equation (9).

In one of the first major experiments carried out to test the Marcus theory, Weller and co-workers measured the fluorescence quenching rate constants for a large number of D-A systems wherein the free energy varied from +6 to -60 kcal  $M^{-1}$ .<sup>14</sup> They observed that the rate constant rapidly rises in the normal region, then

reaches the diffusional limit and remains constant. This behaviour, known today as the "Rehm–Weller behaviour" is exhibited by a large number of D-A systems and it seems to be the rule for processes of luminescence quenching through electron transfer in homogeneous solution.<sup>15</sup> In the Rehm–Weller formalism, the overall quenching rate constant  $k_q$  in a bimolecular electron-transfer reaction is expressed by equation (9)<sup>14</sup>, where  $\Delta G^\#$  is the free energy of activation for electron transfer and is given by equation (10).

$$k_q = \frac{k_{\text{diff}}}{1 + 0.25[\exp(\Delta G^\# / RT) + \exp(\Delta G^0 / RT)]} \quad (9)$$

$$\Delta G^\# = \frac{\Delta G^0}{2} + \left[ \left( \frac{\Delta G^0}{2} \right)^2 + (\Delta G_0^\#)^2 \right]^{1/2} \quad (10)$$

$\Delta G_0^\#$  in equation (10) is the free energy of activation when there is no driving force for the reaction.

We have attempted to fit the  $k_q$  values obtained to the Rehm–Weller equation. To do this, values of  $\Delta G_0^\#$  and  $k_{\text{diff}}$  were required. We have assumed a value of 0.19 eV for  $\Delta G_0^\#$ . For similar systems in water a value of  $6.6 \times 10^9$  is normally used for the diffusion coefficient. The solid line in Figure 2.11 is a fit to equation (9) using these values. Notice that there is good agreement between the observed values and the calculated fit, which confirms that quenching of the CD-appended pyrene by free moving acceptors in solution, obeys the Rehm–Weller

formalism as observed for numerous other diffusion mediated quenching reactions.

Figure 2.12 is a plot of unimolecular rate constant  $k_{et}$  versus  $\Delta G^0$ . It can be seen from Figure 2.12 that as the driving force increases (i.e.,  $\Delta G^0$  becomes more negative),  $k_{et}$  increases initially, reaches a maximum, and then decreases. This is typical of Marcus type electron transfer and the data obtained fitted the Marcus equation very nicely (vide infra).

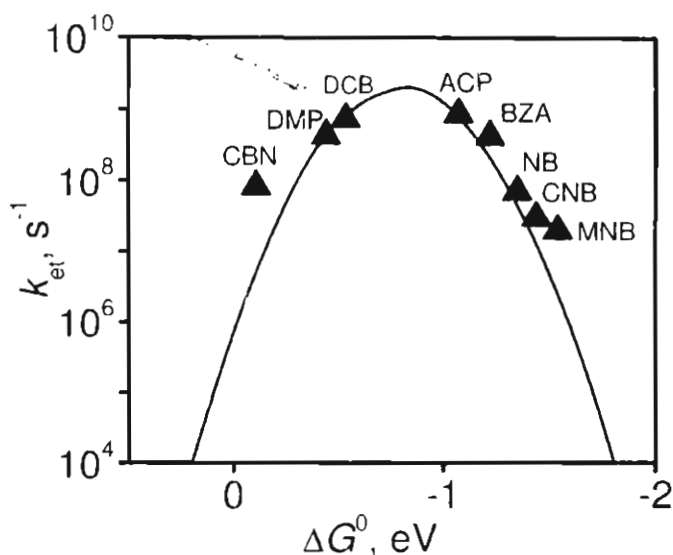


**Figure 2.12.** Plot of electron-transfer rate constant  $k_{et}$  versus  $\Delta G^0$ . The solid curve is the computed curve of equation (1).

Thus we conclude that the intra-ensemble photoinduced electron transfer between the CD-linked pyrene and encapsulated acceptors followed Marcus type behaviour. The photoinduced electron transfer in CD-appended chromophores is thus similar to those in hydrogen-bonded systems, where the unimolecular



component follows Marcus-type behaviour and the bimolecular component obeys the Rehm–Weller pattern.<sup>16</sup>

### 2.3.7. Electronic coupling and Reorganization energy

Our results show that photoinduced electron transfer in the supramolecular-CD dyads follows Marcus-type behaviour (Figure 2.12). The data in Figure 2.12 can be fitted to equation (1) to give  $H_{el}$  and  $\lambda$  values. We have attempted to fit the data to equation (1) by means of various combinations of  $H_{el}$  and  $\lambda$  and the best fit was obtained with values of  $H_{el} = 3 \text{ cm}^{-1}$  and  $\lambda = 0.8 \text{ eV}$ . The fit is shown in Figure 2.12 (solid line). Notice that there is good agreement between the observed values and the calculated fit, confirming the Marcus-type electron transfer taking place in these systems.

Although a few examples of photoinduced electron transfer in CD-appended systems are reported, values of  $H_{el}$  and  $\lambda$  have not been determined in any of these cases. Therefore, we are not able to compare our results with those in similar systems. The  $H_{el}$  values obtained are small, but similar to values reported for hydrogen-bonded donor–acceptor systems.<sup>17</sup> Considering the fact that the donor and acceptor are not linked directly and that they most probably have a through-space interaction, the low value obtained seems reasonable.

The reorganization energy  $\lambda$  obtained from the best fit is 0.8 eV.  $\lambda$  is the sum of inner shell ( $\lambda_{in}$ ) and outer shell ( $\lambda_{out}$ ) reorganization energies.  $\lambda_{out}$  is given by equation (11),<sup>18</sup> where  $\epsilon_{op}$  is the optical dielectric constant of the solvent.

$$\lambda_{out} = \Delta e^2 \left( \frac{1}{2r_P} + \frac{1}{2r_A} - \frac{1}{d} \right) \left( \frac{1}{\epsilon_{op}} - \frac{1}{\epsilon_s} \right) \quad (11)$$

This expression gave  $\lambda_{out} = 0.7$  eV for our systems. This suggested that  $\lambda_{in}$  is only 0.1 eV for these systems. This value of  $\lambda_{in}$  seems to be somewhat lower than expected. In our previous studies with hydrogen-bonded systems, we obtained  $\lambda_{in} = 0.2$  eV for similar donor-acceptor systems.<sup>16</sup> Other groups also have used  $\lambda_{in} = 0.2$  eV for small aromatic donor-acceptor systems.<sup>17a</sup> Because  $\lambda_{in}$  is solvent-insensitive, a similar value was expected here. We use the following argument to explain the low value calculated for  $\lambda_{in}$ .  $\lambda_{out}$  was obtained with equation (11), which gives  $\lambda_{out}$  expected, if both product ions are stabilized by solvation with water molecules. In the present systems, the pyrene moiety is fully exposed to water and the pyrene radical cation formed as a result of PET will be stabilized by solvation with water. However, the acceptor radical anions formed inside the  $\alpha$ -CD cavity are not exposed to water molecules and hence they may not be stabilized by solvation. Thus the actual  $\lambda_{out}$  for the present systems will be somewhat lower than the 0.7 eV obtained from equation (11). If we assume that  $\lambda_{in}$  is 0.2 eV, then  $\lambda_{out}$  will turn out to be 0.6 eV. This may be the correct picture

and based on these arguments we can suggest that encapsulation of the acceptor fragment in  $\alpha$ -CD results in a lowering of the outer shell reorganization energy by 0.1 eV (compared to that in pure water). Fukuzumi et al. reported results similar to this for photoinduced electron transfer between DNA-bound donors and intercalated acceptors.<sup>19</sup> For intramolecular photoinduced electron transfer in these systems, the reorganization energy was found to be reduced by 0.1 eV compared to that of the intermolecular process.

### 2.3.8. The Inverted Region

The most important aspect of Marcus theory was the prediction of an inverted region in electron transfer reactions. This aspect of Marcus theory was controversial from the time the theory was proposed in 1956 until John Miller's group at Argonne National Laboratory found experimental proof of it in 1986. Marcus won the Nobel Prize for Chemistry in 1992 for his contributions to the theory of electron transfer reactions in chemical systems. Though long controversial, the presence of inverted region kinetics is now well established in a large number of charge shift and charge recombination reactions.

In most of the published examples of the inverted region in intramolecular electron transfer reactions, the forward reaction is restricted to the normal region and back electron transfer restricted to the inverted region most probably due to the limited range of free energies available for these reactions. The bulk of

---

experimental observation has shown that intermolecular photoinduced charge separation reactions follow the Rehm-Weller behaviour and observation of the inverted region is restricted to thermal charge recombination or charge shift reactions. Several authors have tried to answer the question as to why the inverted region is generally not observed in PET reactions. In the following section an overview of their results is attempted.

The classical Marcus theory was reanalyzed in the 1980's to include the influence of quantum effects, notably electron tunneling.<sup>20</sup> This treatment increases the rate constant when the thermally activated process becomes slow but it was concluded that this treatment cannot account for the discrepancies of the Marcus and Rehm-Weller type plots. Because of this, the absence of the inverted region in photoinduced electron transfer reactions between neutral partners was attributed to the formation of products in the electronically excited state.<sup>21</sup> If this happens, the actual reaction free energy would be smaller by the excitation energy of the products and will be insufficient to fall within the inverted region. This hypothesis appears quite reasonable because the excitation energies of the radical products are small and these states may be accessible at large driving forces. No experimental evidence exists to prove this hypothesis. The presence of electronically excited molecular ions could in principle be ascertained by the observation of their luminescence, but this is generally very weak and beyond the

detection limit of most currently available instruments. Thus, the intermediacy of electronically excited products remains unproven but is not unreasonable.

The lack of experimental evidence for the formation of products in the excited state has prompted investigators in this area to put forward new theories to explain the absence of inverted region in photoinduced charge separation reactions. The most comprehensive and most debated among these theories is the Mataga-Kakitani (MK theory), which emphasized the role of solvent in controlling electron transfer processes in polar solvents.<sup>22</sup> This theory suggests that the difference in the Marcus and Rehm-Weller behaviour is due to the electric field which acts on the solvent. In the case of ions or ion pairs, the electric field leads to partial dielectric saturation of polar solvents and this will restrict solvent motion. Computer simulations of molecular dynamics following the Monte-Carlo method predicted dielectric saturation up to a distance of about 1 Å from the solvent molecular envelope.<sup>23</sup> In the case of neutral reactants, no such dielectric saturation would exist and the solvent motion remains unhindered resulting in the observation of diffusion controlled rate constants.

The existence of dielectric saturation is not established beyond doubt. Some authors claim that the dielectric saturation becomes important only in the neighbourhood of small ions like  $\text{Li}^+$  in water and is negligible in the solvent shell of larger molecular ions such as those involved in electron transfer reactions.<sup>24</sup> Another complication of M-K theory is that it fails to explain the observation of

the inverted region in non-polar solvents. Dielectric saturation is applicable only to polar solvents and if the M-K theory is correct, inverted region should not be observed in non-saturable solvents such as toluene. Because of all these factors, the MK theory is not considered as the right approach in understanding the difference between Marcus and Rehm-Weller behaviours.

Recently Tachiya and Murata made a distinction between the Marcus and Rehm-Weller types of electron transfers.<sup>25</sup> According to them the Marcus equation gives the first order rate constant for a donor-acceptor pair with a fixed separation, while the Rehm-Weller equation gives a second order rate constant. They have calculated the second order diffusion mediated rate constant by using a recently developed theory of diffusion mediated reactions which takes in to account the donor-acceptor distance of the first order rate constant. This theory also predicted an inverted region at very large driving forces, but this could not be verified experimentally.

Rau and co-workers have suggested that the inverted region is not observed in electron transfer reactions because of the distance dependence of electron transfer rates in the inverted region.<sup>26</sup> This can be explained as follows. In the case of freely moving molecules there will be several quencher molecules around a given probe. In this situation the distance between the probe and quenchers is not fixed but variable. In the Marcus theory, the maximum rate constant (minimum activation energy) occurs when the free energy of the reaction is equal to the

reorganization energy ( $\Delta G^0 = -\lambda$ ). For a probe-quencher system in the normal region, the maximum rate constant occurs at contact distance. For a system in the inverted region,  $\Delta G^0 < -\lambda$  at contact distance. The reorganization energy  $\lambda$ , which is the sum of outer and inner shell reorganization energies, is distance dependent and is expected to be larger at larger separation distance (this comes from the distance dependence of the outer shell reorganization energy). Hence at some particular distance apart,  $\Delta G^0 = -\lambda$  for the systems in the inverted region. The rate will be maximum at this separation distance and electron transfer will occur from this distance. Thus for systems having large driving forces, at very short distances, in particular at van der Waals contact, the free energy could bring the system within the inverted region, but electron transfer would take place at some larger distance where  $\Delta G^0 = -\lambda$  and rate is maximum. This has the effect of truncating the observed rate to the maximum value possible in a solvent, which will be equal to  $k_{diff}$  for the solvent. The inverted region will not be observed for bimolecular reactions if this situation actually exists.

We have recently studied the free energy dependence of electron transfer in a few donor-acceptor systems assembled through hydrogen bonding interactions.<sup>16</sup> Our study showed that when diffusion is prevented, the inverted region can be observed, and when diffusion of the partners is allowed, Rehm-Weller behaviour is observed. The non-observance of the inverted region in charge separation reactions is thus attributed to diffusion in the region of moderately large driving

forces. The results reported here for photoinduced electron transfer in  $\alpha$ -CD appended systems are very similar to those obtained for hydrogen-bonded systems. This confirms our suggestion that the non-observance of the inverted region in PET reactions can be attributed to diffusion limiting of the reaction rates.

It is to be mentioned here that a few reports claimed the observation of inverted region in bimolecular PET reactions.<sup>27</sup> Some of these claims were questioned later.<sup>28</sup> Recently Fukuzumi et al. carried out pulse-radiolytic studies to determine the rate constants of electron transfer from fullerenes ( $C_{60}$ ,  $C_{76}$  and  $C_{78}$ ) to a series of arene radical cations in dichloromethane solution.<sup>29</sup> The driving force dependence of  $k_{et}$  showed a pronounced decrease towards the highly exothermic region, which they claimed as the first definitive confirmation of the inverted region in truly intermolecular electron transfer reactions.

### 2.3.9. Visual demonstration of the inverted region

A very important aspect of the present study is that the raw fluorescence data obtained provide a direct visual observation of the inverted region. Figure 2.13 A-H shows the fluorescence decay profiles of **PYCD** in the presence of different acceptors arranged in the order of increasing driving force (decay curves shown in Figure 2.13 A-H are taken from decay curves presented in Figure 2.8 A-H). Values of  $\Delta G^0$  are also shown in the plots. The biexponential nature of the fluorescence decays can be distinguished by the naked eye in all cases. The intra-



ensemble PET rate constant  $k_{et}$  is obtained from the short lifetime component  $\tau_1$  as per equation (3). As  $1/\tau_1 \gg 1/\tau_0$ ,  $k_{et} \approx 1/\tau_1$ . This means that the faster the initial decay, the higher is the  $k_{et}$  value. An examination of the decay profiles in Figure 2.13 A–H reveals the following: as we proceed from A→B→C, the steepness of the initial decay component (shown in the box on the curve) increases, indicating that  $k_{et}$  increases from A→C. This corresponds to the normal region of the Marcus parabola. The steepness of the initial component is a maximum for C and D, indicating that these systems correspond to the top of the parabola.

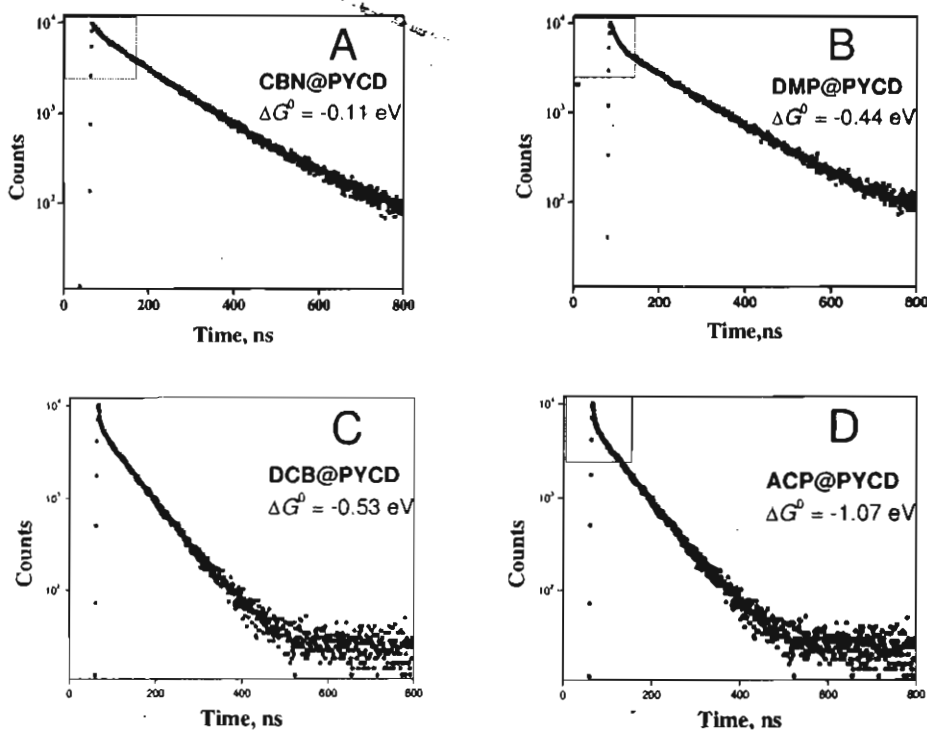
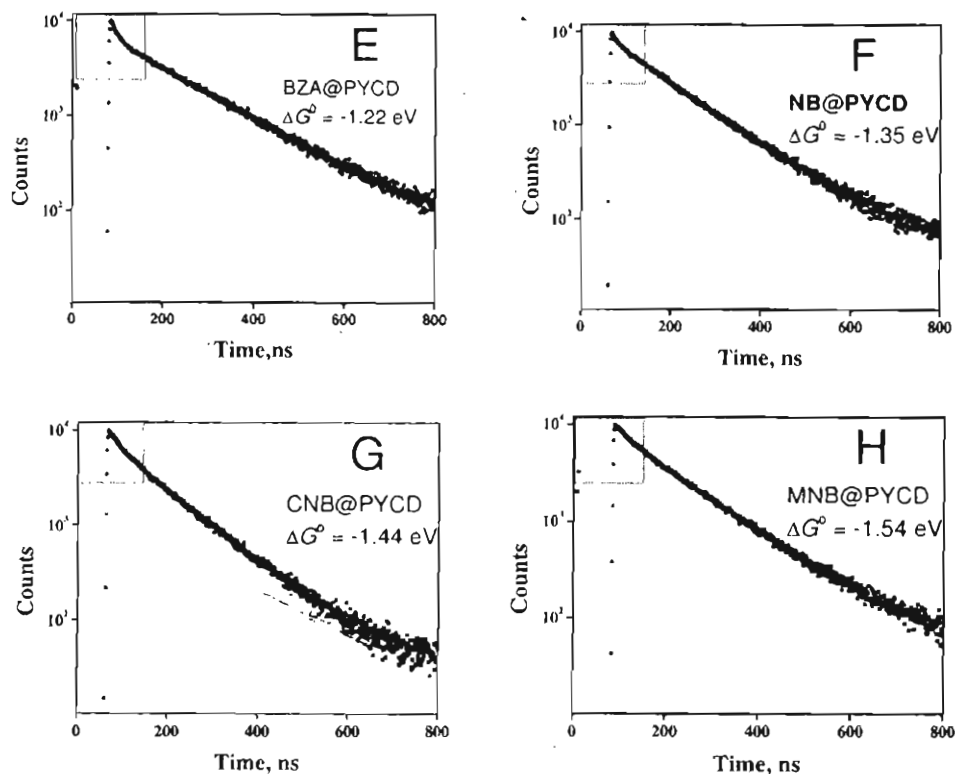


Figure 2.13 A-D. Fluorescence decay profiles of PYCD in the presence of CBN, DMP, DCB, ACP



**Figure 2.13 E-F.** Fluorescence decay profiles of PYCD in the presence of BZA, NB, CNB, MNB

As we proceed further from  $D \rightarrow E \rightarrow F \rightarrow G \rightarrow H$ , the steepness of the initial component decreases, indicating that  $k_{et}$  decreases from  $D \rightarrow H$ . This segment represents the inverted region. The experimental fluorescence profiles thus serve as a visual demonstration of the Marcus parabola in electron-transfer reactions (note that the acceptor concentrations are slightly different for the plots; however, this is immaterial because the short lifetime is independent of the acceptor concentration).

Although the inverted region is now a well-established aspect of Marcus theory, papers dealing with the observation of an inverted region in newer systems

continue to appear frequently in the current literature<sup>19,30</sup> (references 30 list only papers that have appeared in the last three years). Visual observation of the inverted region as shown here was never reported earlier.

When log (counts) is plotted against time (or channel number), bimolecular decays can be clearly distinguished by the naked eye if  $\tau_1 \ll \tau_2$ . For systems at the bottom of the Marcus parabola, both in the normal and inverted regions,  $\tau_1$  is relatively large and the differences between  $\tau_1$  and  $\tau_2$  are small. In the inverted region, diffusion-mediated quenching is maximum, and hence  $\tau_2$  decreases rapidly with quencher concentration. This leads to further decreases in the difference between  $\tau_1$  and  $\tau_2$  in the inverted region. In the hydrogen-bonded systems studied earlier,  $\tau_0 \approx 100$  ns and quencher concentrations required were in the  $(1-5) \times 10^{-3}$  M range.<sup>16</sup> Because of this, the condition that  $\tau_1 \ll \tau_2$  was achieved only for systems near the top of the Marcus parabola. In the present system with the cyclodextrin-appended pyrene,  $\tau_0$  is 204 ns and quencher concentrations employed were about ten times less. Because of this, the condition that  $\tau_1 \ll \tau_2$  was achieved for all the systems studied and this enabled a visual observation of the Marcus parabola from the raw fluorescence lifetime data. Most of the earlier observations of the inverted region actually involved thermal electron-transfer reactions, which are generally not amenable to studies by fluorescence quenching.<sup>21</sup> Thus, in these experiments, the Marcus parabola was built up from different types of

experiments, the normal region constructed on the basis of fluorescence quenching experiments and the inverted region constructed from flash photolysis or pulse radiolysis experiments. Because of this, a visual demonstration of the inverted region could not be achieved from raw data. In our previous experiments with the hydrogen-bonded systems and also in the present system, the complete Marcus parabola was constructed from photoinduced forward electron-transfer reactions. In the present case, we are able to visually demonstrate the existence of the inverted region and also the total Marcus parabola on the basis of fluorescence decay curves and this constituted a very straightforward demonstration of the inverted region.

## 2.4. Conclusions

We have studied the free-energy dependence of PET reactions between  $\alpha$ -cyclodextrin-appended pyrene and small acceptor molecules in aqueous solutions. A fraction of the acceptors associate with **PYCD**, leading to the formation of supramolecular dyads. Upon excitation, both unimolecular and diffusion-mediated electron transfers take place. The former component is attributed to electron transfer in the supramolecular dyad and this component followed the Marcus equation. The dynamic component is attributed to the freely diffusing **PYCD** and acceptors, and this component obeyed the Rehm–Weller equation. Similar to hydrogen-bonded systems, the CD-appended systems also enabled us to simultaneously observe Marcus and Rehm–Weller behaviours. The Marcus

equation was used to determine donor–acceptor coupling and the reorganization energy in the supramolecular dyad systems. Electronic coupling was found to be similar to those reported for hydrogen-bonded systems. It appears that actual  $\lambda_{\text{out}}$  values are somewhat lower than calculated values. An important success of the study is that it enabled us to visually demonstrate the whole Marcus parabola on the basis of raw fluorescence lifetime data.

## 2.5. Experimental section

### 2.5.1. General techniques

$^1\text{H}$  and  $^{13}\text{C}$  NMR spectra were recorded on a 300 MHz Bruker Avance DPX spectrometer. FT-IR spectra were recorded on a Shimadzu IRPrestige-21 FTIR spectrometer. MALDI mass spectrometry was conducted on a Perspective Biosystems Voyager DEPRO MALDI-TOF spectrometer in a matrix of  $\alpha$ -cyano-4-hydroxybenzoic acid. Absorption spectra were recorded on a Shimadzu-3101PC UV/Vis/NIR scanning spectrophotometer. Fluorescence spectra were recorded on a SPEX Fluorolog F112X spectrofluorimeter. Fluorescence lifetimes were determined with an Edinburgh Instruments FL900CD single-photon counting system and the data were analyzed by Edinburgh software.

### 2.5.2. Materials

**Synthesis of PYCD:** PYCD was synthesized by adopting a general procedure for the selective functionalization of a single primary OH of  $\alpha$ -cyclodextrin.<sup>3</sup> 1-

Bromomethylpyrene (0.3 g, 1.05 mmol) was added to a solution of  $\alpha$ -CD (1.0 g, 1.05 mmol) in 2,6-lutidine (90 mL), and the mixture was heated to 150 °C under an argon atmosphere for 3.5 h. Lutidine was then removed under vacuum, and the solid was washed several times with ethyl acetate and purified by chromatography (silica gel, methanol). The crude product was obtained in 30% yield and this was purified by repeated column chromatography over silica gel to get the pure product in less than 10% yield.  $^1\text{H}$  NMR (300 MHz,  $[\text{D}_6]$  DMSO)  $\delta$ (ppm): 3.3–3.7 (m, 36H), 4.5–4.8 (m, 13H), 5.5–5.8 (m, 12H), 7.8–8.4 (m, 9H);  $^{13}\text{C}$  NMR (75 MHz,  $[\text{D}_6]$  DMSO)  $\delta$ (ppm): 60.19, 60.68, 69.34, 71.02, 71.29, 72.23, 72.59, 73.05, 73.45, 82.22, 82.61, 102.10, 102.52, 124.02, 124.59, 124.83, 125.45, 125.96, 126.50, 127.09, 127.59, 128.51, 128.86, 130.47, 130.63, 130.75, 130.89, 131.69, 132.24; FT-IR (KBr)  $\nu_{\text{max}}$ : 1033, 1076, 1151, 1205, 1242, 1296, 1330, 1361, 1406, 1597, 1653, 2839, 2908, 2933, 3566  $\text{cm}^{-1}$ ; UV/Vis (Water): [ $\lambda_{\text{max}}$ , nm ( $\epsilon \text{M}^{-1} \text{cm}^{-1}$ ): 342 (43000)]; MS (MALDI-TOF):  $m/z$  1209.2  $[\text{M}+\text{Na}]^+$ .

**Quencher molecules:** All quencher molecules were commercial samples from Aldrich. These were purified by standard methods before use. Stock solutions of acceptors were prepared as follows: a small amount (10–20 mg) of the acceptors were stirred in water for 2 h. These were then centrifuged and filtered. Concentrations of acceptors in the solution were estimated by means of the measured extinction coefficients in acetonitrile. Solutions used for the

fluorescence lifetime experiments were deaerated by purging with argon for 20 min before use. The fluorescence lifetimes were measured with dilute solutions (OD  $\approx$  0.1 at the excitation wavelength 342 nm), and the emission was monitored at 373 nm.

## 2.6. References

- (a) Marcus, R. A.; Sutin, N. *Biochem. Biophys. Acta* **1985**, *811*, 265-322.  
(b) Marcus, R. A.; Siders, P. *J. Phys. Chem.* **1982**, *86*, 622-630. (c) Siders, P.; Marcus, R. A. *J. Am. Chem. Soc.* **1981**, *103*, 741-747.
- Suppan, P. *Top. Curr. Chem.* **1992**, *163*, 95-130 and references cited therein.
- (a) Tian, S.; Zhu, H.; Forgo, P.; D'Souza, V. T. *J. Org. Chem.* **2000**, *65*, 2624-2630. (b) Khan, A. R.; Forgo, P.; Stine, K. J.; D'Souza, V. T. *Chem. Rev.* **1998**, *98*, 1977-1996.
- (a) Makabe, A.; Kinoshita, K.; Narita, M.; Hamada, F. *Anal. Sci.* **2002**, *18*, 119-124. (b) Narita, M.; Mima, S.; Ogawa, N.; Hamada, F. *Anal. Sci.* **2001**, *17*, 379-386. (c) Hamada, F.; Narita, M.; Kinoshita, K.; Makabe, A.; Osa, T. *J. Chem. Soc., Perkin Trans. 2* **2001**, 388-394. (d) Ueno, A.; Suzuki, I.; Osa, T. *Anal. Chem.* **1990**, *62*, 2461-2466. (e) Ueno, A.; Suzuki, I.; Osa, T. *J. Am. Chem. Soc.* **1989**, *111*, 6391-6397.
- Kano, K.; Takenoshita, I.; Ogawa, T. *J. Phys. Chem.* **1982**, *86*, 1833-1838.

6. (a) Fagnoni, M.; Mella, M.; Albini, A. *J. Org. Chem.* **1998**, *63*, 4026-4033.  
(b) Mann, C. K.; Barnes, K. B. *Electrochemical Reactions in Nonaqueous Systems*; Marcel Dekker: New York, 1970.
7. (a) Zanini, G. P.; Montejano, H. A.; Previtali, C. M. *J. Chem. Soc. Faraday Trans.* **1995**, *91*, 1197-1202. (b) Julliard, M. in *Photoinduced Electron Transfer, Part B*; Fox, M. A., Channon, M., Eds.; Elsevier: New York, 1988; pp 216-313. (c) Tsuchida, A.; Yamamoto, M.; Nishijima, Y. *J. Phys. Chem.* **1984**, *88*, 5062-5064. (d) Baggot, J. E.; Pilling, M. J. *J. Chem. Soc. Faraday Trans. 1* **1983**, *79*, 221-234. (e) Hino, T.; Akazawa, H.; Masuhara, H.; Mataga, N. *J. Phys. Chem.* **1976**, *80*, 33-37.
8. (a) Liu, L.; Guo, Q.-X. *J. Phys. Chem. B* **1999**, *103*, 3461-3467. (b) Rekharsky, M. V.; Inoue, Y. *Chem. Rev.* **1998**, *98*, 1875-1918. (c) Connors, K. A.; Pendergast, D. D. *J. Am. Chem. Soc.* **1984**, *106*, 7607-7614.
9. Park, J. W.; Song, H. E.; Lee, S. Y. *J. Phys. Chem. B* **2002**, *106*, 7186-7192.
10. Lakowicz, J. R. in *Principles of Fluorescence Spectroscopy*; Kluwer Academic: Dordrecht, 1999.
11. de Rege, P. J. F.; Williams, S. A.; Therien, M. J. *Science* **1995**, *269*, 1409-1413.
12. Kavarnos, G. J. *Fundamentals of Photoinduced Electron Transfer*; VCH: New York, 1993; p 62.



13. AM1 calculations of the molecular length were carried out using Titan Version 1 from Wavefunction Inc.; 18401, Von Karman, Suite 370, Irvine, CA 92612.
14. (a) Rehm, D.; Weller, A. *Ber. Bunsen-Ges. Phys. Chem.* **1969**, *73*, 834-839.  
(b) Rehm, D.; Weller, A. *Isr. J. Chem.* **1970**, *8*, 259-271.
15. (a) Nagle, J. K.; Dressick, W. J.; Meyer, T. J. *J. Am. Chem. Soc.* **1979**, *101*, 3993-3995. (b) Breymann, U.; Dreeskamp, H.; Koch, E.; Zander, M. *Chem. Phys. Lett.* **1978**, *59*, 68-70. (c) Martens, F. M.; Verhoeven, J. W.; Gase, R. A.; Pandit, U. K.; Boer, T. J. *Tetrahedron* **1978**, *34*, 443-446. (d) Bock, C. R.; Meyer, T. J.; Whitten, D. G. *J. Am. Chem. Soc.* **1975**, *97*, 2909-2911.
16. (a) Smitha, M. A.; Prasad, E.; Gopidas, K. R. *J. Am. Chem. Soc.* **2001**, *123*, 1159-1165. (b) Prasad, E.; Gopidas, K. R. *J. Am. Chem. Soc.* **2000**, *122*, 3191-3196.
17. (a) Ghaddar, T. H.; Castner, E. W.; Isied, S. S. *J. Am. Chem. Soc.* **2000**, *122*, 1233-1234. (b) Williamson, D. A.; Bowler, B. E. *J. Am. Chem. Soc.* **1998**, *102*, 10902-10911.
18. (a) Marcus, R. A. *Annu. Rev. Phys. Chem.* **1964**, *15*, 155-196. (b) Marcus, R. A. *J. Chem. Phys.* **1956**, *24*, 966-978.
19. (a) Fukuzumi, S.; Tanaka, M.; Nishimine, M.; Ohkubo, K. *J. Photochem. Photobiol. A: Chem.* **2005**, *175*, 79-81. (b) Fukuzumi, S.; Nishimine, M.;

- Ohkubo, K.; Tkachenko, N. V.; Lemmetyinen, H. *J. Phys. Chem. B* **2003**, *107*, 12511-12518.
20. Siders, P.; Marcus, R. A. *J. Am. Chem. Soc.* **1981**, *103*, 748-752.
21. Suppan, P. in *Topics in Current chemistry, Vol. 163*; Mattay, J., Ed.; Springer Verlag: Berlin, 1992; p 94.
22. (a) Kakitani, T.; Mataga, N. *J. Phys. Chem.* **1986**, *90*, 993-995. (b) Kakitani, T.; Mataga, N. *Chem. Phys.* **1985**, *93*, 381-397.
23. Hatono, Y.; Saito, M.; Kakitani, T.; Mataga, N. *J. Phys. Chem.* **1988**, *92*, 1008-1010.
24. Heinziger, K.; Palinkas, G. *Stud. Phys. Theor. Chem.* **1985**, *38*, 313.
25. Tachiya, M.; Murata, S. *J. Phys. Chem.* **1992**, *96*, 8441-8444.
26. (a) Greiner, G.; Pasquine, P.; Weiland, R.; Orthwein, H.; Rau, H. *J. Photochem. Photobiol. A : Chem.* **1990**, *51*, 179-195. (b) Rau, H.; Frank, R.; Greiner, G. *J. Phys. Chem.* **1986**, *90*, 2476-2481.
27. (a) Thanasekaran, P.; Rajendran, T.; Rajagopal, S.; Srinivasan, C.; Ramaraj, R.; Ramamurthy, P.; Venkatachalapathy, B. *J. Phys. Chem. A* **1997**, *101*, 8195-8199. (b) Turró, C.; Zaleski, J. M.; Karabatsos, Y. M.; Nocera, D. G. *J. Am. Chem. Soc.* **1996**, *118*, 6060-6067 (c) Ishiguro, K.; Nakano, T.; Shibata, H.; Sawaki, Y. *J. Am. Chem. Soc.* **1996**, *118*, 7255-7264.

- 
28. (a) Yokoi, H.; Morrizumi, S.; Ishiguro, K.; Sawaki, Y. *J. Photochem. Photobiol. A* **1999**, *125*, 39-46. (b) Li, C.; Hoffman, M. Z. *J. Phys. Chem. A* **1998**, *102*, 6052-6053.
29. Fukuzumi, S.; Ohkubo, K.; Imahori, H.; Guldi, D. M. *Chem. Eur. J.* **2003**, *9*, 1585-1593.
30. (a) Vail, S. A.; Krawczuk, P. J.; Guldi, D. M.; Palkar, A.; Echegoyen, L.; Tomé, J. P. C.; Fazio, M. A.; Schuster, D. I. *Chem. Eur. J.* **2005**, *11*, 3375-3388. (b) Rajkumar, G. A.; Sandanayaka, A. S. D.; Ikeshita, K.-i.; Itou, M.; Araki, Y.; Furusho, Y.; Kihara, N.; Ito, O.; Takata, T. *J. Phys. Chem. A* **2005**, *109*, 2428-2435. (c) Liddell, P. A.; Kodis, G.; Kuciauskas, D.; Andréasson, J.; Moore, A. L.; Moore, T. A.; Gust, D. *Phys. Chem. Chem. Phys.* **2004**, *6*, 5509-5515. (d) Ramos, A. M.; Beckers, E. H. A.; Offermans, T.; Meskers, S. C. J.; Janssen, R. A. J. *J. Phys. Chem. A* **2004**, *108*, 8201-8211. (e) Beckers, E. H. A.; Meskers, S. C. J.; Schenning, A. P. H. J.; Chen, Z.; Würthner, F.; Janssen, R. A. J. *J. Phys. Chem. A* **2004**, *108*, 6933-6937. (f) Sutton, L. R.; Scheloske, M.; Pirner, K. S.; Hirsch, A.; Guldi, D. M.; Gisselbrecht, J.-P. *J. Am. Chem. Soc.* **2004**, *126*, 10370-10381. (g) Schuster, D. I.; Cheng, P.; Jarowski, P. D.; Guldi, D. M.; Luo, C.; Echegoyen, L.; Pyo, S.; Holzwarth, A. R.; Braslavsky, S. E.; Williams, R. M.; Klihm, G. *J. Am. Chem. Soc.* **2004**, *126*, 7257-7270. (h) Chakraborty, A.; Chakrabarty, D.; Hazra, P.; Seth, D.; Sarkar, N. *Chem. Phys. Lett.* **2004**,

387, 517-517. (i) Kumbhakar, M.; Nath, S.; Mukherjee, T.; Pal, H. *J. Chem. Phys.* **2004**, *120*, 2824-2834. (j) Worrall, D. R.; Kirkpatrick, I.; Williams, S. L. *Photochem. Photobiol. Sci.* **2004**, *3*, 63-70. (k) Yamanaka, K.; Fujitsuka, M.; Araki, Y.; Ito, O.; Aoshima, T.; Fukushima, T.; Miyashi, T. *J. Phys. Chem. A* **2004**, *108*, 250-256. (l) Thomas, K. G.; Biju, V.; Kamat, P. V.; George, M. V.; Guldi, D. M. *Chem. Phys. Chem.* **2003**, *4*, 1299-1307. (m) Sun, P.; Li, F.; Chen, Y.; Zhang, M.; Zhang, Z.; Gao, Z.; Shao, Y. *J. Am. Chem. Soc.* **2003**, *125*, 9600-9601. (n) Chakraborty, A.; Chakrabarty, D.; Hazra, P.; Seth, D.; Sarkar, N. *Chem. Phys. Lett.* **2003**, *382*, 508-517. (o) Guldi, D. M.; Hirsch, A.; Scheloske, M.; Dietel, E.; Troisi, A.; Zerbetto, F.; Prato, M. *Chem. Eur. J.* **2003**, *9*, 4968-4979. (p) Yasuda, M.; Kojima, R.; Tsutsui, H.; Utsunomiya, D.; Ishii, K.; Jinnouchi, K.; Shiragami, T.; Yamashita, T. *J. Org. Chem.* **2003**, *68*, 7618-7624. (q) Kumbhakar, M.; Nath, S.; Pal, H.; Sapre, A. V.; Mukherjee, T. *J. Chem. Phys.* **2003**, *119*, 388-399. (r) Guldi, D. M.; Luo, C.; Kotov, N. A.; Da Ros, T.; Bosi, S.; Prato, M. *J. Phys. Chem. B* **2003**, *107*, 7293-7298. (s) Fujitsuka, M.; Tsuboya, N.; Hamasaki, R.; Ito, M.; Onodera, S.; Ito, O.; Yamamoto, Y. *J. Phys. Chem. A* **2003**, *107*, 1452-1458. (t) Fukuzumi, S. *Org. Biomol. Chem.* **2003**, *1*, 609-620. (u) Fukuzumi, S.; Ohkubo, K.; Imahori, H.; Guldi, D. M. *Chem. Eur. J.* **2003**, *9*, 1585-1593.

## Chapter 3

---

### Self-Assembly and Photoinduced Electron Transfer Processes in a $\beta$ -Cyclodextrin-Appended Anthracene - Pyromellitic Diimide Dyad System

---

#### 3.1. Abstract

*An anthracene appended  $\beta$ -cyclodextrin (ANCD) and a pyromellitic diimide derivative (PMDI) were synthesized and characterized. Self-assembly of these molecules into a supramolecular dyad was studied by means of various techniques. Our studies suggested that PMDI is encapsulated in the CD cavity with the aromatic part at the centre and the 2-propyl end at the narrower rim, among the overhanging primary OH groups, and the N-ethylpyridinium end situated at the wider rim exposed to water. Photoinduced electron transfer (PET) in the system was studied by fluorescence quenching and laser flash photolysis techniques. At  $[PMDI] < 10^{-4}$  M, the equilibrium is in favour of the free molecules, and under these conditions fluorescence quenching is negligible and diffusion mediated electron transfer involving the triplet excited state of anthracene predominates. At higher concentrations of PMDI, the equilibrium is largely in favour of the supramolecular dyad and intra-ensemble PET processes predominate. The experimentally determined electron-transfer rate constant*

---

*agrees very well with that calculated by using the Marcus equation. It was observed that a fraction of the ion pairs survived for more than 200  $\mu$ s.*

### 3.2. Introduction

In Chapter 2 of the thesis we have presented a study of the free energy dependence of electron transfer in Cyclodextrin-based donor-acceptor systems. This study has established that electron transfer between a CD-appended chromophore and encapsulated guest is adequately described by the Marcus theory. This enabled us to determine the electronic coupling between the CD-appended chromophore and encapsulated guest molecules. This study has, for the first time, revealed that ~~the~~ encapsulation process leads to a reduction in the solvent reorganization energy for the electron transfer reaction. It is now possible to predict the rates of PET reaction in CD-based systems with reasonable accuracy based on knowledge of  $\Delta G^0$  and  $\lambda$  values.

A very important objective of PET studies is the conversion of solar energy into usable chemical potential.<sup>1</sup> This is possible only if the products of the PET reaction, namely the radical cation of the donor and radical anion of the acceptor, are long-lived and formed with high quantum efficiency.<sup>2</sup> Steady state and time-resolved fluorescence experiments carried out in Chapter 2 of this thesis give information only about the rates of PET reactions and do not provide any information about the fate of the charge separated (CS) state. Detection and monitoring of the radical cation and radical anion products are essential follow up

steps in PET studies. Laser flash photolysis studies, which could provide information about the yields and lifetimes of transient intermediates, are very useful in this context.

We have subjected the systems described in Chapter 2 to laser flash photolysis, but encountered a few difficulties in that process. (1) The pyrene chromophore, which acts as the sensitizer and donor in the study, has practically no absorption in the two laser wavelengths (355 and 532 nm) available in our laboratory. **PYCD** could be excited using 355 nm laser light, but this required very high concentration of **PYCD**. (2) Radical anions of acceptor molecules employed in the study had very weak absorption and are very difficult to observe in the flash photolysis experiments. (3) Association constants for **PYCD**-acceptor systems were low and this has necessitated the use of very high acceptor concentrations. Thus for the laser flash photolysis experiments, high concentrations of **PYCD** and acceptors were used. Under these conditions we could not distinguish between radical ions formed through unimolecular and bimolecular pathways. In fact this is a problem associated with all types of noncovalently bonded donor-acceptor systems, where a dynamic equilibrium exists between the free and complexed forms. In the natural photosynthetic system the donors and acceptors are kept at fixed distance and the diffusion component is absent. In synthetic systems the diffusion component always exists. We propose that the diffusion component could be minimized by adopting two strategies: (1) Increase the association

constant for complex formation and (2) employ low concentration of the sensitizer and higher concentrations of quenchers so as to push the equilibrium to the side of the complex. Under these conditions all the sensitizer molecules are complexed in the ground state and upon excitation the intra-ensemble processes would be favoured over the intermolecular processes.

The present chapter deals with the design and study of a CD-based PET system wherein we addressed some of these issues. The pyrene chromophore was replaced by an anthracene (AN) unit, which can be easily excited using the 355 nm laser light. Association constants are generally lower for  $\alpha$ -CD and hence we replaced it by a  $\beta$ -CD. It is known that association constants are higher if the guest fits tightly in to the CD cavity.<sup>3</sup> We have probed the association process between  $\beta$ -CD and several commonly employed acceptor molecules and found that pyromellitic diimides (PMDI) fit the  $\beta$ -CD cavity rather tightly and the association constants are reasonably high. The radical anion of PMDI has good absorption around 700 nm and hence this acceptor is well suited for laser flash photolysis studies.

The present chapter describes the self-assembly of a  $\beta$ -CD based supramolecular dyad, wherein an anthracene (AN) moiety covalently attached to the smaller rim of  $\beta$ -CD acts as the donor and a pyromellitic diimide (PMDI) derivative encapsulated within the  $\beta$ -CD cavity acts as the acceptor. Anthracene



attached  $\beta$ -CD is designated here as ANCD. Self-assembly of the dyad was studied by absorption, fluorescence and  $^1\text{H}$  NMR spectroscopy, and by circular dichroism and cyclic voltammetry (CV). PET reactions in the supramolecular dyad were studied by fluorescence quenching and laser flash photolysis. Our results suggest that the design of the supramolecular dyad can result in the formation of a long-lived charge-separated (CS) state in moderate yield. Structures of ANCD and PMDI are shown in Chart 3.1. This chart also shows the structures of (9-anthrylmethyl)triethyl ammonium chloride (AMTAC) and adamantyl-ammonium chloride (ADAC), which served as control systems in some of the experiments.

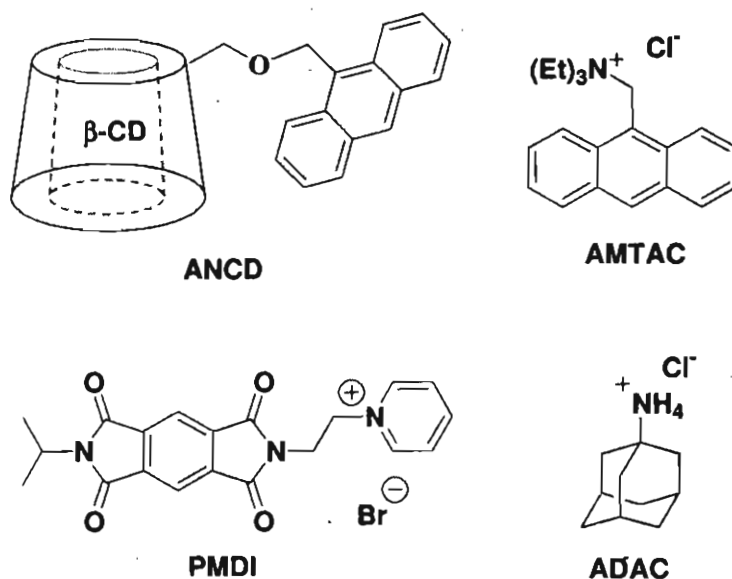
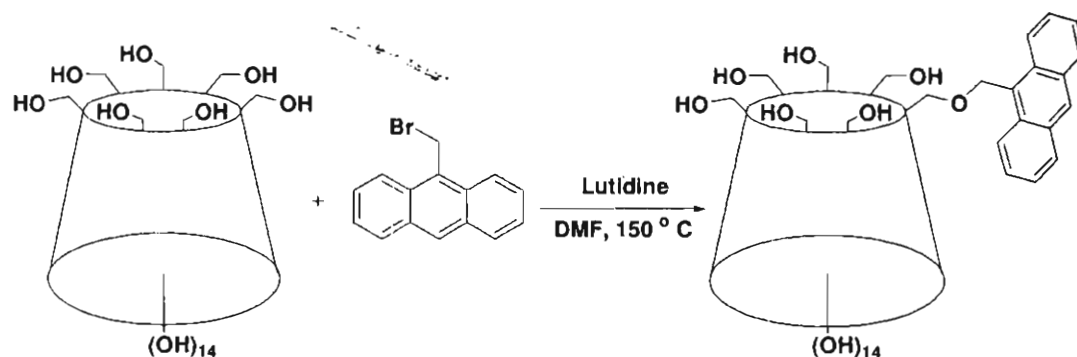


Chart 3.1. Structure of molecules employed.

### 3.3. Results and Discussion

#### 3.3.1. Synthesis and Characterization of ANCD and PMDI

**ANCD** was synthesized by adapting a well-known strategy developed for the selective functionalization of the narrower rim of CDs (Scheme 3.1). A similar method was employed in Chapter 2 for the synthesis of **PYCD**. The crude product was obtained in about 30% yield and this was purified by repeated column chromatography over silica gel. Yield of pure **ANCD** was < 10%.



**Scheme 3.1.** Synthesis of **ANCD**.

The structure of **ANCD** is assigned based on spectral evidence. The MALDI-TOF mass spectrum of **ANCD** (Figure 3.1), for example, showed a peak at  $m/z$ : 1325, which corresponded to  $[\text{ANCD}+\text{H}]^+$ . The peak corresponding to native  $\beta$ -CD was not observed in the MALDI-TOF spectrum.

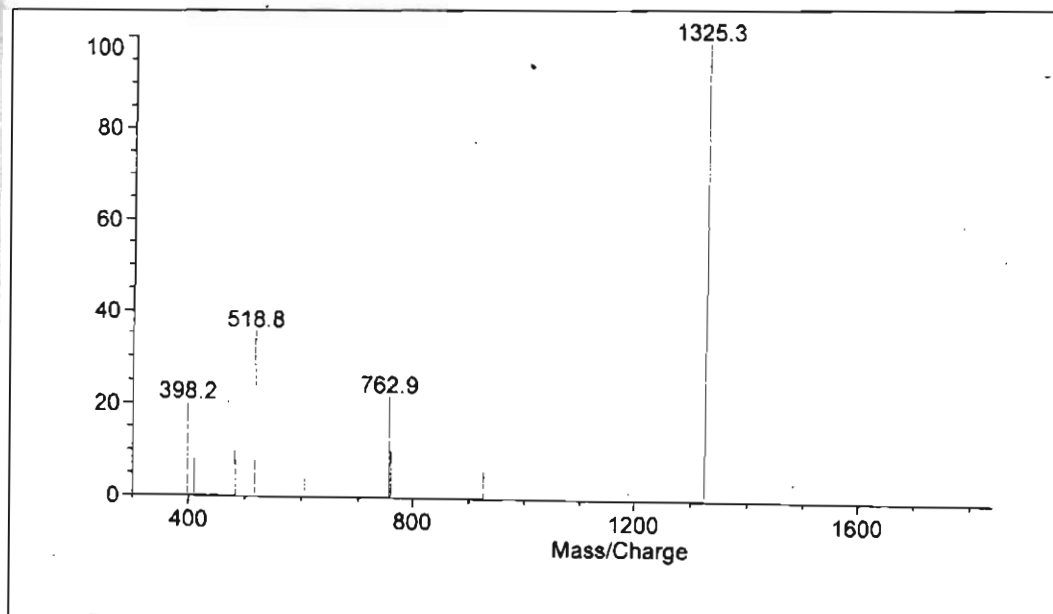


Figure 3.1. MALDI-TOF Spectrum of ANCD.

The  $^1\text{H}$  NMR spectrum of ANCD exhibited peaks due to the  $\beta$ -CD part at  $\delta = 3.2\text{--}5.7$  ppm and the aromatic residue at  $\delta = 7.5\text{--}8.6$  ppm as shown in Figure 3.2. The peaks in the range  $\delta 5.4\text{--}5.7$  are due to 2-OH and 3-OH,  $\delta 4.4\text{--}4.8$  are due to 6-OH and 1-H and all the remaining protons of the CD group appeared in the  $\delta 3.2\text{--}3.8$  region.

The regiochemistry of ANCD was assigned based on a comparison of the  $^{13}\text{C}$  NMR chemical shifts (Figure 3.3) with those reported for similar compounds and also based on our own experience with PYCD reported in Chapter 2.

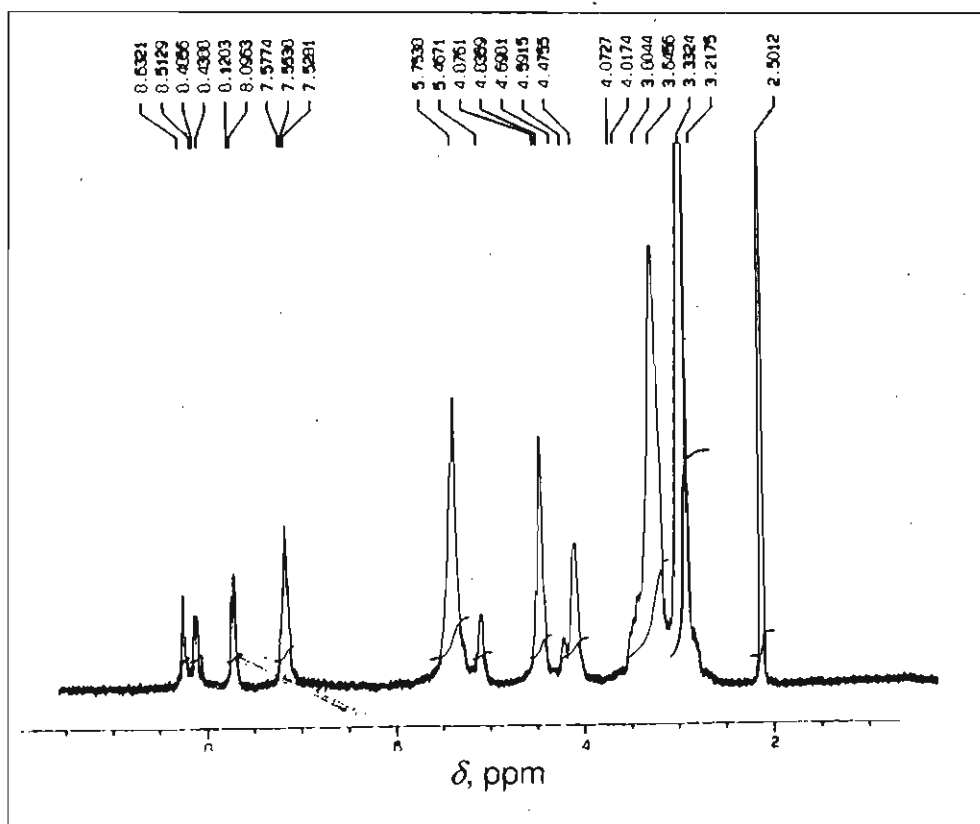


Figure 3.2.  $^1\text{H}$  NMR spectrum of ANCD.

$\beta$ -CD has seven glucose units and in monosubstituted  $\beta$ -CD systems, the  $^{13}\text{C}$  NMR chemical shifts of six of the glucose units remain relatively unaffected by the substitution. The  $^{13}\text{C}$  NMR chemical shifts of the AN-attached glucose unit are expected to be modified as described in Chapter 2. The  $^{13}\text{C}$  NMR spectrum of ANCD exhibited six intense signals and eight small peaks in the carbohydrate region.

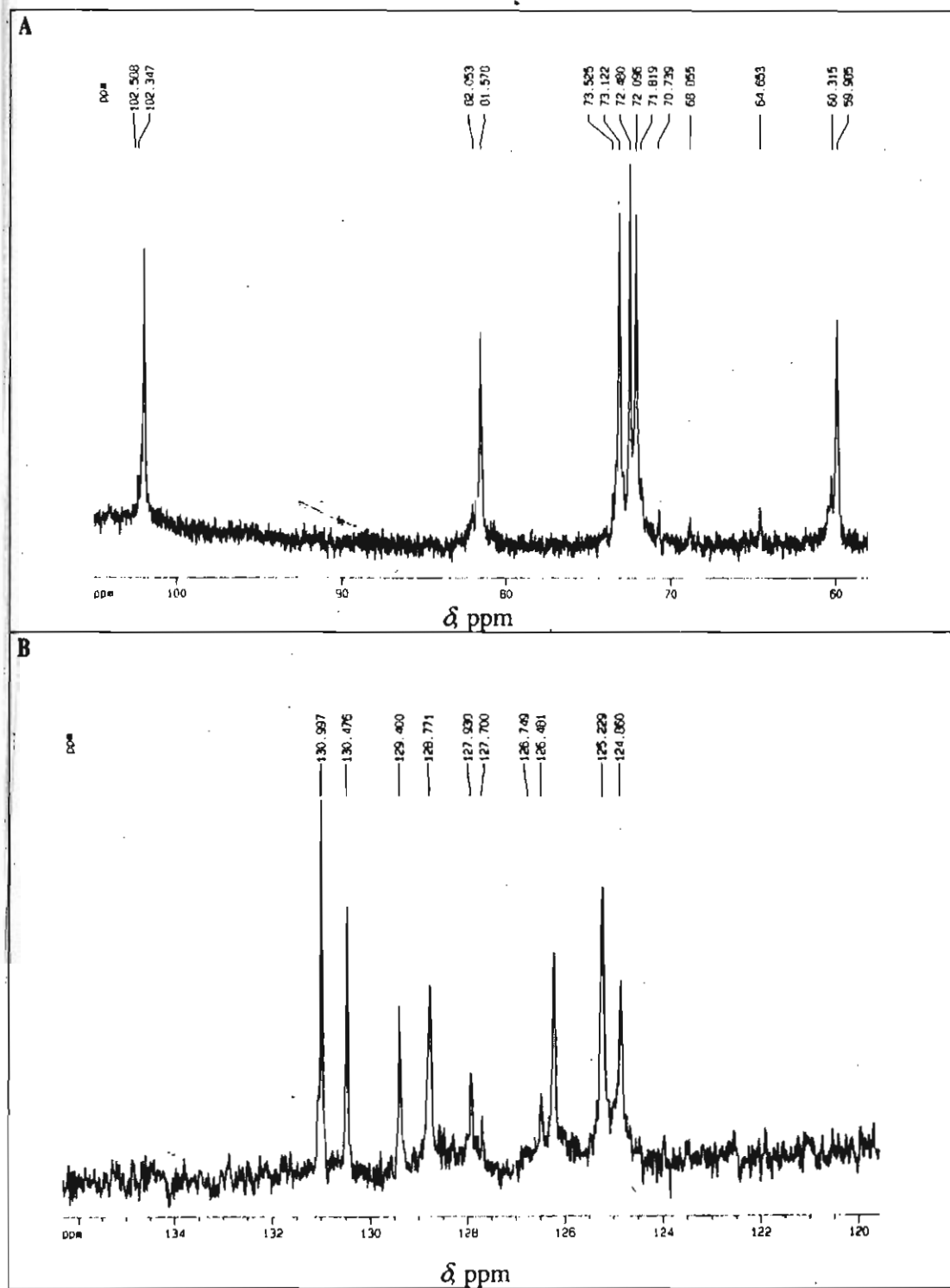
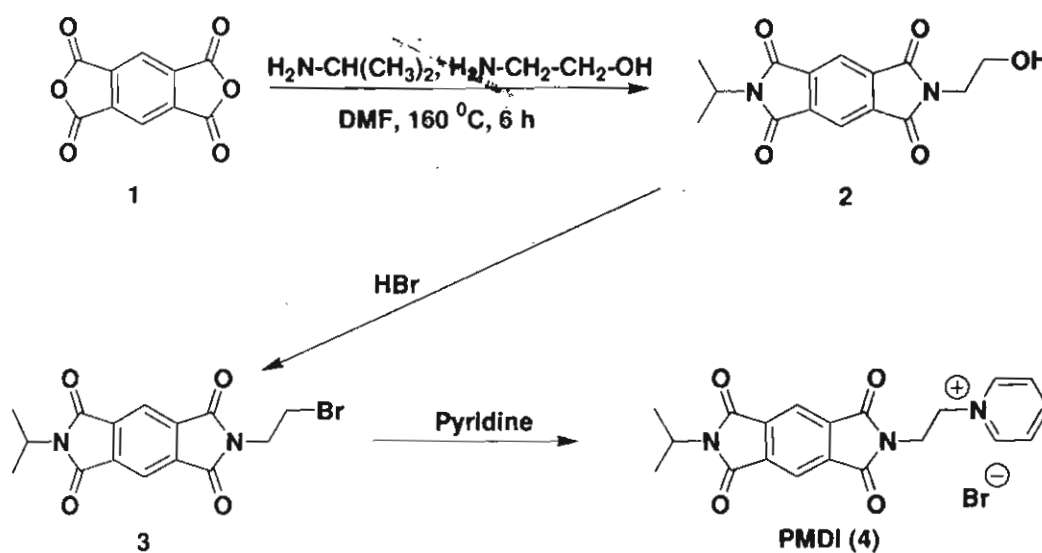


Figure 3.3.  $^{13}\text{C}$  NMR spectrum of ANCD. (A) Cyclodextrin part (B) Aromatic Part.

Based on a comparison with the literature, the six intense signals are assigned to those in the six unsubstituted glucose rings at  $\delta = 102.34$  (C1), 81.57 (C4), 73.12 (C3), 72.48 (C5), 72.09 (C2) and 59.98 ppm (C6). The small peak at  $\delta = 64.65$  ppm is assigned to the  $\text{CH}_2$  group attached to **AN**. Six of the remaining seven peaks must be due to the six carbon atoms in the **AN**-attached glucose ring. Of these, the peak at  $\delta = 68.85$  ppm is assigned to the C6 carbon and this signal is  $\delta = 8.87$  ppm downfield from the normal value because of attachment to the **AN** residue. The other signals were: C5 at  $\delta = 70.73$  (1.75 upfield), C4 at 82.05 (0.48 downfield), C3 at 73.52 (0.4 downfield), C2 at 71.8 (0.29 upfield) and C1 at 102.58 ppm (0.24 ppm downfield). As the C6 signal is shifted by nearly  $\delta = 9$  ppm and C5 is shifted by  $\delta = 1.75$  ppm, we confirm that the **AN** moiety is attached to the C6 carbon atom, which is on the narrower rim of  $\beta$ -CD. A small signal at  $\delta = 60.31$  ppm remains unaccounted. We assign this to the C6 carbon atoms of the glucose units adjacent to the one to which **AN** is attached. (When a relatively large molecule like **AN** is attached to the narrower rim of  $\beta$ -CD, the  $\text{CH}_2\text{OH}$  groups projecting out of the narrower rim may experience steric crowding. This effect may be more on adjacent glucose rings and hence their chemical shifts may be affected. A similar situation was encountered in Chapter 2 of this thesis, while assigning  $^{13}\text{C}$  NMR shifts of **PYCD**).

PMDI was synthesized by adapting a standard procedure (Scheme 3.2).<sup>4</sup> Pyromellitic dianhydride (**1**) was treated with both the amines to give the disubstituted derivative **2** in 30% yield. **2** was then converted into the bromo derivative **3** in 65% yield, by treatment with aqueous HBr. The water-soluble pyridinium derivative **4** was obtained in 73% yield by refluxing **3** in pyridine for 12 h. The final product and intermediates are completely characterized by <sup>1</sup>H, <sup>13</sup>C, IR and HRMS.

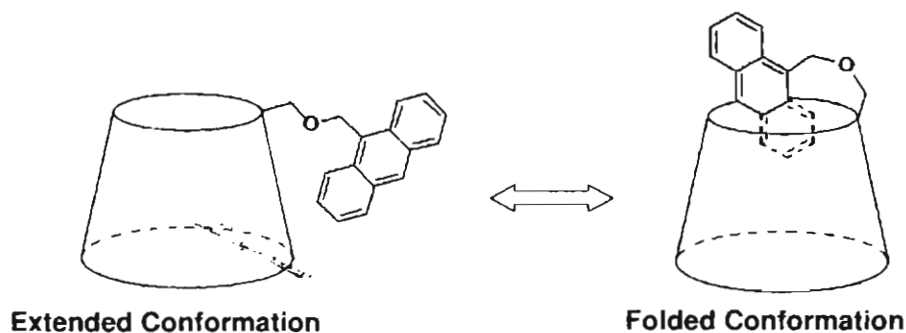


Scheme 3.2

### 3.3.2. Photophysical Properties and Conformation of ANCD

ANCD has an anthracene unit attached to  $\beta$ -CD. The AN moiety acts as the sensitizer and donor. The role of  $\beta$ -CD is to encapsulate the acceptor and bring about the D-A assembly. Determination of actual conformation of ANCD is very

important in this context. The conformation is expected to be in between the two extremes, namely, 1) an extended conformation in which the AN moiety is fully stretched out into solution and 2) a folded conformation in which the AN moiety is folded back, so as to become encapsulated fully or partially in the CD cavity as shown in Scheme 3.3.



**Scheme 3.3.** Scheme showing the extreme conformations of **ANCD**.

In the extended conformation, the AN residue is fully exposed to water and the spectral characteristics are expected to be similar to those of a water-soluble AN derivative, such as **AMTAC**. Figure 3.4 A shows the absorption spectra of **ANCD** and **AMTAC** in water. The absorption spectrum of AN in the relatively non-polar solvent THF (**AN/THF**) is also shown for comparison. The emission spectra of **ANCD** and **AMTAC** in water and AN in THF are compared in Figure 3.4 B. The absorption spectra are characterized by four vibrational bands. The vibrational band maxima in **ANCD** (334, 350, 368 and 388 nm) are in between the values for **AN/THF** (326, 342, 360 and 379 nm) and **AMTAC** in water (338, 355, 373 and 393 nm).



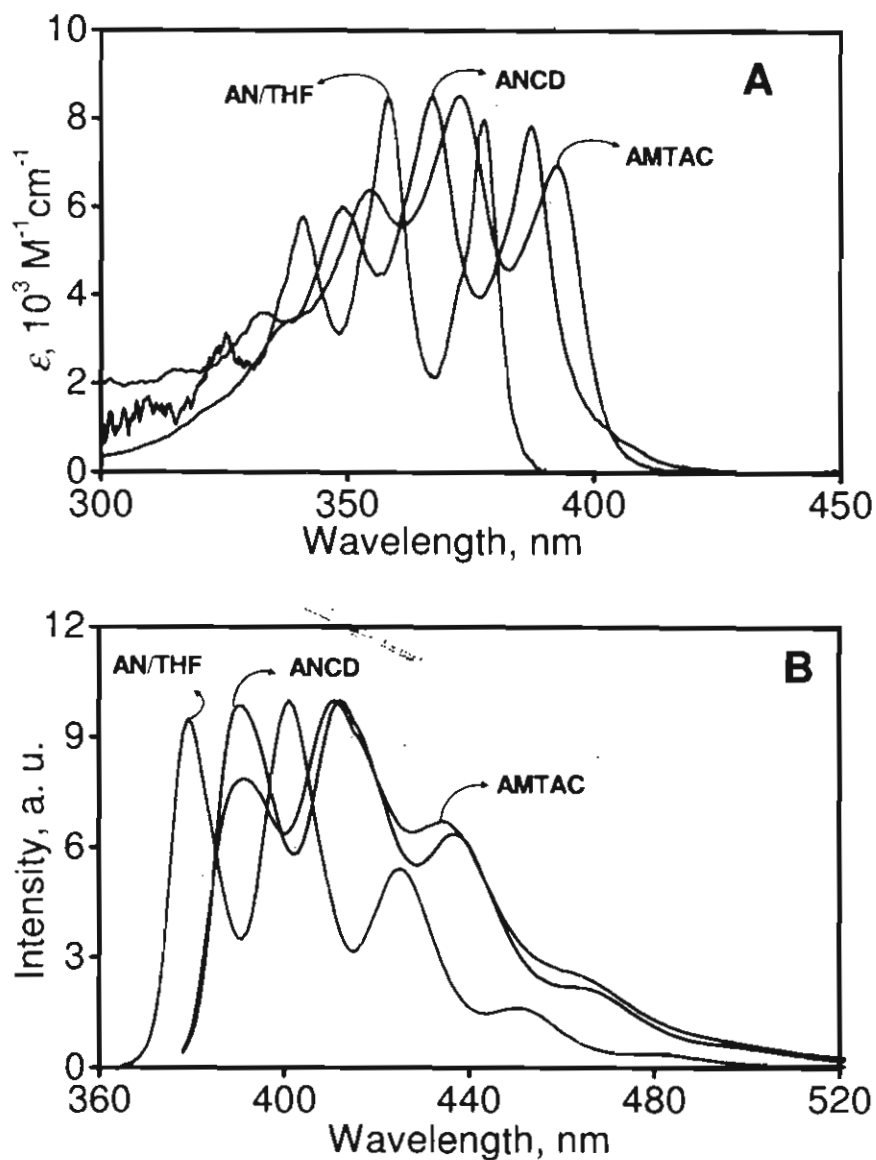


**Figure 3.4.** A) Absorption and B) emission spectra of **AN** in THF (---), **ANCD** in water (—) and **AMTAC** in water (—).

When the emission band maxima are compared, **ANCD** (391, 412, 436 and 468 nm) appears closer to **AMTAC** in water (392, 411, 435 and 466 nm) than to **AN/THF** (382, 402, 373 and 453 nm). The band shapes, however, exhibited some

difference. For example, the intensities of the first and second emission bands are comparable in **ANCD** and **AN/THF**. In **AMTAC** the first band is lower in intensity. Thus, the absorption and emission spectra suggest that the **AN** residue in **ANCD** is not fully exposed to water.

Circular dichroism spectroscopy was employed to obtain further insight into the conformation of **ANCD**. Achiral molecules included in the CD cavity or attached to the rim of the CD often exhibit induced circular dichroism (ICD) spectra, the sign and intensity of which are very sensitive to the orientation of the achiral molecule. The orientation is usually deduced from ICD spectra by using the rules derived for ICD of chiral supramolecular systems, which were initially derived for CD complexes<sup>5</sup> and then generalized for complexes of chiral macrocycles.<sup>6</sup> The rules predict the following: 1) The sign of ICD is positive for a transition polarized parallel to the axis of the macrocyclic host and negative for that polarized perpendicular to the axis. 2) The sign of ICD is reversed when a chromophore moves from the inside of the host cavity to the outside, while keeping the direction of the transition moment unchanged. 3) The absolute value of ICD is greater when a chromophore exists on the outside of the narrower rim than when it is on the outside of the wider rim. 4) The ICD value of a transition polarized perpendicular to the axis of a macrocycle is -1/2 of that of a parallel-polarized one and the sign of ICD changes at 54.7°. These rules were successfully applied for the conformational analysis of several CD-appended chromophores.<sup>7</sup>

The long-wavelength absorption of **AN** in the 300–400 nm region is polarized along its short axis.<sup>8</sup> The length of the **AN** molecule is larger than the diameter of  $\beta$ -CD, and hence **AN** can enter the  $\beta$ -CD cavity only with its long axis parallel to the  $\beta$ -CD axis as shown in the folded conformation of Scheme 3.3. In this conformation, the transition moment of the 300–400 nm absorption would be perpendicular to the  $\beta$ -CD axis and one would expect a negative ICD signal. It should be noted that **AN** is attached to  $\beta$ -CD at the 9-position, and this makes it difficult for complete inclusion of the **AN** moiety within the cavity.

**ANCD** in water exhibits a weak negative ICD signal in the 300–400 nm region as shown in Figure 3.5. The ICD signal was independent of concentration, suggesting that the signal is due to an intramolecular process. Intermolecular processes such as inclusion of the **AN** part of one molecule into the  $\beta$ -CD part of another molecule can thus be ruled out.

According to rules 1 and 2 above, negative ICD can result from two orientations: 1) The **AN** moiety is included within the  $\beta$ -CD cavity with its long axis parallel to the  $\beta$ -CD axis. 2) The **AN** moiety is held outside the cavity with its long axis perpendicular to the  $\beta$ -CD axis. In order to make a distinction between these two possibilities, the ICD of **ANCD** was recorded in the presence of **ADAC**. **ADAC** has a high affinity for encapsulation in  $\beta$ -CD ( $K_a=1.1 \times 10^5 \text{ M}^{-1}$ ).<sup>9</sup>

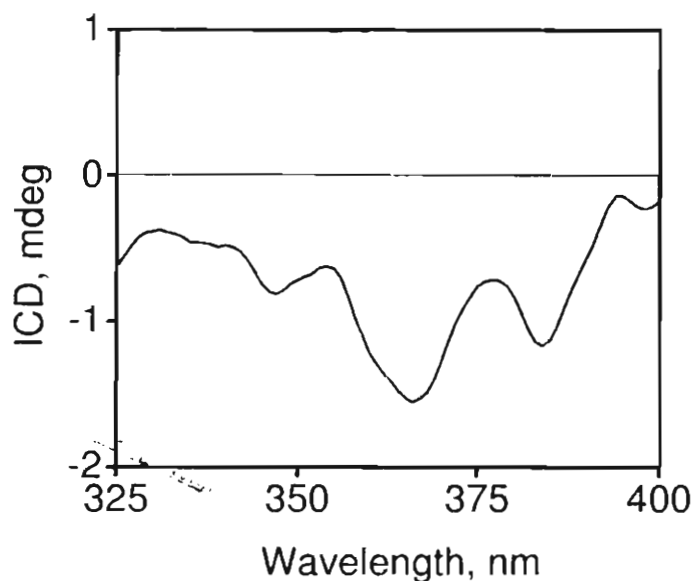
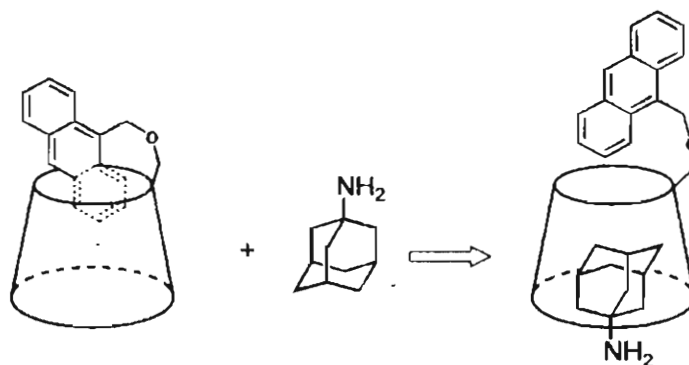


**Figure 3.5.** ICD spectrum of **ANCD** ( $1.2 \times 10^{-4}$  M) in water.

If the **AN** residue is inside the  $\beta$ -**CD** cavity, **ADAC** is expected to displace it to the outside as shown in Scheme 3.4, leading to a reversal in the sign of the ICD signal.



**Scheme 3.4.** Scheme showing the displacement of anthracene from the  $\beta$ -**CD** cavity upon the addition of **ADAC**.

If the **AN** residue is residing outside the cavity, encapsulation of **ADAC** is not expected to affect its orientation. When **ADAC** was added to **ANCD** solution, the

positive ICD spectrum shown in Figure 3.6 was obtained. **ADAC** has no absorption in this region and hence is not expected to contribute to the ICD signal. We propose that **ANCD** exists in a conformation in which the **AN** moiety is partially encapsulated in  $\beta$ -CD with the long axis nearly parallel to the  $\beta$ -CD axis (angle between the two axes  $< 54.78^\circ$ ) and when **ADAC** is added, it is displaced to the outside of the smaller rim as shown in Scheme 3.4.

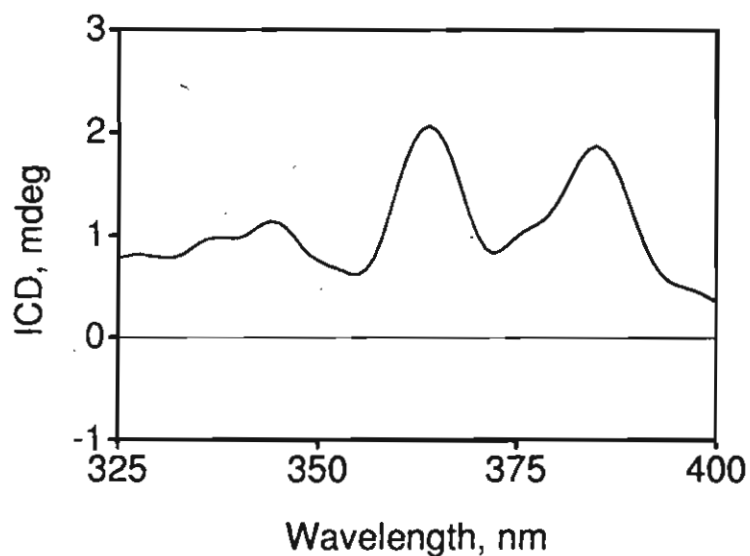


**Figure 3.6.** ICD spectrum of **ANCD** ( $1.2 \times 10^{-4}$  M) in water in the presence of **ADAC** ( $3 \times 10^{-3}$  M).

Photophysical and electrochemical parameters for **ANCD** relevant to our study are presented in Table 3.1.

**Table 3.1.** Relevant photophysical and electrochemical parameters of **ANCD**.

Parameter	Symbol	Value
Singlet energy	$E_S$	3.2 eV
Fluorescence quantum yield	$\Phi_F$	0.71
Fluorescence Lifetime	$\tau_F$	6.8 ns
Fluorescence decay constant	$k_F$	$1.04 \times 10^8 \text{ s}^{-1}$
Rate constant for intersystem crossing	$k_{ST}$	$2.9 \times 10^7 \text{ s}^{-1}$
Triplet energy	$E_T$	1.85 eV
Triplet quantum yield	$\Phi_T$	0.21
Triplet decay constant	$k_T$	$2.1 \times 10^4 \text{ s}^{-1}$
Oxidation potential	$E_{ox}$	1.14 V (vs SCE)

The singlet state parameters were obtained from absorption spectra, emission spectra and emission lifetimes. In order to obtain the triplet-state properties, laser flash photolysis experiments were carried out. Figure 3.7 shows the transient absorption spectrum of **ANCD** in water. The spectrum was very similar to the transient spectrum of **AN** in acetonitrile, and exhibited an absorption maximum at 420 nm and showed a lifetime of 47  $\mu\text{s}$ . The 420 nm absorption was assigned to the T-T absorption of **AN** based on its quenching by oxygen.

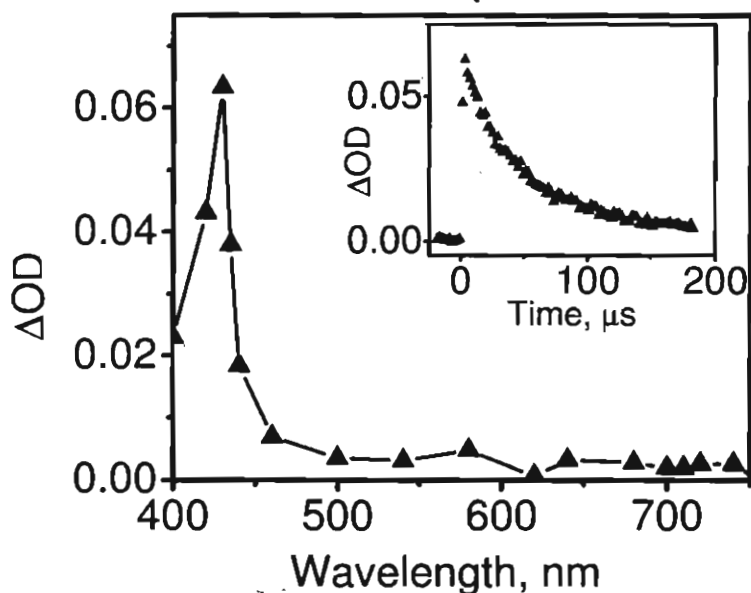


**Figure 3.7.** Transient absorption spectrum of **ANCD** in water recorded at 6.3  $\mu\text{s}$  following the laser flash. Insert shows the decay profile at 420 nm.

Relevant parameters obtained from flash photolysis ( $k_{\text{ST}}$ ,  $\Phi_{\text{T}}$  and  $k_{\text{T}}$ ) are also summarized in Table 3.1. The triplet-state energy of **ANCD** is assumed to be same as that of **AN**, and the value taken from the literature<sup>10</sup> is given in Table 3.1. Notice that  $\Phi_{\text{F}} + \Phi_{\text{T}} < 1$ , indicating a small percentage of non-radiative processes taking place in **ANCD**. This aspect is neglected in subsequent discussions. As the **AN** residue acts as donor in the PET reaction (see below), the oxidation potential ( $E_{\text{ox}}$ ) of this moiety is an important parameter. Attempts were made to record the cyclic voltammogram of **ANCD**, but a good oxidation peak could not be obtained. Hence, the  $E_{\text{ox}}$  of **ANCD** is assumed to be same as that of 9-alkylanthracene, and a value taken from the literature<sup>11</sup> is given in Table 3.1.

### 3.3.3. Properties of Electron Acceptor

**PMDI** is employed in this study because it is a good electron acceptor and its molecular size matches well with the cavity dimensions of  $\beta$ -CD. The use of **PMDI** derivatives as electron acceptors in PET reactions is well documented in the literature.<sup>12</sup> The solubility of **PMDI** in water is very poor. We attached a pyridinium group to one of its nitrogen atoms to make the water-soluble derivative pyromellitic *N*-(2-propyl)-*N'*-(*N*-pyridinium)ethyl diimide (termed **PMDI**) for use in this study.

**PMDI** was found to interact with native  $\beta$ -CD in aqueous solution. Addition of  $\beta$ -CD to an aqueous solution of **PMDI** ( $1 \times 10^{-4}$  M) results in a blue shift of the absorption maximum along with slight enhancement in the absorbance as shown in Figure 3.8. A clear isosbestic point was also observed.

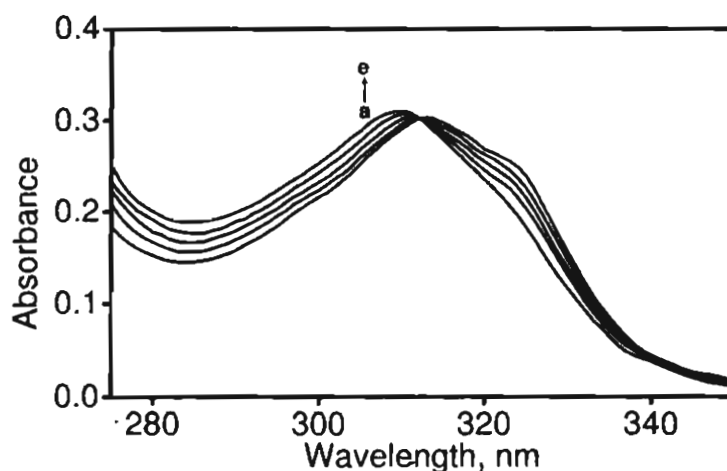
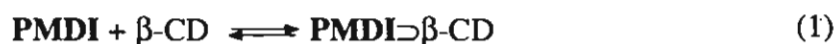


**Figure 3.8.** Absorption spectra of **PMDI** ( $1 \times 10^{-4}$  M) in the presence of various concentrations of  $\beta$ -CD ( $1.14 \times 10^{-4}$  –  $5 \times 10^{-3}$  M).



Formation of the isosbestic point indicated that the following equilibrium exists in the solution,



where,  $\text{PMDI}\supset\beta\text{-CD}$  represents the 1:1 inclusion complex.

### 3.3.4. Interaction of ANCD with PMDI: Self-Assembly and Characterization of $\text{PMDI}\supset\text{ANCD}$ dyad

Upon mixing aqueous solutions of ANCD and PMDI, the  $\beta\text{-CD}$ -based supramolecular dyad (designated as  $\text{PMDI}\supset\text{ANCD}$ ) is formed spontaneously. The self-assembly process was studied by using ICD,  $^1\text{H}$  NMR, MALDI-TOF, CV and fluorescence techniques. The self-assembly process could not be studied by absorption spectroscopy because the absorption due to AN masks the PMDI absorption. Compared to  $\beta\text{-CD}$ , the solubility of ANCD is very poor in water and this imposed some constraints in determining the association constant.

An aqueous solution of PMDI did not exhibit circular dichroism. ANCD exhibited a weak negative ICD signal in aqueous solution (Figure 3.5). When PMDI is added to a solution of ANCD, the weak negative signal due to ANCD is replaced by a strong positive ICD signal with a maximum at 312 nm as shown in Figure 3.9. The ICD maximum corresponds to PMDI absorption and this clearly indicates that PMDI is associated with the  $\beta\text{-CD}$  part of ANCD. The lowest-energy absorption (314 nm) in PMDI derivatives is known to be polarized along the long axis connecting the two imide nitrogen atoms.<sup>13</sup> As per the ICD rules

described earlier, the strong positive signal indicates that **PMDI** enters the  $\beta$ -CD cavity with its long axis parallel to the  $\beta$ -CD axis, with the isopropyl group inside the cavity and the pyridinium moiety projecting out into the aqueous environment.

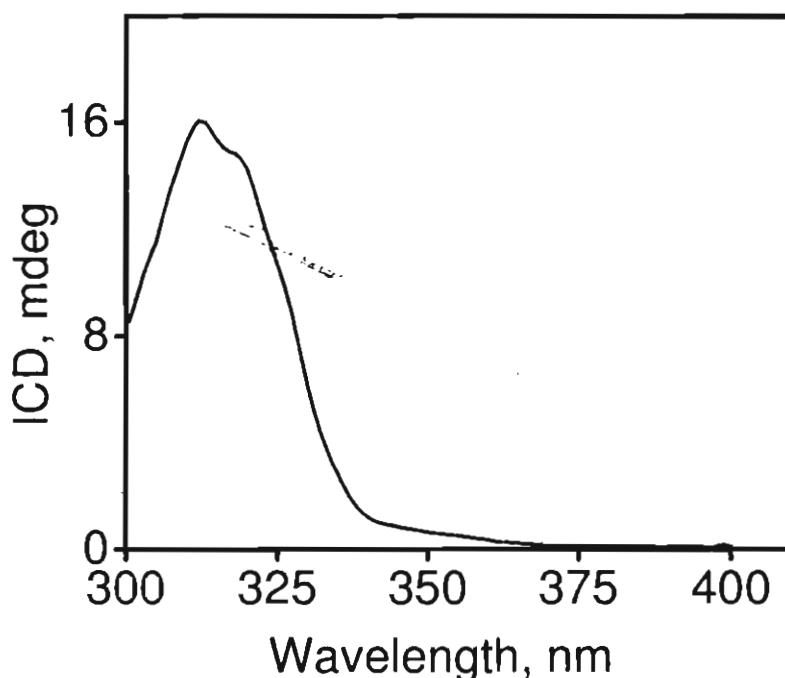


**Figure 3.9.** ICD spectrum of a mixture of **ANCD** ( $1.3 \times 10^{-4}$  M) and **PMDI** ( $3 \times 10^{-4}$  M).

A parallel orientation in which the pyridinium moiety remains inside and the isopropyl group remains outside is ruled out, based on the hydrophilicity/hydrophobicity properties of these groups. When **PMDI** enters the cavity, the **AN** residue, which is partially included within the cavity, has to be displaced. A weak positive ICD signal can result at  $\lambda > 350$  nm if the displaced **AN** remains just outside the  $\beta$ -CD cavity. The signal above 350 nm is very weak

and does not give any information about the conformation of the displaced AN moiety.

A positive ICD signal from **PMDI** may also arise if it remains outside the cavity with its long axis perpendicular to the  $\beta$ -CD axis. We have discarded this conformation for the following reasons. If **PMDI** lies on a rim, it can do so only at the larger rim because the smaller rim is crowded due to the presence of an AN residue. The ICD signal intensity will be very low in this case (rule 3). In such a conformation, the absorption polarization is perpendicular to the CD axis, leading to further reduction in the ICD signal intensity (rule 4). The ICD signal obtained is very strong and does not support this conformation. The ICD signal shown in Figure 3.9 decreases upon addition of **ADAC**, and this clearly indicates that **PMDI** is actually included within the cavity.

Further evidence for the encapsulation of **PMDI** in the cavity of **ANCD** is obtained from Cyclic Voltammetric studies. Square-wave voltammogram of **PMDI** in presence of 1:1 concentration of **ANCD** is shown in Figure 3.10 and Cyclic voltammogram is shown in Figure 3.11. The voltammograms of **PMDI** consisted of two reversible reduction peaks at -0.58 and -0.74 V (versus SCE). Addition of **ANCD** resulted in a reduction of the peak current, which is indicative of complex formation between the two species.

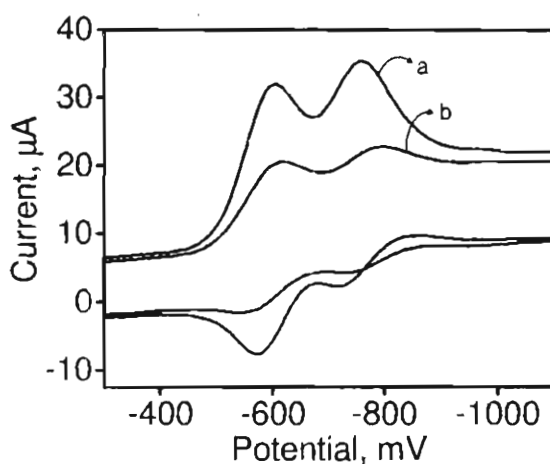


**Figure 3.10.** Square-wave voltammogram of **PMDI** ( $1.3 \times 10^{-3}$  M) in the absence (a) and presence (b) of **ANCD** ( $1.3 \times 10^{-3}$  M).

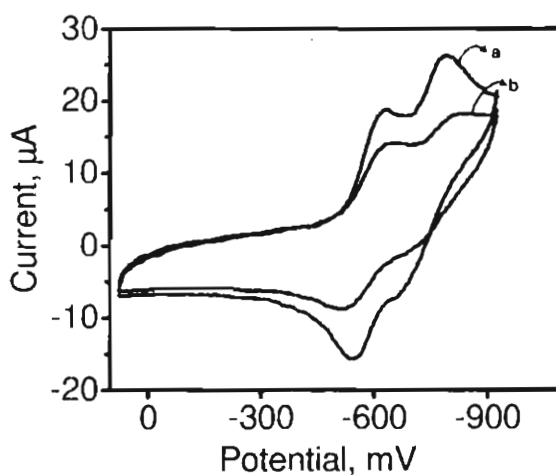


**Figure 3.11.** Cyclic Voltammogram of **PMDI** ( $1.3 \times 10^{-3}$  M) in the (a) absence and (b) presence of **ANCD** ( $1.3 \times 10^{-3}$  M)

Association of an electroactive guest with a bulky host, such as  $\beta$ -CD, always results in substantial reduction of the effective diffusion coefficient, leading to a decrease in the current associated with the redox process.<sup>14</sup> In addition to the decrease in current, addition of **ANCD** also resulted in a slight shift (0.04 V)

in the second reduction peak to a more negative  $E_{1/2}$  value. A negative shift in the reduction potential indicates destabilization of the reduced state (or reduction has become more difficult). It has been suggested that the redox process in an included guest will occur only after the dissociation of the inclusion complex,<sup>15</sup> leading to a positive shift in the oxidation potential and a negative shift in the reduction potential. These results suggested that **PMDI** is included in the cavity of **ANCD** with one of its imide groups deeply buried inside the cavity and the other imide group relatively exposed to water and accessible for reduction at the electrode.

Further evidence for the association of **PMDI** with **ANCD** was obtained from  $^1\text{H}$  NMR spectroscopic studies. The  $^1\text{H}$  NMR spectrum of **PMDI** in  $\text{D}_2\text{O}$  is shown in the lower panel of Figure 3.12. The assignments of the different signals are also indicated (the large peak around  $\delta = 4.8$  ppm is due to HOD present in  $\text{D}_2\text{O}$ ) in the figure. Upon addition of **ANCD**, noticeable changes are observed in the chemical shifts of several protons. The  $\text{CH}_3$  protons of the isopropyl group (labeled *a*) appeared as a doublet at  $\delta = 1.47$  ppm. Upon addition of **ANCD**, the doublet changed into a broad singlet and shifted upfield. The CH proton of the isopropyl group (labelled *b*), which originally was a multiplet, shifted upfield and changed into a broad singlet. The  $\text{CH}_2$  group attached to the imide nitrogen (labelled *d*) also showed similar changes. The most observable change, however, was that of the aromatic pyromellitic imide proton (labelled *c*). This proton underwent an upfield shift of about 0.4 ppm. The protons in the pyridinium ring (*f*,

*g* and *h*) did not exhibit any change, and any change in the *e* signal is obscured by the  $\beta$ -CD protons of ANCD. The new peaks that appear in the aromatic region are due to the AN moiety of ANCD.

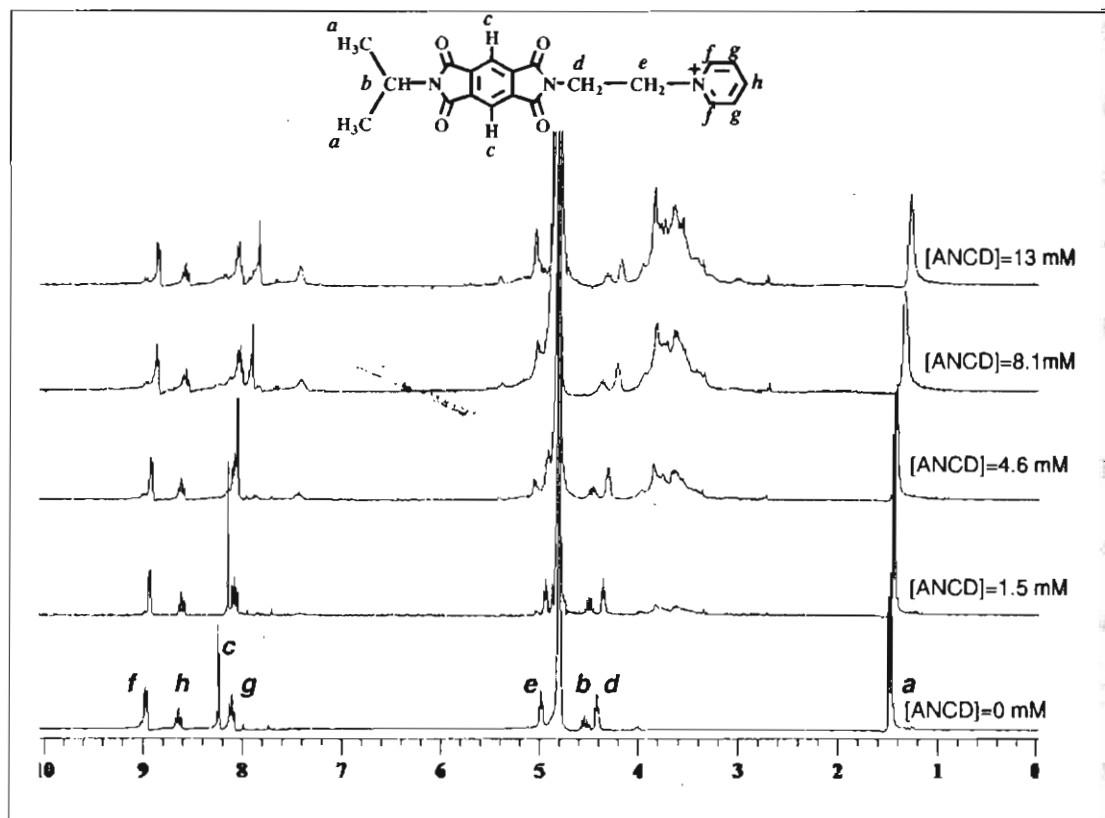


**Figure 3.12.**  $^1\text{H}$  NMR spectra of PMDI in  $\text{D}_2\text{O}$  in the presence of an increasing concentration of ANCD.

Figure 3.13 shows the changes observed in the chemical shifts ( $\Delta\delta$ ) for the various protons. It can be seen that even at the highest possible concentration of ANCD, the  $\Delta\delta$  values have not reached a plateau region. Hence, a  $K_a$  value could not be determined from the data in Figure 3.13.

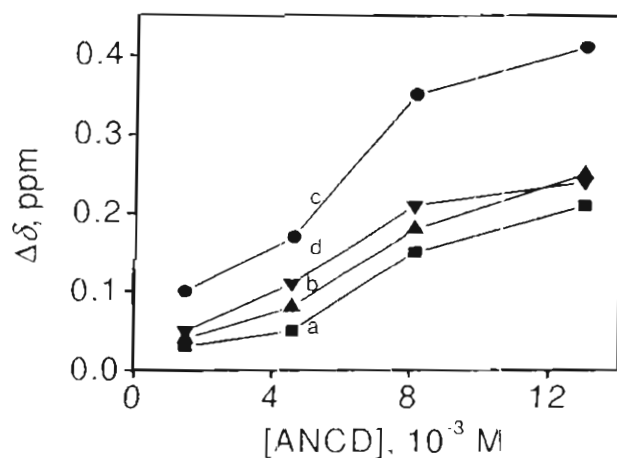


Figure 3.13. Plot of  $\Delta\delta$  against ANCD concentration.

Further evidence for the formation of the supramolecular dyad is provided by MALDI-TOF spectroscopy. The MALDI-TOF spectrum of a 1:1 ANCD / PMDI mixture exhibited peak at  $m/z = 1768.4$ , which corresponded to the molecular mass of the dyad (Figure 3.14).

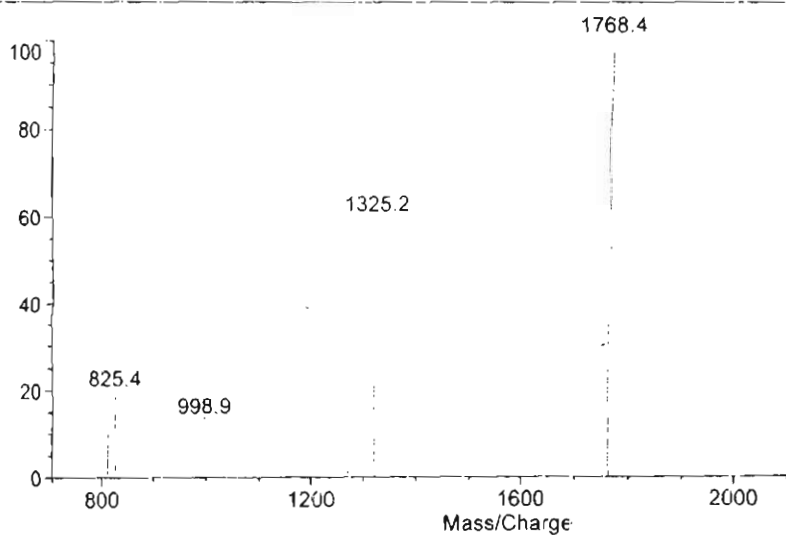
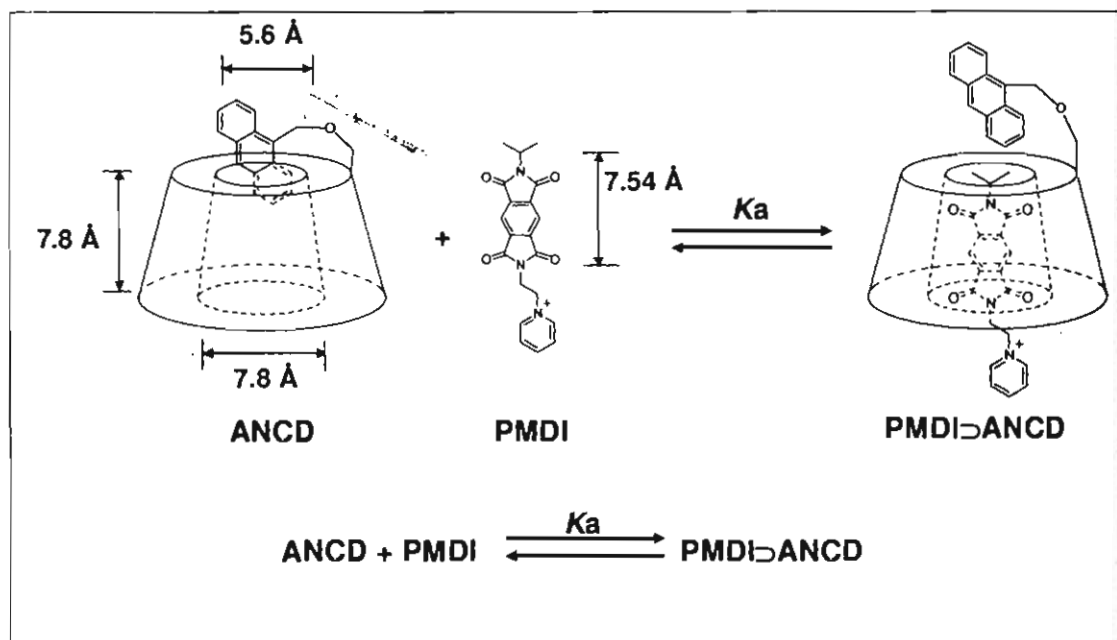


Figure 3.14. MALDI-TOF spectrum of 1:1 concentration of ANCD and PMDI.

The dimensions of the  $\beta$ -CD cavity taken from the literature<sup>16</sup> and the molecular dimensions of **PMDI** obtained from AM1 calculations,<sup>17</sup> along with results from the ICD, CV and <sup>1</sup>H NMR studies were put together to obtain a clear picture of the structure of the inclusion complex **PMDI**⊂**ANCD**. Relevant molecular dimensions and a possible structure of the inclusion complex are shown in Scheme 3.5.



**Scheme 3.5.** Inclusion of **PMDI** into **ANCD**. Molecular dimensions are also shown.

As the smaller rim of **ANCD** is capped by **AN**, **PMDI** may enter the cavity through the wider rim with the hydrophobic *N*-(2-propyl) end going into the cavity and the hydrophilic *N'*-(2-ethylpyridinium) end remaining outside at the wider rim, as shown in Scheme 3.5. The <sup>1</sup>H NMR signals for the *a* and *b* protons have



broadened considerably, indicating that free rotation of the 2-propyl group is constrained. The distance between the farthest hydrogen atoms in the 2-propyl group (obtained from AM1) is 4.32 Å. The diameter of the smaller rim of the  $\beta$ -CD cavity is 5.6 Å. The AN moiety and six CH<sub>2</sub>OH groups are also present at the smaller rim and hindrance to free rotation of the 2-propyl group is interpreted to mean that this group is situated very close to the narrow rim and flanged by the overhanging CH<sub>2</sub>OH and AN residues. The *c* proton experienced the maximum shift, which indicates that this proton is near the centre of the  $\beta$ -CD cavity. The *d*-proton signal is also affected and we suggest that this group is present near the wider rim of ANCD. The protons in the pyridinium ring (*f*, *g* and *h*) are unaffected and it can be safely assumed that the pyridinium ring is present outside the cavity fully exposed to water. All of these assignments are consistent with the conformation shown in Scheme 3.5. The imide group at the pyridinium end is near the wider rim slightly exposed to water and the imide group at the 2-propyl end is buried inside the cavity, supporting the results from CV studies.

Since the diameter of the smaller rim of the  $\beta$ -CD cavity is only 5.6 Å, encapsulation of **PMDI** in this fashion would lead to the displacement of the AN residue, as shown in Scheme 3.5. The edge-to-edge distance between the **PMDI** and AN residues is an important parameter in the electron transfer process and we assume that this distance is very small ( $< 2$  Å).

### 3.3.5. Photoinduced Electron Transfer between ANCD and PMDI

When aqueous solutions of ANCD and PMDI are mixed, a fraction of the molecules exist as **PMDI**⊃**ANCD** as shown in Scheme 3.5. Photoexcitation of the system would then lead to unimolecular and bimolecular electron-transfer processes, as demonstrated previously for  $\alpha$ -CD-appended systems in Chapter 2 and also for hydrogen bonded systems.<sup>18</sup> An important difference in the present study is that the triplet excited state of the AN chromophore is also involved in the electron-transfer process.

#### 3.3.5.1. Fluorescence-quenching experiments

Fluorescence of ANCD is quenched very efficiently by millimolar concentrations of PMDI as shown in Figure 3.15.

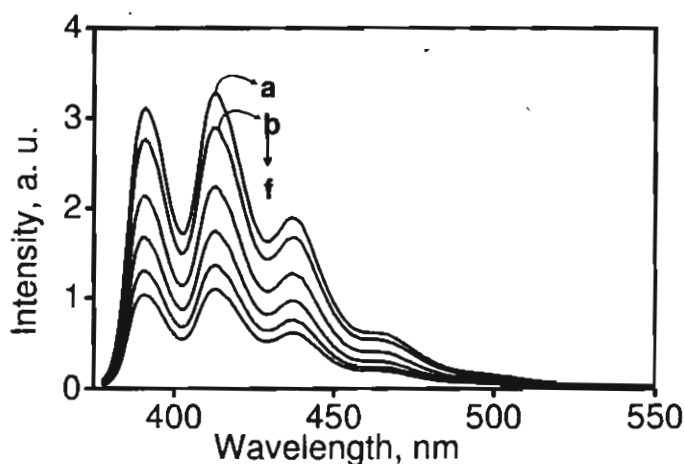
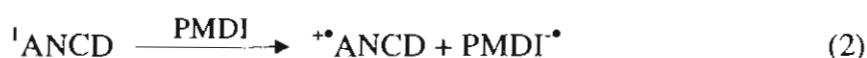


**Figure 3.15.** Fluorescence spectra of ANCD in the absence (a) and in the presence (b–f) of PMDI.

Concentration of PMDI varied from  $1 \times 10^{-4}$  -  $3 \times 10^{-3}$  M.

Fluorescence quenching can occur by way of energy transfer or electron transfer mechanisms. As the singlet energy of **PMDI** is greater than the singlet energy of **AN**, quenching by energy transfer mechanism is ruled out and the quenching is attributed to electron transfer from the singlet excited state of **AN** to **PMDI**, as shown in equation (2).



The change in free energy associated with this electron-transfer process can be calculated by using the Weller equation [equation (3)].

$$\Delta G_{(S)}^0 = E_{\text{ox}} - E_{\text{red}} - E_S - e^2/\epsilon d \quad (3)$$

In equation (3),  $E_{\text{ox}}$  is the oxidation potential of **AN**,  $E_{\text{red}}$  is the first reduction potential of **PMDI**,  $E_S$  is the singlet energy of **AN**,  $\epsilon$  is the dielectric constant of water and  $d$  is the distance separating the donor and acceptor. Since  $\epsilon$  for water is very high, the last term can be neglected in the calculation. Substitution of the various values gave  $\Delta G_{(S)}^0 = -1.48$  eV. The highly negative  $\Delta G_{(S)}^0$  value suggests that the singlet-state mediated electron-transfer process lies in the Marcus inverted region.

The singlet-state quenching process can occur by a unimolecular mechanism (intramolecular quenching within **PMDI**⊃**ANCD**), a diffusion mediated mechanism or a combination of these mechanisms. For CD-appended systems, the diffusion coefficient ( $k_{\text{diff}}$ ) in water is determined to be  $6.6 \times 10^9 \text{ M}^{-1}$

$s^{-1}$ .<sup>19</sup> If the quenching occurred by the diffusion mechanism, the maximum possible rate constant  $k_q = k_{diff}$ . By definition,  $k_q \tau_0 = K_{SV}$ , in which  $K_{SV}$  is the Stern–Völmer constant. Substituting  $k_{diff}$  and  $\tau_0$ , we obtain  $K_{SV} = 45 \text{ M}^{-1}$ . By definition, the reciprocal of  $K_{SV}$  gives the concentration (of the quencher) required to quench 50% of the fluorescence.<sup>20</sup> This calculation revealed that  $2.2 \times 10^{-2} \text{ M}$  **PMDI** is required for 50% quenching, if quenching is to occur by the diffusion mechanism. Figure 3.15 shows that nearly 75% of the fluorescence is quenched by  $3 \times 10^{-3} \text{ M}$  **PMDI**. We propose that in the concentrations employed for the fluorescence quenching experiments, the diffusion-mediated reaction does not contribute significantly to singlet-state deactivation.

The fluorescence quenching data in Figure 3.15 can be analyzed in the following way to obtain the rate constant for electron transfer  $k_{et(S)}$ . In the absence of diffusion-mediated quenching, the observed fluorescence quantum yield ( $\Phi_{F(obs)}$ ) can be related to the fluorescence quantum yields of the uncomplexed ( $\Phi_F$ ) and complexed ( $\Phi_{F(PMDI \rightleftharpoons ANCD)}$ ) forms by equation (4).<sup>21</sup>

$$\Phi_{F(obs)} = (1-\alpha)\Phi_F + \alpha\Phi_{F(PMDI \rightleftharpoons ANCD)} \quad (4)$$

In equation (4)  $\alpha$  is the fraction of associated molecules. Equation (4) could be simplified to equation (5).<sup>21</sup>

$$\frac{1}{\Phi - \Phi_{F(obs)}} = \frac{1}{\Phi_F - \Phi_{F(PMDI \rightleftharpoons ANCD)}} + \frac{1}{K_d(\Phi_F - \Phi_{F(PMDI \rightleftharpoons ANCD)})[PMDI]} \quad (5)$$

According to equation (5), plot of  $1/(\Phi_F - \Phi_{F(\text{obs})})$  vs  $1/[\text{PMDI}]$  should be a straight line. The association constant  $K_a$  and the fluorescence quantum yield of the complex  $\Phi_{F(\text{PMDI} \supset \text{ANCD})}$  could be obtained from the intercept and slope of such a plot.

Figure 3.16 is a plot of  $1/(\Phi_F - \Phi_{F(\text{obs})})$  vs  $1/[\text{PMDI}]$  for the above quenching. A straight line is obtained which supports equations (4) and (5). Dividing the intercept by slope, we obtained  $K_a = 1800 \text{ M}^{-1}$  and  $\Phi_{F(\text{PMDI} \supset \text{ANCD})} = 0.214$ . The rate constant for electron transfer  $k_{\text{et(S)}}$  within **PMDI**⊃**ANCD** can be obtained by using equation (6):

$$k_{\text{et(S)}} = \frac{1}{\tau_F} \left[ \left( \frac{\Phi_F}{\Phi_{F(\text{PMDI} \supset \text{ANCD})}} \right) - 1 \right] \quad (6)$$

Substituting the values, we obtain  $k_{\text{et(S)}} = 3.4 \times 10^8 \text{ s}^{-1}$ .

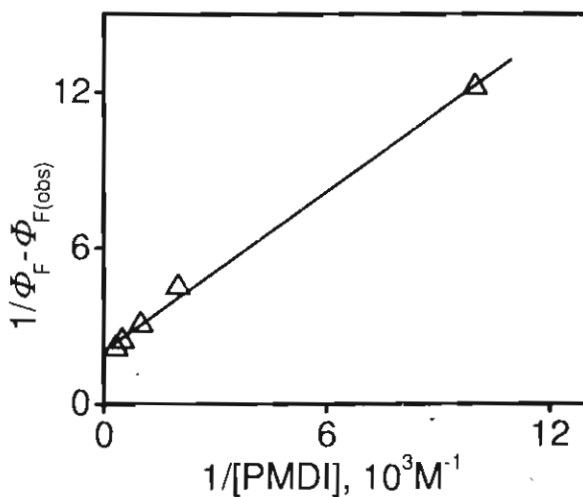
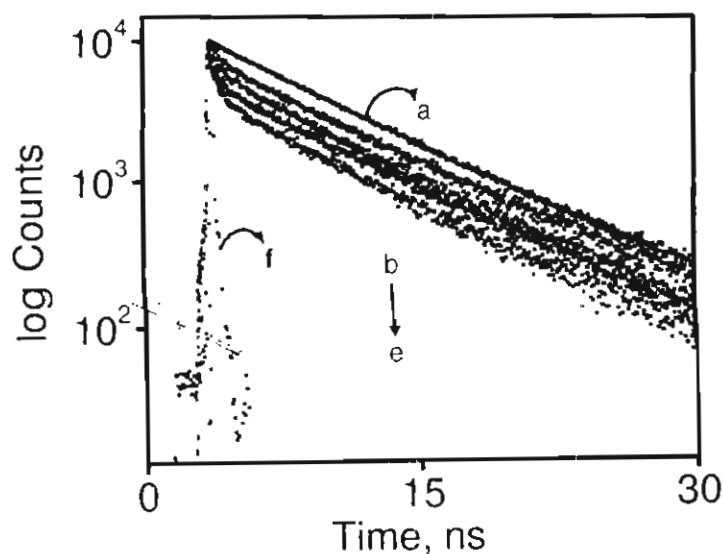


Figure 3.16. Plot of  $1/(\Phi_F - \Phi_{F(\text{obs})})$  vs  $1/[\text{PMDI}]$ .

Further insight into the mechanism of fluorescence quenching was obtained by fluorescence lifetime experiments. In the absence of any quencher, the fluorescence decay of **ANCD** was monoexponential as shown in Figure 3.17 a. The decays become biexponential in the presence of **PMDI** as shown in Figure 3.17 b-e.



**Figure 3.17.** Fluorescence decay profiles of **ANCD** in the absence (a) and presence (b-e) of different concentrations ( $1-8 \times 10^{-4}$  M) of **PMDI**. (f) is the lamp profile.

All the fluorescence decay profiles were fitted by using the biexponential function equation (7).

$$I_t = \chi_{(\text{PMDI} \rightarrow \text{ANCD})} \exp(-t/\tau_1) + \chi_{(\text{ANCD})} \exp(-t/\tau_2) \quad (7)$$

where,  $\chi_{(\text{PMDI} \rightarrow \text{ANCD})}$  is the mole fraction of the complexed species and  $\chi_{(\text{ANCD})}$  is the mole fraction of free **ANCD**. Values of  $\tau_1$ ,  $\tau_2$ ,  $\chi_{(\text{PMDI} \rightarrow \text{ANCD})}$ ,  $\chi_{(\text{ANCD})}$  along with  $\chi^2$  values obtained from the fit are given in Table 3.2.

The short lifetime component  $\tau_1$  arises due to electron-transfer quenching within the ensemble **PMDI**⊃**ANCD** and hence  $\tau_1 = (k_0 + k_{\text{et(S)}})^{-1}$ , in which  $k_{\text{et(S)}}$  is the rate constant for electron transfer within **PMDI**⊃**ANCD**.  $k_{\text{et(S)}}$  can be calculated by using equation (8) as described in Chapter 2.

$$k_{\text{et(S)}} = 1/\tau_1 - 1/\tau_0 \quad (8)$$

**Table 3.2.** Fluorescence lifetimes ( $\tau_1$  and  $\tau_2$ ), fractional contributions ( $\chi_{(\text{PMDI} \supset \text{ANCD})}$  and  $\chi_{(\text{ANCD})}$ ) and  $\chi^2$  values obtained for fluorescence lifetime quenching of **ANCD** by **PMDI**.

[PMDI]	$\tau_1$ , ns	$\chi_{(\text{PMDI} \supset \text{ANCD})}$	$\tau_2$ , ns	$\chi_{\text{ANCD}}$	$\chi^2$
0	-----	-----	6.8	100	1.2
$1 \times 10^{-4}$ M	2.4	8.36	6.8	91.64	1.1
$2 \times 10^{-4}$ M	2.5	13.09	6.7	86.91	1.1
$3 \times 10^{-4}$ M	2.5	16.06	6.7	83.94	1.2
$5 \times 10^{-4}$ M	2.5	38.91	6.7	61.09	1.1
$8 \times 10^{-4}$ M	2.6	49.98	6.6	50.02	1.1

The value of  $k_{\text{et}}$  thus obtained was  $(2.5 \pm 0.1) \times 10^8 \text{ s}^{-1}$ . The  $k_{\text{et(S)}}$  value calculated from steady-state quenching (see above) was very close to this value. It can be noticed from Table 3.2 that the long lifetime component  $\tau_2 \approx \tau_0$ , which indicated that the contribution due to diffusion-mediated quenching of the singlet excited state is negligible.

$K_a$  for the encapsulation process can be calculated from the fractional contributions  $\chi_{(\text{PMDI} \supset \text{ANCD})}$  and  $\chi_{(\text{ANCD})}$ . As the concentration of **PMDI** is large compared to that of the complex, we can write equation (9).

$$K_a = \frac{\chi_{(\text{PMDI} \supset \text{ANCD})}}{\chi_{\text{ANCD}}[\text{PMDI}]} \quad (9)$$

Figure 3.18 shows a plot of  $\chi_{(\text{PMDI} \supset \text{ANCD})}/\chi_{(\text{ANCD})}$  against  $[\text{PMDI}]$ . The plot was linear and gave  $K_a = 1390 \text{ M}^{-1}$ . This value is somewhat smaller than the value obtained from the steady-state fluorescence method (see above).

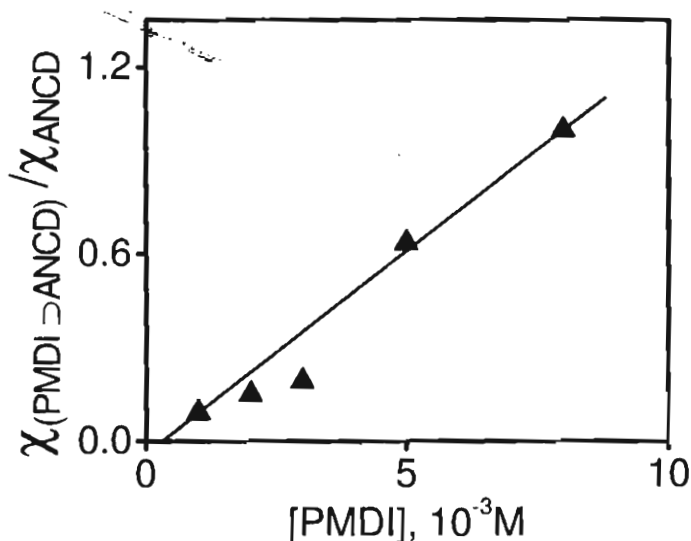


**Figure 3.18.** Plot of  $\chi_{\text{PMDI} \supset \text{ANCD}} / \chi_{\text{ANCD}}$  against  $[\text{PMDI}]$

Electron transfer within **PMDI** $\supset$ **ANCD** is an example of non-adiabatic electron transfer involving a weakly interacting donor and acceptor for which the rate constant can be obtained by using equation (10), which is a modified form of the Marcus equation.<sup>22</sup>



$$k_{\text{el}} = (2\pi/\hbar) H_{\text{el}}^2 (4\pi\lambda_0 k_B T)^{-1/2} \sum_{m=0}^{\infty} (e^{-s} s^m / m!) \times \exp[-(\lambda_0 + \Delta G^0 + m h \nu)^2 / (4\lambda_0 k_B T)] \quad (10)$$

In equation (10),  $\hbar$  is Planck's constant divided by  $2\pi$ ,  $H_{\text{el}}$  is the coupling matrix element,  $\lambda_0$  is the outer-sphere reorganization energy,  $k_B$  is the Boltzmann constant,  $T$  is the absolute temperature,  $\Delta G^0$  is the free energy change for the reaction,  $s = \lambda_i/h\nu$ ,  $m$  is an integer, and  $\lambda_i$  is the inner-sphere reorganization energy. In Chapter 2 with  $\alpha$ -CD appended pyrene and encapsulated acceptors we obtained  $H_{\text{el}} = 3 \text{ cm}^{-1}$ . Using  $H_{\text{el}} = 3 \text{ cm}^{-1}$ ,  $\lambda_0 = 0.8 \text{ eV}$ ,  $\lambda_i = 0.2 \text{ eV}$ ,  $h\nu = 0.15 \text{ eV}$ ,  $T = 298 \text{ K}$  and  $\Delta G^0 = -1.48 \text{ eV}$ , we obtain  $k_{\text{el}(S)} = 3.83 \times 10^8 \text{ s}^{-1}$ . Notice that this value is very close to the values obtained from steady state ( $3.4 \times 10^8 \text{ s}^{-1}$ ) and time resolved ( $2.5 \times 10^8 \text{ s}^{-1}$ ) fluorescence quenching measurements.

### 3.3.6. Laser Flash Photolysis Studies

Laser flash photolysis of ANCD resulted in the formation of the AN triplet state absorbing at 420 nm as shown in Figure 3.7. We observed that the triplet is quenched by PMDI. The quenching rate constant ( $k_{q(T)} = 1.6 \times 10^8 \text{ M}^{-1} \text{ s}^{-1}$ ) was obtained by plotting the observed pseudo-first-order rate constants against [PMDI] as shown in Figure 3.19. The triplet energy of PMDI (2.45 eV) is 0.6 eV higher than the triplet energy of AN.<sup>23</sup> Hence, quenching by an energy transfer mechanism is ruled out. Based on the evidence obtained from flash photolysis

experiments, we attribute the quenching to an electron-transfer process that takes place from the triplet state of AN as shown in equation (11):

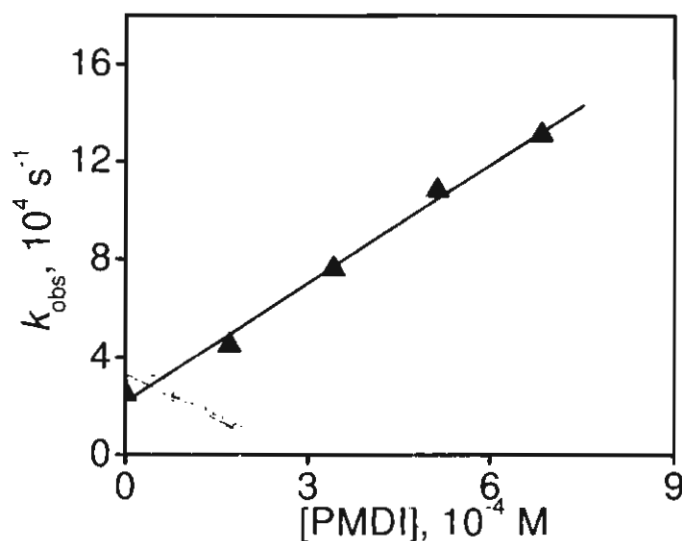
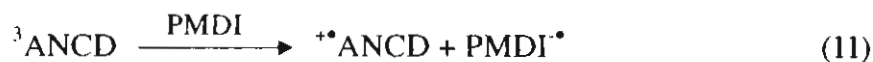


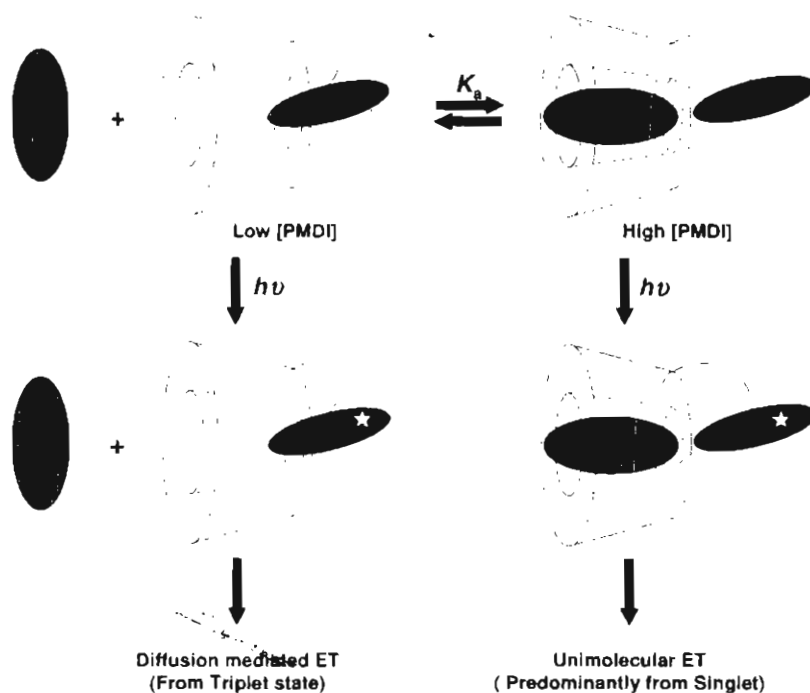
**Figure 3.19.** Plot of  $k_{\text{obs}}$  against [PMDI].

The change in free energy for electron transfer from the triplet state ( $\Delta G^0_{(\text{T})}$ ) can also be calculated from equation (3), by substituting the triplet energy  $E_{\text{T}}$  instead of  $E_{\text{S}}$ . We obtained  $\Delta G^0_{(\text{T})} = -0.12$  eV. The  $k_{\text{q}(\text{T})}$  value obtained is much lower than the diffusion limited value, probably because of the low driving force for this reaction. As mentioned previously,  ${}^3\text{ANCD}$  was quenched by oxygen. In order to make a comparison, the rate constant for oxygen quenching  $k_{\text{q}}(\text{O}_2)$  was determined as follows. The  $k_{\text{obs}}$  values were determined at three different concentrations of oxygen, namely, 0 M (Argon atmosphere),  $2.9 \times 10^{-4}$  M (air saturated aqueous

solution) and  $1.39 \times 10^{-3}$  ( $O_2$  saturated aqueous solution).<sup>24</sup>  $k_{\text{obs}}$  values were then plotted against oxygen concentration and  $k_q(O_2)$  was obtained from the slope of this plot.  $k_q(O_2)$  value thus obtained was  $9.0 \times 10^8 \text{ M}^{-1} \text{ s}^{-1}$ , indicating that quenching of  $^3\text{ANCD}$  by oxygen is five times more efficient than quenching by **PMDI**.

**PMDI** has no absorption above 350 nm and hence **AN** can be selectively excited in the presence of **PMDI** by using the 355 nm laser light. The photoprocesses taking place in the system are expected to depend on the position of the equilibrium shown in Scheme 3.6. At lower concentrations of **PMDI**, the equilibrium is in favour of intermolecular reactions involving  $^3\text{ANCD}$ . At higher concentrations of **PMDI**, we expect the equilibrium to shift to the intra-ensemble process as shown in Scheme 3.6.

In order to understand these processes in detail, transient absorption spectra of **ANCD** were recorded at several different concentrations of **PMDI**. Figure 3.20 A and B show the transient absorption spectra taken at  $[\text{PMDI}] = 7 \times 10^{-5}$  and  $5 \times 10^{-3} \text{ M}$ , respectively. In both cases the spectra exhibited maxima at 420 and 720 nm.



**Scheme 3.6.** Photoprocesses taking place in the ANCD-PMDI system.

The 720 nm absorption is due to  $\text{PMDI}^{\bullet}$  and  $\text{AN}^{+\bullet}$ <sup>25</sup> and the 420 nm absorption is due to  $^3\text{ANCD}$  and  $\text{AN}^{+\bullet}$ . At low  $[\text{PMDI}]$ , the 420 nm band due to  $^3\text{ANCD}$  is very strong (Figure 3.20 A). Kinetic traces taken in a small time window show decay of the triplet at 420 nm and a matching growth of the radical-ion products at 720 nm (insets in Figure 3.20 A), confirming that the products originate through the triplet pathway shown in equation (11).

The quantum yield ( $\Phi_{cs}$ ) for the formation of the CS state was estimated by assuming that the absorption at 720 nm is due to equimolar amounts of  $\text{PMDI}^{\bullet}$  and  $\text{AN}^{+\bullet}$  (see experimental section for details).

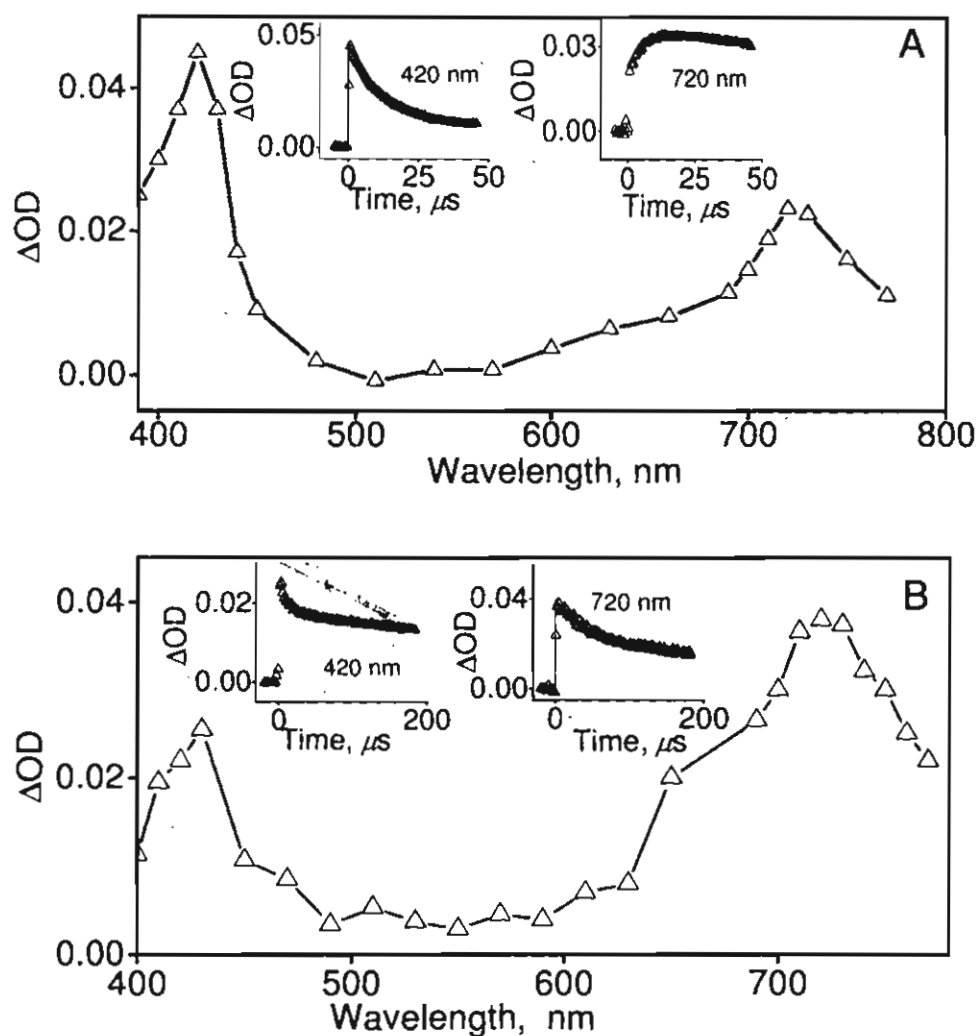


**Figure 3.20.** Transient absorption of **ANCD** ( $7 \times 10^{-5}$  M) in the presence of A)  $7 \times 10^{-5}$  M **PMDI** recorded at  $0.46 \mu\text{s}$  and B)  $5 \times 10^{-3}$  M **PMDI** recorded at  $1.0 \mu\text{s}$  following the laser flash. Insets show the decays at 420 and 720 nm.

$\Phi_{cs}$  was found to increase with  $[\text{PMDI}]$  and reach a maximum at  $[\text{PMDI}] = 5 \times 10^{-3}$  M as shown in Figure 3.21. This result suggests that the yield of the radical ion products increases with an increase in the fraction of the **PMDI**-**ANCD** complex.

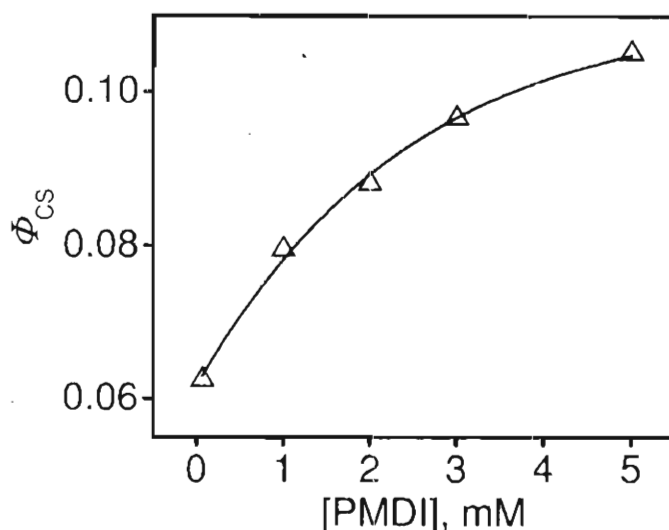


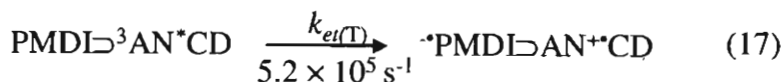
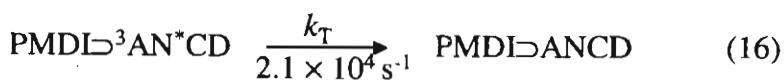
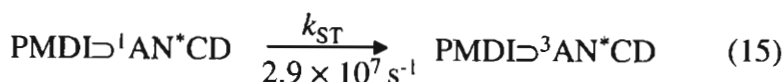
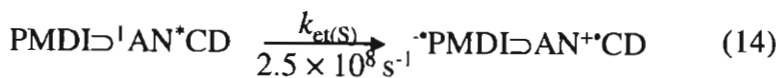
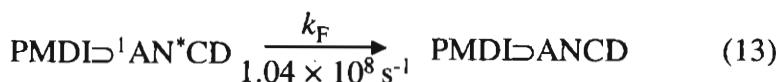
**Figure 3.21.** Plot of  $\Phi_{CS}$  at 720 nm against **PMDI** concentration.

In the transient spectrum taken at  $[\text{PMDI}] = 5 \times 10^{-3} \text{ M}$  (Figure 3.20 B), the 720 nm band is much stronger than the 420 nm band, indicating that the contribution from the triplet state is small. At 420 nm, the decay exhibited a fast component due to decay of  $^3\text{AN}$  and a very slow component due to decay of  $\text{AN}^{+\bullet}$  (see inset in Figure 3.20 B). Notice that the absorption due to the radical-ion products at 720 nm is very long-lived and persists even after 200  $\mu\text{s}$ .

Results from the fluorescence quenching and flash photolysis experiments can be summarized as shown in equations (12–17) to describe the various intra-ensemble processes taking place in the system. Complex formation will not affect the fundamental photophysical rate constants  $k_F$ ,  $k_{ST}$  and  $k_T$ . Complex formation, however, leads to electron transfer processes from singlet as well as triplet states characterized by rate constants  $k_{et(S)}$  and  $k_{et(T)}$ . The  $k_{et(S)}$  value obtained from

lifetime experiments is given in equations (12–17). The rate constant for electron transfer from the triplet state within the ensemble  $k_{et(T)}$  could not be determined experimentally. This value was calculated by using equation (10) and by employing the same parameters described earlier along with  $\Delta G^0_{(T)} = -0.12$  eV. This treatment gave  $k_{et(T)} = 2.22 \times 10^5 \text{ s}^{-1}$  and this value is shown in equation (17).

The quantum yield of the various intra-ensemble processes can be obtained by using the  $k$  values. For example,  $\Phi_{et(S)} = k_{et(S)} / (k_{et(S)} + k_F + k_{ST})$  and so on. The values so obtained are:  $\Phi_{et(S)}(\text{complex}) = 0.65$ ,  $\Phi_T(\text{complex}) = 0.076$ ,  $\Phi_{et(T)}(\text{complex}) = 0.069$ . Thus, 71.9% of the excited AN in the **PMDI**⊃**ANCD** complex decays by electron-transfer processes. According to the arguments we have presented, at  $[\text{PMDI}] = 5 \times 10^{-3}$  M, **ANCD** is present mostly as the complex **PMDI**⊃**ANCD** and within the complex more than 70% of excited AN decays by electron-transfer processes. The value of  $\Phi_{cs}$ , however, is only 0.105 under these conditions as shown in Figure 3.21. This suggests that a significant fraction of the radical ions formed underwent back electron transfer (BET) before they could be detected.



An important observation here is that a fraction of the CS state survives for more than 200  $\mu\text{s}$ . Generation of a long-lived CS state is an important aim in the study of PET reactions.<sup>26</sup> Long-lived decay, as shown in Figure 3.20 B, is generally associated with intermolecular processes. Covalently bound donor-acceptor dyads in general (with the exception of  $\text{C}_{60}$ -based systems) exhibit very short lifetimes, although a claim to the contrary has been made recently.<sup>27</sup> For a few CD-based dyads for which data are available, the CS-state lifetimes were extremely small.<sup>28</sup> In this context it was important to know if the long-lived CS state (shown in insets of Figure 3.20 B) has any contribution from the intra-ensemble electron-transfer processes. Laser flash photolysis in oxygen-saturated solutions suggested that a fraction of the long-lived CS state actually originated through the intra-ensemble pathway.



The concentration of oxygen in oxygen-saturated aqueous solutions is  $1.39 \times 10^{-3}$  M.<sup>24</sup> We have already shown that for  $^3\text{ANCD}$ ,  $k_q$  for oxygen is five times larger than  $k_q$  for **PMDI**. Under conditions in which  $[\text{O}_2] > [\text{PMDI}]$ , quenching of  $^3\text{ANCD}$  by **PMDI** is not expected to be efficient. Laser flash photolysis of the system under the conditions described for Figure 3.20 A was carried out after saturating the solution with oxygen. Under these conditions the only transient observed was a fast-decaying triplet. It should be mentioned that in addition to triplets, oxygen also quenches radical anions very efficiently, but radical cations are generally not quenched. The presence of oxygen is not expected to affect the intra-ensemble processes. As the absorption due to  $\text{AN}^{+\bullet}$  at 720 nm was absent, we conclude that under the conditions used for Figure 3.20 A, only intermolecular electron transfer quenching was possible, and this process was inhibited completely by the oxygen present in the solution.

We carried out oxygen quenching experiments at  $[\text{PMDI}] = 1.0 \times 10^{-3}$  M. If we assume that  $K_a = 10^3 \text{ M}^{-1}$  and  $[\text{PMDI}]_{\text{eq}} \approx [\text{PMDI}]_0$  (in which  $[\text{PMDI}]_0$  is the actual concentration and  $[\text{PMDI}]_{\text{eq}}$  is the equilibrium concentration of **PMDI**), it can be shown that  $[\text{PMDI} \rightarrow \text{ANCD}]/[\text{ANCD}] = 1$  under these conditions. 50% of **ANCD** is present in the free form and undergoes triplet-mediated electron transfer and the remaining 50% is present as the complex and undergoes intra-ensemble electron transfer. It can be shown that nearly 78% of all the PET reactions occur within the ensemble and the remaining 22% occur through the intermolecular

triplet pathway. Saturating the solution with oxygen is expected to remove most of the intermolecular electron transfers and any radical ions observed under these conditions could be considered as arising from the intra-ensemble pathway.

Figure 3.22 shows the kinetic traces at 420 and 720 nm for the oxygen-saturated **ANCD** ( $7 \times 10^{-5}$  M) solution in the presence of  $1 \times 10^{-3}$  M **PMDI**. At 420 nm, the initial fast decay is due to the triplet and the long-lived residual absorption is due to **AN<sup>+</sup>\***. At 720 nm, the fast decay is assigned to oxygen quenching of **PMDI<sup>\*</sup>** and the residual absorption is due to **AN<sup>+</sup>\***. By using the residual absorption,  $\Phi_{cs}$  was calculated and the value obtained was 0.056. In the absence of oxygen,  $\Phi_{cs}$  was 0.08. This study prompted us to suggest that more than 50% of the CS state observed under argon-saturated conditions originated from the intra-ensemble pathway at high **PMDI** concentrations.

The reason for the long lifetime of the CS state is not exactly understood. The following factors, however, can contribute. 1) A small fraction of the radical-ion products arise through the triplet pathway [eq. (17)]. BET in the triplet ion pair is spin forbidden and hence slow. 2) **AN** and **PMDI** units in **PMDI**⊃**ANCD** are separated by a small distance and if there are no water molecules in this space, the BET has to occur either through space or through several bonds of the  $\beta$ -CD framework, leading to low BET rates.

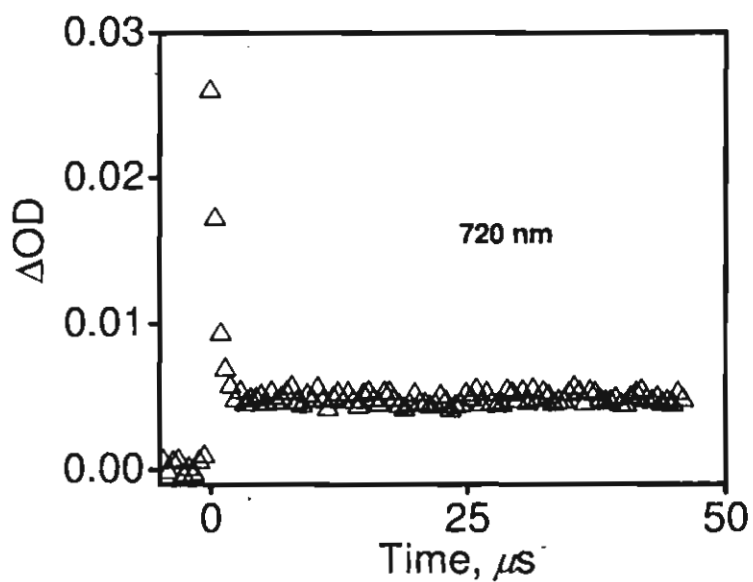
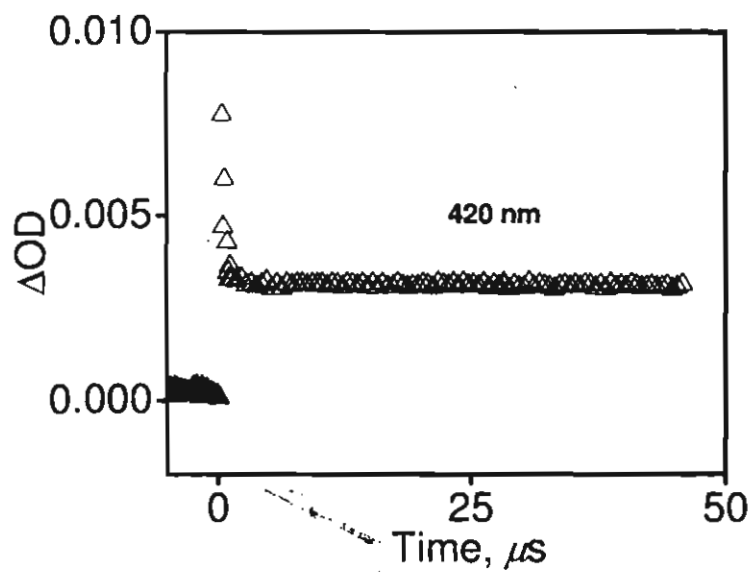


**Figure 3.22.** Kinetic traces at 420 (a) and 720 nm (b) for the oxygen-saturated ANCD ( $7 \times 10^{-5}$  M) solution in the presence of  $1 \times 10^{-3}$  M PMDI.

3) The **PMDI**<sup>•</sup> formed is polar and may exhibit a tendency to move out to the polar aqueous environment, leading to an increase in distance between **AN**<sup>•+</sup> and **PMDI**<sup>•</sup>. Control of BET by this latter mechanism has been suggested in a few cases.<sup>29</sup> 4) For the **AN**–**PMDI** system studied here,  $\Delta G_{(\text{BET})}^0 = -1.72$  and  $\lambda \approx 1$  eV. Thus, the BET process occurs in the deep inverted region and this can also result in an enhanced lifetime for the CS state. Fukuzumi and co-workers have recently observed a long lifetime for the CS state in a  $\pi$ -complex formed between co-facial free-base bisporphyrin and the acridinium ion.<sup>30</sup> The long lifetime of the CS state was attributed to inverted region effects in this case.

### 3.4. Conclusion

A supramolecular dyad **PMDI**⊃**ANCD** with the **AN** donor covalently attached to  $\beta$ -CD and a **PMDI** acceptor encapsulated within the  $\beta$ -CD cavity was assembled. The encapsulation process was studied by UV/Vis, ICD, <sup>1</sup>H NMR, CV, MALDI-TOF and fluorescence techniques. The association constant was determined by three methods. The results suggested that the **PMDI** moiety is encapsulated with the aromatic ring at the centre of the cavity. The *N*-(2-propyl) end of **PMDI** is at the narrower rim and the *N*-ethylpyridinium end is at the wider rim exposed to the aqueous medium. **PMDI** quenches the singlet and triplet excited states of **AN** by an electron-transfer mechanism. The radical cation of **AN** and radical anion of **PMDI** were observed in flash photolysis experiments. At

[PMDI] <  $10^{-4}$  M, the system exists as free molecules and fluorescence quenching is negligible. AN radical cations and PMDI radical anions are formed even under these conditions, and this is attributed to diffusion mediated triplet quenching. At higher concentrations of PMDI, the equilibrium is largely in favour of PMDI $\rightarrow$ ANCD and intra-ensemble PET processes are favoured. The rate constant for electron transfer within the ensemble from the singlet excited state of AN was measured. The experimentally determined rate constant agreed very well with that calculated using the Marcus equation. A fraction of the CS state was very long lived, suggesting that the non-covalent approach is useful in the design of artificial photosynthetic systems.

### 3.5. Experimental section

#### 3.5.1. General techniques

NMR spectra were recorded using a 300 MHz Bruker Avance DPX spectrometer. MALDI mass spectrometry was conducted on a Perspective Biosystems Voyager DEPRO MALDI-TOF spectrometer in a matrix of  $\alpha$ -cyano-4-hydroxycinnamic acid. High-resolution mass spectra were obtained by using a JOEL JMS600 mass spectrometer. Absorption spectra were obtained using a Shimadzu 3101PC UV/Vis-NIR scanning spectrophotometer. ICD spectra were obtained using a JASCO J-810 circular dichroism spectropolarimeter. Steady-state fluorescence experiments were performed with a SPEX Fluorolog F112X spectrofluorimeter by using optically dilute solutions. The fluorescence quantum

yield of **ANCD** in water was determined by the relative method employing an optically matched solution of **AN** in ethanol as reference ( $\Phi_R = 0.27$ ).<sup>31</sup> The following equation was used [eq. (18)],<sup>32</sup>

$$\Phi_F = \Phi_R \frac{A OD_R n^2}{A_R OD n_R^2} \quad (18)$$

where, the subscript R refers to the reference, OD is the optical density at the excitation wavelength,  $n$  is the refractive index of the solvent and  $A$  is the area under the fluorescence spectrum. CV experiments were performed by using a BAS 50W voltammetric analyzer. Solutions of the compounds ( $1 \times 10^{-3}$  M) in water containing 0.1 M potassium nitrate were thoroughly deaerated and used for CV experiments. Time-resolved fluorescence experiments were performed by using an IBH picosecond single-photon counting system employing a 401 nm nano-LED excitation source and a Hamamatsu C4878-02 microchannel plate (MCP) detector. Laser flash photolysis experiments were performed by using an Applied Photophysics Model LKS-20 laser kinetic spectrometer by using the third harmonic (355 nm) from a GCR-12 series Quanta Ray Nd:YAG laser. Quantum yields of the triplet ( $\Phi_T$ ) and CS ( $\Phi_{CS}$ ) states were determined by relative actinometry employing a solution of benzophenone (**BP**) in benzene as reference. equation (19) was used for calculating the quantum yields.<sup>33</sup>

$$\Phi_M = \Phi_R \frac{\Delta OD_M \epsilon_R}{\Delta OD_R \epsilon_M} \quad (19)$$

In equation (19), the subscript M refers to the state under consideration (triplet or CS state) and R refers to **BP**;  $\Delta OD$  is the end-of-pulse optical density of transients and  $\epsilon$  the extinction coefficients of transients. For **BP**, values of  $\Phi_R = 1.0$  and  $\epsilon_R = 7600 \text{ M}^{-1} \text{ cm}^{-1}$  at  $530 \text{ nm}$ <sup>34</sup> were used. For calculating  $\Phi_T$ , the reported extinction coefficient of the triplet-triplet absorption of **AN** ( $\epsilon_T = 45,500 \text{ M}^{-1} \text{ cm}^{-1}$  at  $420 \text{ nm}$ )<sup>35</sup> was used. For the calculation of  $\Phi_{CS}$ , known extinction coefficients of the **AN** radical cation ( $\epsilon_{AN^{+\bullet}} = 11,600 \text{ M}^{-1} \text{ cm}^{-1}$  at  $720 \text{ nm}$ )<sup>36</sup> and **PMDI** radical anion ( $\epsilon_{PMDI^{\bullet-}} = 41,700 \text{ M}^{-1} \text{ cm}^{-1}$  at  $720 \text{ nm}$ )<sup>24</sup> were employed. Rate constants ( $k$ ) for the various processes were obtained from  $\Phi$  and  $\tau_F$  values by using standard equations.<sup>37</sup> Solutions for laser flash photolysis studies were deaerated by purging with argon for 20 min before experiments. Unless stated otherwise, all experiments were performed at  $20 \text{ }^\circ\text{C}$ .

### 3.5.2. Materials

**Synthesis of ANCD:** ANCD was prepared as shown in Scheme 3.1. 9-Bromomethylantracene (0.4 g) was added to a solution of  $\beta$ -CD (1.7 g, 1.49 mmol) in 2,6-lutidine (40 mL) and dry DMF (40 mL) and the mixture was heated at  $150 \text{ }^\circ\text{C}$  under an argon atmosphere for 3.5 h. The solvents were removed under vacuum and the solid was washed several times with ethyl acetate and purified by

chromatography over silica gel by using methanol/ethyl acetate 1:1 as the eluent. The product was further purified by chromatography (Sephadex column) by using deionized water as the eluent. The crude product was obtained in about 30% yield and this was purified by repeated column chromatography over silica gel. Yield of pure ANCD was < 10%.

$^1\text{H}$  NMR (300 MHz,  $[\text{D}_6]$  DMSO)  $\delta$ (ppm): 3.2-3.8 (m, 42 H), 4.4-4.8 (m, 15 H), 5.4-5.7 (m, 14 H), 7.5-8.6 (m, 9 H);  $^{13}\text{C}$  NMR (75 MHz,  $[\text{D}_6]$  DMSO)  $\delta$ (ppm): 59.98, 60.31, 64.65, 68.85, 70.73, 71.80, 72.09, 72.48, 73.12, 73.52, 81.57, 82.05, 102.34, 102.58, 124.86, 125.22, 126.48, 126.74, 127.7, 127.93, 128.77, 129.40, 130.47, 130.99 ppm; FT-IR (KBr)  $\nu_{\text{max}}$ : 1031, 1080, 1153, 1246, 1334, 1365, 1448, 1587, 1662, 2895, 2939  $\text{cm}^{-1}$ ; UV/Vis (Water): [ $\lambda_{\text{max}}$ , nm ( $\epsilon$ ,  $\text{M}^{-1} \text{cm}^{-1}$ ): 368 (8,500)]; MS (MALDI-TOF):  $m/z = 1325 (M + \text{H})^+$ .

**Synthesis of PMDI:** PMDI was obtained by the 3-step reaction shown in Scheme 3.2.

**Preparation of 2:** Pyromellitic anhydride (1 g, 4.6 mM) was dissolved in DMF (9 mL). Isopropylamine (0.27 g, 4.6 mM) and ethanolamine (0.28 g, 4.6 mM) were added and the mixture refluxed for 6 h. Cooled and poured in to ice cold water and the precipitate formed was filtered, dried and chromatographed over silica gel. The product was eluted in 5% MeOH- $\text{CHCl}_3$  and the pure product was obtained in 29% yield.



$^1\text{H}$  NMR (300 MHz,  $[\text{D}_6]$  DMSO)  $\delta$ (ppm): 1.42 (d, 6H), 3.58-3.63 (t, 2H), 3.67-3.71 (t, 2H), 4.41 (m, 1H), 8.15 (s, 2H);  $^{13}\text{C}$  NMR (75 MHz,  $[\text{D}_6]$  DMSO)  $\delta$ (ppm): 19.76, 40.91, 42.97, 57.81, 116.95, 136.86, 136.91, 166.19, 166.41; FT-IR (KBr)  $\nu_{\text{max}}$ : 3332, 1722, 1776, 2945, 2983  $\text{cm}^{-1}$ ; HRMS:  $m/z = 303.16$  ( $\text{M}^+$ ).

**Preparation of 3: 2** (0.15 g, 0.49 mM) was added to a mixture of aqueous HBr (1 mL) and Conc.  $\text{H}_2\text{SO}_4$  (0.4 mL). Conc.  $\text{H}_2\text{SO}_4$  (0.4 mL) was again added and the solution refluxed for 3 h. The mixture was cooled and the product was extracted with dichloromethane and recrystallized from dichloromethane-methanol mixture to get the pure product in 65% yield.

$^1\text{H}$  NMR (300 MHz,  $[\text{D}_6]$  DMSO)  $\delta$ (ppm): 1.42 (d, 6H), 3.72-3.76 (t, 2H), 4.03-4.07 (t, 2H), 4.41-4.45 (m, 1H), 8.2 (s, 2H);  $^{13}\text{C}$  NMR (75 MHz,  $[\text{D}_6]$  DMSO)  $\delta$ (ppm): 19.74, 29.71, 40.33, 42.97, 117.32, 136.50, 137.18, 165.95, 166.10  $\text{cm}^{-1}$ ; FT-IR (KBr)  $\nu_{\text{max}}$ : 2983, 2941, 1774, 1724. HRMS:  $m/z = 365.13$  ( $\text{M}^+$ ).

**Preparation of PMDI:** A mixture of **3** (100 mg, 0.2 mM) and Pyridine (1.5 mL) was refluxed for 8 h and cooled. The crude product was washed with hexane and chloroform and was recrystallized from dichloromethane-methanol mixture. The yield of the product was 73%.

$^1\text{H}$  NMR (300 MHz,  $\text{D}_2\text{O}$ )  $\delta$ (ppm): 1.47 (d, 6 H), 4.41 (t, 2 H), 4.52-4.56 (m, 1 H), 4.98 (t, 2 H), 8.09 (t, 2 H), 8.23 (s, 2 H), 8.63 (t, 1 H), 8.96 (d, 2 H);  $^{13}\text{C}$  NMR (75 MHz,  $[\text{D}_6]$  DMSO)  $\delta$ (ppm): 19.75, 40.34, 42.99, 59.58, 117.29, 128.09,

136.67, 136.99, 145.47, 146.20, 166.05, 166.10; FT-IR (KBr)  $\nu_{\max}$ : 1631, 1709, 1768, 2985, 3055  $\text{cm}^{-1}$ ; UV/Vis (Water): [ $\lambda_{\max}$ , nm ( $\epsilon$ ,  $\text{M}^{-1} \text{cm}^{-1}$ )]: 314 (2840); HRMS:  $m/z = 364.02$  ( $\text{M}^+$ ).

The 9-chloromethylantracene used in the study was purchased from Aldrich and converted to **AMTAC** by adapting standard procedures. 1-Adamantylamine was purchased from Aldrich and converted to **ADAC** by treatment with aqueous hydrochloric acid. **AN** and **BP** were purchased from Aldrich and recrystallized before use.

### 3.6. References

1. (a) Balzani, V.; Juris, A. *Coord. Chem. Rev.* **2001**, *211*, 97-115. (b) Armaroli, N. *Chem. Soc. Rev.* **2001**, *30*, 113-124. (c) Kitamura, T.; Wada, Y.; Yanagida, S. *J. Fluorine Chem.* **2000**, *105*, 305-311. (d) Borja, M.; Dutta, P. K. *Nature* **1993**, *362*, 43-45. (e) Amouyal, E. *Sol. Energy Mater. Sol. Cells* **1995**, *38*, 249-276. (f) Kirch, M.; Lehn, J.-M.; Sauvage, J.-P. *Helv. Chim. Acta* **1979**, *62*, 1345-1384.
2. (a) Flamigni, L.; Baranoff, E.; Collin, J.-P.; Sauvage, J.-P. *Chem. Eur. J.* **2006**, *12*, 6592-6606. (b) Weber, J. M.; Rawls, M. T.; MacKenzie, V. J.; Limoges, B. R.; Elliot C. M. *J. Am. Chem. Soc.* **2007**, *129*, 313-320. (c) Frank, R.; Rau, H. *Helv. Chim. Acta* **2001**, *84*, 3837-3838. (d) Schuster, G. B. *Acc. Chem. Res.* **2000**, *33*, 253-260.

3. Szejtli, J. in *Comprehensive Supramolecular Chemistry, Vol. 3*; Atwood, J. L., Davies, J. E. D., MacNicol, D. D., Vögtle, F., Szejtli, J., Osa, T., Eds.; Pergamon: Oxford, 1996; pp 189-204.
4. Linn, B. O.; Paege, L. M.; Doherty, P. J.; Bochis, R. J.; Waksmunski, F. S.; Kulsa, P.; Fisher, M. H. *J. Agric. Food Chem.* **1982**, *30*, 1236-1242.
5. (a) Kodaka, M. *J. Phys. Chem.* **1991**, *95*, 2110-2112. (b) Shimizu, H.; Kaito, A.; Hatano, M. *Bull. Chem. Soc. Jpn.* **1981**, *54*, 513-519. (c) Shimizu, H.; Kaito, A.; Hatano, M. *Bull. Chem. Soc. Jpn.* **1979**, *52*, 2678-2684. (d) Harata, K.; Uedaira, H. *Bull. Chem. Soc. Jpn.* **1975**, *48*, 375-378.
6. (a) Kodaka, M. *J. Phys. Chem. A* **1998**, *102*, 8101-8103. (b) Kodaka, M. *J. Am. Chem. Soc.* **1993**, *115*, 3702-3705.
7. (a) Park, J. W.; Lee, S. Y.; Song, H. J.; Park, K. K. *J. Org. Chem.* **2005**, *70*, 9505-9513. (b) Pagliari, S.; Corradini, R.; Galaverna, G.; Sforza, S.; Dossena, A.; Montalti, M.; Prodi, L.; Zaccheroni, N.; Marchelli, R. *Chem. Eur. J.* **2004**, *10*, 2749-2758. (c) Park, J. W.; Song, H. E.; Lee, S. Y. *J. Phys. Chem. B* **2002**, *106*, 7186-7192. (d) Takakusa, H.; Kikuchi, K.; Urano, Y.; Higuchi, T.; Nagano, T. *Anal. Chem.* **2001**, *73*, 939-942. (e) Zhang, X.; Nau, W. M. *Angew. Chem. Int. Ed.* **2000**, *39*, 544-547. (f) Hossain, M. A.; Matsumura, S.; Kanai, T.; Hamasaki, K.; Mihara, H.; Ueno, A. *J. Chem. Soc., Perkin Trans. 2* **2000**, 1527-1533. (g) Hamai, S.; Koshiyama, T. *J. Photochem. Photobiol. A: Chem.* **1999**, *127*, 135-141. (h)

- 
- Nau, W. M.; Zhang, X. *J. Am. Chem. Soc.* **1999**, *121*, 8022-8032. (i)  
Bonomo, R. P.; Pedotti, S.; Vecchio, G.; Rizzarelli, E. *Inorg. Chem.* **1996**,  
*35*, 6873-6877. (j) Ueno, A.; Suzuki, I.; Osa, T. *J. Am. Chem. Soc.* **1989**,  
*111*, 6391-6397. (k) Kano, K.; Hitoshi, M.; Yoshimura, Y.; Hashimoto, S.  
*J. Am. Chem. Soc.* **1988**, *110*, 204-209. (l) Yorozu, T.; Hoshino, M.;  
Imamura, M.; Shizuka, H. *J. Phys. Chem.* **1982**, *86*, 4422-4426.
8. Chakrabarti, S. K. *Mol. Phys.* **1970**, *18*, 275-277.
9. Rekharsky, M. V.; Inoue, Y. *Chem. Rev.* **1998**, *98*, 1875-1918.
10. Jardon, P.; Gautron, R. *J. Chim. Phys. Phys.-Chim. Biol.* **1985**, *82*, 353-360.
11. Fukuzumi, S.; Nakanishi, I.; Tanaka, K. *J. Phys. Chem. A* **1999**, *103*,  
11212-11220.
12. (a) Sessler, J. L.; Brown, C. T.; O'Connor, D.; Springs, S. L.; Wang, R.;  
Sathiosatham, M.; Hirose, T. *J. Org. Chem.* **1998**, *63*, 7370-7374. (b)  
Osuka, A.; Marumo, S.; Wada, Y.; Yamazaki, I.; Yamazaki, T.; Shirakawa,  
Y.; Nishimura, Y. *Bull. Chem. Soc. Jpn.* **1995**, *68*, 2909-2915. (c)  
Wiederrecht, G. P.; Niemczyk, M. P.; Svec, W. A.; Wasielewski, M. R. *J.*  
*Am. Chem. Soc.* **1996**, *118*, 81-91. (d) Nagata, T. *Bull. Chem. Soc. Jpn.*  
**1991**, *64*, 3005-3016. (e) Freilich, S. C.; *Macromolecules* **1987**, *20*, 973-  
978.
13. Gawroński, J.; Brzostowska, M.; Kacprzak, K.; Kolbon, H.; Skowronek, P.  
*Chirality* **2000**, *12*, 263-268.

14. (a) Kaifer, A. E. in *Comprehensive Supramolecular Chemistry*, Vol. 8; Atwood, J. L., Davies, J. E. D., MacNicol, D. D., Vögtle, F., Ripmeester, J. A., Eds.; Pergamon: Oxford, 1996; pp 499-534. (b) Boulas, P. L.; Gómez-Kaifer, M.; Echegoyen, L. *Angew. Chem. Int. Ed.* **1998**, *37*, 216-247.
15. (a) Isnin, R.; Salam, C.; Kaifer, A. E. *J. Org. Chem.* **1991**, *56*, 35-41. (b) Diaz, A.; Quintela, P. A.; Schuette, J. M.; Kaifer, A. E. *J. Phys. Chem.* **1988**, *92*, 3537-3542. (c) Matsue, T.; Evans, D. H.; Osa, T.; Kobayashi, N. *J. Am. Chem. Soc.* **1985**, *107*, 3411-3417.
16. Szejtli, J. *Cyclodextrin Technology*; Kluwer-Academic: Dordrecht, 1988.
17. AM1 calculations of the molecular length were carried out using Titan Version 1 from Wavefunction Inc.; 18401, Von Karman, Suite 370, Irvine, CA 92612.
18. (a) Smitha, M. A.; Prasad, E.; Gopidas, K. R. *J. Am. Chem. Soc.* **2001**, *123*, 1159-1165. (b) Prasad, E.; Gopidas, K. R. *J. Am. Chem. Soc.* **2000**, *122*, 3191-3196.
19. Wang, Y.-H.; Zhang, H.-M.; Liu, L.; Liang, Z.-X.; Guo, Q.-X.; Tung, C.-H.; Inoue, Y.; Liu, Y.-C. *J. Org. Chem.* **2002**, *67*, 2429-2434.
20. Lakowicz, J. R. in *Principles of Fluorescence Spectroscopy*; Kluwer Academic: Dordrecht, 1999.

- 
21. (a) Gopidas, K. R.; Bohorquez, M.; Kamat, P. V. *J. Phys. Chem.* **1990**, *94*, 6435-6440. (b) Kamat, P. V.; Chauvet, J. P.; Fessenden, R. W.; *J. Phys. Chem.* **1986**, *90*, 1389-1394.
22. (a) Miller, J. R.; Bietz, J. V.; Huddleston, R. K. *J. Am. Chem. Soc.* **1984**, *106*, 5057-5068. (b) Jortner, J. *J. Chem. Phys.* **1976**, *64*, 4860-4867.
23. Weiss, E. A.; Chernick, E. T.; Wasielewski, M. R. *J. Am. Chem. Soc.* **2004**, *126*, 2326-2327.
24. Murov, S. L.; Carmichael, I.; Hug, G. L. *Handbook of Photochemistry*; Marcel Dekker: New York, 1993; p 293.
25. (a) Hayes, R. T.; Walsh, C. J.; Wasielewski, M. R. *J. Phys. Chem. A* **2004**, *108*, 2375-2381. (b) Worrall, D. R.; Williams, S. L.; Wilkinson, F. *J. Phys. Chem. B* **1997**, *101*, 4709-4716. (c) Dabestani, R.; Higgin, J.; Stephenson, D.; Ivanov, I. N.; Sigman, M. E. *J. Phys. Chem. B* **2000**, *104*, 10235-10241. (d) Li, W.; Fox, M. A. *J. Phys. Chem. B* **1997**, *101*, 11068-11076.
26. (a) Mauzerall, D. in *Photoinduced Electron Transfer, Part A*; Fox, M. A., Channon, M., Eds.; Elsevier: Amsterdam, 1988; pp. 228-244. (b) Fukuzumi, S. *Org. Biomol. Chem.* **2003**, *4*, 609-620. (c) Segura, S. L.; Martin, N.; Guldi, D. M. *Chem. Soc. Rev.* **2005**, *34*, 31-47. (d) Mallouk, T. E.; Hoertz, P. G. *Inorg. Chem.* **2005**, *44*, 6828-6840. (e) Guldi, D. M.; Imahori, H.; Tamaki, K.; Kashiwagi, Y.; Yamada, H.; Sakata, Y.; Fukuzumi, S. *J. Phys. Chem. A* **2004**, *108*, 541-548. (f) Imahori, H.; Guldi,

- D. M.; Tamaki, K.; Yoshida, Y.; Luo, C.; Sakata, Y.; Fukuzumi, S. *J. Am. Chem. Soc.* **2001**, *123*, 6617-6628.
27. Fukuzumi, S.; Kotani, H.; Ohkubo K.; Ogo, S.; Tkachenko, N. V.; Lemmetyinen, H. *J. Am. Chem. Soc.* **2004**, *126*, 1600-1601.
28. (a) Quaranta, A.; Zhang, Y.; Filippone, S.; Yang, J.; Sinay, P.; Rassat, A.; Edge, R.; Navaratnam, S.; McGarvey, D. J.; Land, E. J.; Brettreich, M.; Hirsch, A.; Bensasson, R. V. *Chem. Phys.* **2006**, *325*, 397-403. (b) Faiz, J. A.; Williams, R. M.; Silva, M. J. J. P.; De Cola, L.; Pikramenou, Z. *J. Am. Chem. Soc.* **2006**, *128*, 4520-4521. (c) Pal, S. K.; Sahu, T.; Misra, T.; Ganguly, T.; Pradhan, T. K.; De, A. *J. Photochem. Photobiol. A: Chem.* **2005**, *174*, 138-148. (d) Haider, J. M.; Chavarot, M.; Weidner, S.; Sadler, I.; Williams, R. M.; De Cola, L.; Pikramenou, Z. *Inorg. Chem.* **2001**, *40*, 3912-3921. (e) Hamachi, I.; Takashima, H.; Hu, Y.-Z.; Shinkai, S.; Oishi, S. *Chem. Commun.* **2000**, 1127-1128.
29. (a) Willner, I.; Willner, B. in *Frontiers in Supramolecular Organic Chemistry and Photochemistry*; Schneider, H.-J., Dürr, H., Eds.; VCH: Weinheim, 1991; pp 337-370. (b) Adar, E.; Degani, Y.; Goren, Z.; Willner, I. *J. Am. Chem. Soc.* **1986**, *108*, 4696-4700. (c) Manoj, N.; Gopidas, K. R. *Phys. Chem. Chem. Phys.* **1999**, *1*, 2743-2748.
30. Tanaka, M.; Ohkubo, K.; Gros, C. P.; Guillard, R.; Fukuzumi S. *J. Am. Chem. Soc.* **2006**, *128*, 14625-14633.

- 
31. Melhuish, W. H. *J. Phys. Chem.* **1961**, 65, 229-235.
  32. Eaton, D. F. in *Handbook of Organic Photochemistry, Vol. 1*; Scaiano, J. C., Ed.; CRC Press: Boca Raton, Florida, 2000; p 234.
  33. Lutz, H.; Breheret, E.; Lindqvist, L. *J. Phys. Chem.* **1973**, 77, 1758-1762.
  34. Bensasson, R.; Land, E. J. *J. Photochem. Photobiol. Rev.* **1978**, 3, 163-191.
  35. Carmichael, I.; Hug, G. L. in *Handbook of Organic Photochemistry, Vol. 1*; Scaiano, J. C., Ed.; CRC Press: Boca Raton, Florida, 2000; p 377.
  36. Wang, Y.; Tria, J. J.; Dorfman, L. M. *J. Phys. Chem.* **1979**, 83, 1946-1951.
  37. Turro, N. J. in *Modern Molecular Photochemistry*; University Science Books: California, 1992.



## Chapter 4

---

### Self-Assembly and Photoinduced Electron Transfer Processes in a Donor-Cyclodextrin-Acceptor Type Ternary System

---

#### 4.1. Abstract

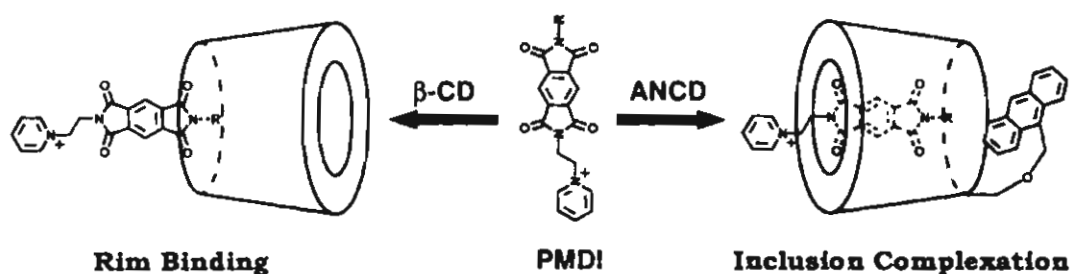
*In this chapter self-assembly of an adamantane-attached pyrene donor and a pyromellitic diimide acceptor into a  $\beta$ -CD scaffold to yield a donor- $\beta$ -CD-acceptor type ternary system, is reported. The propensity of pyromellitic diimides for rim binding with the primary side of  $\beta$ -CD and the high affinity of adamantane moiety for  $\beta$ -CD cavity are utilized in the design of this ternary system. Self-assembly of the ternary system did not involve synthesis or purification of CD-appended systems.  $\beta$ -CD has three functions in the self-assembled system, namely, partial encapsulation of donor, rim-binding of acceptor and serving as a rigid spacer between donor and acceptor. Formation of the ternary complex was established using  $^1\text{H}$  NMR, induced circular dichroism (ICD) and MALDI-TOF data. PET in the ternary system was studied by steady state and time resolved fluorescence experiments.*

---

## 4.2. Introduction

In the earlier chapters we have employed chromophore appended CDs to assemble supramolecular D-A systems for PET reactions in water. Photoexcitation would then lead to electron transfer between the appended chromophore and encapsulated guest. The hydrophobic nature of the CD cavity acts as the assembler of the D-A system here. This approach suffers from two major disadvantages: (1) The CD assembles only one component and the other component needs to be assembled by covalent linkage; (2) Synthesis and purification of the chromophore-appended CD is a very tedious process. These reactions generally proceed with modest yields. But purification of the CD appended chromophores from the unreacted cyclodextrin is very difficult. This latter aspect is particularly important for photophysical studies where CD-appended systems of extremely high level of purity are required. In this context, development of alternate strategies for assembling supramolecular D-A systems that does not involve synthesis and purification of CD-appended systems, gain considerable importance. A useful strategy in this context was to search for donor (or acceptor) molecules that can selectively bind to the rim or to the outside of CD cavity. The acceptor (or donor) molecule can then be encapsulated into the CD cavity, leading to the formation of CD-based, non-covalent ternary systems capable of undergoing photoinduced electron or energy transfer reactions.

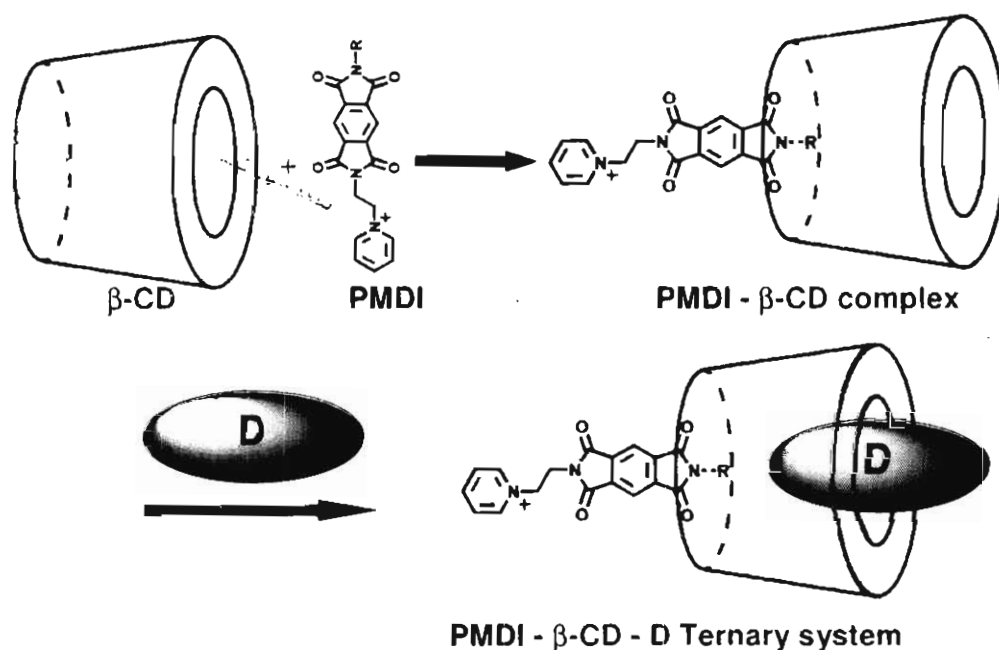
In Chapter 3 of this thesis we have presented a detailed investigation of the interaction of a pyromellitic diimide (**PMDI**) derivative with an anthracene-appended  $\beta$ -CD (**ANCD**). These studies have clearly established that the **PMDI** is encapsulated into the cavity of **ANCD** with the aromatic part placed at the centre of the cavity, the *N*-alkyl group sitting at the narrow rim among the overhanging primary hydroxyl groups and the *N*-ethylpyridinium moiety sitting at the secondary rim exposed to water. During the course of these investigations we have noticed that **PMDI** has an entirely different mode of interaction with native  $\beta$ -CD. In order to have a clear understanding of this interaction we have carried out a detailed investigation of the self-assembly of three **PMDI** derivatives with native  $\beta$ -CD and **ANCD**. These studies have unequivocally established that **PMDI**s get themselves encapsulated into the cavity of **ANCD**, whereas with native  $\beta$ -CD they prefer to remain just outside of the narrow rim as shown in Scheme 4.1.



Scheme 4.1

We have coined the term 'Rim-binding' to describe the complexation mode of **PMDI** with  $\beta$ -CD as shown in Scheme 4.1. In the rim binding mode most of the

CD cavity is empty and one could in principle design specific guest molecules capable of inclusion into the partially filled cavity through the secondary side leading to the formation of CD based ternary system as shown in Scheme 4.2.



Scheme 4.2

**PMDI** is a well known acceptor in PET reactions and if the guest molecule is capable of donating an electron in its excited state to **PMDI**, then the strategy shown in Scheme 4.2 could result in the assembly of a CD based donor-acceptor assembly. The important advantage of this strategy is that it does not involve any covalent synthesis of CD-appended systems. In this chapter we report, for the first time, the self-assembly of such a ternary system.

This chapter is arranged in two sections. In the first section, rim-binding of PMDI with  $\beta$ -CD is described in detail. In order to distinguish clearly between rim-binding and encapsulation, interaction of PMDI with ANCD is also investigated and a comparison is made between the two binding modes. In the second section, assembly of the functional ternary system is described. Steady state and time resolved fluorescence experiments which clearly demonstrated the PET processes in the ternary system are then described.

### 4.3. Results and Discussion

#### 4.3.1. Interactions of PMDI Derivatives with $\beta$ -CD and ANCD

In this section the interactions of PMDI derivatives with ANCD and  $\beta$ -CD are studied using induced circular dichroism and  $^1\text{H}$  NMR spectroscopies. Structures of ANCD and PMDI derivatives employed are shown in Chart 4.1.

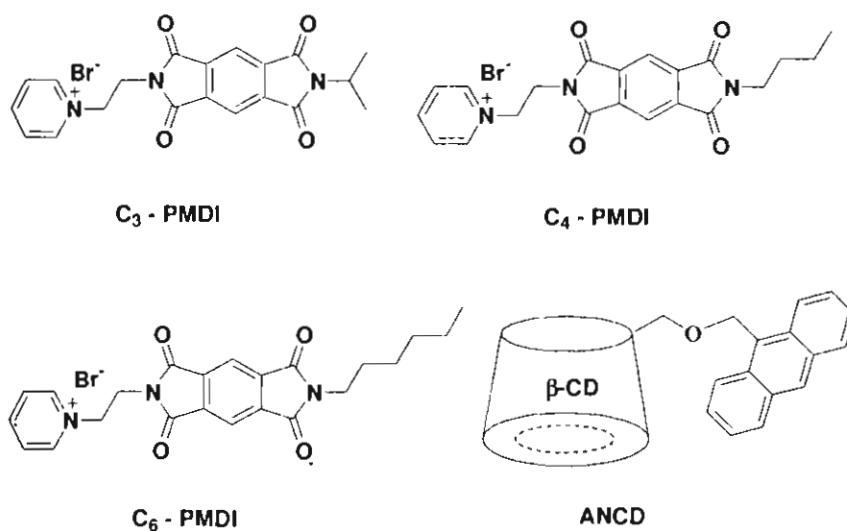
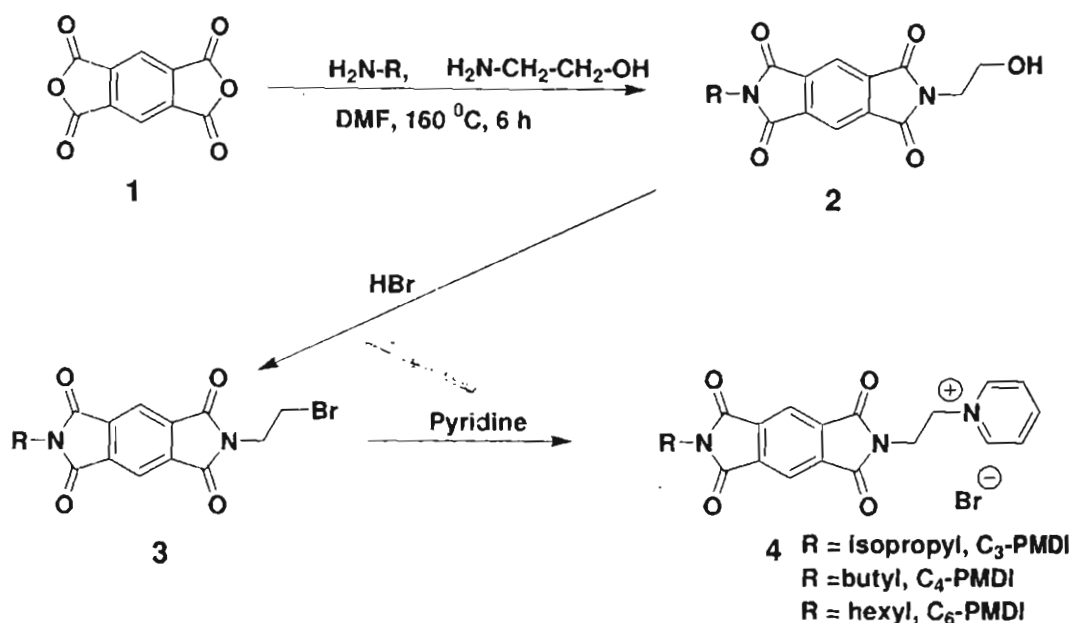


Chart 4.1

### 4.3.1.1. Synthesis and Characterization of PMDIs

The **PMDI** derivatives were synthesized by the route shown in Scheme 4.3. Structures of the **PMDI** derivatives were confirmed by all spectroscopic methods (see experimental section for details).



Scheme 4.3

### 4.3.1.2. Inclusion Complexation and Rim-Binding

All the **PMDI** derivatives exhibited similar absorption spectra with  $\lambda_{\text{max}} = 314 \text{ nm}$  and  $\epsilon_{\text{max}} = 2.8 \times 10^3 \text{ M}^{-1} \text{ cm}^{-1}$ . The **C<sub>4</sub>-PMDI** and **C<sub>6</sub>-PMDI** exhibited slight aggregation in water and as a result the absorption spectra of these derivatives showed residual absorption at long wavelength region. Although the absorption spectra of **PMDIs** exhibited changes in the presence of  $\beta$ -CD, the

residual absorption exhibited by these derivatives made it difficult to extract the association constant from absorption spectroscopy. In this section complexation of **PMDIs** with  $\beta$ -CD and ANCD are studied using ICD and  $^1\text{H}$  NMR techniques.

Figure 4.1 shows ICD spectra of the **PMDIs** in presence of  $\beta$ -CD and Figure 4.2 shows ICD spectra of **PMDIs** in presence of ANCD. ICD spectra shown in Figures 4.1 and 4.2 differ in several respects. (1) The  $\beta$ -CD:**PMDI** systems exhibit negative ICD signals where the signal intensity increased with alkyl chain length. (2) The ANCD:**PMDI** systems showed strong positive ICD signals where the signal intensity decreased with alkyl chain length.

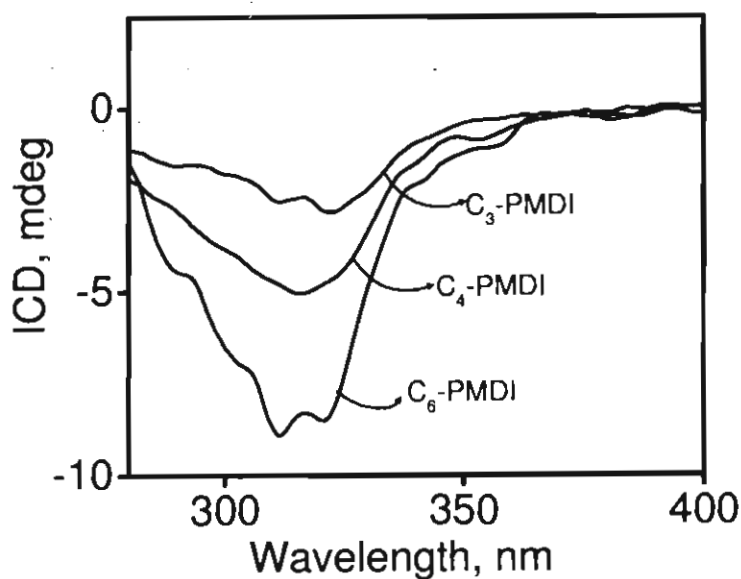


Figure 4.1. ICD of **PMDIs** ( $3.5 \times 10^{-4}$  M) in presence of  $\beta$ -CD ( $1.4 \times 10^{-3}$  M).

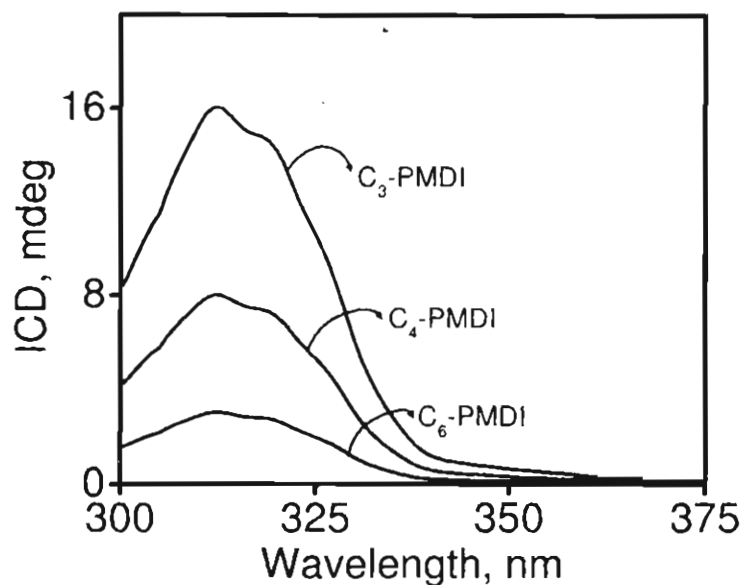


Figure 4.2. ICD of PMDIs ( $3.5 \times 10^{-4}$  M) in presence of ANCD ( $1.2 \times 10^{-5}$  M).

(3) For  $\beta$ -CD:PMDI, millimolar amounts of  $\beta$ -CD were required to obtain ICD signals whereas for ANCD:PMDI good ICD signals were obtained with  $10^{-5}$  M ANCD.

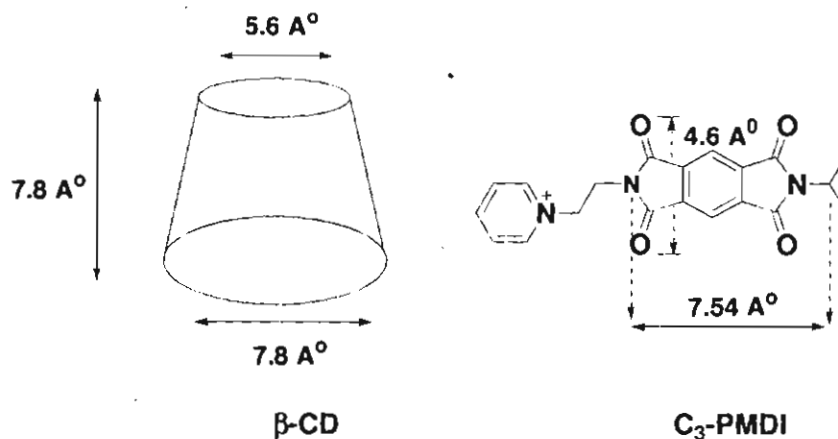
As described in the previous chapter, the sign and intensity of the ICD signal are very sensitive to the orientation of the guest with respect to the CD. The orientation of the guest is usually deduced using a set of rules introduced first by Harata et al.<sup>1</sup> and later modified by Kodaka.<sup>2</sup> The rules predict the following: (1) the sign of ICD is positive for a transition polarized parallel to the axis of the macrocyclic host, and negative for that polarized perpendicular to the axis; (2) the sign of ICD is reversed when a chromophore moves from the inside of the host cavity to the outside, keeping the direction of the transition moment unchanged;



---

(3) the absolute value of ICD is greater when a chromophore exists on the out side of the narrower rim than when it is on the out side of the wider rim; (4) the ICD value of a transition polarized perpendicular to the axis of a macrocycle is  $-1/2$  of that of a parallel-polarized one and the sign of ICD changes at  $54.7^\circ$ .

For **PMDI**s, the lowest energy absorption (314 nm) is polarized along the long axis connecting the two imide nitrogen atoms.<sup>3</sup> Thus in a parallel orientation we would expect positive ICD if **PMDI** is inside the cavity and negative ICD if **PMDI** is outside. The molecular dimensions of  $\beta$ -CD taken from literature and **PMDI** calculated using AMI method are shown in Scheme 4.4. The **PMDI** nucleus is very rigid and it is very clear from Scheme 4.4 that **PMDI** cannot be accommodated into the  $\beta$ -CD cavity with its N-N axis perpendicular to the  $C_7$  axis of the CD. On the basis of these factors and the  $^1\text{H}$  NMR data (vide infra), the strong positive ICD of **ANCD:PMDI**s is assigned to parallel orientation of **PMDI** within the cavity and the negative ICD for the  $\beta$ -CD:**PMDI** systems is assigned to parallel orientation outside the cavity as shown in Scheme 4.1. An orientation in which **PMDI** lies just outside of the wider rim (for  $\beta$ -CD:**PMDI**) is ruled out based on geometrical considerations (vide infra).



Scheme 4.4

The association constants ( $K_a$ ) for the association of **PMDIs** with  $\beta$ -CD and **ANCD** were obtained from ~~ICD~~ ICD experiments using the Benesi-Hildebrand plots of the ICD data, assuming 1:1 stoichiometry. Consider the following equilibrium,



where,  $G \supset H$  represents the 1:1 inclusion complex in which G is the guest and H is the host and  $K_a$  is the equilibrium constant for the complex formation. Under the assumption that the concentrations of guest is much higher than that of host, the Benesi-Hildebrand relation for such an equilibrium is given by equation (2)<sup>4</sup>

$$1/(\varepsilon - \varepsilon_0) = a \{ 1/[H]_0 + 1/([H]_0 K_a [G]_0) \} \quad (2)$$

Where  $\varepsilon_0$  is the molar ellipticity of host in the absence of the guest,  $\varepsilon$  is the molar ellipticity in the presence of guest,  $[H]_0$  and  $[G]_0$  are the initial concentrations of H and G and  $a$  is a constant. If a 1:1 complex is formed, a plot of  $1/(\varepsilon - \varepsilon_0)$  vs  $1/[G]$  would yield a straight line.

For the  $\beta$ -CD/PMDI systems,  $\beta$ -CD was taken in excess. Hence [G] is replaced by  $[\beta\text{-CD}]$  and [H] is replaced by [PMDI] in equation (2) and the data obtained were analyzed. The double reciprocal plots were straight lines as shown in Figure 4.3. For  $\beta$ -CD:PMDI systems  $K_a$  values were 300 ( $C_3$ -PMDI), 700 ( $C_4$ -PMDI), and 1800 ( $C_6$ -PMDI)  $M^{-1}$  and increased in the order 2-propyl < *n*-butyl < *n*-hexyl.

For the ANCD:PMDI systems, higher concentration of ANCD could not be employed due to lack of solubility in water. Hence [G] is [PMDI] and [H] is [ANCD] for these systems. The double reciprocal plots obtained for these systems are shown in Figure 4.4.  $K_a$  values thus obtained were 1249 ( $C_3$ -PMDI), 596 ( $C_4$ -PMDI), and 533 ( $C_6$ -PMDI)  $M^{-1}$ . It is to be mentioned that the values increased in the reverse order here compared to  $\beta$ -CD/PMDI systems.

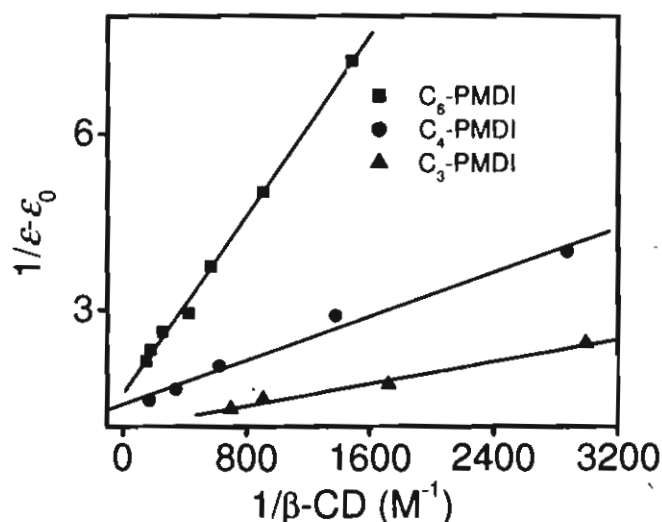


Figure 4.3. Benesi-Hildebrand plot of  $1/\Delta\epsilon$  vs  $1/[\beta\text{-CD}]$ .

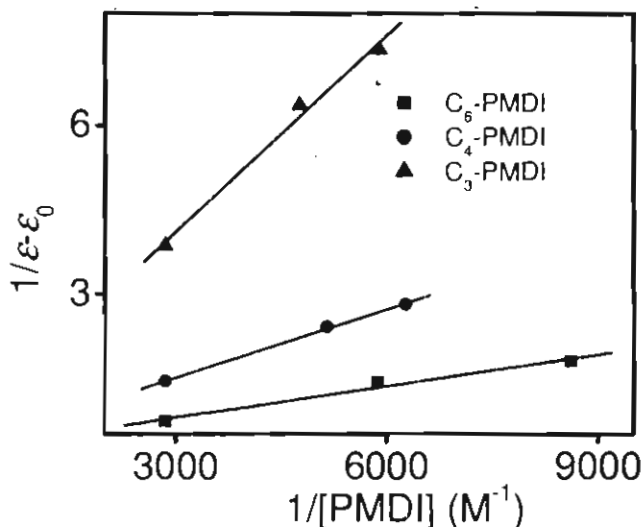


Figure 4.4. Benesi-Hildebrand plot of  $1/\Delta\epsilon$  vs  $1/[PMDI]$ .

Orientations for the complexes shown in Scheme 4.1 were confirmed by  $^1H$  NMR studies. Figure 4.5 and 4.6 shows the changes in the  $^1H$  NMR spectra of  $C_4$ -PMDI upon the addition of  $\beta$ -CD and ANCD, respectively. Assignments of the various protons are also indicated in the figures. For the  $C_4$ -PMDI/ $\beta$ -CD system, addition of  $\beta$ -CD leads to small changes for the alkyl (0.06 – 0.14 ppm for protons *a*, *b* and *c*) and aromatic (0.09 ppm for proton *e*) protons. The changes in the  $\Delta\delta$  value for these protons upon the addition of  $\beta$ -CD are shown in Figure 4.7. Protons of the pyridinium group (*h*, *i* and *j*) are unaffected indicating that this moiety is placed away from the CD. Effect of addition of  $\beta$ -CD on the  $^1H$  NMR of  $C_3$ -PMDI and  $C_6$ -PMDI were also very small.

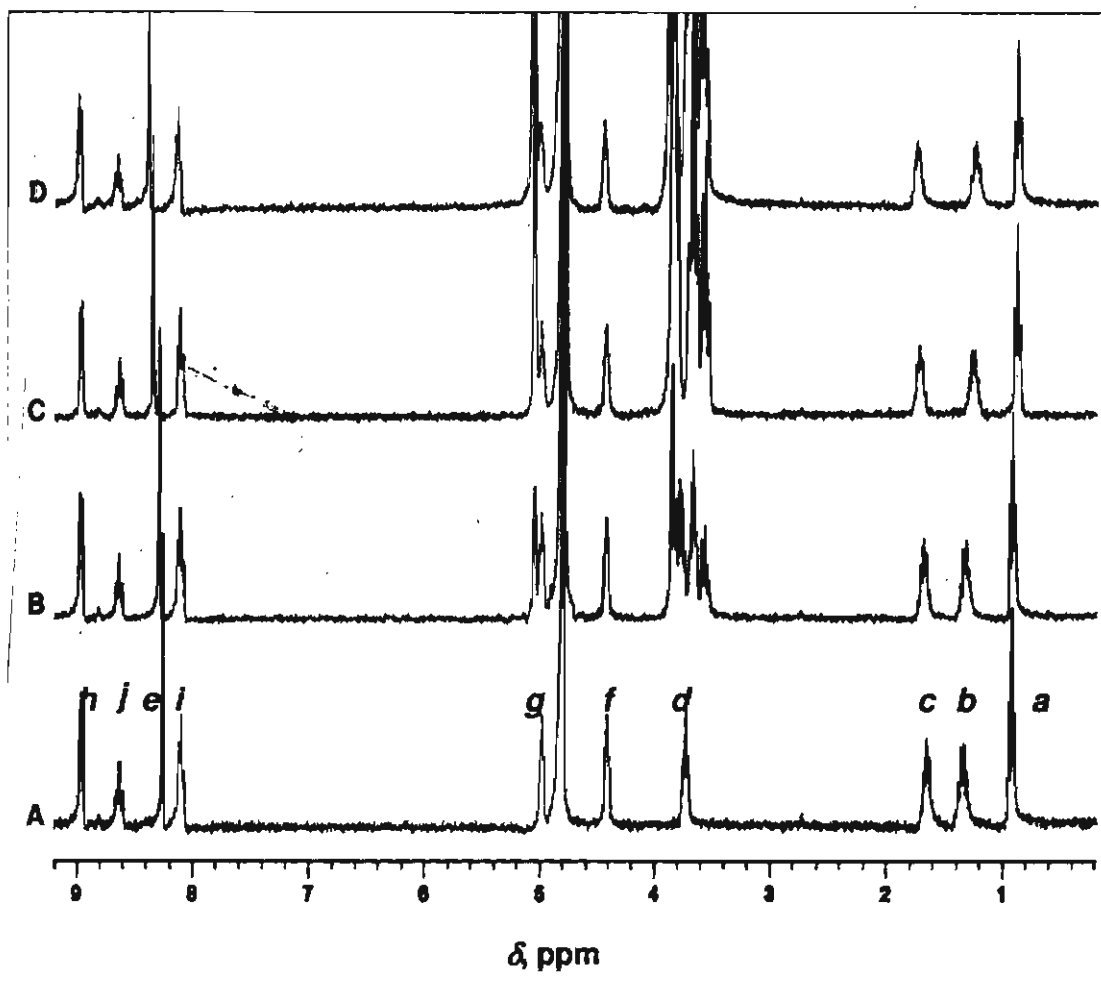
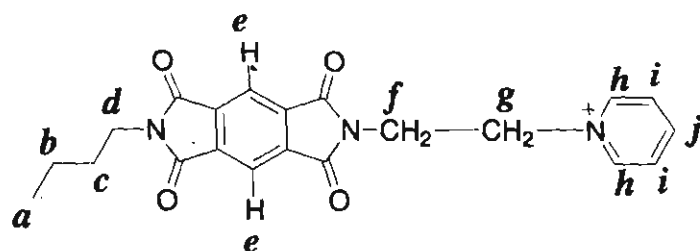


Figure 4.5. NMR Spectra of  $C_4$ -PMDI ( $1.1 \times 10^{-2}$  M) in the (A) absence and (B) - (D) presence of  $\beta$ -CD. Concentration of  $\beta$ -CD were (B)  $0.4 \times 10^{-2}$  M (C)  $0.8 \times 10^{-2}$  M (D)  $1.1 \times 10^{-2}$  M.

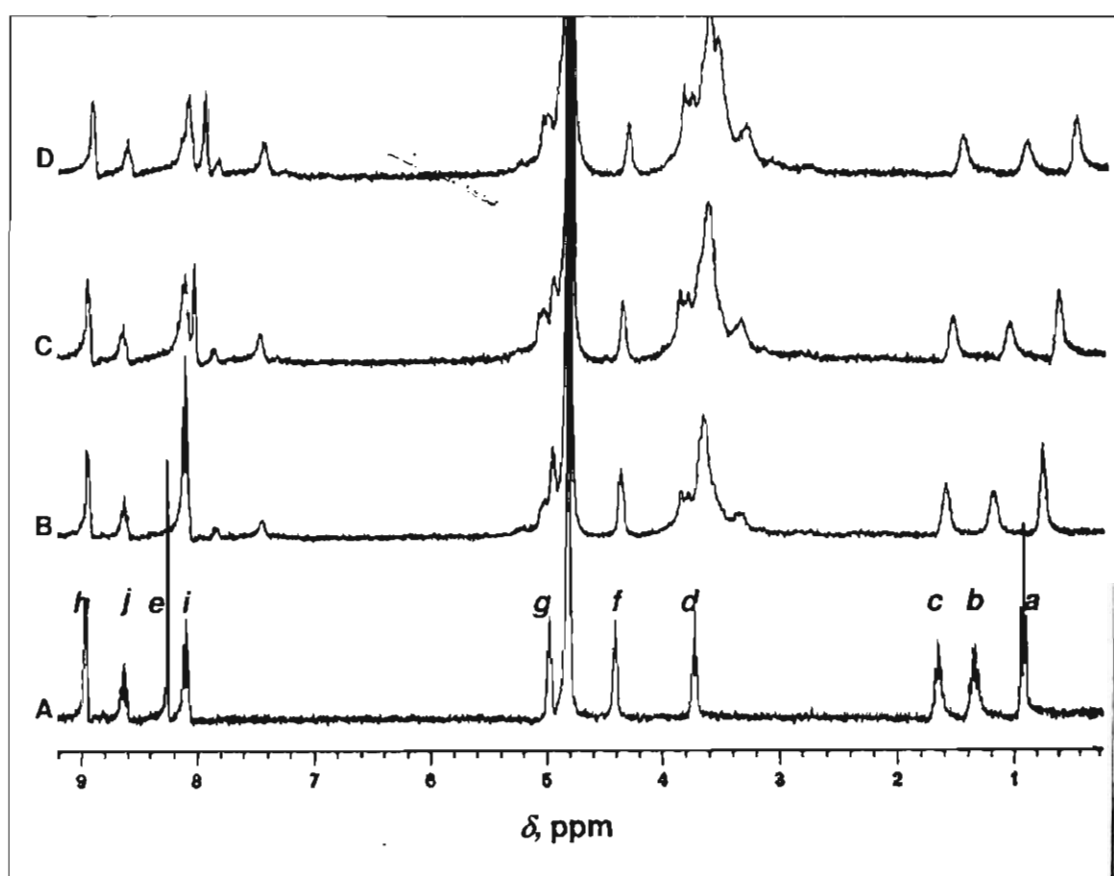
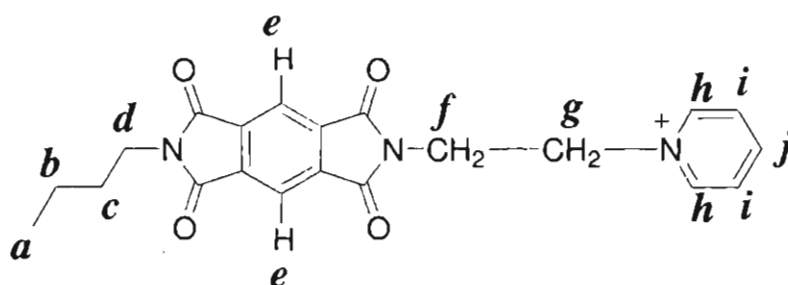


Figure 4.6. NMR Spectra of  $C_4$ -PMDI ( $1.1 \times 10^{-2}$  M) in the (A) absence and (B) - (D) presence of ANCD. Concentration of ANCD were (B)  $0.4 \times 10^{-2}$  M (C)  $0.8 \times 10^{-2}$  M (D)  $1.1 \times 10^{-2}$  M.

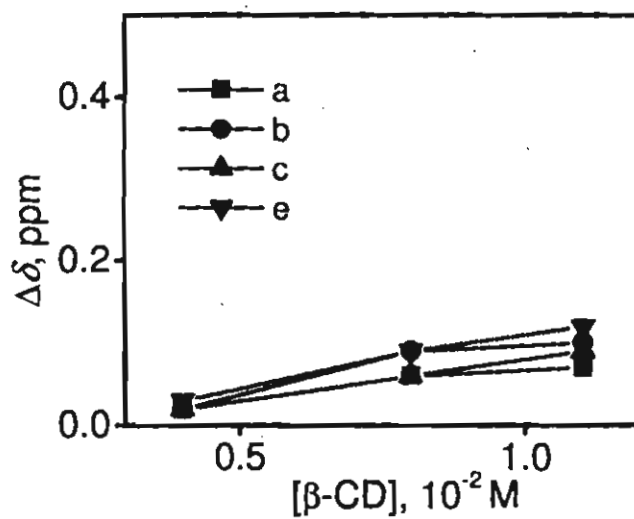


Figure 4.7. Changes in the  $^1\text{H}$  NMR chemical shifts of  $\text{C}_4\text{-PMDI}$  upon addition of  $\beta\text{-CD}$ . Assignments of the various protons are also indicated.

Addition of ANCD, on the other hand, led to drastic shifts in the signals of all PMDI protons except for the pyridinium protons as shown in Figure 4.6 and 4.8.

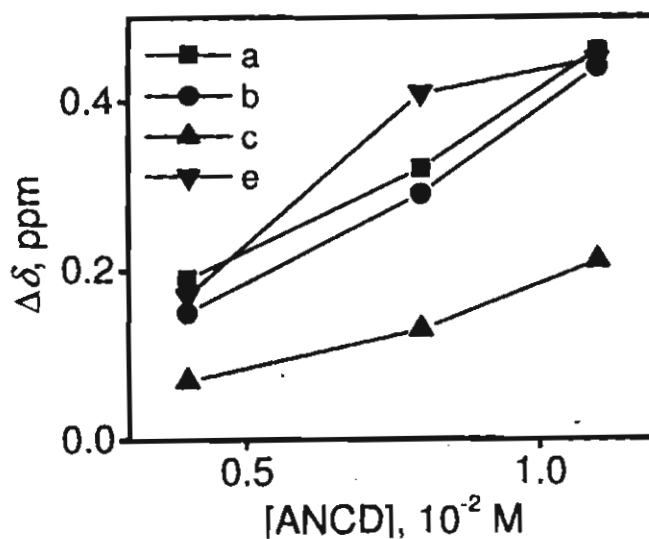


Figure 4.8. Changes in the  $^1\text{H}$  NMR chemical shifts of  $\text{C}_4\text{-PMDI}$  upon addition of ANCD. Assignments of the various protons are also indicated.

---

The alkyl protons experienced considerable broadening, loss of splitting pattern and shifts in the 0.3 – 0.7 ppm range. The aromatic proton is shifted by 0.4 ppm along with broadening, indicating that this moiety is tightly bound within the CD cavity. Results similar to these are obtained for complex formations of **ANCD** with **C<sub>3</sub>-PMDI** (shown in Chapter 3) and **C<sub>6</sub>-PMDI**.

In the conformation shown for  $\beta$ -CD:**PMDI** systems (Scheme 4.1) most parts of the **PMDI** molecule are exposed to water. Native  $\beta$ -CD contains about six water molecules inside the cavity. When the alkyl group inserts into the cavity through the narrow rim, a few water molecules might be displaced, but the alkyl chain is still exposed to water that can enter and leave the cavity through the wider rim. The microenvironment around **PMDI** chromophore does not change much and hence changes observed for the aromatic protons are very small. It is not clear as to why **PMDIs** associate with  $\beta$ -CD in this fashion, although some conclusions can be drawn from general considerations. The most hydrophobic part in **C<sub>3</sub>-PMDI** for example, is the 2-propyl group. The pyridinium moiety is very hydrophilic and prefers to be in water. The imide moieties have two carbonyl groups each, capable of hydrogen bond formation with water, making them relatively hydrophilic. In the conformation shown in Scheme 4.1, the imide group at the pyridinium end remains unaffected. The imide group at the 2-propyl end can engage itself in hydrogen bonding interactions with the primary OH groups at the narrow rim. Since the diameter of the narrow rim (5.6 Å) and the O-O distance of



---

the imide group are similar (4.6 Å), H-bonding can result in the formation of a rigid structure. Hence we categorize these as “Rim-Binding” type complexes.  $K_a$  values in these systems increase with increase in alkyl chain length due to the cooperative interactions of hydrogen bonding and alkyl group insertion.

The conformation shown for **ANCD:PMDI** is a closed conformation. The anthracene moiety present at the small rim acts as a lid for the CD. The **PMDI** gets inserted into the cavity through the wider rim with the alkyl group near the narrow rim and the pyridinium group remaining in the aqueous phase near the wider rim. The aromatic moiety of **PMDI** is relatively large and provides a tight fit near the wider rim. In such a conformation all water molecules present in the cavity would be displaced to the outside and the cavity becomes highly hydrophobic, leading to substantial shifts in the NMR signals. As the alkyl chain becomes larger, more and more of the aromatic moiety will be displaced to the outside of the wider rim. The cavity becomes more open leading to decrease in hydrophobicity resulting in lower association constants and NMR shifts. When anthracene group is attached to one of the primary OH groups, the **AN** moiety undergoes partial self-inclusion through the narrow rim forcing the **PMDI** molecule to approach the cavity through the wider rim with the more hydrophobic alkyl chain entering it first. The **ANCD:PMDI** systems are true inclusion complexes. In this conformation one of the imide groups is forced inside the CD cavity and no hydrogen bonding interaction is available to it. The cavity is highly

---

hydrophobic, which stabilizes the alkyl groups and compensates for the loss of H-bonding interaction suffered by one of the imide groups. As the alkyl chain length increases the aromatic moiety of **PMDI** is gradually pushed out leading to a decrease in the hydrophobicity of the cavity, which results in a reduction in the ICD signal intensity,  $^1\text{H}$  NMR shifts and  $K_a$  values.

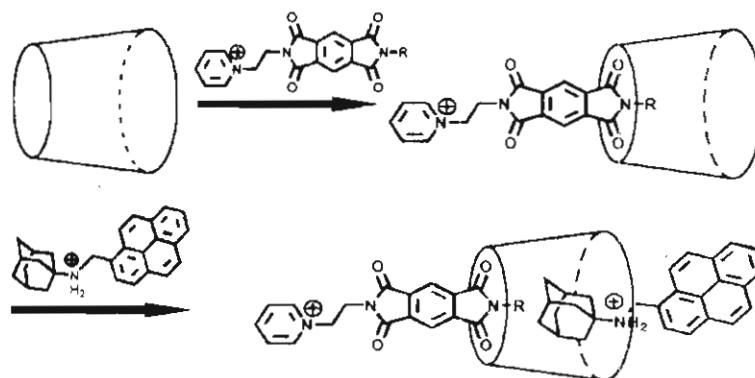
In most of the CD complexes reported in literature, the guest molecules are either completely or partially encapsulated into the CD cavity and hence these are generally known as inclusion complexes. Nearly a thousand papers appear every year on CD systems and ~~about~~ 22% of these papers deal with studies of inclusion complexes,<sup>5</sup> leading to the common belief that all CD complexes are inclusion complexes. A large number of CD complexes are reported in the literature and at least in some of these cases where the substrates are loaded with hydrogen bond acceptor groups, non-inclusion complexes of the type described here for  $\beta$ -CD/**PMDI** are probable. It should be mentioned here that binding of guests to the rim of  $\beta$ -CD has been reported, but in most of these cases the studies are carried out at high pH values where the OH groups deprotonate.<sup>6</sup> The case presented here is clearly different. The rim-binding-type association described here could be very important in the context of designing supramolecular structures. In the following section we utilize the rim-binding property of  $\beta$ -CD/**PMDI** system for designing donor- $\beta$ -CD-acceptor type ternary systems.

---

### 4.3.2. Design and Study of Donor- $\beta$ -CD-Acceptor Ternary System

In section 4.3.1 we have shown that **PMDI** derivatives form 'Rim-binding' complexes with  $\beta$ -CD. Rim-binding type association described here could be very important in the context of designing supramolecular systems. In the rim-binding conformation most of the CD cavity is empty and this aspect can be utilized to design a ternary system as outlined in Scheme 4.2. In this section design and self-assembly of the ternary system are described. This is followed by fluorescence quenching studies which clearly established the donor-spacer-acceptor type properties of the self-assembled system.

Pyrene attached adamantane (**Py-Ad**, Scheme 4.5) was used as the guest in this study. Pyrene is a well known electron donor and is capable of donating an electron to **PMDI** from its excited state. Adamantane derivatives are well known for their binding to  $\beta$ -CD ( $K_a \geq 10^5 \text{ M}^{-1}$ ).<sup>7</sup> Using molecular models Breslow et al. had previously shown that adamantane derivatives bind to  $\beta$ -CD cavity through the secondary side and that the adamantane nucleus occupies only 65% of the cavity space.<sup>8</sup> In the rim-bound state **PMDI** indeed lies outside of the primary rim and one can in principle use **Py-Ad** as an encapsulating guest and assemble a supramolecular ternary system as shown in Scheme 4.5.



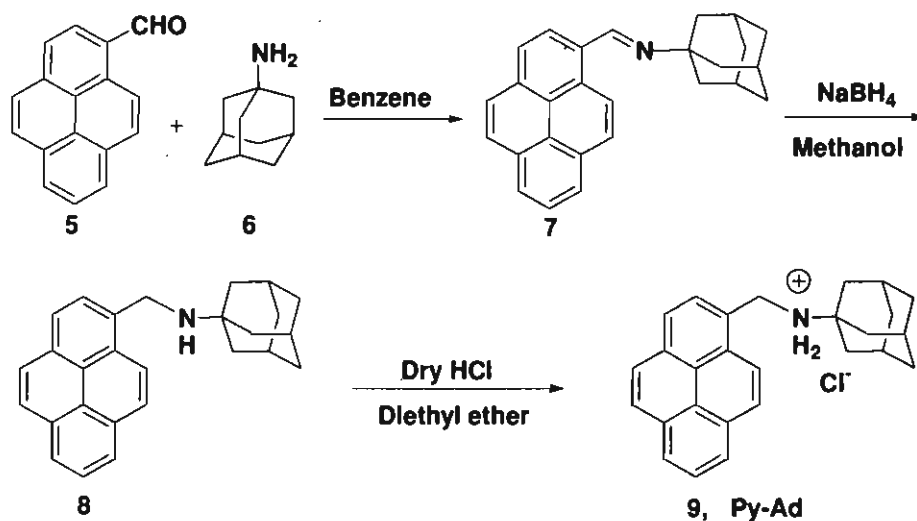
Scheme 4.5

The greatest advantage of this design is that covalent synthesis of CD-appended systems is not required for this self-assembly. A simple mixing of the constituents is sufficient. It is to be mentioned that CD based ternary systems of uncertain structures were known previously.<sup>9</sup> Ternary complexes are proposed to be formed when fluorophores such as naphthalene or pyrene are dissolved in aqueous solutions of  $\beta$ -CD or  $\gamma$ -CD in the presence of small aliphatic amines<sup>9b</sup> or alcohols.<sup>9c</sup> Pyrene forms a loose complex with  $\beta$ -CD where the pyrene is only partially encapsulated into the cavity. The empty space available within the cavity can host small molecules leading to the formation of ternary complexes. In the pyrene/ $\beta$ -CD/diethylamine ternary complex, the amine is sitting close to the pyrene leading to static quenching of pyrene fluorescence. Although few ternary systems of this type are reported, detailed studies to elucidate their structure or relative orientation have not been attempted. In the context of mimicking photosynthesis, static quenching systems are not at all useful, as they do not lead

to charge separation. The ternary system assembled here is a donor-spacer-acceptor type system and is clearly superior to the co-encapsulated systems.

#### 4.3.2.1. Synthesis and Characterization of Py-Ad

Synthetic strategy for the preparation of **Py-Ad** is shown in Scheme 4.6. Pyrene Carboxaldehyde (**5**) was condensed with adamantylamine (**6**) to form the imine derivative (**7**), which was reduced with sodium borohydride to form the amine derivative (**8**). It was finally converted into a water-soluble derivative **9** by passing dry HCl through a solution of the amine (**8**) in diethyl ether.



Scheme 4.6

The <sup>1</sup>H NMR spectrum of **Py-Ad** in D<sub>2</sub>O:CD<sub>3</sub>OD (98:2) is shown in Figure 4.9. Assignments of the aliphatic protons are also shown in the Figure. 1-substituted adamantane derivatives have three chemically different types of

protons, which are denoted as  $H_a$ ,  $H_b$  and  $H_c$  in Figure 4.9. For most 1-substituted adamantanes these protons appear as two or three broad singlets. In the case of **Py-Ad** in  $D_2O: CD_3OD$  (98:2), the  $H_a$  protons appear as a quartet (Figure 4.9). To the best of our knowledge this quartet pattern is not reported for the  $H_a$  protons of any adamantane derivatives. It is very interesting to note that the  $H_a$  quartet pattern transforms to a broad singlet in the  $^1H$  NMR of **Py-Ad** in  $CD_3OD$ . We try to explain these observations by invoking a folded conformation for **Py-Ad** in  $D_2O$ .

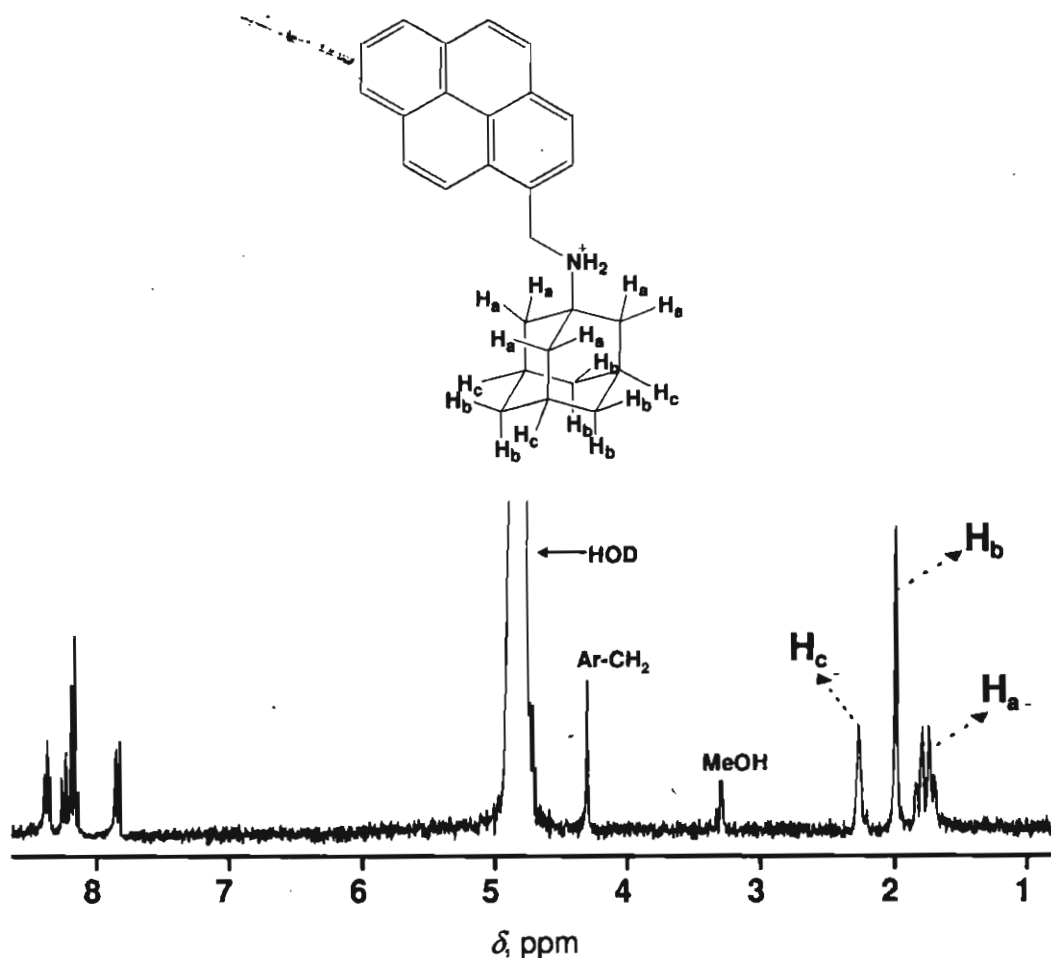


Figure 4.9.  $^1H$  NMR of **Py-Ad** in  $D_2O/CD_3OD$  (98:2).

The pyrene and adamantane moieties in **Py-Ad** are highly hydrophobic. **Py-Ad** is sparingly soluble in water because of the presence of the ammonium ( $\text{NH}_4\text{Cl}$ ) moiety in the molecule. Because of the hydrophobicity of pyrene and adamantane moieties **Py-Ad** would most probably exist in water in a folded conformation so as to minimize the area exposed to water. In the folded conformation the pyrene moiety comes very close to the  $\text{H}_a$  protons. Because of the steric crowding, the  $\text{H}_a$  protons undergo geminal coupling leading to the observed quartet pattern. Folded conformation of **Py-Ad** obtained through the AM1 method is shown in Figure 4.10. When **Py-Ad** is dissolved in  $\text{CD}_3\text{OD}$  hydrophobic interactions are absent and the molecule assumes the extended conformation shown in Figure 4.10. There is no steric crowding in the extended conformation and consequently the quartet pattern coalesces into a broad singlet.

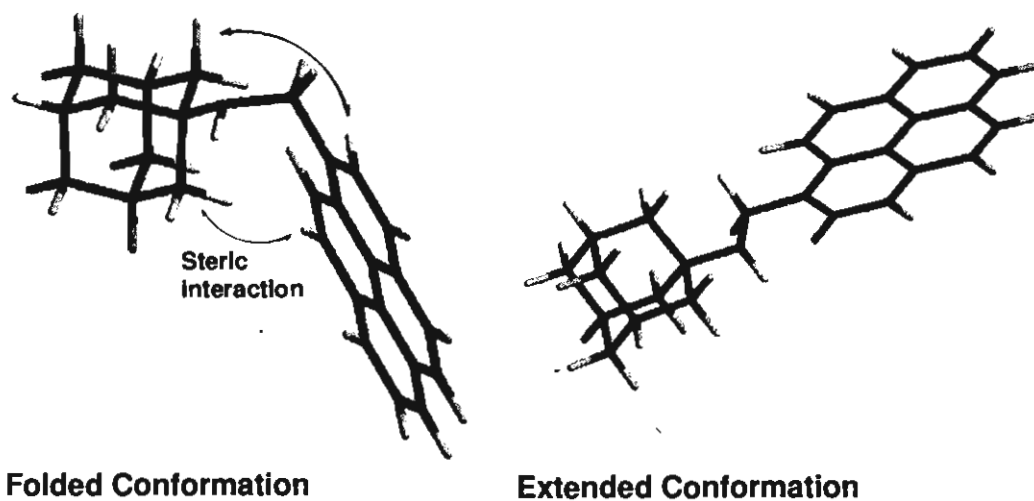


Figure 4.10. Folded and extended conformations of **Py-Ad**.

#### 4.3.2.2. Self-Assembly of the Ternary-system

Self assembly of the constituents namely **PMDI**,  $\beta$ -CD and **Py-Ad**, into the ternary system was studied using  $^1\text{H}$  NMR, induced circular dichroism and MALDI-TOF techniques. Figure 4.11 A is the  $^1\text{H}$  NMR of **C<sub>6</sub>-PMDI**. This molecule tends to aggregate in aqueous solution and hence all signals are broad and exhibit no splitting. However NMR taken in  $\text{CD}_3\text{OD}$  shows expected splitting patterns for all protons. Upon addition of one equivalent of  $\beta$ -CD, spectrum 4.11 B is obtained. The aliphatic and aromatic protons of **C<sub>6</sub>-PMDI** exhibit shifts (indicated by arrows) in the presence of  $\beta$ -CD. In addition to the shifts, splitting patterns appear for most protons. These changes, particularly the down field shift of the aromatic proton at 8.27 ppm is due to rim binding of **PMDI** with  $\beta$ -CD. Appearance of splittings for **PMDI** protons is attributed to breaking of aggregates as a result of rim binding with  $\beta$ -CD. Up on addition of one equivalent of **Py-Ad** to the above solution we obtain the  $^1\text{H}$  NMR spectrum in Figure 4.11 C and the major changes observed up on going from the components to the ternary system are indicated by arrows. On the **PMDI** side, only the aromatic proton showed a significant shift (0.43 ppm up field). On the **Py-Ad** side, several significant changes were observed (For a comparison,  $^1\text{H}$  NMR of **Py-Ad** is shown in Figure 4.11 D).



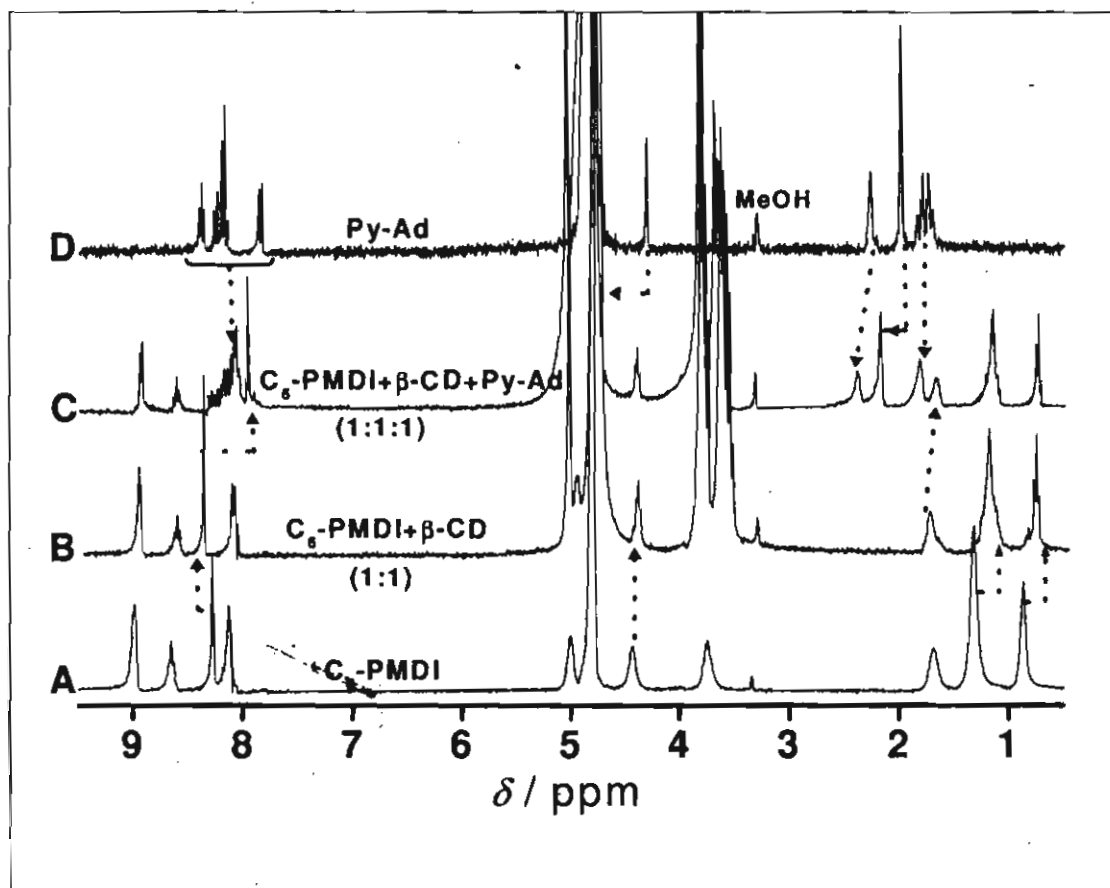


Figure 4.11. <sup>1</sup>H NMR spectra in D<sub>2</sub>O : CD<sub>3</sub>OD (98:2) of (A) C<sub>6</sub>-PMDI; (B) C<sub>6</sub>-PMDI +  $\beta$ -CD (1:1); (C) C<sub>6</sub>-PMDI +  $\beta$ -CD + Py-Ad (1:1:1) and (D) Py-Ad.

(1) The quartet due to H<sub>a</sub> protons collapsed to a broad singlet and exhibited slight down field shift, (2) the H<sub>b</sub> and H<sub>c</sub> protons shift down field by 0.2 and 0.12 ppm, respectively, (3) the N-CH<sub>2</sub> protons shift down field by nearly 0.45 ppm and merges with the HOD peak (in the <sup>1</sup>H NMR of Py-Ad in CD<sub>3</sub>OD this peak appears at  $\delta$  4.85, and very close to the HOD peak), and (4) protons of the pyrene moiety showed drastically different splitting pattern. These changes are consistent with encapsulation of the adamantane group in to the CD cavity. As mentioned

---

previously, **Py-Ad** exists in a folded conformation leading to a quartet for the  $H_a$  protons. When encapsulation occurs, a part of the CD rim gets inserted between the pyrene and adamantane moieties thereby forcing **Py-Ad** to assume an extended conformation. In this conformation, the  $H_a$  protons do not experience steric crowding from pyrene and consequently the quartet pattern collapses into a broad singlet. Changes in the splitting patterns for the pyrene protons are also attributed to the conformational change. Since the adamantane unit is inserted only partially into the cavity, the  $H_a$  protons are outside the cavity and experience little change in chemical shift. The  $H_b$  and  $H_c$  protons go deep into the cavity and experience significant down field shifts. In section 4.3.1 we have shown that **PMDI**s bind to the primary rim of  $\beta$ -CD with the alkyl group inserted into the cavity. In this configuration water molecules can enter and leave the cavity through the secondary side. When the adamantane group inserts through the secondary side and occupies nearly 65% of the cavity, all water molecules are driven out. As a result the free space (35%) now available at the narrow rim becomes highly hydrophobic. It is known that  $K_a$  values are higher for capped CDs because of increased hydrophobicity of the cavity.<sup>10</sup> The 0.43 ppm up field shift of the **PMDI** aromatic proton is attributed to the increased hydrophobicity at the primary rim, which might cause small changes in the rim-binding conformation. Thus the NMR spectra are consistent with the formation of ternary complex as shown in Scheme 4.5. In this study the binary and ternary systems are designated as **Py-Ad** $\supset$  $\beta$ -CD,

**PMDI**⊃β-CD and **Py-Ad**⊃β-CD⊃**PMDI**. We have noted that the order of addition of the components had no influence on the NMR spectrum of the ternary system. Spectrum 4.11 C is obtained regardless of whether **PMDI** is added first or **Py-Ad** is added first. For **C<sub>3</sub>-PMDI** and **C<sub>4</sub>-PMDI** also, formation of ternary complexes were studied by <sup>1</sup>H NMR. Similar results were obtained in these cases also. It may be mentioned that the ternary system studied here has its own NMR pattern which is different from those of uncomplexed or binary constituent systems like **PMDI**, **Py-Ad**, **Py-Ad**⊃β-CD or **PMDI**⊃β-CD. This completely rules out the possibility that the observed NMR is due to a mixture of **Py-Ad**⊃β-CD and **PMDI**⊃β-CD systems. Another important point is that the concentrations of **Py-Ad**:β-CD:**PMDI** employed is in a 1:1:1 ratio. The association constant  $K_a$  for **C<sub>6</sub>-PMDI**⊃β-CD is 1800 M<sup>-1</sup>.  $K_a$  for adamantane systems are known to be greater than 10<sup>5</sup> M<sup>-1</sup>. So the addition of one equivalent of **PMDI** to 1:1 **Py-Ad**⊃β-CD system is not expected to displace the **Py-Ad** moiety from the CD complex. So if a ternary system is not formed, most of the **PMDI** exist as free **PMDI** and signals corresponding to free **PMDI** should be seen in NMR. But we are not observing the signal due to free **PMDI** which again confirms the formation of the ternary system.

Further evidence for the formation of the ternary complex is provided by ICD studies. **PMDI** derivatives do not show circular dichroism, but when

associated with  $\beta$ -CD they exhibit negative ICD signal due to rim-binding (vide supra). Figure 4.12 A shows the ICD spectrum of  $C_6$ -**PMDI** $\supset\beta$ -CD in water. **Py-Ad** also does not show circular dichroism, but in the presence of  $\beta$ -CD gave the ICD spectrum in Figure 4.12 B. The 300-350 nm band of pyrene is polarized along the long axis.<sup>11</sup> As per ICD rules the negative ICD signal arises due to pyrene sitting outside of the rim with its long axis nearly parallel to  $\beta$ -CD axis (angle between the two axes  $< 54.7^\circ$ ).<sup>2</sup> Figure 4.12 C is the ICD spectrum of  $C_6$ -**PMDI**/ $\beta$ -CD/**Py-Ad** (5:1:1) system in water. The ICD signal has peaks due to **PMDI** and pyrene moieties and constitutes another evidence for formation of **Py-Ad** $\supset\beta$ -CD. As in the case of NMR studies, the order of addition of the components had no influence on the ICD signal due to **PMDI** $\supset\beta$ -CD $\subset$ **Py-Ad**. For the  $C_3$ -**PMDI** and  $C_4$ -**PMDI** cases also, ICD spectra similar to those shown in Figure 4.12 were obtained. ICD intensities, however, were lower for these systems.

It may be noted that ICD of **Py-Ad** $\supset\beta$ -CD $\subset$ **PMDI** is not a simple sum of the ICDs of **Py-Ad** $\supset\beta$ -CD and **PMDI** $\supset\beta$ -CD. This is due to the fact that the conformation of **PMDI** or pyrene in the ternary system is not identical to those in the binary systems. The alkyl group of **PMDI** and a part of the adamantyl group co-exist in the cavity and depending up on the available space and hydrophobicity of groups, minor realignments might occur. As a result, the pyrene or **PMDI**

chromophore move slightly into or out of the cavity causing changes in the ICD signal shape and intensity. Using the same argument as in NMR, we can rule out the presence of mixtures of **Py-Ad** and  $\beta$ -CD and **PMDI** and  $\beta$ -CD causing the observed ICD pattern. Here also, **Py-Ad** and  $\beta$ -CD are in 1:1 ratio. If **PMDI** has to complex with CD, it should displace some of the **Py-Ads** from the CD complex and as a result the signal intensity due to **Py-Ad** should decrease. But this is not observed. In fact the signal intensity due to **Py-Ad** actually increases, which means that the ternary complex is more tightly bound than the binary systems.

For circular dichroism measurements optical density of sample should be less than 1. For **PMDIs**, extinction coefficient of the 314 nm absorption is only  $2,800 \text{ M}^{-1} \text{ cm}^{-1}$ . Hence relatively high concentration of **PMDI** ( $> 3 \times 10^{-4} \text{ M}$ ) is required to get good ICD signals. At  $3 \times 10^{-4} \text{ M}$  concentration, optical density of the 340 nm ( $\epsilon = 45,000 \text{ M}^{-1} \text{ cm}^{-1}$ ) absorption of **Py-Ad** would be  $> 4$ . Thus it was not possible to do the ICD experiments with 1:1:1 **PMDI**/ $\beta$ -CD/**Py-Ad**. In order to circumvent this difficulty, we have carried out ICD experiments with adamantylammonium chloride (**ADAC**) (see Chapter 3 for structure) also.

**ADAC** has no absorption above 300 nm and hence high concentrations can be used in ICD experiments. An aqueous solution containing  $1.5 \times 10^{-3} \text{ M}$  each of **ADAC** and  $\beta$ -CD did not exhibit any ICD above 300 nm. Addition of **C<sub>6</sub>-PMDI**

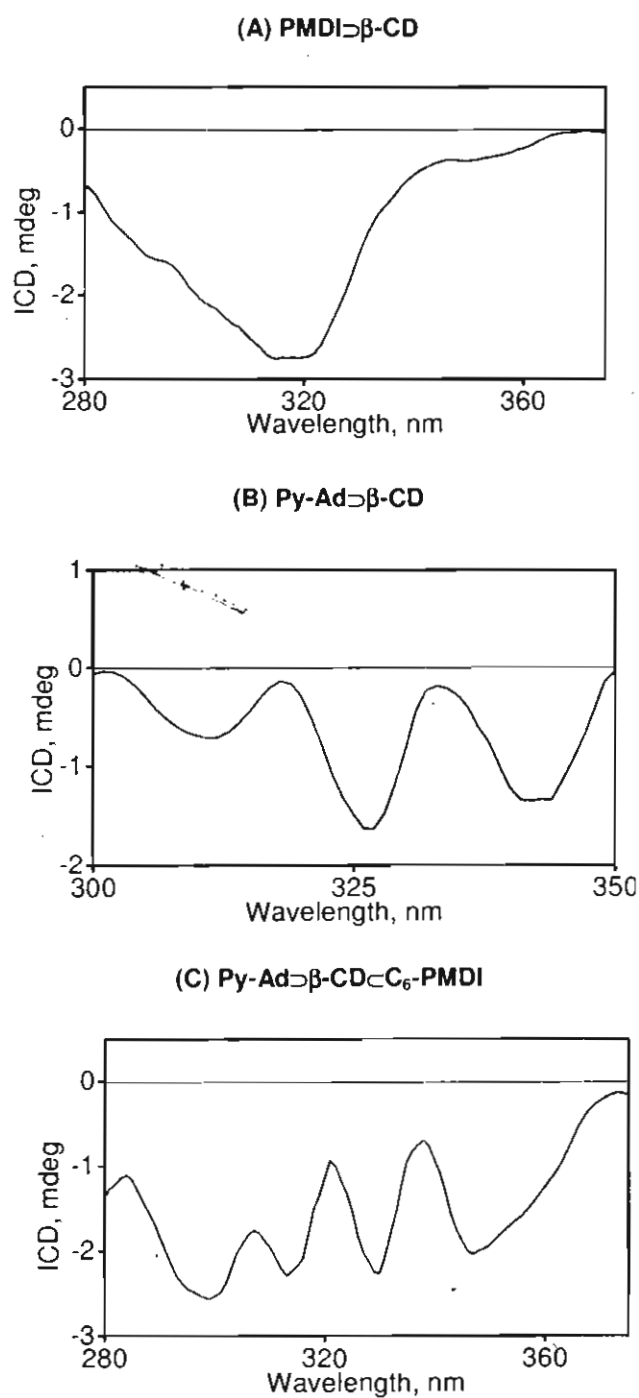


**Figure 4.12.** ICD spectra of (A) C<sub>6</sub>-PMDI +  $\beta$ -CD (1:1) (B) Py-Ad +  $\beta$ -CD (1:1) (c) C<sub>6</sub>-PMDI +  $\beta$ -CD + Py-Ad (1:1:1).

to the above solution leads to observation of ICD signal due to the **PMDI** as shown in Figure 4.13. **ADAC** complexes strongly with  $\beta$ -CD and **PMDI** is not expected to displace **ADAC** from the  $\beta$ -CD cavity. Under these conditions observation of ICD due to **PMDI** confirms formation of the ternary complex  $\text{ADAC} \supset \beta\text{-CD} \subset \text{PMDI}$ , which arises through rim binding of **PMDI** to  $\text{ADAC} \supset \beta\text{-CD}$ .

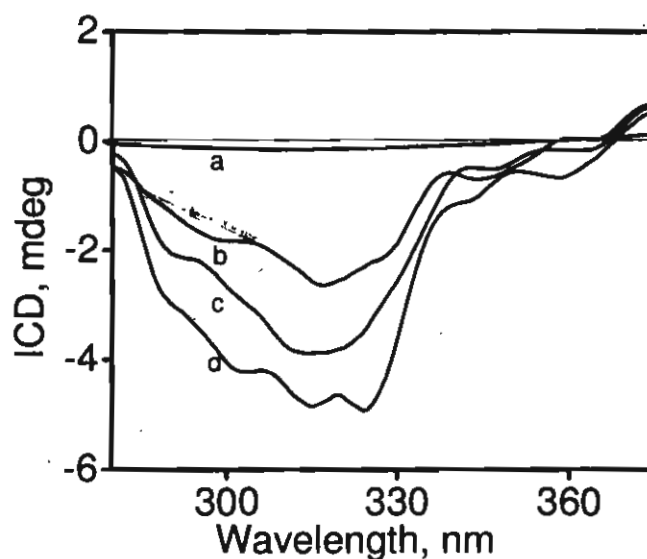
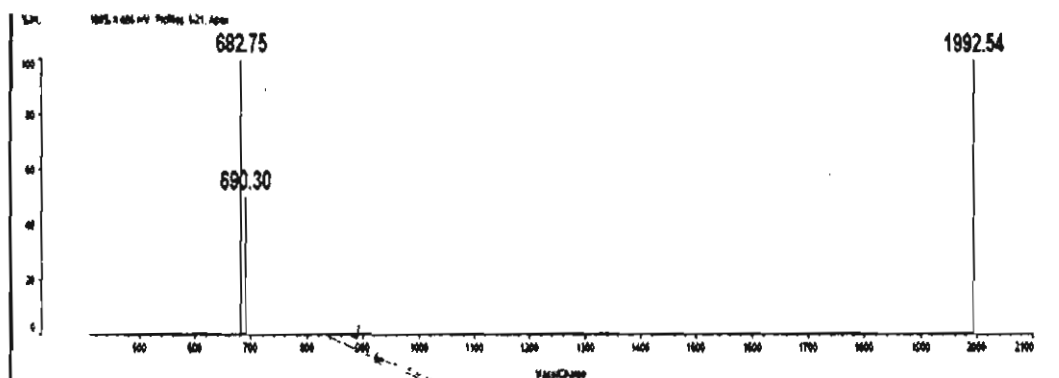


**Figure 4.13.** ICD of **ADAC**/ $\beta$ -CD (1:1, each  $1.5 \times 10^{-3}$  M) in the (a) absence and (b-d) presence of various amounts of **C<sub>6</sub>-PMDI**. [**C<sub>6</sub>-PMDI**] varied in the range  $0.74 \times 10^{-4}$  –  $3.5 \times 10^{-4}$  M.

Final evidence for the existence of the ternary system comes from MALDI-TOF spectroscopy. MALDI-TOF spectra of all **PMDI**/ $\beta$ -CD/**Py-Ad** systems exhibited masses corresponding to the ternary systems. For example, MALDI-

TOF of **Py-Ad**+ $\beta$ -CD+C<sub>4</sub>-PMDI exhibited peak at 1992 which corresponded to the sum of molecular masses of **Py-Ad**,  $\beta$ -CD and C<sub>4</sub>-PMDI (Figure 4.14 A).

**A**



**B**

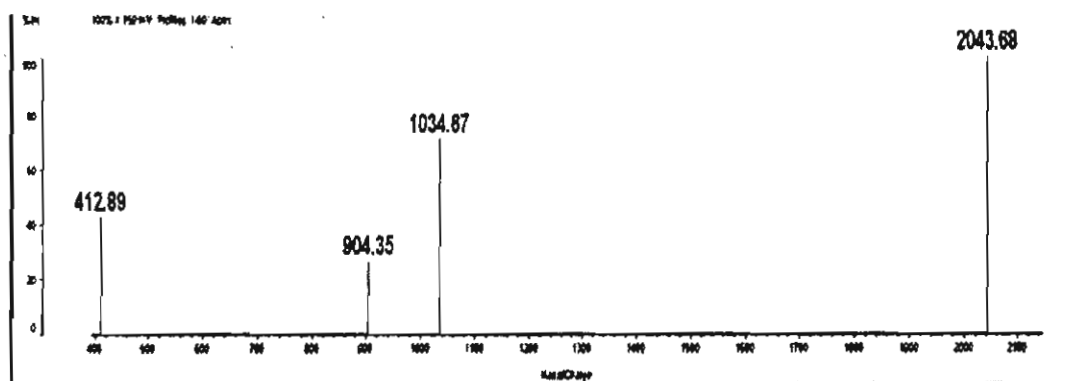


**Figure 4.14.** MALDI-TOF spectra of (A) **Py-Ad** +  $\beta$ -CD + C<sub>4</sub>-PMDI ( $M^+$  Calcd. 1992.33 Found: 1992.54) (B) **Py-Ad** +  $\beta$ -CD + C<sub>6</sub>-PMDI + Na (Calcd. 2043.65 Found: 2043.68)

In the case of the **Py-Ad**+ $\beta$ -CD+C<sub>6</sub>-PMDI ternary system, the mass peak was observed at 2043 (Figure 4.14 B) which corresponded to **Py-Ad**+ $\beta$ -CD+C<sub>6</sub>-



---

**PMDI+Na**. Thus maldi studies also confirmed the formation of the ternary system.

#### 4.3.2.3. Photoinduced Electron Transfer in the Ternary system

Pyrene is a well known excited state electron donor<sup>12</sup> and pyromellitic diimides are good electron acceptors.<sup>13</sup> The free energy change ( $\Delta G^0$ ) for electron transfer between <sup>1</sup>pyrene\* and **PMDI**, calculated using Weller equation (see Chapter 2 and 3 for details), was highly negative (-2.0 eV) indicating that this reaction is thermodynamically allowed. Hence the strategy presented in Scheme 4.5 is capable of delivering a **CD**-based ternary supramolecular system capable of undergoing PET reaction.

##### 4.3.2.3.1. Steady State Fluorescence Quenching Experiments

In the self-assembled **Py-Ad**⊃**β-CD**⊂**PMDI**, excitation of the pyrene moiety triggers transfer of an electron from pyrene chromophore to the **PMDI**. To study this process the binary complex **Py-Ad**⊃**β-CD** was assembled and its fluorescence quenching by added **PMDIs** was studied. Fluorescence of **Py-Ad** was unaffected by complexation with **β-CD**. This is due to the fact that the pyrene moiety remains above the hydrophilic secondary rim and not encapsulated into the **β-CD** cavity. Fluorescence spectrum of **Py-Ad**⊃**β-CD** is shown in Figure 4.15 a. Addition of **C<sub>6</sub>-PMDI** leads to quenching of the fluorescence as shown in Figure 4.15 b-j. Similar behaviour was observed for **C<sub>3</sub>-PMDI** and **C<sub>4</sub>-PMDI** also.

Because of the very high association constant, we assume that all of the **Py-Ad** is complexed with  $\beta$ -CD

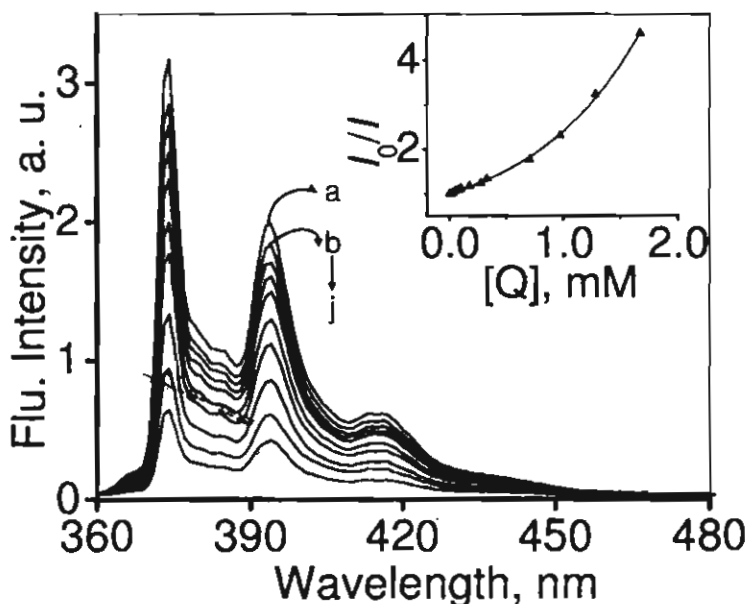
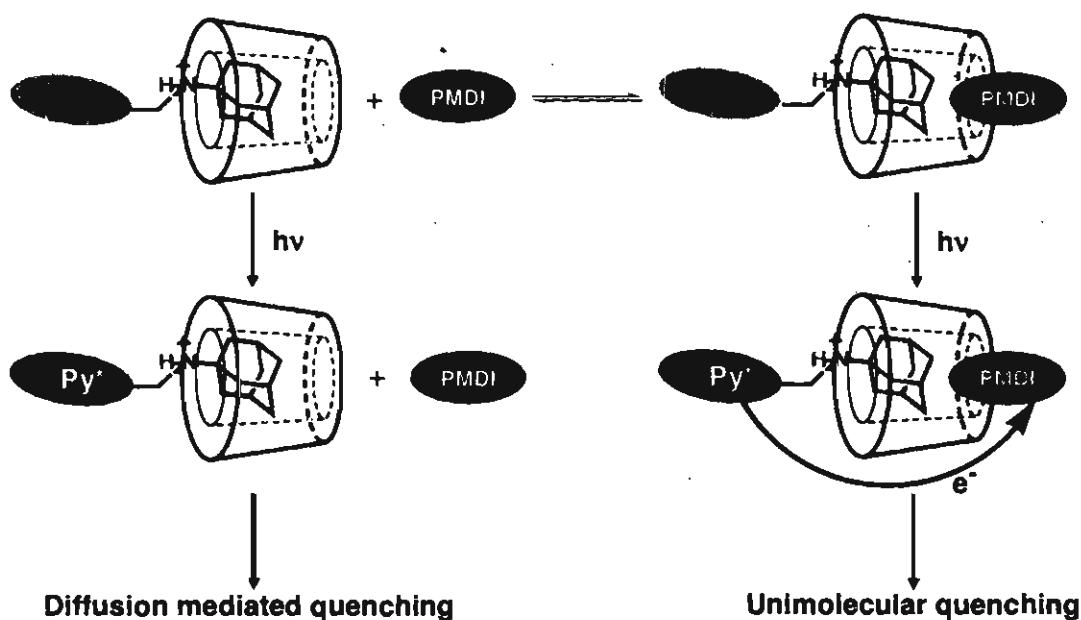


**Figure 4.15.** Fluorescence spectra of **Py-Ad**⊃ $\beta$ -CD in the absence (a) and presence (b-j) of **C<sub>6</sub>-PMDI**. Inset is a plot of  $I_0/I$  for this quenching.

When **PMDI** is added to **Py-Ad**⊃ $\beta$ -CD, a fraction of **PMDI** undergoes rim binding and assembles as the ternary system **Py-Ad**⊃ $\beta$ -CD⊃**PMDI** and the remaining fraction freely diffuses in solution. The free moving fraction of **PMDI** quenches the fluorescence of **Py-Ad**⊃ $\beta$ -CD in a diffusion mediated reaction and fluorescence in **Py-Ad**⊃ $\beta$ -CD⊃**PMDI** is quenched by the bound **PMDI** in a unimolecular reaction as shown in Scheme 4.7. The Stern-Völmer plot for the quenching shows upward curvature as shown in the inset of Figure 4.15, which confirms the unimolecular and diffusion mediated quenching processes.



**Scheme 4.7.** Unimolecular and diffusion mediated quenching pathways in **PMDI/β-CD/Py-Ad** system.

#### 4.3.2.3.2. Time Resolved Fluorescence Experiments

Unimolecular and diffusion mediated quenching pathways are further confirmed by fluorescence lifetime quenching experiments. Decay of **Py-Ad** in water was mono exponential with a lifetime ( $\tau_0$ ) of 151 ns. Addition of  $\beta$ -CD did not cause any change in the lifetime which supports our contention that almost all the **Py-Ad** molecules are present as **Py-Ad**⊃ $\beta$ -CD. Addition of **PMDI** leads to bi-exponential decays, which gave two lifetime values. Fluorescence decay profiles of **Py-Ad**⊃ $\beta$ -CD in presence of **C<sub>3</sub>-PMDI** and **C<sub>6</sub>-PMDI** are shown in Figures 4.16 and 4.17.

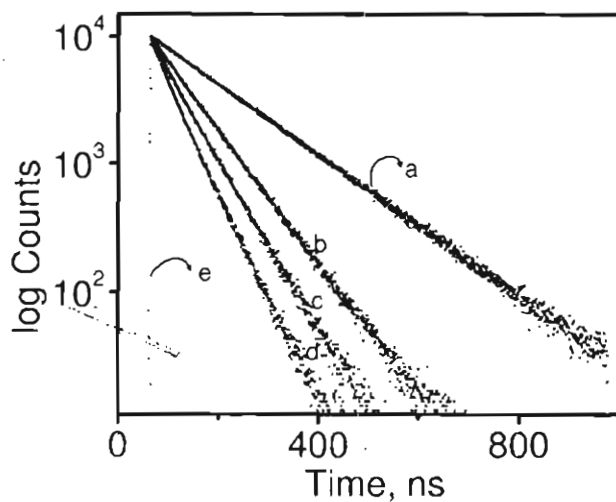


**Figure 4.16.** Fluorescence decay profiles of **Py-Ad** $\beta$ -CD (1:1,  $7 \times 10^{-4}$  M), in the (a) absence and (b-d) presence of **C<sub>3</sub>-PMDI** ( $2 - 4.6 \times 10^{-3}$  M). e is lamp profile.

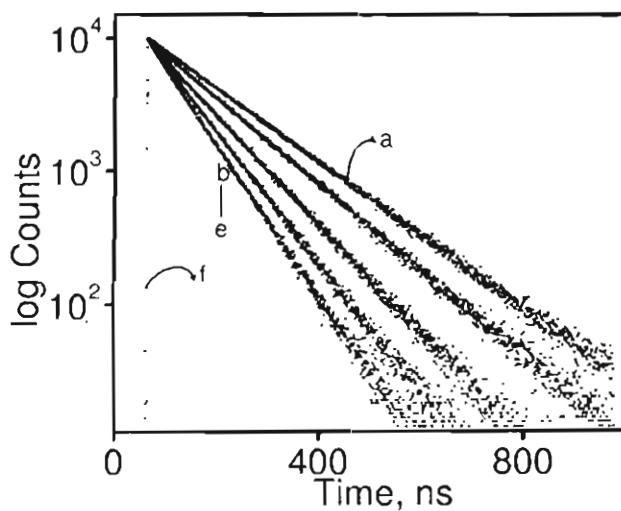


**Figure 4.17.** Fluorescence decay profiles of **Py-Ad** $\beta$ -CD (1:1,  $7 \times 10^{-4}$  M), in the (a) absence and (b-e) presence of **C<sub>6</sub>-PMDI** ( $0.4 - 3.13 \times 10^{-3}$  M). f is lamp profile.

The fluorescence decays were analyzed using the function,

$$I_1 = \chi_1 \exp(-t/\tau_1) + \chi_2 \exp(-t/\tau_2) \quad (3)$$

$$\tau_1 = (k_0 + k_{et})^{-1} \quad (4)$$

$$\tau_2 = (k_0 + k_q \tau_0 [\text{PMDI}])^{-1} \quad (5)$$

$\chi_1$  and  $\chi_2$  are the contributions due to the ternary (Py-Ad $\beta$ -CD $\subset$ PMDI) and binary (Py-Ad $\beta$ -CD) systems, respectively. According to equations (3)-(5), the short lifetime component ( $\tau_1$ ) is independent of the PMDI concentration and the long lifetime component ( $\tau_2$ ) is dependent on PMDI concentration. The short lifetime component  $\tau_1$  arises due to electron transfer quenching within the ternary system and hence the rate constant for electron transfer can be calculated using equation (6).

$$k_{et} = 1/\tau_1 - 1/\tau_0 \quad (6)$$

Data shown in Figures 4.16 and 4.17 were fitted using equation (3) and the fit parameters obtained are shown in Tables 4.1 and 4.2.

**Table 4.1.** Fluorescence lifetimes ( $\tau_1$  and  $\tau_2$ ), fractional contributions ( $\chi_1$  and  $\chi_2$ ) and  $\chi^2$  values obtained in the fluorescence lifetime quenching of Py-Ad $\beta$ -CD by C<sub>3</sub>-PMDI.

[C <sub>3</sub> -PMDI], mM	$\tau_1$ , ns	$\tau_2$ , ns	$\chi_1$	$\chi_2$	$\chi^2$
0		151		100	1.1
2	32	82.3	5	95	1.1
3.5	35	63.6	6.64	93.36	1.0
4.6	30	50.5	8.80	91.2	1.1

**Table 4.2.** Fluorescence lifetimes ( $\tau_1$  and  $\tau_2$ ), fractional contributions ( $\chi_1$  and  $\chi_2$ ) and  $\chi^2$  values obtained in the fluorescence lifetime quenching of **Py-Ad $\beta$ -CD** by **C<sub>6</sub>-PMDI**.

[ <b>C<sub>6</sub>-PMDI</b> ], mM	$\tau_1$ , ns	$\tau_2$ , ns	$\chi_1$	$\chi_2$	$\chi^2$
0		151		100	1.1
0.44	51.69	135	3.97	96.03	1.1
1.49	48.6	107	5	95	1.0
2.49	52	87.7	5.34	94.66	1.1
3.13	52	75.80	6.8	93.2	1.0

The short lifetime component ( $32 \pm 3$  ns for **C<sub>3</sub>-PMDI** and  $50 \pm 2$  ns for **C<sub>6</sub>-PMDI**) was independent of **PMDI** concentration and the long lifetime component decreased with **PMDI** concentration. Results similar to these were described in previous chapters and in line with these observations we assign the short lifetime component ( $\tau_1$ ) to electron transfer within the **Py-Ad $\beta$ -CD****C<sub>6</sub>-PMDI** ensemble and the long lifetime component to diffusion mediated electron transfer quenching of **Py-Ad $\beta$ -CD** by **PMDI**. Accordingly the rate constant for electron transfer within **Py-Ad $\beta$ -CD****C<sub>6</sub>-PMDI**,  $k_{et}$ , was calculated using the expression,  $k_{et} = (1/\tau_1 - 1/\tau_0)$ .  $k_{et}$  values obtained for **C<sub>3</sub>-PMDI** and **C<sub>6</sub>-PMDI** systems were  $2.4 \times 10^7$  and  $1.33 \times 10^7$  s<sup>-1</sup>, respectively.

The intra-ensemble rate constant  $k_{et}$  obtained for the ternary systems can be used to derive useful information about the donor-acceptor distance in the ternary

system. In Chapter 2 of this thesis, we have studied the dependence of  $k_{et}$  on free energy change for CD based systems wherein the acceptor is assumed to be encapsulated fully into the cavity and the donor is placed above the CD cavity at a distance of about 2 Å above the narrow rim. The donor-acceptor distance in this conformation was about 6 Å and we obtained the D-A coupling constant as 3 cm<sup>-1</sup>. The situation here is somewhat similar. The donor (pyrene) is placed slightly above the wider rim and the acceptor (**PMDI**) is placed near the narrow rim. The centre-to-centre distance between the **PMDI** and pyrene moieties is slightly more than the height of β-CD as shown in Scheme 4.5. For the present discussion, we assumed that this distance is 9 Å for the ternary system **Py-Ad**⊃β-CD⊃**C<sub>3</sub>-PMDI**. The free energy change  $\Delta G^0$  and solvent reorganization energy  $\lambda_0$  are distance dependent as per equations (7)<sup>14</sup> and (8).<sup>15</sup>

$$\Delta G^0 = E_{ox} - E_{red} - E_{0,0} - \frac{e^2}{2} \left( \frac{1}{r_P} + \frac{1}{r_Q} \right) \left( \frac{1}{37} - \frac{1}{\epsilon_s} \right) - \frac{e^2}{\epsilon_s d_{cc}} \quad (7)$$

$$\lambda_{out} = \Delta e^2 \left( \frac{1}{2r_P} + \frac{1}{2r_Q} - \frac{1}{d_{cc}} \right) \left( \frac{1}{\epsilon_{op}} - \frac{1}{\epsilon_s} \right) \quad (8)$$

In these equations,  $E_{ox}$  is the oxidation potential (in acetonitrile) of the pyrene moiety in **Py-Ad**,  $E_{red}$  is the reduction potential of **C<sub>3</sub>-PMDI** (in acetonitrile),  $r_P$  and  $r_Q$  are the radii of the pyrene and **PMDI** moieties, respectively,  $\epsilon_s$  and  $\epsilon_{op}$  are the static and optical dielectric constants of water and  $d_{cc}$  is the distance separating the donor and acceptor units. For the **C<sub>3</sub>-PMDI**/pyrene system we have calculated

$\Delta G^0$  and  $\lambda_0$  as per equations 7 and 8 using the following values.  $r_P = 4 \text{ \AA}$ ,  $r_Q = 2.75 \text{ \AA}$  and  $d_{cc} = 9 \text{ \AA}$ . We obtained  $\lambda_0 = 1.55 \text{ eV}$  and  $\Delta G^0 = -2.07$ . The coupling constant  $H_{el}$  is also distance dependent according to equation (9),<sup>16</sup>

$$H_{el}^2 = (H_{el}^0)^2 \exp [-\beta(d-d_0)] \quad (9)$$

where  $H_{el}^0$  is the coupling constant at distance  $d_0$ ,  $H_{el}$  is the coupling constant at distance  $d$  and  $\beta$  is the damping factor. For a large number of donor-acceptor systems in solution  $\beta$  values are known to vary in the  $1.0 - 1.4 \text{ \AA}^{-1}$  range.<sup>16</sup> Our work in Chapter 2 gave  $H_{el} = 3 \text{ cm}^{-1}$  for similar systems. With  $H_{el}^0 = 3 \text{ cm}^{-1}$  at  $d_0 = 6 \text{ \AA}$ , and using values of  $\beta = 1.2 \text{ \AA}^{-1}$  and  $d = 9 \text{ \AA}$ , we obtained  $H_{el}$  as  $0.6 \text{ cm}^{-1}$ , using equation (9). The  $k_{et}$  value can be obtained using equation (10).

$$k_{et} = (2\pi/\hbar) H_{el}^2 (4\pi\lambda_0 k_B T)^{-1/2} \sum_{m=0}^{\infty} (e^{-s} s^m / m!) \times \exp[-(\lambda_0 + \Delta G^0 + m h \nu)^2 / (4\lambda_0 k_B T)] \quad (10)$$

Equation (10) is a modified form of the Marcus equation where,  $\hbar$  is Planck's constant divided by  $2\pi$ ,  $H_{el}$  is the coupling matrix element,  $\lambda_0$  is the outer-sphere reorganization energy,  $k_B$  is the Boltzmann constant,  $T$  is the absolute temperature,  $\Delta G^0$  is the free energy change for the reaction,  $s = \lambda_i / h \nu$ ,  $m$  is an integer, and  $\lambda_i$  is the inner-sphere reorganization energy. Using  $H_{el} = 0.6 \text{ cm}^{-1}$  ( $6.14 \times 10^{-5} \text{ eV}$ ),  $\Delta G^0 = -2.07 \text{ eV}$ ,  $\lambda_0 = 1.55 \text{ eV}$ ,  $\lambda_i = 0.2 \text{ eV}$  and  $h \nu = 0.15 \text{ eV}$ , we obtained  $k_{et} = 2.35 \times 10^7 \text{ s}^{-1}$ . It is to be noted that the experimental value of  $k_{et}$  for the **Py-Ad** $\rightarrow$  **$\beta$ -CD** $\rightarrow$ **C<sub>3</sub>-PMDI** system ( $2.4 \times 10^7 \text{ s}^{-1}$ ) is very close to the calculated value.



---

Thus we have integrated a donor and acceptor into a supramolecular ensemble involving a  $\beta$ -CD framework without expending any effort towards CD functionalization. The rim-binding type of association described in this chapter could be very important in the context of designing supramolecular structures. Simple mixing of equimolar amounts of the constituent molecules in water results in the formation of the ternary ensemble. In the CD based ternary systems reported earlier, CD cavities co-host the chromophore and quencher systems. These types of systems are of no use in the context of mimicking natural photosynthesis. In the ternary system described here CD act as a scaffold to keep the donor and acceptor moieties at a fixed distance,  $d_{cc}$ . For the **Py-Ad $\supset$  $\beta$ -CD $\subset$ C<sub>3</sub>-PMDI** ternary system,  $d_{cc}$  is 9 Å and for the **Py-Ad $\supset$  $\beta$ -CD $\subset$ C<sub>6</sub>-PMDI** system  $d_{cc}$  was slightly larger.  $\beta$ -CD has a three fold function in this ensemble: (1) Encapsulate the adamantane unit and keep the pyrene moiety above the secondary rim, (2) rim bind **PMDI** and keep it at the primary rim and (3) act as a spacer between the donor and acceptor. The donor-spacer-acceptor configuration of the ternary systems could facilitate photoinduced charge separation. This is the first report of the assembly of a  $\beta$ -CD based ternary system capable of vectorial electron transfer. Self-assembly of donor and acceptor components in aqueous solution and study of PET processes in such systems is an extremely important task in the context of understanding and mimicking natural photosynthetic process.

---

#### 4.4. Conclusions

In this chapter complex formation of pyromellitic diimide derivatives (**PMDI**) with  $\beta$ -cyclodextrin and anthracene-appended  $\beta$ -cyclodextrin were studied using induced circular dichroism and  $^1\text{H}$  NMR spectroscopies. Pyromellitic diimides form rim-binding type complexes with  $\beta$ -CD and in these complexes the pyromellitic diimides lie just outside of the narrow rim of the CD. When the smaller rim was blocked by a relatively large molecule like anthracene the pyromellitic diimides form true inclusion complexes. The ability of **PMDI** to form rim binding complexes was exploited to assemble *Acceptor- $\beta$ -CD-Donor* Ternary complexes. The very high affinity of adamantane moiety for  $\beta$ -CD cavity and the propensity of **PMDI** for rim binding with the primary rim of  $\beta$ -CD cavity were utilized in this design. Simple mixing of equimolar amounts of the constituent molecules in water resulted in the formation of the ternary ensemble as evidenced by NMR, ICD and MALDI-TOF experiments.  $\beta$ -CD has a three fold function in the ensemble: (1) Encapsulate the adamantane unit and keep the pyrene moiety above the secondary rim, (2) rim bind **PMDI** and keep it at the primary rim and (3) act as a spacer between the donor and acceptor. The donor-spacer-acceptor configuration of the assembly could facilitate photoinduced charge separation. Steady state and time resolved fluorescence experiments confirm photoinduced electron transfer in **Py-Ad** $\supset$  $\beta$ -CD $\subset$ **PMDI**.

## 4.5. Experimental section

### 4.5.1. General techniques

NMR spectra were recorded on a 300 MHz Bruker Avance DPX spectrometer. ICD spectra were obtained on a JASCO-J-810 Circular Dichroism Spectropolarimeter. MALDI mass spectrometry was conducted on a Perspective Biosystem Voyager DEPRO MALDI-TOF Spectrometer in a matrix of  $\alpha$ -cyano-4-hydroxycinnamic acid. Steady state fluorescence experiments were performed using SPEX Fluorolog F112X spectrofluorimeter and fluorescence lifetime experiments were carried out using a IBH picosecond Single Photon Counting system employing a 335 nm NanoLED excitation source and Hamamatsu C4878 MCP detector.

### 4.5.2. Materials

#### 4.5.2.1. Synthesis and Characterization of PMDI derivatives

General Procedure:

**Preparation of 2:** Pyromellitic anhydride (1 g, 4.6 mM) was dissolved in DMF (9 mL). The amine R-NH<sub>2</sub> (4.6 mM) and ethanolamine (0.277 mL, 4.6 mM) were added and the mixture refluxed for 6 h. Cooled and poured in to ice cold water and the precipitate formed was filtered, dried and chromatographed over silica gel. **2** was obtained upon elution with MeOH-CHCl<sub>3</sub> (5:95) mixture. Yield 29-30%.

**Preparation of 3:** **2** (0.49 mM) was added to a mixture of aqueous HBr (1 mL) and Conc. H<sub>2</sub>SO<sub>4</sub> (0.4 mL). Conc. H<sub>2</sub>SO<sub>4</sub> (0.4 mL) was again added and the solution refluxed for 3 h. The mixture was cooled and the product was extracted with dichloromethane and recrystallized from dichloromethane-methanol mixture. Yield 62-65%.

**Preparation of 4:** A mixture of **3** (0.2 mM) and Pyridine (1.5 mL) was refluxed for 8 h and cooled. The crude product was washed with hexane and chloroform and was recrystallized from dichloromethane-methanol mixture. Yield 73-75%.

Data for **2a**, **3a** and **4a** were given in Chapter 3.

**2b:** <sup>1</sup>H NMR (300 MHz, [D<sub>6</sub>] DMSO)  $\delta$  ppm: 0.89 (t, 3H), 1.27-1.34 (m, 2H), 1.57-1.62 (m, 2H), 3.59-3.64 (m, 4H), 3.69 (t, 2H), 4.88 (t, 1H), 8.17 (s, 2 H); HRMS (FAB)  $m/z = 317.40$  (M + H<sup>+</sup>) (calculated mass = 316.11).

**3b:** <sup>1</sup>H NMR (300 MHz, CDCl<sub>3</sub>, TMS)  $\delta$  (ppm): 0.96 (t, 3H), 1.34-1.44 (m, 2H), 1.64-1.74 (m, 2H), 3.66 (t, 2H), 3.75 (t, 2H), 4.18 (t, 2H), 8.30 (s, 2 H); HRMS (FAB)  $m/z = 378.13$  (calculated mass = 378.02).

**4b:** <sup>1</sup>H NMR (300 MHz, D<sub>2</sub>O, TMS)  $\delta$  (ppm): 0.93 (t, 3H), 1.29-1.39 (m, 2H), 1.61-1.71 (m, 2H), 3.73 (t, 2H), 4.43 (t, 2H), 5.00 (t, 2H), 8.10 (t, 2 H), 8.25 (s, 2 H), 8.65 (t, 1 H), 8.99 (d, 2 H); <sup>13</sup>C NMR (75 MHz, CDCl<sub>3</sub>)  $\delta$  (ppm): 13.52, 19.99, 29.64, 30.34, 38.41, 59.95, 118.49, 128.37, 136.88, 137.31, 146.06, 166.16, 166.23; FT-IR (KBr)  $\nu_{\max}$ : 1631, 1712, 1776, 2870, 2958, 3041 cm<sup>-1</sup>; HRMS (FAB)  $m/z = 378.20$  (calculated mass = 378.15).

**2c:**  $^1\text{H}$  NMR (300 MHz,  $[\text{D}_6]$  DMSO)  $\delta$  (ppm): 0.84 (t, 3H), 1.27 (broad singlet, 6H), 1.61 (t, 2H), 3.58-3.63 (m, 4H), 3.69 (t, 2H), 4.87 (t, 1H), 8.18 (s, 2 H); HRMS (FAB)  $m/z = 344.34$  (calculated mass = 344.14).

**3c:**  $^1\text{H}$  NMR (300 MHz,  $\text{CDCl}_3$ )  $\delta$  (ppm): 0.88 (t, 3H), 1.25-1.31 (m, 4H), 1.65-1.71 (m, 4H), 3.64-3.76 (m, 4H), 4.18 (t, 2H), 8.30 (s, 2 H); HRMS (FAB)  $m/z = 406.15$  (calculated mass = 406.05).

**4c:**  $^1\text{H}$  NMR (300 MHz,  $\text{D}_2\text{O}$ , TMS)  $\delta$  (ppm): 0.86 (broad singlet, 3H), 1.31 (broad singlet, 6H), 1.66 (broad singlet, 2H), 3.70 (broad singlet, 2H), 4.43 (broad singlet, 2H), 5.00 (broad singlet, 2H), 8.10-8.21 (m, 4 H), 8.64 (t, 1 H), 9.00 (d, 2 H);  $^{13}\text{C}$  NMR (75 MHz,  $\text{CDCl}_3$ )  $\delta$  (ppm): 13.94, 22.43, 26.45, 28.31, 29.63, 31.23, 38.67, 59.84, 118.43, 128.29, 136.86, 137.32, 146.07, 166.13, 166.23; FT-IR (KBr)  $\nu_{\text{max}}$ : 1633, 1712, 1724, 1774, 2854, 2929, 3043  $\text{cm}^{-1}$ ; HRMS (FAB)  $m/z = 406.38$  (calculated mass = 406.18).

#### 4.5.2.2. Synthesis and Characterization of Py-Ad

**Preparation of 7:** Pyrenecarboxaldehyde (1 g, 2.1 mM) was dissolved in dry benzene (15 mL). Adamantylamine (656 mg, 2.1 mM) was added and the mixture refluxed for 3 h in a Dean-Stark apparatus. Benzene was distilled out and the crude material obtained was recrystallized from ethanol to give pure product.

Yield: 90%

$^1\text{H}$  NMR (300 MHz,  $\text{CDCl}_3$ )  $\delta$  (ppm): 1.80 (s, 6H), 2.09 (d, 6H), 2.25 (s, 3H), 7.97-8.20 (m, 7H), 8.54 (d, 1H), 8.25 (d, 1H), 9.32 (s, 1H) ppm; FT-IR (KBr)  $\nu_{\text{max}}$ : 1448, 1597, 1620, 2845, 2904, 3043  $\text{cm}^{-1}$ . HRMS (FAB)  $m/z = 363.12$  (calculated mass = 363.20)

**Preparation of 8:** ~~7~~ (100 mg, 0.2 mM) was dissolved in methanol (20 mL) and  $\text{NaBH}_4$  (10 mg, 0.2 mM) was added to it with stirring. The reaction was completed in 10 minutes. Then it was filtered through a neutral alumina column and concentrated to get the pure product. Yield: 98%

$^1\text{H}$  NMR (300 MHz,  $\text{CDCl}_3$ )  $\delta$  (ppm): 1.57 (s, 1H), 1.74 (s, 6H), 1.88 (s, 6H), 2.16 (s, 3H), 4.45 (s, 2H), 7.95-8.18 (m, 8H), 8.37 (d, 1H) ppm; FT-IR (KBr)  $\nu_{\text{max}}$ : 1141, 1182, 1305, 1355, 1452, 1593, 1635, 2845, 2900, 3041, 3307  $\text{cm}^{-1}$ . HRMS (FAB)  $m/z = 365.20$  (calculated mass = 365.22)

**Preparation of 9:** **8** was dissolved in Diethyl ether (25 mL) and dry HCl was passed through it for 5-10 minutes. Hydrochloride salt of **Py-Ad** was precipitated out in 100% yield.

$^1\text{H}$  NMR (300 MHz, 98:2  $\text{D}_2\text{O}:\text{CD}_3\text{OD}$ )  $\delta$  (ppm): 1.70-1.83 (m, 6H), 2.20 (s, 6H), 2.26 (s, 3H), 4.30 (s, 2H), 7.82-7.85 (d, 2H), 8.13-8.39 (m, 7H) ppm;  $^{13}\text{C}$  NMR (75 MHz, DMSO  $\delta$  ppm): 29.07, 35.51, 37.81, 58.01, 123.14, 124.03, 124.37, 125.04, 125.93, 126.04, 126.13, 126.83, 127.51, 128.47, 128.59, 129.71, 129.76, 130.54, 131.10, 131.89 ppm; FT-IR (KBr)  $\nu_{\text{max}}$ : 842, 1068, 1305, 1365, 1456,

---

1593, 2436, 2594, 2638, 2754, 2848, 2916, 3045  $\text{cm}^{-1}$ . HRMS (FAB)  $m/z = 365.18$  (calculated value 365.22).

#### 4.6. References

1. Harata, K.; Uedaira, H. *Bull. Chem. Soc. Jpn.* **1975**, *48*, 375-378.
2. (a) Kodaka, M. *J. Phys. Chem.* **1991**, *95*, 2110-2112. (b) Kodaka, M. *J. Am. Chem. Soc.* **1993**, *115*, 3702-3705.
3. Gawroński, J.; Brzostowska, M.; Kacprzak, K.; Kolbon, H.; Skowronek, P. *Chirality* **2000**, *12*, 263-268.
4. Matsushita, Y.; Suzuki, T.; Ichimura, T.; Hikida, T. *J. Phys. Chem. A* **2004**, *108*, 7490-7496.
5. Szejtli, J. *Pure Appl. Chem.* **2004**, *76*, 1825-1845.
6. (a) Komiyama, M. *J. Am. Chem. Soc.* **1989**, *111*, 3046-3050. (b) Tee, O. S.; Hoeven, J. J. *J. Am. Chem. Soc.* **1989**, *111*, 8318-8320.
7. Rekharsky, M. V.; Inoue, Y. *Chem. Rev.* **1998**, *98*, 1875-1917.
8. (a) Breslow, R.; Czarniecki, M. F.; Emert, J.; Hamaguchi, H. *J. Am. Chem. Soc.* **1980**, *102*, 762-770. (b) Emert, J.; Breslow, R. *J. Am. Chem. Soc.* **1975**, *97*, 670-672.
9. (a) Kano, K.; Takenoshita, I.; Ogawa, T. *Chem. Lett.* **1980**, 1035-1038. (b) Kano, K.; Takenoshita, I.; Ogawa, T. *J. Phys. Chem.* **1982**, *86*, 1833-1838. (c) Kano, K.; Hashimoto, S.; Imai, A.; Ogawa, T. *J. Inclusion Phenom.*

- 
- 1984**, 2, 737-746. (d) Hamai, S. *Bull. Chem. Soc. Jpn.* **1991**, 64, 431-438.
- (e) Kano, K.; Takenoshita, I.; Ogawa, T. *Chem. Lett.* **1982**, 321-324.
10. Engeldinger, E.; Arinspach, D.; Matt, D. *Chem. Rev.* **2003**, 103, 4147-4173.
11. (a) Langkilde, F. W.; Gisin, M.; Thulstrup, E. W.; Michl, J. *J. Phys. Chem.* **1983**, 87, 2901-2911. (b) Kobayashi, N.; Minato, S.; Osa, T. *Macromol. Chem.* **1983**, 184, 2123-2132 (c) Ueno, A.; Suzuki, I.; Osa, T. *J. Am. Chem. Soc.* **1989**, 111, 6391-6397.
12. Julliard M. in *Photoinduced Electron Transfer, Part B*; Fox, M. A., Channon, M., Eds.; Elsevier: New York, 1988; pp 216-313.
13. (a) Sessler, J. L.; Brown, C. T.; O'Connor, D.; Springs, S. L.; Wang, R.; Sathiosatham, M.; Hirose, T. *J. Org. Chem.* **1998**, 63, 7370-7374. (b) Osuka, A.; Marumo, S.; Wada, Y.; Yamazaki, I.; Yamazaki, T.; Shirakawa, Y.; Nishimura, Y. *Bull. Chem. Soc. Jpn.* **1995**, 68, 2909-2915. (c) Wiederrecht, G. P.; Niemczyk, M. P.; Svec, W. A.; Wasielewski, M. R. *J. Am. Chem. Soc.* **1996**, 118, 81-91. (d) Nagata, T. *Bull. Chem. Soc. Jpn.* **1991**, 64, 3005-3016. (e) Freilich, S. C.; *Macromolecules* **1987**, 20, 973-978.
14. Kavarnos, G. J. *Fundamentals of Photoinduced Electron Transfer*; VCH: New York, 1993; p 62.
15. (a) Marcus, R. A. *Annu. Rev. Phys. Chem.* **1964**, 15, 155-196. (b) Marcus, R. A. *J. Chem. Phys.* **1956**, 24, 966-978.



- 
16. (a) Paddon-Row, M. N. in *Electron Transfer in Chemistry, Vol. 3*; Balzani, V., Ed.; Wiley-VCH: Weinheim, 2001; pp 179-271. (b) Marcus, R. A.; Siders, P. J. *J. Phys. Chem.* **1982**, *86*, 622-630. (c) Siders, P. J.; Marcus, R. A. *J. Am. Chem. Soc.* **1981**, *103*, 741-747. (d) Sutin, N. *Acc. Chem. Res.* **1982**, *15*, 275-282. (e) Marcus, R. A. *Int. J. Chem. Kinet.* **1981**, *13*, 865-872. (f) Marcus, R. A. *Faraday Discuss. Chem. Soc.* **1982**, *74*, 7-15.

## List of Publications

1. Photoinduced Electron Transfer in  $\alpha$ -Cyclodextrin-Based Supramolecular Dyads: A Free-Energy Dependence study.

**Bijitha, B.;** Gopidas, K. R. *Chem. Eur. J.* **2006**, *12*, 6701-6710.

2. An Anthracene-Appended  $\beta$ -Cyclodextrin-Based Dyad: Study of Self Assembly and Photoinduced Electron-Transfer Processes.

**Bijitha, B.;** Gopidas, K. R. *Chem. Eur. J.* **2007**, *13*, 5173-5185.

3. Interaction of Pyromellitic Diimide Derivatives with  $\beta$ -Cyclodextrin and Anthracene-Appended  $\beta$ -Cyclodextrin: Rim-Binding vs Inclusion Complexation.

**Bijitha, B.;** Sivadas, D. L.; Gopidas, K. R. *Org. Lett.* **2007**, *9*, 2709-2712.

4. A Donor- $\beta$ -Cyclodextrin - Acceptor Ternary System: Study of Self-Assembly and Photoinduced Electron Transfer Processes.

**Bijitha, B.;** Sivadas, D. L.; Gopidas, K. R. (submitted)

## Papers presented at conferences

1. Photoinduced Electron Transfer in  $\alpha$ -Cyclodextrin-Based Supramolecular Dyads: A Free-Energy Dependence study. (Oral Presentation)

**Bijitha Balan** and K. R. Gopidas, International Conference on Materials for the Millennium, Cochin University of Science and Technology, Kerala, India, March 1-3, 2007.

2. Study of Competition between Energy and Electron transfer in a Hydrogen-Bonded Donor-Acceptor System. (Poster presentation)

**Bijitha Balan** and K. R. Gopidas, 7<sup>th</sup> CRSI National Symposium in Chemistry, IACS, Kolkata, India, February 4-6, 2005.

R

NATIONAL INSTITUTE FOR INTER DISCIPLINARY SCIENCE  
AND TECHNOLOGY (CSIR) TVPM  
KNOWLEDGE RESOURCE CENTRE

Acc. No. 3/2931

Call. No. 547.15:458:8]:6 P7

This book is to be returned on or before the date last stamped below:

--	--	--